RITA ALVES COSTA

# PHYSIOLOGY OF HOMEOSTASIS AND REPAIR OF SKIN IN TELEOSTS AND THE ROLE OF METABOLIC AND ENDOCRINE FACTORS

**UNIVERSIDADE DO ALGARVE**
DEPARTMENTO DE CIÊNCIAS BIOMÉDICAS E MEDICINA
2016

RITA ALVES COSTA

# PHYSIOLOGY OF HOMEOSTASIS AND REPAIR OF SKIN IN TELEOSTS AND THE ROLE OF METABOLIC AND ENDOCRINE FACTORS

Doutoramento em Ciências Biomédicas

Trabalho efetuado sob a orientação de
Professora Doutora Deborah Power

**UNIVERSIDADE DO ALGARVE**
DEPARTMENTO DE CIÊNCIAS BIOMÉDICAS E MEDICINA
2016

*Physiology of homeostasis and repair of skin in teleosts and the role of metabolic and endocrine factors*

Declaração de autoria de trabalho

Declaro ser a autora deste trabalho, que é original e inédito. Os autores e trabalhos consultados estão devidamente citados no texto e constam da listagem de referências incluída.

# Acknowledgements

I would like to acknowledge my supervisor, Professor Deborah Power for her continuous support and guidance during all these years. Thank you Professora Deborah for your encouragement, motivation, for trusting my work and for you mentoring that was fundamental in keeping me focused.

Very special thanks to Doctor João Cardoso, from whom I`ve learned so much, for all the valuable suggestions and positive comments which helped me in preparing and improving the manuscripts and for being such a dear friend and colleague.

Thanks to the colleagues in the laboratory of Comparative Endocrinology and Integrative Biology that helped me along these years, either by the practical help they provided but mainly by the friendship along these journey: Elsa Couto, Rute Félix, Nádia Silva, Liliana Guerreiro, Rute Martins and Patrícia Pinto. Special thanks to Silvia Gregório, Ana Patrícia Mateus and Ricardo Alves for the daily friendship and support when things were more difficult and to share the happiness when things were going forward.

Finally, I would like to thank my family for the support and encouragement, even when distance kept us apart.

# Abstract

The skin is a multifunctional organ and the primal frontier to the external environment. It is the first line of defence against external aggressors and any injuries inflicted in the vertebrate skin are rapidly repaired to re-establish immune defence and integument homeostasis. In mammals the outcome of skin injury is repair and scaring but in other vertebrates such as amphibians and fishes' regeneration of the skin occurs and the disrupted tissue is replaced by skin of the same architecture and functionality as the original. Skin regeneration in vertebrates has been poorly explore and comparisons of the healing process in animals that heal scar free with mammalian wounds that scar will provide novel insights on the skin repair program and identify novel drug targets for mammalian skin disorders.

The aim of this thesis was to identify key factors involved in skin homeostasis and repair and to generate a simple model for skin repair integrating metabolic, endocrine and immune considerations. The model species of this study was the gilthead sea bream (*Sparus aurata*) and using morphological and gene expression analysis the processes involved in wound healing in the regenerating fish skin in response to superficial damage caused by scale removal are described. Two gene families related to tissue repair in mammals (Angiopoietin-like family, ANGPTLs and Osteoglycin, OGN) were studied in detailed and compared and the effect of the diet supplement alpha-ketoglutarate (AKG), an inducer of collagen synthesis, in the integumentary system of adult sea bream explored.

In overall the results obtained contribute to improve the current state of the art on the morphology and physiology of adult teleost skin and its regeneration after damaged and highlights for the importance of fish skin as a comparative model to study cutaneous repair in vertebrates.

**Keywords**: skin, teleosts, wound healing, regeneration, angiopoietin-like family, small leucine-rich proteoglycan, osteoglycin, duplicate genes, alpha-ketoglutarate, metabolism, scales

# Resumo

O integumento é composto pela pele e os seus apêndices (pêlos, glândulas e escamas) e constitui a primeira linha de defesa do organismo a agressões externas e agentes patogénicos em vertebrados. A pele é o maior órgão do corpo e o primeiro a ser formado durante o desenvolvimento embrionário. É um órgão de estrutura simples, no entanto, biologicamente complexo e essencial à sobrevivência, e para além do seu papel na imunidade inata, é também um importante órgão sensorial e neuro-endócrino. Devido à sua importância, a pele quando danificada, recupera rapidamente para restabelecer as defesas imunitárias e a homeostasia do integumento. Em mamíferos, o processo de reparação cutânea leva à formação de uma cicatriz com consequente perda de funcionalidade do tecido afetado, mas noutros vertebrados, tais como anfíbios e peixes, cuja estrutura da pele é semelhante aos mamíferos existe a capacidade de regeneração tecidular e a pele danificada é reconstruída com igual topologia e funcionalidade. Em peixes teleósteos, o processo de regeneração da pele é pouco estudado sendo, no entanto, relevante uma vez que uma melhor compreensão sobre este processo permitirá estabelecer comparações do processo de reparação da pele em indivíduos adultos que têm mecanismos de regeneração como a de mamíferos, que perdem essa capacidade ainda na vida fetal e formam cicatrizes. Isto proporcionará um melhor entendimento dos processos regenerativos em vertebrados e permitirá a descoberta de novas moléculas que podem ajudar na compreensão das desordens da pele em mamíferos.

O objetivo desta tese consistiu em identificar os fatores chave envolvidos na homeostasia e reparação da pele, e estabelecer um modelo simples de reparação da pele em vertebrados integrando considerações metabólicas, endócrinas e imunitárias. O organismo experimental utilizado neste estudo foi a dourada (*Sparus aurata*), um peixe teleósteo marinho de elevado valor económico e comercial na Europa, para qual já existem vários estudos fisiológicos e moleculares sobre o crescimento, metabolismo e homeostasia da energia e função imune. Recorrendo a várias análises morfológicas e moleculares esta tese descreve o processo de reparação da pele em dourada após uma agressão superficial ao integumento provocada pela remoção das escamas. Uma análise de dados de *microarray* de pele da dourada a 3 e 7 dias após a remoção das escamas (disponíveis no grupo) permitiu caracterizar os processos biológicos sub-expressos durante a regeneração da pele (capitulo 2). Neste estudo, verificou-se que no modelo utilizado a inflamação é independente da reepitelização do tecido, e que componentes da imunidade inata e adquirida estão suprimidos nas fases iniciais de reparação e só depois da

função de barreira da pele ser reestabelecida é que o integumento amadurece e adquire a sua funcionalidade original. Duas famílias de genes associadas à reparação tecidular em mamíferos e possivelmente envolvidas na regeneração da pele em teleósteos foram selecionadas com base em estudos anteriores realizados pelo grupo de investigação, e ainda pouco caracterizadas em peixes, foram estudadas em detalhe: os membros da família das proteínas tipo angiopoietinas – (ANGPTLs) (capitulo 3) e o membro da família dos *small leucine-rich proteoglycan* o proteoglicano osteoglicina (OGN) (capitulo 4) e a sua evolução e papel no processo de regeneração tecidular em dourada comparada com os homólogos em tetrápodes. As ANGPTLs são uma família numerosa em peixes (10-13 membros) com vários genes homólogos de mamíferos duplicados. A analise evolutiva e comparativa identificou um novo membro desta família (*angptl9*) em peixes e outros tetrápodes (anfíbios e aves) mas não em mamíferos e que o gene dos mamíferos *ANGPTL8* está ausente em outros vertebrados. Vários genes candidatos expressos na pele de peixes foram identificados, no entanto, o *angptl1b*, *angptl2b* e *angptl7* parecem ter um papel importante no processo de regeneração pois são diferencialmente expressos durante as fases iniciais do processo de regeneração em dourada em pele intacta e regenerada. A existência e expressão de alguns membros da ANGPTL na pele de peixes e mamíferos, a sua ligação com a reparação do integumento, especificamente na dourada e a sua expressão associada a processos essenciais no programa de reparação sugere que o seu papel na regeneração e homeostasia da pele de vertebrados é conservada. Analises *in silico* identificaram dois genes para a OGN em peixes teleósteos (*ogn1* e *ogn2*), e estudos de expressão tecidular e em culturas de células primárias *in vitro* de osso e mióticos de dourada sugerem que estes poderão estar envolvidos em múltiplas funções em peixes e que após duplicação diferenciaram-se e possivelmente adquiriram funções especificas. No entanto, no modelo de regeneração em estudo ambas as cópias duplicadas possuem funções conservadas na reparação da matriz da pele de peixes, tal como em mamíferos. O efeito do suplemento alimentar ácido alfa-cetoglutarato (AKG), estimulador da síntese de colagénio em mamíferos e aves, foi estudado no integumento e na regeneração da pele em douradas adultas (capitulo 5). A presença desta molécula quando na dieta dos peixes, estimula a biomineralização das escamas, acelera o crescimento das escamas em regeneração e promove a proliferação das células da epiderme, sugerindo que têm um papel importante na homeostasia da pele dos peixes e que tal como em mamíferos parece acelerar o processo de reepitelização após uma agressão.

Os resultados obtidos nesta tese, contribuíram para um aumento da informação previamente disponível sobre a morfologia e a fisiologia da pele em peixes teleósteos adultos,

e sobre a sua regeneração após uma agressão. Novos genes e moléculas que partilham a mesma origem evolutiva, motivos funcionais e papel biológico conservado no processo de regeneração com a dos mamíferos foram identificadas em peixes. Este trabalho realça a importância da pele dos peixes como um importante modelo comparativo para o estudo da reparação cutânea em vertebrados.

**Termos chave:** pele, regeneração, reparação, família do tipo das angiopoietinas, proteoglicanos, osteoglicina, genes duplicados, ácido alfa-cetoglutarato, metabolism, escamas

# Table of contents

# List of tables

# List of figures

# List of supplementary tables



# List of supplementary figures

# 1

# General introduction

## 1.1 General introduction

The present thesis is focussed on the skin, the largest organ in the body with an essential role in numerous physiological processes in vertebrates. It has generally been overlooked by anatomists and physiologists, although in recent years it has received increasing attention due to its function as an innate immune barrier and the ease of access for studies of aging and molecular processes. The target organism of this thesis is a teleost fish (sea bream, *Sparus aurata*), that belongs to the most successful extant vertebrates with over 28,000 species identified (Nelson et al. 2001). Studies of skin in fish are of relevance for veterinary medicine, are essential for an important production sector, aquaculture and can also contribute as a biomedical model for regeneration. The advantages of fish skin as an experimental model is the ease of access and experimentation, the epidermis is living and not obscured by a layer of dead cornified cells, it has a high regenerative capacity, does not wrinkle or scar and physiological systems, including the immune system, tend to be less complex in fish, which facilitates interpretation of results. The following introduction is organized to provide a working knowledge about key aspects that are targeted in the experimental studies reported in the thesis and includes considerations about: 1) the anatomy of the skin in vertebrates, 2) the molecular and cellular elements of skin, 3) wound healing and regeneration, 4) the immune system and the skin and 5) model systems for regeneration.

## 1.2 The skin

In vertebrates the integumentary system comprises the skin and its appendages. It is the primary interface between an organism and the environment and provides protection against mechanical insults and physiological stress playing a key role in communication, locomotion and in the detection and reception of external stimulus. Vertebrates possess diverse types of integuments and they have evolved a wide variety of multicellular appendages such as hair, scales, feathers, hooves and nails that perform a wide variety of functions adapted to the different environment that each organism inhabits (Vickaryous and Sire 2009; Hildebrand 1974; Busam 2010). These may include mechanical protection of the soft tissues below, control of water passage in and out of the body to prevent desiccation and disturbance of water balance, regulation of heat transfers to the environment, protection against the entry of injurious organisms and materials, and behavioural aspects such as adaptive coloration and locomotion. The skin may also have a role in respiration, secretion, excretion, sense reception, and also in the storage of fat and glycogen. In vertebrate's colour is also vested in the skin and different colour pigments exist in the chromatophores (Hyman 1956) and the combined action of the different chromatophores (in fish, xanthophores, erythrophores, iridophores, leucophores, melanophores, and cyanophores and in mammals melanophores) produce distinct colour effects that are tightly regulated by hormones produced in the pituitary (eg: melanocyte-stimulating hormone), thyroid (eg: thyroxine) and adrenals (eg: cortisol) glands (Bentley 1998; Hildebrand 1974; Hyman 1956). Colour is used by various vertebrates for concealment or to make themselves conspicuous (as warning, social releaser or sexual attractant), for control of heat absorption or conservation, and in terrestrial vertebrates for control of vitamin D synthesis.

The skin is the largest organ in the body, it is crucial for survival and has an innate ability to regulate its functions but is also coordinated with the rest of the body through the nervous and endocrine systems that mediate its sensory functions and regulate its blood supply (Slominski et al. 2013; Bentley 1998). Skin cells produce hormones, neurotransmitters and neuropeptides and their respective functional receptors having a role as a neuroendocrine organ. They are capable of local immune and steroidogenic activities to protect the body against external environmental and biological factors to maintain local homeostasis (Slominski et al. 2013; Slominski et al. 2008) as reflected by the presence of an HPA (Hypothalamic-Pituitary-Adrenal) (Slominski et al. 2013; Slominski et al. 2008; Slominski et al. 2007) and HPT (Hypothalamic-Pituitary-Thyroid) (Paus 2010) axis in the skin of mammals. Skin is structurally simple but biologically complex and is composed of two principal layers - the epidermis, a superficial layer and a deeper layer - the dermis (figure 1.1) (Hildebrand 1974; Hyman 1956).

It is the first organ to emerge in embryonic development and the ectoderm (the outer layer of the gastrula) forms the outer part of the skin, the epidermis and also the nervous system and parts of the eye and ear. The mesoderm (the middle layer of the gastrula) forms the skeletal, muscular, circulatory, urogenital systems and the inner part of the skin, the dermis (Hildebrand 1974).

## 1.3 General structure of the vertebrate skin

### 1.3.1 The epidermis and its derivatives

The epidermis is the outer part of the skin, it is relatively thin in most animals and is a stratified epithelium. In the epidermis basal cells are attached to the basement membrane and the most superficial of the supra-basal cell layers form the epithelia. Only the cells in the *stratum basale* (figure 1.1), also known as *stratum germinativum*, are mitotically active and their function is to replenish the loss of cells on the surface of the superficial stratum. In the intermediate stratum (*stratum spinosum* and *granulosum* in figure 1.1) of a stratified epithelium, the cells can undergo various processes of differentiation, such as keratinization (Busam 2010; Bragulla and Homberger 2009).

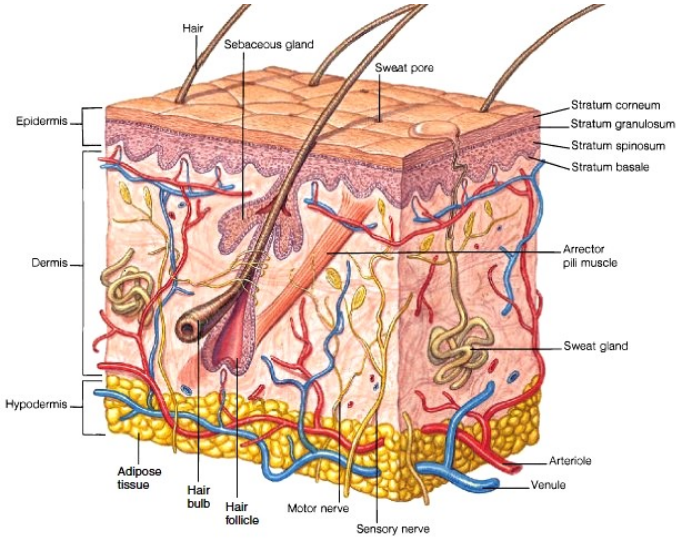


**Figure 1. 1 - A representation of skin structure in mammals. Taken from [http://pulpbits.net/7-skin-structure-anatomy-diagrams/structure-of-skin/](http://pulpbits.net/7-skin-structure-anatomy-diagrams/structure-of-skin/)**

In vertebrates, the epidermis is stratified into two or more layers (figure 1.1). In land vertebrates, the outer layer of the epidermis is composed of dead keratinized cells that protect the skin against water loss and bacterial infections. Epidermal cells are continuously replenished by cells produced in the *stratum germinativum* and as they move toward the upper

layer they start producing keratin (a water-insoluble protein) and differentiate from cuboidal cells to flattened keratinized cell that are shed. In humans the epidermis is shed continuously but in the reptiles such as snakes and lizards the whole epidermis is shed at intervals during moulting (Seeley et al. 2001; Hildebrand 1974; Hyman 1956). The epidermis in aquatic vertebrates such as cyclostomes, fish and tailed amphibians differs from terrestrial vertebrates as it is composed of mitotically active cells and contains numerous mucous cells, the secretion of which keeps the skin moist and slimy and confers protection from the aquatic milieu (Hildebrand 1974; Hyman 1956).

#### 1.3.1.1 Epidermal Derivatives

##### 1.3.1.1.1 Glands

In mammals, three types of cutaneous glands of ectodermal origin are present: the sebaceous, sweat (figure 1.1) and mammary glands and they are responsible for lubrication and protection against water loss, thermo-regulation and milk production, respectively. The sebaceous glands are limited to the mammals and are branched alveolar glands that drain into each hair follicle (figure 1.1) and are related to the nipples, lips and genitalia. Sweat glands (figure 1.1) are tubular, simple (not lobulated) and coiled at their inner ends and form from invagination of the epidermis into the dermis. The mammary glands produce and secrete milk to suckle the young and are formed when the epidermis sinks into the dermis and branches into solid cords. In females, these cords enlarge at puberty, pushing under the skin and becoming lobulated and alveolar (Hildebrand 1974; Hyman 1956).

##### 1.3.1.1.2 Keratinized and cornified structures

Vertebrates have a range of divergent keratinized structures, that includes beaks and feathers in birds and epidermal scales in lizards and in the legs of birds. Claws are strong keratinized structures that wrap around the tapering terminal bones of the digits. Hooves are derived from claws. The shells of the turtle and the armadillo have a heavily keratinized epidermis and the baleen plates of whales are outgrowths of the buccal epithelium and serve as strainers for feeding. The horns and antlers of tetrapods come in different shapes and sizes. The horns of the rhinoceros grow continuously from the epidermis, and the keratinized fibres are compacted into a solid structure (cornified material) that is never shed. The antlers of the deer family are bony outgrowths of the skull covered in skin (“velvet”) and they are shed and replaced each year while the in the pronghorns the skin covering the antlers forms horn and not

hair. The hairs (figure 1.1) or fur in mammals also have the same epidermal origin and are composed of a keratinized shaft that expands from the root below the skin and is hidden in an epidermal sheath or hair follicle. These keratinized epidermal appendages confer protection and resistance to abrasion, but also provide insulation and protection against water loss (Bragulla and Homberger 2009; Hildebrand 1974).

### 1.3.2 The dermis and its derivatives

The dermis is usually thicker than the epidermis (figure 1.1). It commonly has an outer, vascular *stratum spongiosum* and a deeper, thicker *stratum compactum* that are interconnected to secure the skin to the connective tissue covering the muscles of the body wall. The dermis is composed of numerous collagenous fibres but have fewer elastic fibres that are randomly oriented in a three dimensional network (Hildebrand 1974) that is supported by the extracellular matrix (ECM) which confers support and guidance for the cells.

#### 1.3.2.1 Dermal derivatives: Fish Scales

The scales in modern teleosts are of dermal origin. These specialized dermal appendages are the elasmoid scales (cycloid or ctenoid) that are thin, flexible and transparent structures that are rich in calcium (Ca) and phosphorus (P) and are built by osteoblasts and resorbed and remodelled by osteoclasts (de Vrieze et al. 2011; Rotllant et al. 2005b; Persson et al. 1999; Witten 1997). The bulk of the elasmoid scale consists of the basal layer, an acellular structure that contains collagenous fibres running in various directions and an outer hypermineralized layer devoid of collagen (Sire and Akimenko 2004). The scales are responsible for physical protection and for the hydrodynamic properties of the integument (Elliot 2011b; Hildebrand 1974) and are part of the dermal skeleton, accounting for up to 20 % of the total body calcium (Berg 1968; Flik et al. 1986).

## 1.4 Major proteins that are part of the skin

Skin is a complex tissue and approximately 63% of all the human proteins are expressed in this organ (Uhlen et al. 2015). Some of the most important proteins involved in skin function are briefly described below.

### 1.4.1 Collagens

Collagens are the major structural components of the extracellular matrix (ECM) of all metazoans and are also the most abundant connective proteins in the skin. Collagens make up 70-80% of the dry weight of the skin, contributing to its stability and structural integrity (Colgravea et al. 2008; Son et al. 2007; Seeley et al. 2001). They can form large stable extracellular fibrils and complex fibrous superstructures that are responsible for the tensile strength of the tissues and are also part of the cytoskeletal system of epithelial cells (Castillo-Briceno et al. 2009; Bragulla and Homberger 2009; Perumal et al. 2008). Fibrillar collagens (I, II, III, V, XI, XXIV and XXVII) are composed of three polypeptide chains with a triple helix arrangement and each collagen $\alpha$ chain is characterized by a unique repeating amino acid structure, Gly-X-Y, where Y is often proline. Hydroxyproline is essential for the formation of the collagen triple helix (Heino et al. 2009; Taşkiran et al. 1999). The deposition of collagen is finely controlled and is dependent on the physiological status of the body. Dysregulation of collagen deposition and remodelling can originate pathological conditions that result from excessive accumulation of type I collagen in the tissue, as in the keloids (Sasaki et al. 1987) or disorders of the connective tissue like the Ehlers-Danlos syndrome, where the fragility and reduced tensile strength of the skin is one of the cutaneous manifestations of the disease.

### 1.4.2 Keratins

Keratins account for about 25-35% of the extracted proteins in human and murine stratified epidermis (Bowden et al. 1984) and form intermediate filaments found only in vertebrates (Fuchs 1983). The keratins are part of a large multi-gene family that are all characterised by their high cysteine content, which contributes through intermolecular disulphide bond formation to keratins strength and stability (Bragulla and Homberger 2009). The main functions of keratins are to provide resistance to mechanical and non-mechanical stresses and act as a scaffold for the maintenance of cellular architecture (Infante et al. 2007). Evolution of the keratinization of the skin in the tetrapods was accompanied by its association with lipid molecules and these modifications allowed adaptation to the terrestrial environment by providing protection against desiccation. Keratins are also involved in non-structural functions such as cell signalling, proliferation and apoptosis (Gu and Coulombe 2007). Keratins in epithelial cells are not characteristic of entire tissues but of some particular functional properties of cells and tissue regions. In fact, unlike other vertebrates, in teleost fish, hagfishes,

lampreys and amphibians keratins are not restricted to epithelial tissues and extracellular keratins have been described (Schaffeld and Schultess 2006).

### 1.4.3 Elastin

Elastin is a highly elastic protein in the skin, lungs and arteries allowing them to resist deformity and to restoring their shape after stretching or contracting. It is rich in hydrophobic amino acids and in tissue multiple tropoelastin molecules are cross-linked through lysine to desmosine and isodesmosine to generate a massive insoluble and durable complex (Muiznieks and Keeley 2013). In human skin, elastin is a minor component and though it is difficult to identify in histological sections it forms a highly crossed-linked network with the collagens to confer tissue resistance and elasticity.

### 1.4.4 Matricellular proteins

Matricellular proteins are proteins of the extracellular matrix (ECM) that do not have a structural role (Midwood et al. 2004). Matricellular proteins include galectins, osteopontin, SPARC, tenascins, thrombospondins, vitronectin that act temporally and spatially to provide signals that trigger specific cell activities (Midwood et al. 2004; Bornstein and Sage 2002). They are expressed at high levels during development but not in adult tissues and are up-regulated at sites of tissue remodelling (Midwood et al. 2004). In the skin, some small leucine-rich proteoglycans (SLRPs) have a matricellular function, such as decorin and lumican (Iozzo and Schaefer 2010; Yeh et al. 2010; Merline et al. 2009).

## 1.5 Skin ageing and skin diseases

### 1.5.1 Ageing skin

In young skin, the structural properties provided by the cross-linking of the abundant collagens and elastin in the dermis provides an effective support to the epidermis, which is also thinner. Ageing leads to a reduction in the amount and quality of the connective tissue (figure 1.2), which becomes disorganized causing the epidermis to wrinkle, sag and appear lax.

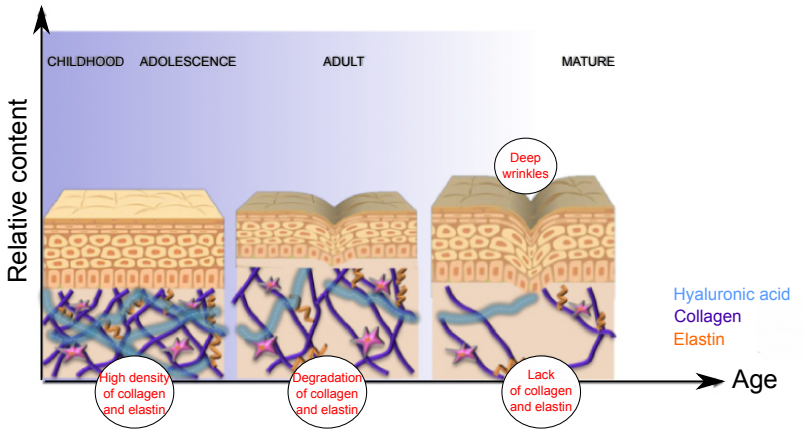


**Figure 1. 2 - Ageing skin in mammals. Highly crossed-linked collagen and elastin fibres are abundant in young skin.** The altered hormonal status with age accompanied by photo-aging of the skin leads to a decrease in cellular activity so that production of collagen and elastin decreases. The skin starts to lack the necessary tensely strength to keep the epidermis in place, and wrinkles start to form. Image taken from http://www.ortron.com.au/ortron-blog/latest

Ageing is a complex multifactorial process (Kishi et al. 2009) and age-related changes that occur during cutaneous wound healing are considered to be potentially negative, especially in the elderly population. Disturbances in protein metabolism, one of the main symptoms of ageing and oestrogen deficiency contribute to less efficient wound healing in the elderly (Harrison and Pierzynowski 2008).

A number of recent studies of teleost aging/senescence suggest that homeostasis and repair in their aging skin may give insight into important molecular/structural factors underlying normal skin function. Several ageing markers have been detected in the skin of zebrafish (*Danio rerio*) namely increased activity of senescence-associated ß-galactosidase and accumulation of oxidized proteins in the muscle (Kishi et al. 2009; Kishi et al. 2003). In the medaka (*Oryzias latipes*) signs of ageing were identified in the skin, and the dermis of 24-month old individuals had an age-dependent decline in the number of dividing cells and an increase in senescence-associated ß-galactosidase. Other tissues such as the liver (spongiosis hepatitis, steatosis, ballooning degeneration, inflammation and nuclear pyknosis), the heart (fibrosis and lipofucsin accumulation), and the eyes (loss of pigmented cells from the retinal epithelium) had a characteristic age associated change (Ding et al. 2010). These studies provided a set of markers that can be used to trace the process of normal tissue aging and to evaluate the impact of environmental stressors.

### 1.5.2 Skin disorders

There is a broad spectrum of lesions that have in common the mechanical fragility of the skin with frequent blister formation and an underlying genetic aetiology (Busam 2010). Mutations of keratins are associated with several disorders that have a clear phenotype in human and murine skins (Pekny and Lane 2007). In epidermis bullosa simplex, an epidermal blister disease, which involves the breakdown of basal cells in stratified epithelia, either *KRT5* or *KRT14* is altered. When *KRT14* is mutated, the type I keratin K15 can compensate for K14 to combine with the type II keratin K5, the usual partner of K14. This results in less severe symptoms than when *KRT5* is mutated, since there is no compensating keratin (Pekny and Lane 2007) (Steinert 2001). The same is true for K6 and its partners K16/17 (Coulombe and Wong 2004). In the skin disorder epidermolytic hyperkeratosis, another epidermal blister disease (Busam 2010), *KRT1* and *KRT10*, characteristic of keratinizing suprabasal cells in the stratified epidermis are mutated. The disease white sponge nevus, which affects the oral and genital stratified epithelia, is caused by mutations of *KRT14* and *KRT13* (Pekny and Lane 2007).

Hyperpigmentation skin disorders, such as Acanthosis nigricans, where there is hyperkeratosis and darkening of the skin, are directly associated with insulin resistance (IR), but the most common associated complications of diabetes in the skin are impaired wound healing, foot ulcers and an increased incidence of skin infections (Perez and Kohn 1994). The molecular basis of the condition is unclear but is linked to insulins role in regulating differentiation and glucose transport by keratinocytes and also proliferation as shown by IR mice with diabetes mellitus (Wertheimer et al. 2001).

Several skin disorders are attributed to alterations of the dermal connective tissue (deposition disorders) (Busam 2010). Namely, prolidase deficiency (PD), which is a rare, autosomal recessive, inborn error of amino acid metabolism that affects collagen maturation and is characterized by severe dermatological manifestations, particularly ulcers of the lower extremities (Haywood 2011). There is currently no cure for this condition.

Psoriasis is a chronic, inflammatory skin disease that results from a complex interplay between genetic and environmental factors that stimulates the activation of the dendritic cells. The activated dendritic cells stimulate the differentiation and migration of effector T cells (Th1 and Th17) to the skin, which subsequently leads to the release of inflammatory cytokines that promote further recruitment of immune cells, stimulation of keratinocyte proliferation and sustains a state of chronic inflammation (Nestle et al. 2009). In this condition there is a generalized epidermal barrier dysfunction with immune dysregulation.

## 1.6 Skin repair and regeneration

Skin is in the frontline of defence from external insults and is frequently subject to injuries (Gawronska-Kozak et al. 2014). The efficacy of skin repair is essential to re-establish immune defence since integument homeostasis is essential for health and survival as it confers protection against pathogens. Wound repair also involves two major clinical issues: a) the rate of healing, a prominent problem in the elderly population, and b) the quality of healing, a major concern in cosmetic appearance especially amongst the young population. The outcome of skin trauma can be regarded as a continuum of possible solutions that range from debilitating scars to complete regeneration and restitution of functionality (Seifert and Maden 2014; Seifert et al. 2012b; Redd et al. 2004). Therefore, the primary therapeutic goal of the treatment of wounds involves rapid wound closure with minimal scar formation (Li et al. 2001). The relevance of wound healing for human health has led to many studies to characterise the physical and molecular mechanisms underlying skin repair to control scaring and ameliorate the effects of aging (Schreml et al. 2010; Philips et al. 2011).

### 1.6.1 Stages of skin wound healing

In mammals, the response of skin to damage is a complex cascade of events and includes: inflammation, proliferation and maturation. These events overlap in time and space and lead to restoration of tissue integrity and homeostasis (figure 1.3 and table 1.1). Skin damage triggers an inflammatory response and is rapidly repaired by dermal fibroblasts and keratinocytes leading to scaring (Schreder et al. 2010; Gilliver et al. 2007). Immediately after injury (figure 1.3A and 1.3D), the platelet plug forms a provisional wound matrix composed of fibrin that attracts inflammatory cells like neutrophils and monocytes to the wound. Neutrophils and monocytes differentiate into macrophages and phagocytize foreign particles (such as bacteria and necrotic tissues) and also participate in angiogenesis (blood vessel repair) and matrix deposition. Within hours of injury re-epithelialization of the wound is initiated and (figure 1.3B) epidermal cells migrate to cover the wound, fibroblasts attracted to the injured area proliferate and form granular tissue, and a network of blood vessels are formed by angiogenesis. The remodelling stage is stimulated by matrix metalloproteinases that are released from fibroblasts and macrophages and modulate the extracellular matrix (ECM). In mammals, the initial deposition of collagen III is replaced by collagen I, fibroblasts differentiate into myofibroblasts that contract to decrease the scar surface and later endothelial cells, macrophages and myofibroblasts undergo apoptosis so that a scar (figure 1.3C) is the final

product of the tissue healing process (Richardson et al. 2013; Gurtner et al. 2008; Braiman-Wiksman et al. 2007; Midwood et al. 2004; Werner and Grose 2003; Philips et al. 2011).

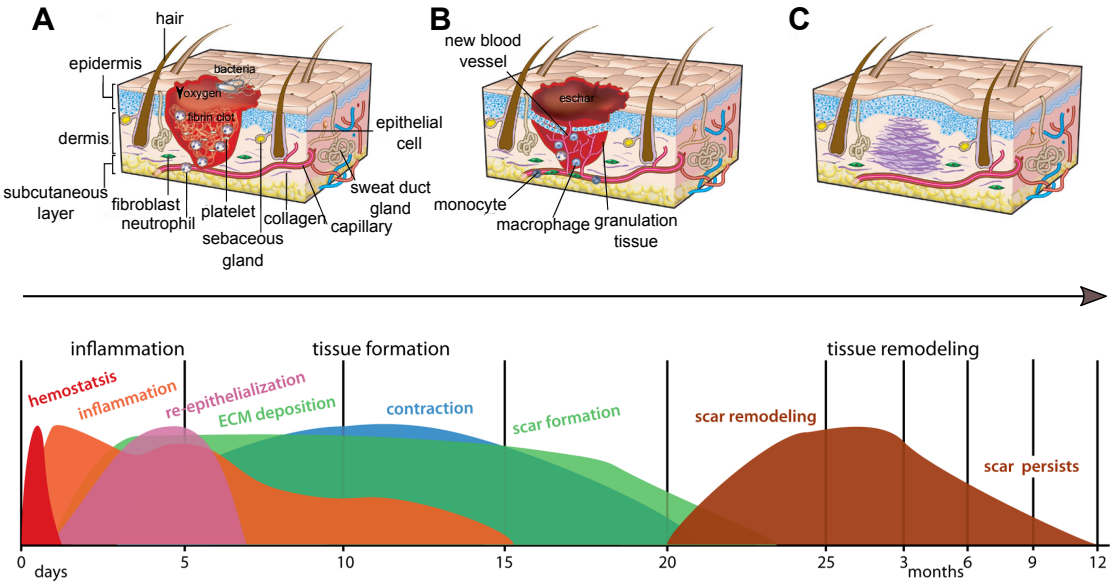


**Figure 1. 3 - Stages of skin wound repair in mammals.** There are three major classical stages of wound repair: inflammation, 0-48 h after injury (A), new tissue formation, 2-21 days after injury (B) and remodelling, up to 1 year (C). **A**: During inflammation (immediately after wounding), a fibrin clot forms that contains bacteria, degranulated platelets, inflammatory cells and many growth factors. **B**: Re-epithelialization occurs in 2-6 days and new tissue formation within 2-21 days after injury. These are accompanied by the formation of a scab (eschar) on the surface under which the keratinocytes from the wound margins migrate to re-epithelialize the wound and new blood vessels infiltrate the fibrous granulation tissue of the wound site. **C**: The dense and disorganized collagen network laid down by the fibroblasts will form a scar which is often raised relative to the surrounding surface. The original architecture of the skin is completely ablated by the scar, there are no hairs, sweat glands or sebaceous glands present in the repair region. Coloured peaks at the bottom represent the range of time periods of individual events during wound healing. The y-axis represents percent maximal response for indicated processes. Adapted from Seifert et al. 2014, 2012 and Gurtner et al. 2008.

Wounds that do not follow the established sequence of events in mammals are not repaired and are called chronic wounds, and are frequently associated with human diseases such as Diabetes (Schreml et al. 2010; Midwood et al. 2004; Perez and Kohn 1994).

Cutaneous repair and regeneration has mainly been explored in tetrapods (mammals and amphibians) but recently the relevance of teleost fish as a valid experimental model to investigative dermatology has been recognized (Rakers et al. 2013; Rakers et al. 2010; Ding et al. 2010; Kishi et al. 2009; Rakers et al. 2011) as the skin of teleosts does not scar, skin damage is rapidly repaired and the bony scales and overlying epithelia are replaced within a few weeks (Guerreiro et al. 2013; Guerra et al. 2008; Ohira et al. 2007b; Fast et al. 2002; Bereiter-Hahn and Zylberberg 1993).

**Table 1.1 – Description of wound healing**. Overview of the cellular elements and proteins involved in each stage of wound healing. Wound healing stages are conserved in teleosts and tetrapods however the timing and duration of their occurrence differs between the evolutionary groups and dictates the outcome of the skin repair programme. Adapted from Krasnov et al. 2012.

| Stage | Cells, structures | Processes | Proteins |
|---|---|---|---|
| **Haemostasis** | Platelets | Formation of provisional matrix | Fibrinogen and related proteins |
| | | Cell signalling | Cytokines, growth factors |
| **Inflammation** | Neutrophils | Pathogen killing, clearance | Humoral factors |
| | Monocytes, macrophages, lymphocytes T-cells B-cells | Sensing, transduction, differentiation | Lectins, receptors, kinases, transcription factors |
| | | Cell signalling | Cytokines, chemokines, lipid regulation |
| | | Phagocytosis | Regulators |
| | | ECM destruction | Enzymes |
| | | Antigen presentation | MHC |
| **Proliferation** | Fibroblasts | ECM formation | Collagens and structural proteins, enzymes |
| | Chondrocytes, osteoblasts | Connective tissue formation | Glycans, growth factors |
| | Keratinocytes | Re-epithelialization | Growth factors |
| | Endothelial cells | Angiogenesis | Structural proteins |
| | Neural cells | Neurogenesis | |
| | Myofibroblasts | Wound contraction | Motor proteins |
| **Maturation** | Connective tissue cells | Formation of mature ECM | Collagens and structural proteins, enzymes |

### 1.6.2 Role of the immune system in cutaneous repair

The efficacy of skin repair to re-establish immune defense and integument homeostasis is essential for health and survival since it also confers protection against pathogens. The skin is the primary site of defense against external aggressors and the involvement of the immune system in cutaneous repair and regeneration has been described in tetrapods and teleosts fish and in the latter differs significantly from mammals as both the immune response and skin (e.g. it is not keratinized, does not scar and does not develop wrinkles) has substantial differences.

In fact, the evolutionary distance between mammals and teleost fish is reflected in the complexity of their immune systems. While higher vertebrates have a complex innate and acquired immune response that involves a large repertoire of cytokines, growth factors, immunoglobulins, specialized receptors, memory-cells and dedicated sites for their production (such as the bone marrow that produces T- and B-cells and the thymus where T-cell maturation occurs), teleosts possess a less developed immune system with fewer pathways and a limited number of immunoglobulins (figure 1.4). Despite the lower complexity of the immune system in teleosts it also plays a key role during regeneration since immune cells destroy pathogens, damaged cells and extracellular structures, and this process is an essential prerequisite for the onset of tissue repair (Gomez et al. 2013; Richardson et al. 2013; Midwood et al. 2004).

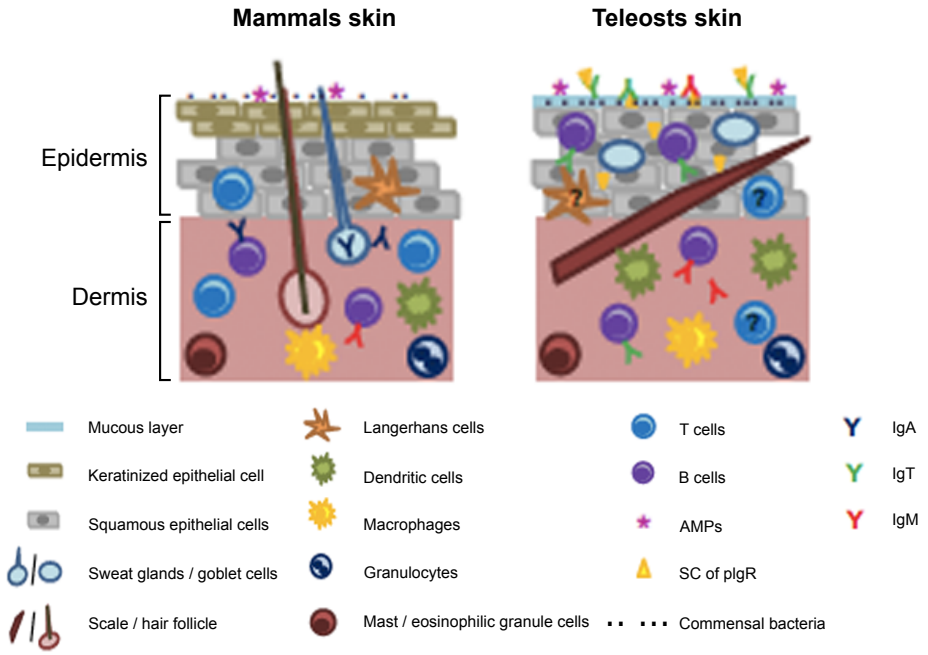


**Figure 1. 4 - Integumentary immune system in the skin of mammals and teleosts**. In mammals the epidermis is composed of dead keratinized cells while in teleosts the cells are alive and a mucus layer protects the animals from the external environment. Similar cellular components of the innate immune system, like the Langerhans cells, dendritic cells, macrophages, granulocytes and mast cells are found in mammals as well as in teleosts. Differences relate to the localization of B and T cells, the isotype of immunoglobulins and the presence of the secretory component (SC) of the polymeric immunoglobulin receptor (pIgR). The presence of commensal bacteria and anti-microbial peptides (AMPs) is shown in the outer mucosal surface or over the keratin layer. Elements that are suspected to be present in a tissue but have not been studied so far are marked as unknown (?). Adapted from Gomez et al. 2013.

In mammals, cortisol inhibits wound healing and retards reparation of damage (Christian et al. 2006). Increased secretion of cortisol mobilises energy from storage to muscles and shuts down metabolic processes involved in growth and immunity (Barton 2002) and it remains the first-line therapy for suppression of inflammation in human skin (Jackson et al. 2007).

## 1.7 Animal models of skin regeneration

Skin wound healing with concomitant scar tissue formation has been widely investigated however tissue regeneration is poorly studied due to the lack of suitable animal models. Comparing adult wounds in animals that heal scar free with mammalian wounds that scar may produce new insights particularly with regard to the local environment and how it might relate to dedifferentiation. Adult individuals with regenerative capacities are found in vertebrates such as amphibians and teleosts.

### 1.7.1 Mammalian models

Mammalian foetal wounds heal perfectly and represent one of the few examples of tissue regeneration in mammals (Yates et al. 2012; Dang et al. 2003). The foetal immune system is not fully developed and there are fewer neutrophils, monocytes, macrophages and lymphocytes and the length of time the inflammatory cells are present at the wound site is reduced (Cowin et al. 1998). The reduced inflammatory reaction combined with the reticular pattern formed by collagens I and III during foetal wound healing (Cuttle et al. 2005) and the up-regulation of the metalloproteinases (MMPs) relative to the tissue inhibitors of metalloproteinases (TIMPs) are contributing factors that favour the regenerative ability of the foetuses (Gill and Parks 2008; Dang et al. 2003). Nevertheless, the regenerative capacity of the foetus is lost in the second trimester of gestation and thereafter cutaneous repair results in scar formation. The goal of wound healing studies is to identify mechanisms to redirect reparative pathways from debilitating scar formation to regenerative pathways that lead to normal tissue functionality (Gawronska-Kozak et al. 2014). The studies of foetal healing have provided important into the cellular and molecular pathways that lead to the regeneration of tissues and its appendages. Due to the cellular and molecular differences between the foetus and adults, it has been very difficult to develop effective human therapies based on fetal wound healing studies. Adult tissues are fully differentiated and a dedifferentiation process (loss of the differentiated phenotype and re-entry into the cell cycle) is induced after damage while damage in the foetus probably does not have to reactivate the genetic program to repair the damage and instead the excised tissue may simply "carry on" developing, which is may be misinterpreted as scar-free healing (Seifert and Maden 2014).

Few adult mammals are capable of regenerating the skin but some mammalian models have been described. Namely, nude mice and African spiny mice. The nude mice have no hairs, as a consequence of a mutation in the *FOXN1* gene, and also lack a thymus and are therefore immune-deficient as a consequence of the of lack T-lymphocytes (Nehls et al. 1994). The timing of the main wound healing stages in the skin of the nude mice is accelerated in comparison to wild type mice. Incisional wounds in the skin of nude mice are completely repaired in 1 to 3 days and granulated tissue is present at day 3 and is largely reduced by 7 days' post-injury. Thirty-six days' post injury, the wounded area is virtually absent of collagen fibres while the wild type mice have well-defined and disorganized collagen bundles penetrating the dermis, subcutaneous pads and underlying muscle (Gawronska-Kozak 2011). However, although the inflammatory response plays a role in the regenerative outcome it remains to be categorically demonstrated that it is a determining factor of this process. Particularly since other

studies indicate that the regenerative response may be dependent on the bimodal pattern of expression of matrix metalloproteinases (MMPs) *MMP9* and *MMP13*. These proteins are highly expressed in the epidermis during the early phase of repair and in the dermis in the late phase of repair and this pattern is associated with scarless healing (Gawronska-Kozak 2011; Manuel and Gawronska-Kozak 2006).

The African spiny mice (*Acomys kempi* and *Acomys percivali*) can shed up to 60% of the total dorsal surface area of their skin as a predator escape behaviour. In the spiny mice the skin regrows and the wound heals without a scar and hairs rapidly regrow (Seifert et al. 2012a) and it is the only mammal capable of skin regeneration. The general structure of the skin in the African spiny mouse is the same as the house mouse (*Mus musculus*) but the mechanical properties are different. The skin in *Acomys* is brittle and requires much less energy/force to tear it while the skin of *Mus* displays elastic properties before breaking and is 20 times stronger than *Acomys* skin. The ability of *Acomys* to heal full-thickness excisional skin wounds (4mm and 1.5cm) is characterized by rapid formation of a scab and haemostasis followed by fast re-epithelialization (~64% in 24h, as opposed to 5-7 days in adult rats (Soo 2000). The collagen layers are less densely packed in *Acomys* during wound contraction and collagen III is the predominant structural component, as opposed to collagen I in *Mus musculus* (Seifert et al. 2012b). Recently, a similar regenerative capacity was recorded for a third *Acomys* species, *Acomys cahirinus* (Matias Santos et al. 2016).

### 1.7.2 Amphibians and teleosts

Amputated limbs in salamanders and fins, jaws and the tip of the heart in zebrafish all undergo a regeneration process that results in full functional reconstruction of lost/damaged tissues (Petrie et al. 2014; Seifert et al. 2012b; Brockes and Kumar 2005; Poss et al. 2003). What these experimental models have in common is a low inflammatory response, a short homeostasis period, lack of scab formation and a relatively long phase of new extracellular matrix production and remodelling.

Urodele amphibians (salamanders like the newts and axolots) maintain their ability to repair wounds without scaring, and regenerate a range of organs and tissues throughout their lives. The regeneration of whole adult limbs in the salamander is complex and involves different cell types with distinct embryonic origins and can be divided into 3 distinct phases: the initial wound healing phase, the progenitor cell activation phase and finally the phase of re-development, that is thought to be a recapitulation of embryonic development on a larger scale in an adult context (Godwin and Rosenthal 2014). The Anurans (frogs and toads) developmental

stages are characterized by variable capacities to scar-free repair and regeneration is restricted to the early stages of development (Godwin and Rosenthal 2014). The innate and adaptive immune system of amphibians are generally considered similar to mammals but specific differences exist that justify their different regenerative capacity. Urodele amphibians are regarded to have a week immune system (Tournefier et al. 1998) while anurans such as the *Xenopus* sp. Have a more robust immune response and less regenerative potential (Murawala et al. 2012).

Teleosts, in common with amphibians, have the ability to regenerate amputated fins and scales through epimorfic regeneration (Petrie et al. 2014). The caudal fin of zebrafish regenerates fast and several gene markers reviewed by (Poss et al. 2003) have been identified that relate to the different phases of the process, like the wound healing, the blastema formation and the regenerative outgrowth and the link between inflammation and adult regeneration as also been described (Petrie et al. 2014). Teleost skin is specialized and scales form late in ontogeny. Most teleosts loose some of their scales at least once during their lifetime (Bereiter-Hahn and Zylberberg 1993) and when scales are lost, the epidermis is also lost and the superficial dermis and scale pocket are directly exposed to the aquatic environment (Guerreiro et al. 2013; Vieira et al. 2011; Quilhac and Sire 1999) Loss of scales creates a failure in a key barrier of the innate immune system and wounds caused by scale loss are rapidly repaired and re-epithelialization from the wound margins is triggered (Quilhac and Sire 1999; Iger and Abraham 1990). According to Sire and Akimenko (2004), the late development of scales is a disadvantage for studies of their development but facilitates studies of the squamation pattern, scale development and ossification/mineralization processes as they can be easily accessed at the body surface (Metz et al. 2012; Thamamongood et al. 2012). The relevance of scales development for understanding tissue development becomes even more compelling with the identification of several genes known to be involved in the control of organogenesis. Developmental processes such as epidermal-dermal interactions, cell proliferation and differentiation can be easily studied during scale formation since they occur in larger animals (late larval phases) compared to embryos and their development occurs over a relatively short period of time. Also, teleosts skin is rich in collagen and elastin and has regenerative properties which makes them an interesting model to study cutaneous wound repair.

## 1.8 Objectives and Organisation of the thesis

The overall aim of the study was to identify key factors involved in skin homeostasis and repair and through inductive research and hypothesis testing generate a simple model for skin repair integrating metabolic, endocrine and immune considerations. The model species of this study was the gilthead sea bream (*Sparus aurata*), a perciform fish with high commercial value in South-Atlantic and Mediterranean aquaculture. Due to its economic value numerous biological studies have been conducted to investigate growth and metabolism, energy homeostasis and immune function in sea bream (Pavlidis and Mylonas 2011).

The specific objectives of the thesis were to:

1) determine the molecular, structural and functional modifications of skin repair in fish and identify important target genes/proteins of the skin and immune system;
2) test the hypothesis that angiopoietin-like family members are involved in skin repair and homeostasis in teleosts, as it has been reported in mammals;
3) test the hypothesis that osteoglycine, a SLRP matrix protein, previously identified in the skin proteome of regenerating sea bream functions as an osteoinductive factor associated with scale eruption;
4) test the hypothesis that intermediates in the tricarboxylic acid cycle (TCA cycle), such as the metabolite alpha-ketoglutarate (AKG) modulate cellular metabolism and that this causes increased skin connective tissue anabolism such that the skins integrity and function is improved.

The first study was directed at characterizing skin and scale regeneration in the sea bream (chapter 2). Analysis of microarray data from a previous study (Vieira et al. 2011) yielded the main biological processes down-regulated during sea bream skin regeneration after scale removal. Even though initial stages of skin regeneration in sea bream are associated with strong down-regulation of gene transcription, most studies have focussed on up-regulated genes. In chapter 2 of the thesis I identify using Gene Ontology (GO) annotation the main processes that were down-regulated 3 days after scale removal in sea bream. Biological markers representative of the modified GO processes was selected and used to build a detailed model of the early stages of skin regeneration in response to superficial damage caused by scale removal. The initial stages of repair (0h – 4 days) in teleosts fish were characterized and particular attention was given to immune system markers and the simultaneous process of extracellular matrix and cytoskeletal remodelling post-injury. A baseline comparison of intact and

regenerating skin is presented and the regenerative capacity of the integument in teleosts is discussed.

Previous studies in the host laboratory identified several proteins in regenerating skin of sea bream, which have also been identified during repair of mammalian skin. For example, in a study of the developing trout embryo the human orthologue of angiopoietin like-7 (*ANGPTL7*) was identified in the dermomyotome (Bricard et al. 2014) and another family member, *ANGPTL4*, was up-regulated in the sea bream skin 3 days after scale removal in fasting fish (Vieira et al. 2011). In mammals, angiopoietin-like (ANGPTL) family members are involved in tissue repair, cell proliferation and in blood vessel formation, a process that remains largely unexplored in other vertebrates. Taking into consideration the existing data about ANGPTL family member function in mammals and their presence in fish skin I hypothesised that if the gene family and structural organisation is conserved across vertebrates then function in skin repair may also be conserved. For this reason, in chapter 3 of the thesis the evolution of the angiopoietin-like family members is studied. Taking into consideration the role of ANGPTL in tissue repair, cell proliferation and angiogenesis in mammals, the expression patterns of *angptl1b*, *angptl2b*, *angptl4a*, *angptl4b* and *angptl7* are correlated with the initial phases of piscine skin regeneration to assess the putative function of ANGPTLs in fish skin repair.

A proteomic study of regenerating sea bream skin 5 days after scale removal identified a novel protein, osteoglycin (OGN), in a cluster with other proteins enriched during anatomical repair and immune activation (Ibarz et al. 2013a). OGN is a matrix protein and a member of the small leucine-rich proteoglycan family and in mammals is essential for the regulation of collagen fibrillogenesis, an essential process in matrix deposition or repair (Tasheva et al. 2002). In order to establish the function of OGN in teleosts skin repair (chapter 4) the the way in which life in an aquatic environment shaped Ogn evolution, structure and function in teleosts is established. *In vitro* culture of fish primary cell lines are used to establish cell specific expression and putative function. *Ogn2* is associated with osteoinduction and myotube formation and *ogn1* has primarily an adipogenic-related expression. The contribution of *ogn* to scale regeneration and skin repair is also evaluated.

The skin is the first line of defence against external aggressors and a fast recovery after injury is fundamental to restitute the barrier. Taking into consideration the importance of collagens in barrier organisation and function in chapter 5 of the thesis I aimed to manipulate this protein production. In mammals, alpha-ketoglutarate (AKG) an intermediate metabolite in the TCA cycle, stimulates collagen synthesis in bone (Harrison et al. 2004) and improves the elasticity of the blood vessels indicating the extracellular matrix is modified (Harrison et al.

2011). AKG is administered to sea bream and its effect on the scale regeneration in sea bream is evaluated. The results reveal the long term effect of AKG supplementation ($0.1 g \cdot kg^{-1} \cdot day$) on the metabolism, integrity and function of the integumentary system of sea bream.

Overall, the results presented in this thesis contribute to improve the current state of the art on the morphology and physiology of adult teleost skin and its regeneration after damage. The results obtained highlight the importance of fish skin as an alternative model to study cutaneous repair in vertebrates. New genes and molecules were identified and characterized in the skin of adult teleosts that share functional motifs and biological roles that are evolutionary conserved. Exploitation of the fish molecules that regulate skin function may provide additional molecular targets that could help to develop novel drug targets for mammalian skin disorders.

# 2

*Manuscript in preparation*

# Characterization of skin and scale regeneration in the sea bream, *Sparus aurata*

Rita A Costa[1] and Deborah M Power[1]

[1]Comparative Endocrinology and Integrative Biology, Centre of Marine Sciences, University do Algarve, Campus de Gambelas, 8005-139 Faro, Portugal,

## 2.1. Abstract

Injuries inflicted on tissues with a barrier function like the skin of vertebrates have to be rapidly repaired in order to avoid osmotic shock but also to re-establish the broken physical and the protective immune barrier. Skin wound healing has been widely studied in mammalian models but the information on teleosts cutaneous healing is sparse and frequently considered in the context of viral or bacterial infections in aquaculture animals. In the present study, the main biological processes down-regulated at 3 and 7 days after scale removal in sea bream (*Sparus aurata*) were identified using microarray and Gene Ontology (GO). A detailed time course of skin regeneration after damage at 0h, 6h, 1, 2, 3 and 4 days after scale removal was established using morphology and gene expression analysis. The integrity of the integument, as indicated by the expression of extracellular matrix (ECM) genes (*fn1a*, *collα1*, *colVα2*, *colXα1*, *ogn1*, *ogn2*, *crtac2*, *cyr61*, *pcna*, *krt2*, a*mmp9*), is restored within 2 days. Epithelial-mesenchymal interactions assessed by expression of *edar* and *shh* are associated with epidermal closure, the re-establishment of the basement membrane and scale eruption. In sea bream regenerating skin histological observations suggest inflammation is independent of tissue re-epithelialization and that humoral and cellular elements of the innate (*mpo*, *cyba* and *csf1r*) and acquired (*cd48* and *cd200*) immune system are supressed in the early stages of skin repair after injury. Overall, the results indicate that only after the physical barrier has been reconstructed does the integument mature and acquire full functionality as reflected by the re-appearance of the mucus and immune-related cells that confer protection against microorganisms and are associated with re-establishment of immune surveillance.

**Keywords:** skin, regeneration, wound healing, teleost

## 2.2. Introduction

The skin of all vertebrates has a similar organisation and is composed of two main layers, the epidermis and the dermis, although they have acquired specific adaptations to life on land and aquatic environments. The outcome of skin trauma in vertebrates is variable but depending on the species and injury inflicted can span from healing with the formation of a scar and loss of function to total regeneration and recovery of tissue functionality (Seifert and Maden 2014). Scaring results from the inflammatory response when the integument is damaged and is rapidly repaired by dermal fibroblasts and keratinocytes (Schreder et al. 2010; Gilliver et al. 2007). In contrast, regeneration is the capacity to replace or restore lost or damaged parts of the body so they resemble the initial tissue. For example, teleost fish and urodele amphibian tissues have remarkable regenerative capacity and amputated fins or limbs regrow (Godwin and Rosenthal 2014; Poss et al. 2003).

Injuries inflicted on tissues with a barrier function have to be rapidly repaired in order to avoid osmotic shock but also to re-establish the broken physical barrier and the protective immune barrier. Fish skin is often compared to a mucosal surface as it is rich in mucous-producing cells, lacks keratinization and is composed of living epithelial cells that are in direct contact with the external aquatic environment (Gomez et al. 2013; Salinas et al. 2011). The skin of all vertebrates is continuously exposed to microorganisms and a specific local immune response has been described in mammals (Cerutti and Rescigno 2008; Bangert et al. 2011) as well as in fish (Xu et al. 2013; Zhang et al. 2010) that involves the secretion of specific immunoglobulins by B-lymphocytes. The evolutionary distance between mammals and teleost fish is reflected in the complexity of their immune systems. While higher vertebrates have a complex acquired immune response that involves a large repertoire of cytokines, growth factors, immunoglobulins, specialized receptors, memory-cells and dedicated sites for their production (such as the thymus that produces T- and B-cells and the lymphatic system), teleosts possess a less developed acquired immune system with fewer pathways and a limited number of immunoglobulins. The differences in the immune system between advanced vertebrates and teleost means the response to injury is not identical. In teleosts the immune system plays a key role during regeneration since immune cells destroy pathogens, damaged cells and extracellular structures, and this process is an essential prerequisite for the onset of tissue repair (Midwood et al. 2004). The sequence of events that leads to repair or regeneration in tetrapods and teleosts, respectively occurs through similar biological events that overlap in time and space to restore tissue integrity. The main stages of wound repair are the inflammatory phase, followed by re-epithelialization and new tissue formation and remodelling (Olczyk et al. 2014; Richardson et

al. 2013; Esteban 2012; Eming et al. 2009). The overall series of events associated with repair in tetrapods (Godwin et al. 2014; Godwin and Rosenthal 2014; Olczyk et al. 2014; Yates et al. 2012; Midwood et al. 2004) and teleosts (Richardson et al. 2013; Rai et al. 2012; Guerra et al. 2008) have been characterised and their timing is dependent on the type of injury and leads to different outcomes such as the formation of a scar or tissue regeneration (Seifert and Maden 2014; Seifert et al. 2012a; Seifert et al. 2012b; Gomez et al. 2013).

There are relatively few studies of cutaneous wound healing in fish but based on the studies available it is clear that the severity of wounding affects the repair program. When damage is superficial and affects mainly the epidermis and loose dermis, such as occurs during scale removal, repair is rapid. For example, re-epithelialization and differentiation of scale-forming cells is completed within 1- 2 days after scale removal in medaka (*Oryzias latipes)* and sea bass (*Dicentrarchus labrax*), by 3 - 5 days the bony matrix of the scale is produced, then at 6 -14 days the basal-plate matrix is produced, followed by calcification at days 14 – 28 (Ohira et al. 2007b; Guerreiro et al. 2013) When wounding is more severe and is associated with bleeding, in teleosts cutaneous wound healing starts immediately but unlike mammals it is independent of signals released from the blood clot (Richardson et al. 2013). The increased interest in fish skin and its repair is linked not only to its importance for innate immunity and homeostasis but also because of its potential as a means for non-invasive monitoring of fish welfare during aquaculture. Also, understanding how regeneration occurs in adult tissues of different animal models that do not scar may produce new insights into the molecules and metabolic pathways that are involved in scar-free repair in vertebrates which can ultimately be applied in biomedicine for human therapy or in the cosmetic and pharmaceutical industry (Seifert and Maden 2014).

Several recent studies have targeted fish skin due to its importance for whole animal homeostasis (Rakers et al. 2010) and to evaluate the impact on fish production of loss of skin integrity due to damage or ectoparasites during aquaculture. In a microarray study of sea bream (*Sparus aurata*) in which fish were fasted and the skin was damaged by scale removal, up-regulated genes and inferred processes at 3 and 7 days after damage were identified (Vieira et al. 2011). The study revealed that genes of immune surveillance, tissue regeneration and mitotic checkpoint and cell proliferation were up-regulated presumably due to the need for immediate protection and as illustrated by histology for the rapid re-establishment of the barrier (Vieira et al. 2011). In Atlantic salmon (*Salmo salar*) affected by sea lice (*Lepeophtheirus salmonis*) microarray was also used to characterize the skin specific response in the presence and absence of chronic stress (Krasnov et al. 2012; Skugor et al. 2008). A rapid induction of a mixed

inflammatory response occurred in sea lice infected salmon skin followed by hyporesponsiveness and delayed healing (Skugor et al. 2008). However, increased levels of cortisol to simulate stress had a far greater impact on the immune and healing response compared to sea lice infection alone (Krasnov et al. 2012). A notable and intriguing feature of the studies on salmon was both strong down- and up-regulation of transcripts linked to the immune system, the inflammatory response, tissue remodelling and wound healing, indicating complex tissue repair dynamics occur. To better understand skin regeneration in fish, more detailed studies across time of regeneration and associated molecular and cellular responses are required.

In the present study, we aimed to better characterise the regenerative process in response to superficial damage caused by scale removal by using a detailed time course of skin regeneration after damage. Since the previous microarray study of skin regeneration in sea bream did not consider down-regulated transcripts (that were more numerous and more profoundly modified than up-regulated transcripts) we started by annotating the down-regulated probes at days 3 and 7 after scale removal. The aim was to identify which processes are repressed during scale regeneration in sea bream in order to contribute to characterization of the regenerative process in teleost fish. We hypothesized that most of the molecular and cellular events associated with tissue repair after injury should happen in the first 2 days after scale removal based on histomorphological observations. To respond to the hypothesis, we studied groups of genes indicative of key events during healing over a detailed time course during regeneration. The response of the immune system was characterized along with the response of cytoskeletal remodelling post-injury. A baseline comparison of intact and regenerating skin is presented and discussed in the context of the regenerative capacity of the integument in teleosts.

## 2.3. Materials and Methods

### 2.3.1. Annotation of down-regulated probes during regeneration of seabream skin

#### 2.3.1.1.The microarray experiment

The biological processes and candidate genes associated with skin regeneration in gilthead sea bream used as a starting point the microarray study of Vieira et al. (2011), which did not consider down-regulated transcripts. In the present study a detailed analysis of the down-regulated transcripts reported 3 days after skin damage in Vieira et al. (2011) fed sea bream was performed. The data of the microarray study is available in the NCBI's Gene

Expression Omnibus (GEO Series accession number GSE30717; http://www.ncbi.nlm.nih .gov/geo/query/acc.cgi?acc=GSE30717). The microarray used by Vieira et al. (2011) was composed of 39,379 sea bream oligonucleotide probes, which represent 2 non-overlapping probes covering 19,715 unique transcripts. Hybridizations were performed using the Agilent One-Colour Microarray-Based Gene Expression Analysis protocol and were analysed with an Agilent G2565BA DNA microarray scanner (resolution 5 μm; sensitivity, XDR Hi 100% and XDR Lo 10%). Recorded data was extracted using the Agilent Feature Extraction Software 9.5.1 and analysed using the R limma package. Five samples were analysed for each experimental group (control versus descaled fish) and transcripts were only considered to be differentially expressed when both probes had as a minimum a 2-fold change relative to the control.

Analysis was focused on the significantly down-regulated genes in gilthead sea bream skin 3 days after scale removal (109 probes) and 7 days after scale removal (4 probes). The fasta sequences of the down-regulated genes were extracted and annotated using Blast2Go 3.2.7 (Conesa et al. 2005). The fasta sequences were submitted by blastx to the nr database (NCBI) using an e-value threshold for identity assignment of $1e^{-3}$ (73 probes, and only 34% of the probes were annotated); to increase probe annotation manual screening of the NCBI database was performed using blastx followed by blastn and this resulted in annotation of 72% of the down-regulated probes.

#### 2.3.1.2. Functional annotation

Functional annotation of down-regulated genes was carried out using DAVID resources v6.7 (http://david.abcc.ncifcrf.gov/, (Huang da et al. 2009b, 2009a)). Of the 79 annotated probes that were down-regulated 3 and 7 days after scale removal 76 probes were assigned a gene symbol and 73 were unique (not duplicates). Seventy of the 73 annotated genes matched genes found in humans and in the teleosts *Danio rerio*, *Oncorhynchus mykiss*, *Salmo salar*, *Takifugu rubripes* and *Oryzias latipes* (see table 2.1 for annotation statistics). GO annotation (level 2) was retrieved for the 70 annotated genes and pie charts for biological process, molecular function and cellular compartment constructed. Information regarding the enrichment of protein domains (InterPro) in the dataset was also retrieved.

**Table 2. 1 - Annotation statistics of the down-regulated probes in the microarray.**

| | # Down-regulated probes |
|---|---|
| Total number of sequences | 110 |
| Sequences with / without a Blast hit | 79 / 31 |
| Sequences with / without GO annotation | 75 / 4 |
| Sequences with /without a Gene Symbol | 76 / 3 |
| Sequences with unique / duplicated Gene Symbols | 73 / 3 |
| Probes included / excluded from functional annotation | 70 / 3 |

### 2.3.2. Selection of candidate genes

A comprehensive description of the molecular profile of candidate genes across time was established by quantitative PCR (QRT-PCR) during skin regeneration in sea bream. Candidate genes were chosen based upon analysis of transcripts down-regulated in the microarray and reported in previous studies (Ibarz et al. 2013a), and included transcripts related to extracellular matrix deposition, remodelling and tissue maturation as well as genes related to the immune function (innate and acquired). Eighteen genes were chosen and these (table 2.2) were grouped according to the described cellular and molecular events of the healing process into: 1) ECM (*fn1a*, *colIα1*, *colVα2* and *colXα1*) and matricellular proteins (*ogn1*, *ogn2*, *crtac2* and *cyr61*); 2) proliferation (*pcna*), remodelling (*mmp9*), cytoskeletal development (*krt2*) and epithelial-mesenchymal interaction (*edar* and *shh*), and 3) immune-related genes (*mpo*, *cyba*, *csf1r*, *cd48* and *cd200*).

### 2.3.3. Skin regeneration challenge

#### 2.3.3.1.Fish

A stock of adult sea bream (*Sparus aurata*) of the same age class (1-year-old) were purchased from a commercial supplier (CUPIMAR SA, Cádiz, Spain) and transferred to Ramalhete the experimental station of the Centre of Marine Sciences, Universidade do Algarve (Faro, Portugal). Fish were acclimated to 1000 L tanks supplied with a continuous flow of aerated sea water at 18 - 20°C, pH 7.8 – 8.1, 37 ppt salinity, > 80% oxygen saturation and at a density of < 5 $kg \cdot m^{-3}$. For maintenance fish were fed *ad libitum* twice daily with a commercial feed (Excel; Skretting, Burgos, Spain).

**Table 2. 2 - Candidate transcripts selected for expression analysis in sea bream skin.**

| Gene | Gene name | Function | Presence in the oligoarray |
|---|---|---|---|
| *fn1a* | *fibronectin 1a* | Ubiquitous cell adhesive ECM protein that plays important roles throughout wound repair (Midwood et al. 2004) | -- |
| *colIa1* | *collagen type I* | Major protein component of cartilage, bone and skin | SAPD01318 |
| *colVa2* | *collagen type V* | Minor collagen in fish skin and scales (Guellec and Zylberberg 1998) | SAPD03530 |
| *colXa1* | *collagen type X* | Marker of chondrogenesis in sea bream (Estêvão et al. 2011) | SAPD03342 |
| *ogn1* | *osteoglycin 1* | Regulates collagen fibrillogenesis (Tasheva et al. 2002) | -- |
| *ogn2* | *osteoglycin 2* | Unknown function in teleost | -- |
| *crtac2* | *cartilage acidic protein 2* | Promotes piscine epithelial cell outgrowth *in vitro* (Anjos et al. 2013) | -- |
| *cyr61* | *cysteine-rich angiogenic inducer 61* | Inducer of angiogenesis (Chen et al. 2001) | SAPD00346 |
| *pcna* | *proliferating-cell nuclear antigen* | Marker of proliferation during wound healing (Braiman-Wiksman et al. 2007) | SAPD02155 |
| *krt2* | *keratin 2* | Type II keratin expressed in fish skin (Infante et al. 2007) | -- |
| *mmp9* | *matrix metalloproteinase 9* | Tissue degradation and removal of cellular debris (Gawronska-Kozak 2011) | SPAD23115 |
| *shh* | *sonic-hedgehog* | Important roles in organogenesis, including epithelial-mesenchymal interactions (Sire and Akimenko 2004) | SAPD33953 |
| *edar* | *ectodysplasin a receptor* | Development of integumentary appendages (Harris et al. 2008; (Cui and Schlessinger 2006) | -- |
| *mpo* | *myeloperoxydase* | Marker of leukocyte activation in sea bream (Rodriguez et al. 2003) | SAPD02565 |
| *csf1r* | *colony-stimulating factor receptor 1* | Macrophage marker in sea bream (Roca et al. 2006) | -- |
| *cyba* | *cytochrome b-245* | Antimicrobial response of primary phagocytes (neutrophils) (Grayfer et al. 2011) | SAPD00344 |
| *cd48* | *cd48 antigen* | Surface antigen in mammalian lymphocytes but with undescribed function in teleosts (Sameshima et al. 2012) | -- |
| *cd200* | *ox-2 membrane glycoprotein* | Immunosuppressive molecule biomarker of hair follicle bulge in human and dog skin (Gorczynski et al. 2010; Jiang et al. 2010; Kobayashi et al. 2010) | SAPD20935 |

### 2.3.3.2. Skin regeneration experiment

For the skin regeneration challenge adult sea bream (n = 40, length = 34 ± 1.3 cm) were randomly divided between five 500 L tanks (n = 8 per tank) supplied with a continuous flow of aerated seawater at 20 ± 2°C and maintained under the conditions described above. Each fish provided both regenerating and control tissue since scales were removed from only one flank

(regenerating) and the undamaged flank was used as the control. The material was stored in such a way as to permit direct comparison of intact and regenerating skin from the same individual.

For scale removal fish were anesthetised with 2-phenoxyethanol in seawater (1:10,000; Sigma-Aldrich) and scales were removed from the left flank of the body by gently stroking the skin with forceps to minimise damage of the dermis. A group of fish (n = 8) were killed immediately (time zero) after scale removal and blood was collected by caudal puncture, centrifuged (10,000 rpm for 5 minutes) and the plasma transferred to a micro-centrifuge tube, frozen in liquid nitrogen and stored at -80 °C until analysis. Fish were killed by decapitation and the skin below the dorsal fin on the left (regenerating skin) and right hand side (intact skin) of the same fish was collected and a portion frozen in liquid nitrogen and the other portion fixed in 4 % paraformaldehyde (PFA), pH 7.4 for histological examination. To avoid undue stress caused by sampling repeatedly from the 5 tanks each tank represented a different time point in the experiment: 6 h and day 1, 2, 3 and 4. Intact and regenerating skin samples (1.5 $cm^2$; n = 8 per time point) were collected by anaesthetising fish in 2-phenoxyethanol (1:10,000, Sigma-Aldrich), weighing them, measuring their length and photographing them. Blood and skin samples were collected as previously described.

The maintenance of fish and subsequent experiments complied with the Guidelines of the European Union Council (86/609/EU) and was covered by a group 1 license to DMP (emitted by the Direção-Geral de Veterinária, Portugal). The behaviour and health of animals was monitored visually each day and no evidence of infection, modified behaviour or mortality occurred during the experiment.

#### 2.3.3.2.1. Quantification of plasma osmolality

To assess if scale removal (35% of body scales) affected plasma osmolality this parameter was determined using a vapour pressure osmometer (Vapro Wescor 5520, South Logan, Utah, USA) and expressed in mOsmol·kg-1.

#### 2.3.3.2.2. Histology of sea bream skin

To characterise the chronology of skin regeneration in sea bream, intact and regenerating skin samples (0, 6h, 1, 2, 3 and 4 days after scale removal) fixed in 4% PFA were decalcified overnight in 0.5 M ethylenediaminetetraacetic acid (EDTA, pH 8). Subsequently samples were dehydrated in ethanol (70%, 90% and 100%), saturated in xylene and

impregnated and embedded in low melting point paraffin wax (Histosec, Merck). Serial 5 µm sections of skin were mounted on APES coated glass slides, dried overnight at 37°C, cooled to room temperature and stored until required. Masson`s trichrome staining was used to distinguish collagen rich and/or mineralized and non-mineralized tissue as previously described (Vieira et al. 2011).

#### 2.3.3.2.3. RNA extraction and cDNA synthesis

Total RNA was extracted from intact and regenerated sea bream skin using a Maxwell® 16 MDx Instrument (Promega) and a Maxwell 16 Total RNA Purification Kit (Promega), according to the manufacturer`s instructions. Quality and integrity of total RNA was verified using a NanoDrop 1000 Spectrophotometer (Thermo Scientific). Purified total RNA (1-3 µg) was treated with 1.5 U DNAse (Ambion DNA-*free*™ kit) following the manufacturer`s instructions. DNA free total RNA (100 or 250 ng) was used for first strand cDNA synthesis in a 20 µl reaction volume containing 100 mM p6 random hexamers (GE Healthcare, UK), 100 U of RevertAid™ Reverse Transcriptase (Fermentas) and 8 U of RiboLock™ RNase Inhibitor (Fermentas). cDNA was synthesized by incubating for 10 minutes at 20°C, followed by 50 minutes at 42°C and 5 minutes at 72°C. The quality of cDNA was checked by PCR amplification of *rps18* using the following cycle: 10 minutes at 95°C, followed by 25 cycles of 95°C for 30 seconds, 60°C for 30 seconds and 72 °C for 30 seconds and a final 5 minutes at 72°C. The PCR products were run on a 1 % agarose gel to confirm amplicon size and the absence of contamination with genomic DNA.

#### 2.3.3.2.4. Quantitative expression analysis (QRT-PCR)

The expression of the target genes (table 2.3) during sea bream skin regeneration was analysed in detail by quantitative real-time PCR. QRT-PCR was carried out in duplicate 10 µl reactions of 1x SsoFast-Evagreen Supermix (Biorad) containing cDNA (≈ 16.7 ng) and 300 nM of forward and reversed primers. Quantification was performed in a StepOnePlus thermocycler (Applied Biosystems) using the standard-curve method (software StepOne™ Real-Time PCR Software v2.2) and the following program: 30 seconds at 95°C, 45 cycles of 5 seconds at 95°C and 15 seconds at the primer Ta (°C) (table 2.3). A standard curve was included to permit the initial quantity of target template to be related to amplification cycle. A final melting curve was carried out between 60°C and 95°C and produced a single product dissociation curve for each gene. Relative expression (log2(fold-change)) was estimated using the geometric mean of *rps18*

and *ß-actin* neither of which varied significantly ($p > 0.05$) between samples. The qPCR results in log2(fold-change) are illustrated with a heat map generated in Cluster 3.0 (http://bonsai.hgc.jp/~mdehoon/software/cluster/software.htm#ctv) and analysed with Java TreeView version 1.1.6r4 (http://jtreeview.sourceforge.net) in figures 2.5 – 2.7. The bar graphs corresponding to these data are in supplementary files 2.2 – 2.4.

**Table 2. 3 - List of the primers used for gene expression analysis by quantitative RT-PCR in sea bream (*Sparus aurata*) skin.** Accession number, primer sequence, amplicon length (bp), annealing temperature (T ºC) and qPCR efficiency and coefficient of correlation ($R^2$) are indicated for each pair of primers. F: forward primer and R: reverse primer.

| Gene | Accession number | Primers sequences 5 ⓟ3 | Amplicon (bp) | Ta (ºC) | Eff (%) | $R^2$ |
|---|---|---|---|---|---|---|
| *fn1a* | FG262933 | F: CGGTAATAACTACAGAATCGGTGAG<br>R: CGCATTTGAACTCGCCCTTG | 104 | 60 | 85 | 0.99 |
| *colIα1* | P02452 | F: AGACCTGCGTATCCCCAACTC<br>R: GCCACCGTTCATAGCCTCTCC | 110 | 57 | 81 | 0.99 |
| *colVα2* | IPI00293881 | F: ACCTGTGACGACCTGAAGAGATGC<br>R: TGGATGGGTTGGCGGAGATGC | 145 | 62 | 91 | 0.99 |
| *colXα1* | FP333454 | F: GGGCTTCCTGGATCAAATGTC<br>R: GCTGCAAATATACCATTACTCTCC | 105 | 56 | 95 | 0.99 |
| *ogn1* | KM603667 | F: GAAGTCTCTCTTATTCACCTGT<br>R: CAAAGGGTCACTGAAGTATCCA | 136 | 60 | 94 | 0.99 |
| *ogn2* | KM603668 | F: TGTTATTCTCCCATGGATCCTG<br>R: GATCCCCCGCTGCATCTGTGG | 125 | 60 | 101 | 0.99 |
| *crtac2* | DQ384627 | F: TCTTCACCTATTCGCACAGTCATCG<br>R: GCATCGGCTCTCCTCAACACC | 131 | 58 | 95 | 0.99 |
| *cyr61* | AM962203/AM957653 | F: AGAGGCGGTAGAAGGGGTAG<br>R: TGCGAGGACGGCGAGA | 109 | 60 | 107 | 0.99 |
| *pcna* | P12004 | F: GAGCAGCTGGGTATTCCAGA<br>R: CTGTGGCGGAGAACTTGACT | 148 | 60 | 94 | 0.99 |
| *krt2* | FM155497 | F: CTGTCAGTGCTGGTATTTGCT<br>R: TTGTTAAATGCAGTGAGGGAG | 128 | 60 | 93 | 0.99 |
| *mmp9* | AM905938 | F: ATTCAGAAGGTGGAGGGAGCG<br>R: CATTGGGGACACCACCGAAGA | 151 | 60 | 91 | 0.99 |
| *edar* | DLAgn_00049460 | F: GCCGTGGTGAAGACGTGGAG<br>R: GTAGCCCGCCGTGCT | 114 | 62 | 98 | 0.99 |
| *shh* | FM153740 | F: TGTCCTTGGTGTCCTCTGGGATGGG<br>R: GGAGTTTCTTGTGATCTTGCCTTC | 167 | 60 | 74 | 0.99 |
| *mpo* | FM148574 | F: TTGGTCCAGACATCCTCG<br>R: ATGGGCAAAGCGGTAG | 110 | 62 | 102 | 0.99 |
| *cyba* | AM966128 | F: TGCCACCGTCCTGGGATGTGTCTGC<br>R: GGTGGATTCTGAGGGGGATTCTTGA | 153 | 60 | 90 | 0.99 |
| *csf1r* | AM050293 | F: ACGTCTGGTCCTATGGCATC<br>R: AGTCTGGTTGGGACATCTGG | 129 | 62 | 102 | 0.99 |
| *cd48* | AM958473 | F: GCATGGTATTTGTACACTTG<br>R: TATCAATTACAATGTTAGGTTA | 147 | 56 | 93 | 0.99 |
| *cdk1* | AM965126 | F: ACGGACAGTACATACGCCAA<br>R: CTTGTGCCTTCCCTTATACA | 116 | 60 | 95 | 0.99 |
| *cd200* | SRR278741_isotig03093 | F: CTGGCAGAAAGTTTTACCTGAGG<br>R: CGATAGCAGCCTTCATCTTGG | 171 | 60 | 96 | 0.99 |
| *rps18* | AM490061 | F: AGGGTGTTGGCAGACGTTAC<br>R: CTTCTGCCTGTTGAGGAACC | 164 | 60 | 88 | 0.99 |
| *ß-actin* | X89920 | F: CCCTGCCCCACGCCATCC<br>R: TCTCGGCTGTGGTGGTGAAGG | 94 | 60 | 92 | 0.99 |

### 2.3.4. Statistical analysis

A Two-way ANOVA followed by a Fisher`s Least Significant Difference (LSD) post-test was performed using StatPlus:mac LE v5.9.80 (AnalystSoft Inc., StatPlus:mac - statistical analysis program for Mac OS, Version v5, www.analystsoft.com/en/) to reveal differences between experimental groups in gene transcript abundance during skin regeneration. The significance cut-off was set at $p < 0.05$ and data are presented as the mean ± standard error of the mean (sem). A Spearman correlation analysis ($p < 0.05$) was performed with the expression levels of the quantified genes to look for combined patterns of variation using GraphPad Prism version 6.00 for Mac OS (GraphPad Software, La Jolla California USA, www.graphpad.com).

## 2.4.Results

In fed sea bream (*Sparus aurata*) 3 days after scale removal from the left flank 109 genes were down-regulated in regenerating skin relative to intact skin and by day 7 only 4 genes were down-regulated (supplementary table 2.1; see Vieira et al. 2011). Comparison of the down-regulated transcripts at day 3 and day 7 after scale removal (VENNY 2.1) yielded a single probe (SAPD12466 – no match) down-regulated at both time points (figure 2.1), which demonstrated that by 7 days after scale removal expression levels of gene transcripts was already similar to intact skin.

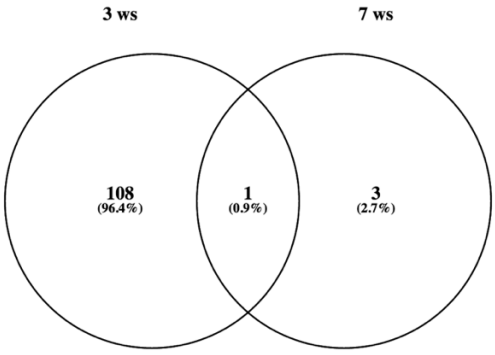


**Figure 2. 1 - Venn diagram with the distribution of the down-regulated genes at 3 (3 ws) and 7 (7 ws) days after scale removal.** The probe SAPD12466 was down-regulated at day 3 and 7 after scale removal but annotation was not possible. The three probes down-regulated in the regenerating skin at day 7 were, cdc42-interacting protein 4 (SAPD0665), coxsackie virus and adenovirus receptor homolog (SAPD19002) and the non-annotated probe SAPD23844. Further details about the 108 down-regulated probes 3 days after scale removal are given in supplementary table 2.1.

### 2.4.1. Expression profile of the down-regulated probes via GO enrichment

The down-regulated microarray probes were classified according to their Gene Ontology (GO) terms using DAVID in order to determine the enrichment in particular biological processes. The down-regulated probes were involved in several biological processes and abundant categories included anatomical structure development (11%), negative regulation of processes (23%) (in detail: cellular 7%, biological 8%, developmental 7% and lipid storage 1%), response to stress (8%) and chemical stimulus (5%), cell adhesion (5%), oxidation reduction (4%), tissue remodelling (2%) and ossification (2%; supplementary figure 2.1A).

The cellular compartments represented by the down-regulated probes related to the membrane (45%) and to the extracellular region/space (18% and 12%, respectively) and extracellular matrix (13%; supplementary figure 2.1B). In terms of molecular function, the most down-regulated probes were involved in protein (47%) and ion binding (28%). The remaining functions involved oxidoreductase activity (8%) and carbohydrate binding (6%) as well as extracellular matrix binding (3%), peroxidase activity (4%) and tetrapyrrole binding (4%; supplementary figure 2.1C). The protein domains of deduced down-regulated proteins were enriched in immunoglobulins (38%), EFG-like (35%) and peroxidase activity (12%; supplementary figure 2.1D).

### 2.4.2. Down-regulated genes 3 and 7 days after scale removal

Analysis of the down-regulated genes reflects the biological processes that were supressed in sea bream skin after scale removal. The “top 20” known genes differently expressed and down-regulated in gilthead sea bream skin 3 and 7 days after scale removal (table 2.4) comprise molecules with pro-inflammatory activity (galactose-specific lectin nattectin-like, L-rhamnose-binding lectin CSL2), recognition (fish-egg lectin) and inactivation of microorganisms (myeloperoxidase, eosinophil peroxidase, cdc42-interacting protein 4) and cytoskeletal reorganization (keratin, type I cytoskeletal 18) and remodelling (meprin A subunit beta, osteopontin).

Detailed analysis of the full list of down-regulated genes (supplementary table 2.1) revealed that the cellular and humoral response of the innate immune system was suppressed and also genes of the acquired immune response related to lymphocyte development (tyrosine-protein kinase Blk) and activation (immunoglobulin lambda-like polypeptide 1). The immaturity of the regenerating skin as a protective barrier was illustrated by the down-regulation of genes associated with epidermal keratinocyte differentiation (mitogen-activated protein kinase 13), tight junction integrity, tissue homeostasis and repair (coxsackie virus and

adenovirus receptor homolog), adhesion molecules (integrin, beta 3 (platelet glycoprotein IIIa, antigen CD61), matricellular proteins involved in collagen fibril assembly (biglycan) and regulation of chondrocyte differentiation (collagen alpha-1 (XXVII) chain B-like, transcription factor Maf, pim-2 oncogene).

**Table 2. 4 - Top 20 known genes down-regulated at 3 and 7 (shaded rows) days after scale removal.**

| Clone | LogFold | adj P-value | Acc. Number | Gene Identification | Putative function |
|---|---|---|---|---|---|
| SAPD02896 | -5.778 | 0.000 | XP_014827725 | galactose-specific lectin nattectin-like | Hemagglutination and pro-inflammatory activity |
| SAPD20552 | -5.534 | 0.000 | XP_012711056 | galactose-specific lectin nattectin-like | Hemagglutination and pro-inflammatory activity |
| SAPD09202 | -5.459 | 0.002 | XM_010736228 | ES1 protein homolog, mitochondrial-like | (Unknown function) |
| SAPD21910 | -4.887 | 0.000 | ABB29990 | FBP32 precursor | Fucose-bindin lectin |
| SAPD02565 | -4.747 | 0.009 | AKM12663 | myeloperoxidase-like protein | Microbicidal activity; host defense system of polymorphonuclear leukocytes |
| SAPD23604 | -4.597 | 0.000 | XP_010737445 | IgGFc-binding protein | Maintenance of the mucosal structure, as a gel-like component of the mucosa |
| SAPD15020 | -4.582 | 0.000 | XM_005476746 | cell adhesion molecule 3 | Involved in cell-cell adhesion |
| SAPD03342 | -4.540 | 0.000 | XP_008296443 | collagen alpha-1(X) chain | Endochondral ossification |
| SAPD02243 | -4.306 | 0.000 | XP_010742298 | meprin A subunit beta-like | Involved in inflammation and tissue remodelling due to its capacity to degrade ECM components |
| SAPD01456 | -4.210 | 0.000 | XP_010752647 | zymogen granule membrane protein 16-like | Protein trafficking |
| SAPD02976 | -4.032 | 0.000 | XP_010734733 | transmembrane protease serine 9-like | Serine-type endopeptidase activity |
| SAPD10113 | -3.970 | 0.001 | XM_010736670 | keratin, type I cytoskeletal 18-like | Role in filament reorganization (when phosphorylated); involved in interleukin-6 (IL-6)-mediated barrier protection |
| SAPD03259 | -3.849 | 0.000 | XP_013996240 | putative ferric-chelate reductase 1 | Ferric to ferrous iron reduction |
| SAPD16032 | -3.451 | 0.008 | XP_010730846 | eosinophil peroxidase-like | Inactivates ROS from microorganisms |
| SAPD07870 | -3.304 | 0.019 | XP_010730906 | eosinophil peroxidase-like | Inactivates ROS from microorganisms |
| SAPD06360 | -3.253 | 0.024 | BAL61198 | Fish-egg lectin | Binds to carbohydrates from microorganisms |
| SAPD18731 | -3.156 | 0.000 | AIT83008 | L-rhamnose-binding lectin CSL2 | Hemagglutination activity and induction of pro-inflammatory cytokines; stimulation of the phagocytic capacity of macrophages |
| SAPD26722 | -3.098 | 0.001 | AAV65951 | osteopontin-like | Cell-matrix interaction; integral part of the mineralized matrix; cytokine involved in type I immunity |
| SAPD26173 | -3.033 | 0.000 | AIT83008 | L-rhamnose-binding lectin CSL2 | Hemagglutination activity and induction of pro-inflammatory cytokines; stimulation of the phagocytic capacity of macrophages |
| SAPD0665 | -2.914 | 0.008 | KKF13527 | Cdc42-interacting protein 4 | Coordinates membrane tubulation with reorganization of the actin cytoskeleton during endocytosis |

### 2.4.3. Skin regeneration challenge

#### 2.4.3.1. Plasma osmolality

Scale removal did not significantly affect plasma osmolality which was maintained between 350 and 375 mOsmol·kg$^{-1}$ during the course of the experiment (figure 2.2).

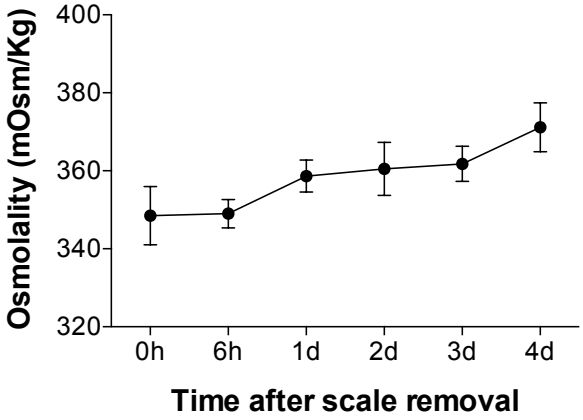


**Figure 2. 2 - Changes of plasma osmolality in sea bream during skin regeneration.** Results are presented as mean ± sem of 6 fish and statistical significance was assessed using a one-way ANOVA followed by the Kruskal-Wallis post-test. Significant differences were considered at $p < 0.05$.

#### 2.4.3.2.Morphology of sea bream intact and regenerating skin

In the intact skin of sea bream stained with Masson`s trichrome several over-imposing scales can be observed imbricated within the scale pockets in the loose dermis, that was limited below by the compact dermis and above by the basement membrane and epidermis (figure 2.3A). With the removal of the scales, the epidermis and scale pocket was disrupted, hence the dermis, became exposed to the ambient water as previously demonstrated in the skin of sea bream (Vieira et al. 2011) and seabass (Guerreiro et al. 2013). Six hours after scale removal (figure 2.3B) the disorganization of the dermis was visible and 1 day after scale removal (figure 2.3C) a rapid reorganization of the basement membrane and epidermis was evident so that by 2 days after scale removal (figure 2.3D) the epidermis already covered the wounded area and in the dermis, the dermal papilla (the cells that will form the new scales) were already defined. The bundles of epidermis that remained attached to the dermis after scale removal serve to protect the exposed dermis while at the wound edges, the progressive deposition of the basement membrane was associated with the differentiation of the disturbed supra-basal cells to form an organised basal cell layer. These two events appeared to contribute to the fast re-epithelialization observed in sea bream skin.

Mucous cells started to appear in the regenerating epidermis 2 days after scale removal (figure 2.4D), as well as signs of vascularization, as indicated by the visible blood vessels in the regenerating skin near the basement membrane (figure 2.4E) and in the dermis (figure 2.4F). Three days after scale removal, the scleroblasts had a cuboidal shape (associated with the active deposition of the new scales) and had established the basement plate of the new scale (figure 2.3E and 2.4H). Putative immune-related cells (identified by their morphology and granular cytoplasm) were observed mainly in the dermis, close to blood vessels (figure 2.4I). These cells were less evident in the epidermis (figures 2.4G) and were relatively abundant in the loose dermis of the undamaged skin (figure 2.4C). By day 4 after scale removal, the epidermis and dermis were more organized, the loose dermis was more pronounced and the new scales inside the scale pockets started to mineralize (figure 2.3F).

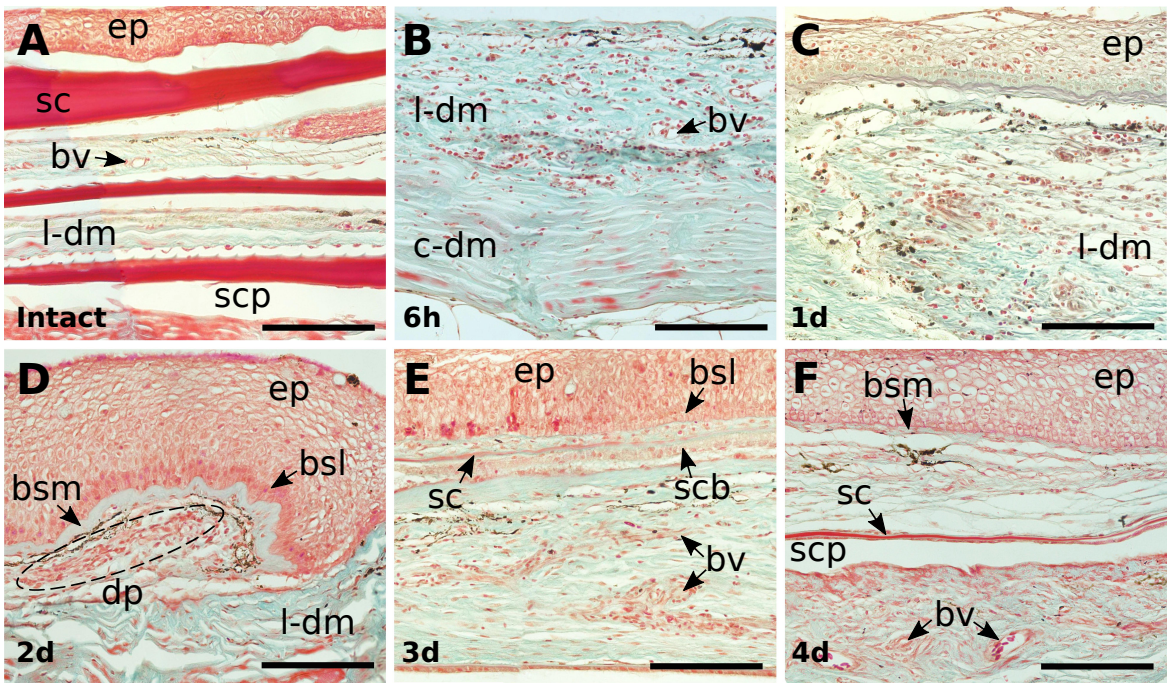


**Figure 2. 3 - Morphological characterization of histological sections stained with Masson Trichrome of intact and regenerating skin from sea bream during the healing period after scale removal**. **A**: Sea bream intact skin revealing the super-imposed scales imbricated in the dermis and covered by the epidermis. Sea bream regenerating skin at **B**: 6h, **C**: 1d, **D**: 2d, **E**: 3d and **F**: 4 days after scale removal. ep: epidermis, sc: scale, l-dm: loose dermis, c-dm: compact dermis, bsm: basement membrane, bsl: basal-cell layer, dp: dermal papilla, scb: scleroblasts, bv: blood vessels, rbc: red-blood cells. Scale bars: 100 µm

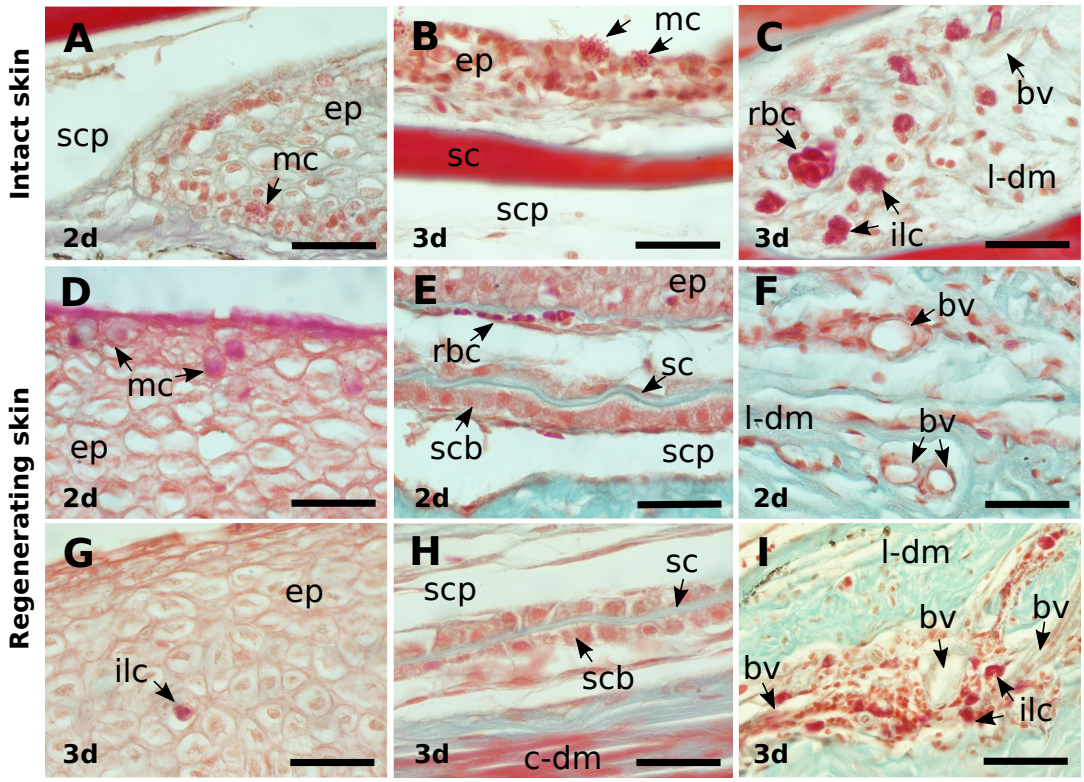


**Figure 2. 4 - Detailed images of histological sections stained with Masson Trichrome of intact and regenerating sea bream skin. A-C:** Detailed images of sea bream intact skin. Regenerating sea bream skin **D-F**: 2d and **G-I**: 3 days after scale removal. scp: scale pocket, sc: scale, ep: epidermis, mc: mucous cell, rbc: red-blood cells, ilc: immune-like cells, bv: blood vessel, l-dm: loose dermis, c-dm: compact dermis, scb: scleroblasts. Scale bars: 25 µm

### 2.4.3.3. The effect of scale removal on gene expression in sea bream skin

Real time qPCR analysis was performed to validate the microarray results and to extend the study by the inclusion of candidate genes that were absent from the microarray platform.

#### 2.4.3.3.1. Expression profile of ECM and matricellular proteins

The profile of expression of the constitutive ECM markers *fn1a*, *collα1*, *colVa2* and *colXa1* and matricellular proteins differed in intact and regenerating skin (figure 2.5A and supplementary figure 2.2), as demonstrated by their different clustering in the two skin conditions. Significant down regulation of biological and structural ECM markers was evident at 6h in regenerating skin (figure 2.5A and supplementary figure 2.2). The expression of *collα1* remained down-regulated in the regenerating skin until day 3 after scale removal and was positively correlated ($r > 0.53$) with the expression of all other genes except fibronectin ($r = 0.145$). The expected down-regulation of collagen X (SAPD03442, -4.54 log-fold; table 2.4) based on the results of the microarray analysis did not occur and it was not significantly

different between intact and regenerating skin. The variable pattern of expression of transcripts in the intact skin may be linked to normal skin homeostasis or the response to damage inflicted on the other flank of the fish and was unexpected.

The expression of *fn1a* in the regenerating skin was constant throughout the experiment, *collα1* and *colXa1* increased significantly at day 2 while the expression of *colVa2* was significantly down-regulated at 6h and re-established to initial levels 2 days after scale removal. Molecular alterations in the skin from the intact flank were also identified and a significant increase ($p < 0.05$) in the expression of *collα1*, *colXα1 ogn1*, *ogn2*, *crtac2* and *cyr61* ocurred at day 1 and/or 2 after scale removal relative to undamaged skin (figure 2.5A and supplementary file 2.2). In general, four days after scale removal gene expression was similar in the intact and regenerating flanks of the experimental animals.

**A**

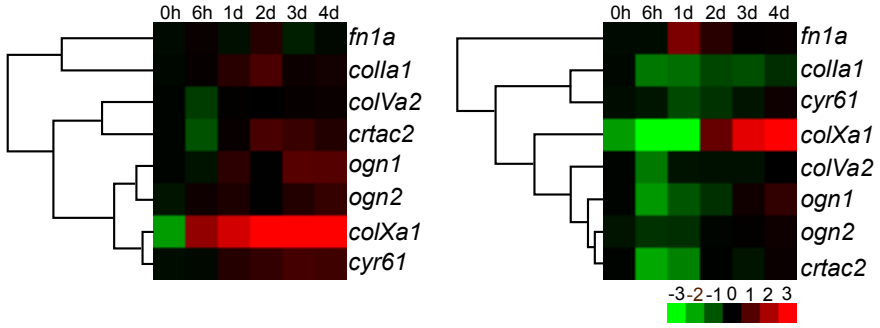


**B**

**intact *vs.* regenerating skin**

| Gene | 0h | 6h | 1d | 2d | 3d | 4d |
|---|---|---|---|---|---|---|
| *fn1a* | 1.0 | 0.49200 | 0.00002 * | 0.92679 | 0.26758 | 0.623 |
| *collα1* | 1.0 | 0.00005 * | 0.00000 * | 0.00001 * | 0.00452 * | 0.03349 |
| *colVα2* | 1.0 | 0.00141 * | 0.23638 | 0.39456 | 0.24503 | 0.61359 |
| *crtac2* | 1.0 | 0.00237 * | 0.00000 * | 0.00753* | 0.00818 * | 0.37265 |
| *ogn1* | 1.0 | 0.00000 * | 0.00000 * | 0.05674 | 0.00717 * | 0.15493 |
| *ogn2* | 1.0 | 0.04510 | 0.02170 * | 0.91687 | 0.35431 | 0.22389 |
| *colXα1* | 1.0 | 0.00000 * | 0.00000 * | 0.11101 | 0.35355 | 0.68892 |
| *cyr61* | 1.0 | 0.62499 | 0.00015 * | 0.00048* | 0.00281 * | 0.08296 |

**Figure 2. 5 - Relative expression of ECM and matricellular genes in intact and regenerating skin during the healing period after scale removal in sea bream**. **A**: Heat map of the expression levels of ECM (*fn1a*, *collα1*, *colVα2*, *colXα1*) and matricellular (*cyr61*, *ogn1*, *ogn2*, *crtac2*) genes. Expression levels were determined using qPCR and relative expression in log2(fold-change) was estimated using the geometric mean of *rps18* and ß-*actin* as reference genes (supplementary file 2). The heat map was generated with Clustal3.0 and analysed with Java TreeView and the colour gradient from green to red indicates down- and up-regulated genes, respectively. Each coloured square represents the mean of 4-6 individuals. **B**: Table representing the direct comparison of the relative genes expression in the intact and regenerating flank during the time course studied. Statistical significance (*, $p < 0.05$) between groups was assessed using a two-way ANOVA followed by the Fisher`s Least Significant Difference (LSD) post-test and significant differences are represented by a difference in colour intensity > 2 points.

#### 2.4.3.3.2. Expression profile of specific cellular events

Gene transcripts associated with cellular events like proliferation, cytoskeletal remodelling, degradation of debris and other elements and epithelial-mesenchymal interactions changed during skin regeneration (figure 2.6 and supplementary figure 2.3A). The removal of cellular debris after skin damage was indicated by the increased ($p < 0.001$) expression of *mmp9* transcripts 6h after removal of scales and was associated with a significant increase ($p < 0.001$) across time in *pcna*, which was indicative of increased proliferation up until 1 / 2 days after scale removal when the histology revealed that the basement membrane and epidermis were re-established (figure 2.3D).

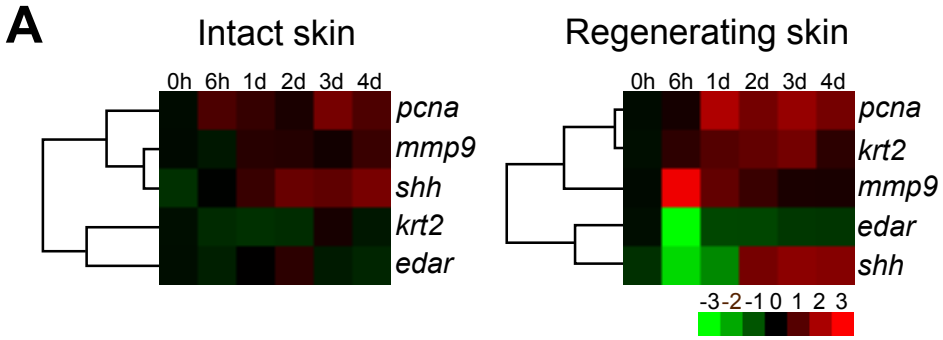


**B**

**intact *vs.* regenerating skin**

| Gene | 0h | 6h | 1d | 2d | 3d | 4d |
|---|---|---|---|---|---|---|
| *pcna* | 1.0 | 0.02580 | 0.00000 * | 0.00044 * | 0.21725 | 0.09905 |
| *mmp9* | 1.0 | 0.00000 * | 0.13319 | 0.59286 | 0.85320 | 0.42081 |
| *shh* | 1.0 | 0.00056 * | 0.00104 * | 0.79996 | 0.43848 | 0.80329 |
| *krt2* | 1.0 | 0.00429 * | 0.00002 * | 7.514E-8 * | 0.00380 * | 0.02508 |
| *edar* | 1.0 | 1.858E-11 * | 0.10177 | 0.01064 * | 0.53050 | 0.70942 |

**Figure 2. 6 - Expression profile of cellular proliferation, remodelling and epithelial-mesenchymal interactions related genes during sea bream healing after scale removal in intact and regenerating skin**. **A**: Heat map of the expression levels of genes related to proliferation (*pcna, krt2*), remodelling (*mmp9*) and epithelial-mesenchyme interactions (*edar*, *shh*). Expression levels were obtained by qPCR and relative expression in log2(fold-change) was estimated using the geometric mean of *rps18* and ß-*actin* as reference genes (supplementary file 3). The heat map was generated with Clustal3.0 and analysed with Java TreeView where the colour gradient from green to red indicates down- and up-regulated genes, respectively. Each coloured square represents the mean of 4-6 individuals. **B**: Table representing the direct comparison of the genes relative expression in the intact and regenerating flank during the time course studied. Statistical significance (*, $p < 0.05$) between groups was assessed using a two-way ANOVA followed by the Fisher`s Least Significant Difference (LSD) post-test and significant differences are represented by a difference in colour intensity > 2 points.

The expression of *krt2*, a marker of keratinization in soft epithelial tissues and an indicator of cell migration through cytoskeletal remodelling, was significantly increased ($p <$

0.01) in the regenerating skin until experimental day 3 (figure 2.3B-F) and was positively correlated (r = 0.696) to the expression of *pcna*. The expression of *shh* and *edar* were positively correlated (r = 0.478; supplementary figure 2.3B) and the two were significantly reduced ($p < 0.01$) in the regenerating flank at 6h but recovered to initial levels 1 day after injury. Additionally, *shh* was significantly increased in both flanks (intact and regenerating) from day 2 onwards, when the basement membrane was reconstituted and scale patterning was established as revealed by the development of the dermal papilla evident in histology (figure 2.3D) of the regenerating skin.

#### 2.4.3.3.3. Expression profile of immune-related genes

Genes associated with innate and acquired immune functions were quantified and their pattern of expression differed in intact and regenerating skin (figure 2.7A and supplementary figure 2.4A), as demonstrated by the different clustering of the genes in the two skin conditions. Briefly, an initial (6h) decrease in transcripts associated with immune function was observed in the regenerating skin that was progressively re-established until day 4 of regeneration. The expression of *mpo* was significantly reduced in the regenerating skin until experimental day 3 compared to intact skin and its expression during the experimental trial was positively correlated ($r > 0.4$) with all other genes quantified (supplementary figure 2.4B).

As predicted from the microarray data, *mpo* and *cyba* were significantly down-regulated (-4.747 and -1.406 fold, respectively; table 2.4 and supplementary table 2.1) in the regenerating skin 3 days after scale removal. Additionally, the expression of *csf1r* and *cd48* was also significantly reduced in the regenerating skin until experimental day 1 whilst expression of *cd200* was up-regulated in the regenerating skin at the same time. Scale removal also impacted immune function at the physiological level, as reflected by significantly increased ($p < 0.05$) expression of *mpo*, *cyba* and *cd48* in the intact skin of experimental fish. This was matched by the identification in histology of immune-like cells (ilc) that were more abundant in the intact relative to the regenerating flank of experimental fish (figures 2.4C, G and I).

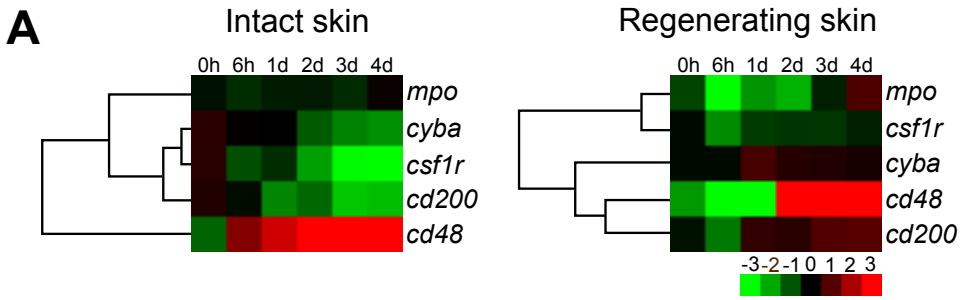


**B**

**intact *vs.* regenerating skin**

| Gene | 0h | 6h | 1d | 2d | 3d | 4d |
|---|---|---|---|---|---|---|
| *mpo* | 1.0 | 0.00021 * | 0.00182 * | 0.00044 * | 0.00881 * | 0.01107 * |
| *csf1r* | 1.0 | 0.03090 | 0.00723 * | 0.53599 | 0.16839 | 0.10662 |
| *cyba* | 1.0 | 0.63727 | 0.69696 | 0.94063 | 0.00412 * | 0.00005 * |
| *cd48* | 1.0 | 0.00001 * | 0.00000 * | 0.46503 | 0.57994 | 0.69932 |
| *cd200* | 1.0 | 0.00517 * | 0.001492 * | 0.59691 | 0.26150 | 0.81487 |

**Figure 2. 7 - Relative expression of immune-related genes during sea bream skin healing after scale removal in intact and regenerating skin. A**: Heat map of the expression levels of immune-related genes (*mpo*, *csf1r*, *cyba*, *cd48*, *cd200*). Expression levels were obtained by qPCR and relative expression in log2(fold-change) was estimated using the geometric mean of *rps18* and ß-*actin* as reference genes (supplementary file 4). The heat map was generated with Clustal3.0 and analysed with Java TreeView where the colour gradient from green to red indicates down- and up-regulated genes, respectively. Each coloured square represents the mean of 4-6 individuals. **B**: Table representing the direct comparison of the genes relative expression in the intact and regenerating flank during the time course studied. Statistical significance (*, $p < 0.05$) between groups was assessed using a two-way ANOVA followed by the Fisher`s Least Significant Difference (LSD) post-test and significant differences are represented by a difference in colour intensity > 2 points.

## 2.5. Discussion

The present detailed study of sea bream skin recovering from superficial injury revealed that the removal of cellular debris happened immediately after tissue aggression, and that this process occurred in the absence of chemical signals released from a blood clot. Proliferation was important for epidermal closure and histology revealed that within 2 days after damage integument integrity was restored. Epithelial-mesenchyme interactions were associated with epidermal closure and with the re-establishment of the basement membrane and determination of scale patterning. The results of histology over the first 2 days of skin repair were congruent with the results of a previous microarray study (Vieira et al. 2011) in which genes involved in proliferation, the mitotic checkpoint and adhesion were up-regulated 3 days after skin damage. A complex immune response has been associated with skin regeneration in teleosts, and although Vieira et al., reported up-regulation of genes of the immune response 3 days after skin

damage, in the present study we identified strongly down-regulated immune related genes over the first 2 days of regeneration. For example, down-regulated genes were associated with pro-inflammatory activity (galactose-specific lectin nattectin-like, L-rhamnose-binding lectin CSL2) and recognition (fish-egg lectin) and inactivation of microorganisms (myeloperoxidase, eosinophil peroxidase, cdc42-interacting protein 4). The expression of gene markers of the immune response over time demonstrated that in sea bream skin after scale removal suppression of the immune system started immediately after wounding and occurred simultaneously with the fast re-epithelialization of the skin. Based on the results we hypothesise that during teleost skin healing priority is given to the reconstitution of the physical barrier that protects the fish from the external environment and only later are other cell types of the skin associated with immune surveillance acquired. Furthermore, by using the same fish to study intact and damaged skin it was possible to establish the direction of the locally inflicted injury independent of the systemic response.

### 2.5.1. Expression of immune genes during skin regeneration in sea bream

In the regenerating skin of sea bream, genes involved in several immune processes and pathways had a modified expression. For example, the expression of the leukocytes marker *mpo* was down-regulated from 6h onwards, the macrophage marker *csf1r* was down-regulated at day 1 and the marker of neutrophils *cyba* was up-regulated at day 1 compared to day 0 and initial levels were restored by 2 days after scale removal. These results suggest that macrophages do not have a specific role in early stages of skin repair in sea bream but that the neutrophils have an important physiological role in the early stages of repair. The expression levels of these genes are related to the types of cells they represent and coincide with the role of neutrophils and macrophages in early stages of cutaneous repair as has been previously demonstrated in the skin of zebrafish (Richardson et al. 2013). A 2 mm circular excisional wound in zebrafish skin revealed neutrophils were present at the margins of the wound in re-epithelialized tissue from 4 hours post-wounding (hpw) and a gradual increase in macrophages occurred from 4 hpw until 4 days post-wounding (dpw) (Richardson et al. 2013). These immune cells are part of the innate immune response and can be recruited to the site of injury or they are resident cell types in the skin (Esteban and Cerezuela 2015; Gomez et al. 2013). Also, the presence of leukocytes was detected at 4 dpw in the skin of zebrafish (Richardson et al. 2013) and the expression of *mpo* in the present study supports the histological finding of cells of innate immunity in the regenerating skin of sea bream.

The skin of teleosts also has resident cell types of the acquired immune response that assure immune surveillance, such as the dendritic cells and the B- and T-cells (Esteban 2012; Gomez et al. 2013; Eming et al. 2009; Lazado and Caipang 2014). Cd48 is a surface marker of lymphocytes (Sameshima et al. 2012) and was down-regulated in the present study at 6h and 1 day after scale removal in the regenerating skin. A significant increase in the expression of *cd48* in both intact and regenerating skin was observed from 2 days onwards and an infiltration of immune-like cells (ilc) both in the intact and regenerating skin (figure 2.4C and I) was observed 3 days after scale removal. Future work will be necessary to identify these "ilc" but based on morphology and timing of appearance we propose they are most likely lymphocytes and associated with the acquired immune response. Cd200 is an immunosuppressive molecule in mammals that delivers inhibitory signals to the macrophage lineage in diverse tissues (Gorczynski et al. 2010) but has an unknown function in teleosts. In the present study, the up-regulation of *cd200* one day after scale removal was coincident with the down-regulation of *csf1r*, and if its function is conserved in vertebrates then its inhibitory function may explain the initial low levels of macrophage in initial phases of sea bream skin regeneration. The down-regulation of acquired immunity markers such as the *cd48* and *cd200* in the regenerating sea bream skin in the early stages of repair (6h and 1 day for *cd48* and 6h for *cd200*) is somewhat similar to the changes in gene expression described in the skin of Atlantic salmon during the inflammatory stage of repair that occurs in the first 24h after infection with salmon lice (Krasnov et al. 2012). In the Atlantic salmon, several genes involved in the differentiation of lymphocytes were down-regulated either by cortisol treatment or during infection with salmon lice revealing that T and B cells were suppressed during the inflammatory stage of repair in the skin of Atlantic salmon (Krasnov et al. 2012).

In the previous study of skin regeneration in sea bream, Cd200 was up-regulated in sea bream skin 3 days after scale removal (Vieira et al. 2011). In the present study with samples from a detailed time course of skin repair in sea bream qPCR analysis failed to reveal up-regulation of *cd200* in regenerating skin relative to intact skin (figure 2.7 and supplementary figure 2.4A). However, reanalysis of the microarray results of Vieira et al (2011) using the currently available transcriptome data for teleosts (2015) revealed that one of the a previously unannotated probes (SAPD20935) on the microarray was annotated as *cd200* in the present study, and is also designated "OX-2 membrane glycoprotein-like", in the down-regulated genes characterised in the present study (supplementary table 2.1). The identification of additional *cd200* probes on the microarray is a reflection of the similarity between the recently identified cd2 family members in fish (Sameshima et al. 2012) and the existence of multiple genes that

share relatively high sequence similarity probably explains the divergent results obtained in the previous (Vieira et al. 2011) and present study.

Overall, the results of the study are in line with the active role of the skin in protection against pathogens and indicates that suppression of immune function appears to be an essential facet of tissue repair in teleosts.

### 2.5.2. Fast re-epithelization in sea bream skin after scale removal

Re-epithelialization involves the *de novo* production of the basement membrane and the overlying cells under the control of epidermal growth factor (Werner and Grose 2003). In the present study, the re-epithelialization of the epidermis after scale removal in sea bream skin was complete in 2 days, as indicated by the re-establishment of the basement membrane and the dermal papilla and the increased expression of *pcna* and *krt2* in the regenerating skin. In zebrafish during cutaneous repair the epidermal barrier is fully recovered and stratified 24h after the lesion (2 mm circular excisional wound), even before inflammation is resolved. Epidermal barrier establishment is independent of the ECM proteins supplied by granulation tissue and the blood cloth (Richardson et al. 2013) and in the African catfish (*Clarias gariepinus*), a scale-less fish, and in the carp (*Cyprinus carpio*) complete epidermal closure occurred 24h post wounding (Guerra et al. 2008; Iger and Abraham 1990), as observed in sea bream. Re-epithelialization of excisional skin wounds in the tail of axolotls occurs 8h after injury and is accompanied by a very low inflammatory response and low fibrosis (Seifert et al. 2012b) and in mammals, the re-epithelialization of 4 mm circular excisional wounds in the ears of *Acomys* mice is complete in 7 days (Matias Santos et al. 2016). The fast recovery of the epidermal barrier in sea bream skin after superficial damage is in accordance with previous studies in teleosts and tetrapods. The results highlight the importance of the type of injury/damage inflicted on the duration of repair since the overall biological events are conserved across species but the timing is not.

### 2.5.3. Scale development during skin regeneration in sea bream

The damage to skin in the present study was caused by removal of the scales which led to disruption of the epidermis, basement membrane and scale pocket. Scales form late in development (greater than 100 days' post hatch) but loss or removal of scales leads to rapid replacement by new regenerating scales. The developmental histomorphology of the scale after their loss in adults has been characterised in several teleost species including the medaka, sea

bass, goldfish and catfish and is a very rapid process (Guerreiro et al. 2013; Guerra et al. 2008; Ohira et al. 2007b; Kondo et al. 2001). Fewer studies have looked at the molecular basis of this rapid regenerative process, although it has been demonstrated that the ectodysplasin a receptor (*edar*) is required for scale development in the medaka (Kondo et al. 2001) and zebrafish (Harris et al. 2008) and also the development of the epidermal appendages in vertebrates. In the regenerating scales of the goldfish the pattern of expression of osteoblast- (dlx5, runx2a, runx2b, osterix, RANKL, type I collagen, ALP and osteocalcin) and osteoclast-specific genes (TRAP and cathepsin K) was characterized (Thamamongood et al. 2012) and a new scale matrix protein identified and named goldfish scale protein-37 (GSP-37) that was related to the calcification of the scales (Miyabe et al. 2012). In the present study on sea bream skin regeneration new scales started to be deposited on the left damaged flank of fish by dermal osteoblasts from 3 days onwards and the deposited extracellular matrix started to calcify by day 4 and this pattern coincides with what has been previously reported in other teleosts (Guerreiro et al. 2013; Sire et al. 1990). Several markers linked to scale regeneration were quantified during scale regeneration such as collagen type I and collagen type V. The pattern of expression of *colIα1* in the sea bream is not only related to dermal and epidermal regeneration but is probably also related to the increase in scale mineralization reported from day 4 onwards. Other new markers quantified in the present study may also be related to scale formation and growth. Namely, collagen X which is a short chain collagen involved in chondrogenesis and endochondral bone ossification and cartilage acidic protein 2 (*crtac2*), which is a high-affinity calcium-binding protein (Anjos et al. 2013). The abundance of these transcripts in sea bream skin up until day 4 after scale removal suggests they may also be involved in deposition of the scale matrix during formation of the new scales.

Fish scales are bony elements that develop in the dermis and in common with amniotes, the loss of *edar* signalling affects the appendages in the integument and both epidermal and dermal derivatives are affected. The integumentary appendages such as hairs and scales develop from reciprocal signalling interactions between the basal epidermis and the subjacent mesenchyme (Harris et al. 2008). The expression of the ectodysplasin a receptor (*edar*) in epidermal cells of the zebrafish and medaka define the location of the growing scales (Harris et al. 2008; Kondo et al. 2001). Also, the expression of sonic hedgehog (*shh*) in the skin of zebrafish suggests a pre-patterning of the skin before scales formation in the dermis since only the cells in the basal epidermal layer express *shh* and they are only detected after the scale papillae have formed and it becomes progressively restricted to the cells that cover the posterior region of the growing scales (Sire and Akimenko 2004). The genes *edar* and *shh* were used in

the present study to reveal the interaction between the epidermis and the dermis in sea bream skin. The expression of *edar* and *shh* in the regenerating sea bream skin was re-established to initial levels 1 day after scale removal and this coincided with the recovery of epidermal coverage. The expression of *shh* increased from day 2 onwards and was coincident with the formation of the dermal papillae that give origin to the new scales and a regional thickening of the basement membrane above the dermal papillae. It was not possible to establish the pattern and cellular distribution of *edar* and *shh* using immunolocalization in the present study but this will be important to establish in future work. Nonetheless, the transcript abundance of the genes suggests that in sea bream pre-patterning of the skin occurs before scale formation and reveals the epithelial-mesenchyme interactions in the skin of sea bream as demonstrated in other teleosts.

### 2.5.4. Deposition and remodelling of ECM components during skin regeneration in sea bream

The timing of occurrence of wound healing stages can vary with the type of wound inflicted (Gawronska-Kozak et al. 2014) and total recovery of the cutaneous layers can occur as fast has 28 days in zebrafish (Richardson et al. 2013) or span over a large period of time leading to scar formation in mammals (Eming et al. 2009). In the present study, a superficial wound was inflicted in sea bream skin and the expression pattern of collagen V and collagen I indicates their importance in skin repair in teleosts. Collagen V is a fibrillar collagen found in tissues containing type I collagen and is widely present in fish skin as a minor collagen and in fish scales (Guellec and Zylberberg 1998). Functionally it regulates the assembly of heterotypic fibres composed of both type I and type V collagen (Birk 2001). The fast recovery of the expression levels of collagen V one day after scale removal, preceded by collagen I four days after the removal of the scales may be related to their importance in the assembly and maturation of new fibres of collagen V and collagen I that are formed to close the wound, and to allow the migration of cells and restore skin integrity. In zebrafish skin wound healing after a full-thickness laser-punch, *colIα1* expression below the wound is sparse at 24 hours post-wounding (hpw) but very prominent by 4 days post-wounding (dpw) not only in dermal fibroblasts but also in basal keratinocytes of the neo-epidermis (Richardson et al. 2013). Considering that the wounds inflicted in the zebrafish study and in the present study are different, but that the behaviour of the ECM is similar reinforces the general idea that a low level of collagen I expression in the early stages of cutaneous healing in teleosts might partially explain the higher regenerative capacity of teleosts relative to mammals (Richardson et al. 2013). In fact, collagen

fibres are laid down during the proliferation phase while maturation of fibres occurs at the final stage of wound healing and involves a gradual change in collagen type, enzymatic modification and formation of other complexes with other protein components of the extracellular matrix (ECM) (Krasnov et al. 2012), such as matricellular proteins. In mammals the matricellular proteins in skin wound healing are essential for interactions between cells and collagens but they are also involved in the induction of keratinocyte proliferation during wound closure (Midwood et al. 2004). The profile of expression of the matricellular proteins *ogn1* and *ogn2* in early developmental stages of development and in adult tissues of sea bream (chapter 4) suggests the two transcripts may have distinct biological roles that are in part linked to their differing abundance in different developmental stages. In the sea bream skin wound healing model, *ogn1* and *ogn2* had different expression profiles during skin regeneration, which is consistent with the hypothesis of divergent function in different developmental stages. The presence of *ogn1* and *ogn2* in intact and regenerating sea bream skin was correlated ($r = 0.3739$ for both transcripts) with the formation of the new collagen fibres to restore tissue integrity.

Matrix metalloproteinases (MMPs) are required for regular skin wound healing and are produced by fibroblasts and/or macrophages at the wound bed where their functions are related to the removal of cellular and wound debris, facilitating epithelialization and preventing wound scars from excess collagen (Philips et al. 2011). Significant up-regulation of mmp9 was registered in the present study immediately after scale removal (6h), although it rapidly fell to control levels (1d) and its profile of expression was consistent with its role in the removal of cellular debris to allow cell migration and tissue reorganization after damage.

## 2.6. Conclusions

The present study expands previous knowledge about regeneration of skin in a marine teleost, the sea bream. Using morphological and gene expression analysis, we demonstrated that in our regeneration model inflammation is independent of tissue re-epithelialization, as has previously been suggested in teleost fish and that humoral and cellular elements of the innate and acquired immune system are supressed in the early stages of skin repair after injury. Only after the physical barrier has been reconstructed does the integument mature and acquire full functionality as reflected by the re-appearance of the mucus and immune-related cells that confer protection against microorganisms and are associated with re-establishment of immune surveillance.

## 2.7. Acknowledgements

This study was financed by the European Regional Development Fund (ERDF) COMPETE and Portuguese funds through Foundation for Science and Technology (FCT) under the project UID/Multi/04326/2013. RAC is funded by FCT SFRH/BD/81625/2011 grant.

## 2.8. Supplementary material

### Supplementary table 2. 1 - Complete list of the newly annotated and differently expressed transcripts at days 3 and 7 (shaded rows) after scale removal.

| Clone | LogFold | adj P-value | Acc. Number | Gene Identification | Putative function |
|---|---|---|---|---|---|
| SAPD16129 | -6.008 | 0.000 | -- | no match | --- |
| SAPD02896 | -5.778 | 0.000 | XP_014827725 | galactose-specific lectin nattectin-like | Hemagglutination and pro-inflammatory activity |
| SAPD20552 | -5.534 | 0.000 | XP_012711056 | galactose-specific lectin nattectin-like | Hemagglutination and pro-inflammatory activity |
| SAPD09202 | -5.459 | 0.002 | XM_010736228 | ES1 protein homolog, mitochondrial-like | (Unknown function) |
| SAPD02853 | -4.933 | 0.000 | -- | no match | --- |
| SAPD21910 | -4.887 | 0.000 | ABB29990 | FBP32 precursor | Fucose-bindin lectin |
| SAPD02565 | -4.747 | 0.009 | AKM12663 | myeloperoxidase-like protein | Microbicidal activity; host defense system of polymorphonuclear leukocytes |
| SAPD23604 | -4.597 | 0.000 | XP_010737445 | IgGFc-binding protein | Maintenance of the mucosal structure, as a gel-like component of the mucosa |
| SAPD15020 | -4.582 | 0.000 | XM_005476746 | cell adhesion molecule 3 | Involved in cell-cell adhesion |
| SAPD03342 | -4.540 | 0.000 | XP_008296443 | collagen alpha-1(X) chain | Endochondral ossification |
| SAPD02243 | -4.306 | 0.000 | XP_010742298 | meprin A subunit beta-like | Involved in inflammation and tissue remodelling due to its capacity to degrade ECM components |
| SAPD01456 | -4.210 | 0.000 | XP_010752647 | zymogen granule membrane protein 16-like | Protein trafficking |
| SAPD02976 | -4.032 | 0.000 | XP_010734733 | transmembrane protease serine 9-like | Serine-type endopeptidase activity |
| SAPD10113 | -3.970 | 0.001 | XM_010736670 | keratin, type I cytoskeletal 18-like | Role in filament reorganization (when phosphorylated); involved in interleukin-6 (IL-6)-mediated barrier protection |
| SAPD03259 | -3.849 | 0.000 | XP_013996240 | putative ferric-chelate reductase 1 | Ferric to ferrous iron reduction |
| SAPD23844 | -3.617 | 0.040 | -- | no match | --- |
| SAPD16032 | -3.451 | 0.008 | XP_010730846 | eosinophil peroxidase-like | Inactivates ROS from microorganisms |
| SAPD07870 | -3.304 | 0.019 | XP_010730906 | eosinophil peroxidase-like | Inactivates ROS from microorganisms |
| SAPD06360 | -3.253 | 0.024 | BAL61198 | Fish-egg lectin | Binds to carbohydrates from microorganisms |
| SAPD12466 | -3.168 | 0.004 | -- | no match | --- |
| SAPD18731 | -3.156 | 0.000 | AIT83008 | L-rhamnose-binding lectin CSL2 | Hemagglutination activity and induction of pro-inflammatory cytokines; stimulation of the phagocytic capacity of macrophages |
| SAPD02942 | -3.102 | 0.001 | -- | no match | --- |
| SAPD26722 | -3.098 | 0.001 | AAV65951 | osteopontin-like | Cell-matrix interaction; integral part of the mineralized matrix; cytokine involved in type I immunity |
| SAPD26173 | -3.033 | 0.000 | AIT83008 | L-rhamnose-binding lectin CSL2 | Hemagglutination activity and induction of pro-inflammatory cytokines; stimulation of the phagocytic capacity of macrophages |
| SAPD12015 | -2.959 | 0.000 | DQ850950 | clone lmos2p07f02 mRNA sequence | --- |
| SAPD05774 | -2.944 | 0.009 | -- | no match | --- |
| SAPD0665 | -2.914 | 0.008 | KKF13527 | Cdc42-interacting protein 4 | Coordinates membrane tubulation with reorganization of the actin cytoskeleton during endocytosis |
| SAPD26362 | -2.882 | 0.000 | -- | no match | --- |
| SAPD17464 | -2.768 | 0.004 | -- | no match | --- |
| SAPD23168 | -2.623 | 0.006 | XP_014186212 | heme-binding protein 2-like isoform X1 | Induction of necrotic cell death and mitochondrial permeabilization |

| | | | | | |
|---|---|---|---|---|---|
| SAPD24471 | -2.471 | 0.002 | XM_010734808 | uncharacterized LOC104922082 | --- |
| SAPD03013 | -2.469 | 0.021 | XP_010727916 | transmembrane protease serine 13 isoform X1 | Epidermal development and acquisition of epidermal barrier function |
| SAPD12208 | -2.417 | 0.002 | -- | no match | --- |
| SAPD09805 | -2.318 | 0.003 | -- | no match | --- |
| SAPD22176 | -2.316 | 0.004 | KKF14187 | Phenylalanine-4-hydroxylase | Protein metabolism; catalyses the hydroxylation of the aromatic side-chain of phenylalanine to generate tyrosine |
| SAPD24318 | -2.312 | 0.002 | -- | no match | --- |
| SAPD06462 | -2.285 | 0.002 | XP_003456807 | normal mucosa of oesophagus-specific gene 1 protein | Suppressive role in the tumorigenesis of the oesophagus |
| SAPD23245 | -2.284 | 0.003 | -- | no match | --- |
| SAPD09340 | -2.256 | 0.023 | -- | no match | --- |
| SAPD16249 | -2.252 | 0.002 | XP_010733392 | hemicentin-1-like | Organization of hemidesmosomes in the epidermis |
| SAPD12466 | -2.247 | 0.043 | -- | no match | --- |
| SAPD05424 | -2.238 | 0.011 | -- | no match | --- |
| SAPD05555 | -2.195 | 0.004 | XM_010795291 | biglycan (bgn) | Role in bone growth, collagen fibril assembly in multiple tissues and muscle development and regeneration |
| SAPD21140 | -2.191 | 0.007 | XP_010739722 | multidrug resistance-associated protein 1-like | Mediates export of organic anions and drugs from the cytoplasm; multidrug-resistance transporter |
| SAPD15726 | -2.185 | 0.000 | XP_014000243 | tropomyosin beta chain isoform X2 | Binds to actin filaments in muscle and non-muscle cells to regulate muscle contraction and cytoskeleton stabilization |
| SAPD13364 | -2.180 | 0.001 | | | |
| SAPD20891 | -2.168 | 0.000 | KR492508 | SOX9 (sox9) gene | Transcription factor for several genes involved in chondrogenesis |
| SAPD19336 | -2.152 | 0.008 | XP_008289680 | KN motif and ankyrin repeat domain-containing protein 4 | Control of cytoskeleton formation by the regulation of actin polymerization |
| SAPD18103 | -2.130 | 0.014 | -- | no match | --- |
| SAPD12211 | -2.105 | 0.002 | XM_010793238 | metalloprotease TIKI1-like | Antagonizes Wnt signalling pathway by acting as Wnt proteases |
| SAPD12876 | -2.082 | 0.050 | CBN80756 | Synaptonemal complex protein 1 | Synaptonemal complex assembly |
| SAPD22495 | -2.035 | 0.003 | -- | no match | --- |
| SAPD21204 | -1.962 | 0.000 | XM_010739866 | protein FAM46A-like | Unknown; linked to retinal diseases and colon cancer |
| SAPD05334 | -1.944 | 0.014 | XP_010748487 | tetraspanin-1-like | Mediates signal transduction events in cell development, activation, growth and motility |
| SAPD14109 | -1.943 | 0.000 | XP_010786982 | vascular endothelial growth factor A-like isoform X1 | Induces endothelial cell proliferation, promotes cell migration, inhibits apoptosis and induces permeabilization of blood vessels |
| SAPD05674 | -1.943 | 0.000 | -- | no match | --- |
| SAPD17176 | -1.924 | 0.002 | XP_010769955 | xaa-Pro aminopeptidase 2 | Role in the inflammatory process in response to injury or infection |
| SAPD15796 | -1.842 | 0.016 | -- | no match | --- |
| SAPD15106 | -1.839 | 0.045 | -- | no match | --- |
| SAPD16053 | -1.829 | 0.014 | -- | no match | --- |
| SAPD23066 | -1.826 | 0.000 | -- | no match | --- |
| SAPD25220 | -1.816 | 0.009 | XR_798497 | uncharacterized LOCLOC104946797 | --- |
| SAPD23962 | -1.758 | 0.017 | HG314000 | *Oryzias latipes* strain Hd-rR, complete genome assembly, chromosome 22 | --- |
| SAPD01275 | -1.740 | 0.006 | XP_008302747 | S-adenosylmethionine synthase isoform type-1 | Catalyses the formation of S-adenosylmethionine from methionine and ATP; involved in neurological development and myelination |

| | | | | | |
|---|---|---|---|---|---|
| SAPD04253 | -1.738 | 0.025 | XP_011604753 | tetraspanin-5 isoform X1 | Role in cell fusion during osteoclastogenesis |
| SAPD12452 | -1.729 | 0.025 | -- | no match | --- |
| SAPD05063 | -1.728 | 0.001 | XM_010745874 | integrin, beta 3 (platelet glycoprotein IIIa, antigen CD61) | Adhesion molecule critical for cell attachment to the extracellular matrix; cell-surface mediated signalling |
| SAPD05108 | -1.727 | 0.021 | KKF31404 | putative AC9 transposase | Insertion and excision of transposable elements; can also encode proteins |
| SAPD19085 | -1.704 | 0.002 | XP_008304640 | glutathione peroxidase 3 | Detoxification of hydrogen peroxide |
| SAPD15369 | -1.670 | 0.001 | XP_006797895 | forkhead box C1-A-like | Regulator of cell viability and resistance to oxidative stress |
| SAPD09070 | -1.643 | 0.008 | -- | no match | --- |
| SAPD20935 | -1.603 | 0.024 | XM_008287318 | OX-2 membrane glycoprotein-like | Co-stimulation of T-cell proliferation; may regulate myeloid cells activity and delivers inhibitory signals to the macrophage lineage in diverse tissues |
| SAPD24489 | -1.592 | 0.001 | CAP47207 | major histocompatibility complex II gamma chains | Chaperone that regulates antigen presentation for immune cells; cell surface receptor for the cytokine MIF, initiating survival pathways and cell proliferation |
| SAPD04337 | -1.565 | 0.013 | -- | no match | --- |
| SAPD22068 | -1.555 | 0.000 | XM_010729369 | sorbin and SH3 domain containing 2 | Adapter protein to assemble signaling complexes in stress fibres |
| SAPD10964 | -1.555 | 0.014 | XM_006801259 | delta-like protein C-like | Ligand for Notch receptors; involved in somitogenesis |
| SAPD05123 | -1.538 | 0.001 | -- | no match | --- |
| SAPD19328 | -1.521 | 0.002 | XM_010744532 | slit homolog 1 (Drosophila) | Formation and maintenance of the nervous system |
| SAPD05109 | -1.510 | 0.022 | XM_008281573 | alpha-2B adrenergic receptor-like | Modulation of neurotransmission, smooth muscle contraction and thermoregulation |
| SAPD19002 | -1.495 | 0.036 | XM_014983745 | coxsackie virus and adenovirus receptor homolog | Cell adhesion molecule essential for tight junction integrity; activation of gamma-delta T-cells involved in tissue homeostasis and repair |
| SAPD05981 | -1.484 | 0.014 | AGQ56873 | phospholipase C gamma 2 | Crucial enzyme in transmembrane signalling; hydrolyzation of phospholipids into fatty acids and other lipophilic molecules |
| SAPD00699 | -1.453 | 0.008 | -- | no match | --- |
| SAPD14708 | -1.453 | 0.004 | XM_004540006 | N-acetylgalactosaminyltransferase 16 | Oligosaccharide biosynthesis; protein glycosylation |
| SAPD05736 | -1.445 | 0.027 | -- | no match | --- |
| SAPD24731 | -1.438 | 0.006 | XP_010730044 | C-C motif chemokine 4-like | Inflammatory and immunoregulatory processes; chemotaxis of pro-inflammatory cells |
| SAPD15414 | -1.431 | 0.003 | XM_013274473 | tyrosine phosphatase, receptor type, D | Promotes neurite growth and regulates neurons axon guidance |
| SAPD00344 | -1.406 | 0.017 | XP_010739797 | cytochrome b-245 light chain | Primary component of microbicidal oxidase system of phagocytes |
| SAPD13152 | -1.394 | 0.007 | AHH30804 | perforin | Secretory granule-dependent cell death and defense against virus-infected or neoplastic cells |
| SAPD11343 | -1.388 | 0.011 | XM_005913547 | sidekick-2-like | Formation of neuronal circuits that detect motion in the eye |
| SAPD04345 | -1.382 | 0.019 | KKF28146 | Tyrosine-protein kinase Blk | Non-receptor tyrosine kinase involved in B-lymphocyte development, differentiation and signaling |
| SAPD05165 | -1.381 | 0.032 | XP_013122635 | immunoglobulin lambda-like polypeptide 1 | B-cell activation |
| SAPD13832 | -1.354 | 0.014 | -- | no match | --- |
| SAPD16242 | -1.348 | 0.014 | XM_008285396 | collagen alpha-1(XXVII) chain B-like | Calcification of cartilage and transition of cartilage to bone; tissue growth and repair |
| SAPD13238 | -1.348 | 0.015 | XP_010732895 | cdc42 effector protein 3-like | Organization of actin cytoskeleton and pseudopodia formation in fibroblasts |

| | | | | | |
|---|---|---|---|---|---|
| SAPD09257 | -1.321 | 0.003 | -- | no match | --- |
| SAPD02250 | -1.302 | 0.008 | XM_004545745 | apelin | Mediator of cardiovascular function, fluid homeostasis and adipocyte endocrine secretion |
| SAPD18720 | -1.278 | 0.006 | XM_014332401 | mitogen-activated protein kinase kinase kinase 13 | Regulation of epidermal keratinocyte differentiation, apoptosis and skin tumour development |
| SAPD12212 | -1.273 | 0.002 | -- | no match | --- |
| SAPD05745 | -1.270 | 0.033 | XM_010781273 | transcription factor Maf | Chondrocyte terminal differentiation and embryonic lens fibre cell development; increases T-cell susceptibility to apoptosis |
| SAPD08110 | -1.260 | 0.003 | XM_008295124 | ATPase, aminophospholipid transporter, class I, type 8A, member 1 | Translocation of phospholipids from the outer to the inner leaflet of various membranes, ensuring its asymmetric distribution |
| SAPD25131 | -1.244 | 0.002 | ACQ58626 | SH3 domain-binding glutamic acid-rich like protein 2 | Putative regulator of redox activity |
| SAPD18946 | -1.226 | 0.002 | XP_003451108 | cysteine dioxygenase type 1 | Critical regulator of cellular cysteine concentrations |
| SAPD06309 | -1.214 | 0.002 | XM_008293058 | pim-2 oncogene | Prevents apoptosis and promotes cell survival; positive regulation of chondrocyte survival and autophagy in the epiphyseal growth plate |
| SAPD04995 | -1.210 | 0.009 | XM_010785894 | transcription factor COE1-like | Preserves B-lymphocyte identity during differentiation |
| SAPD16101 | -1.209 | 0.010 | XM_010765910 | tweety homolog 3-like | Ca2+ signalling transduction |
| SAPD06699 | -1.194 | 0.006 | XM_010784982 | sprouty homolog 2-like | Antagonist of fibroblast growth factor (FGF) pathways |
| SAPD03822 | -1.190 | 0.035 | XM_010734289 | insulin-like growth factor-binding protein 5 | Prolongs the half-life of IGFs, inhibiting or stimulating their growth promoting effects |
| SAPD11866 | -1.188 | 0.015 | -- | no match | --- |
| SAPD23938 | -1.180 | 0.010 | XP_008406995 | ras-related protein Rab-37-like isoform X3 | Control of vesicle trafficking, docking and fusion |
| SAPD12331 | -1.137 | 0.004 | -- | no match | --- |
| SAPD01425 | -1.133 | 0.007 | XM_008294138 | fasciculation and elongation protein zeta-2-like | Involved in axonal outgrowth and fasciculation |
| SAPD18685 | -1.126 | 0.001 | XM_010730706 | extracellular serine/threonine protein kinase FAM20C-like | Binds calcium and phosphorylates proteins involved in bone mineralization, lipid homeostasis, wound healing an cell migration and adhesion |
| SAPD15540 | -1.085 | 0.004 | XM_008306421 | TNFAIP3-interacting protein 1-like | Involved in the anti-inflammatory response of macrophages; prevention of autoimmunity; leukocyte integrin activation during inflammation |

**Supplementary figure 2. 1 - Functional annotation according to Gene Ontology (GO) level 2 of the down-regulated genes 3 and 7 days after scale removal. A:** Biological process **B:** Cellular compartment **C:** Molecular function **D:** Proteins domains (IterPro). The number of genes included in each process/compartment/function and protein domai nis indicated and they are coloured annotated according to their role.

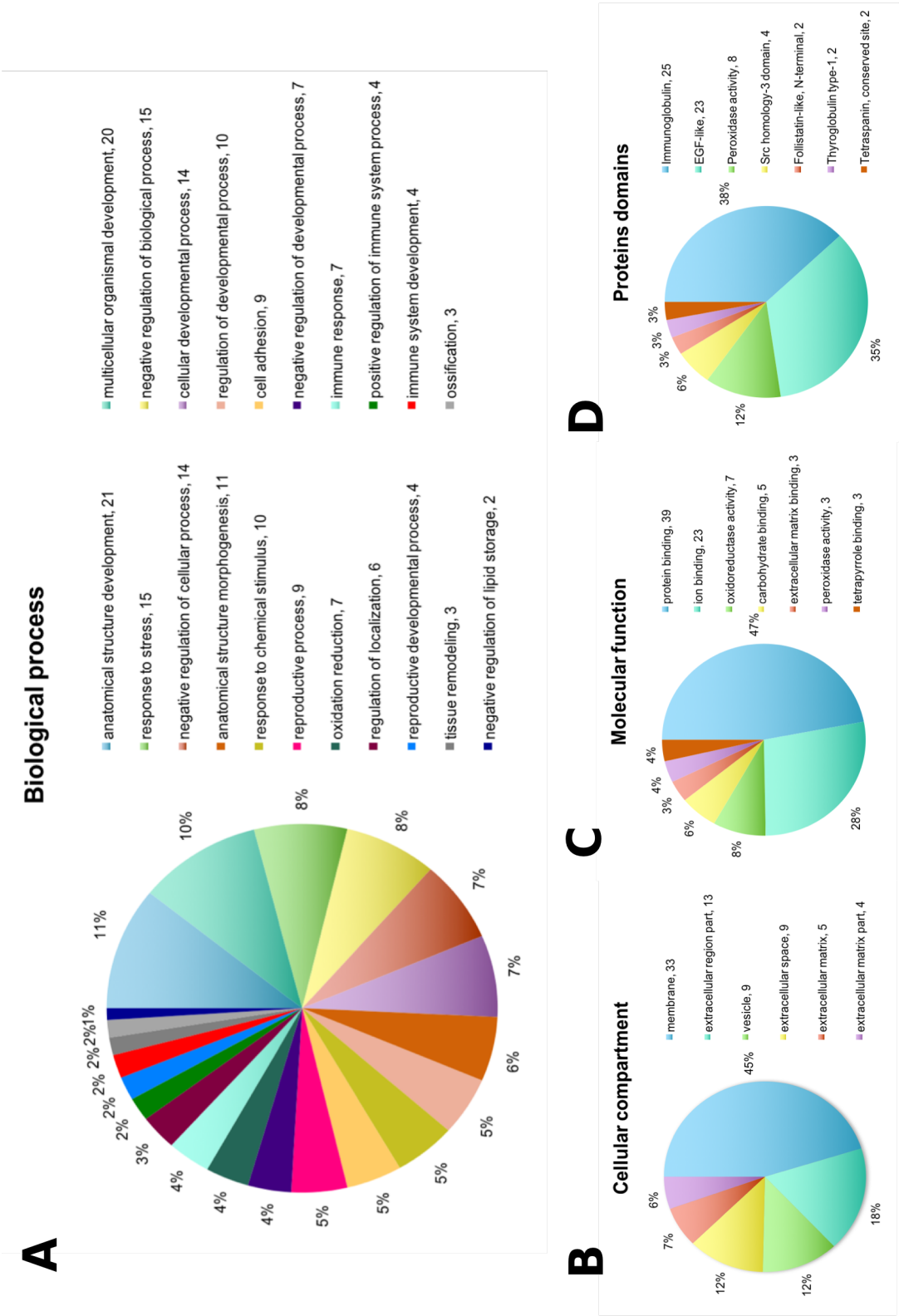

**Supplementary figure 2. 2 - Relative expression obtained by qPCR of ECM and matricellular proteins during sea bream skin healing after scale removal in intact and regenerating skin. A:** Relative expression levels of the ECM (*fn1a*, *collα1*, *colVα2* and *colXα1*) and matricellular proteins (*cyr61*, *ogn1*, *ogn2* and *crtac2*) was estimated in log2(fold-change) using the geometric mean of *rps18* and ß-*actin* as reference genes. Results are presented as mean ± sem of 4-6 individuals. Statistical significance ($p < 0.05$) between groups was assessed using two-way ANOVA followed by the Fisher`s Least Significant Difference (LSD) post-test. Differences in intact and regenerating skin during the experimental trial are annotated with different letters and comparisons between intact and regenerating skin at the same time point are indicated with an *asterisk*. **B:** Spearman correlation analysis (r) between the group of genes ($p < 0.05$).

**A**

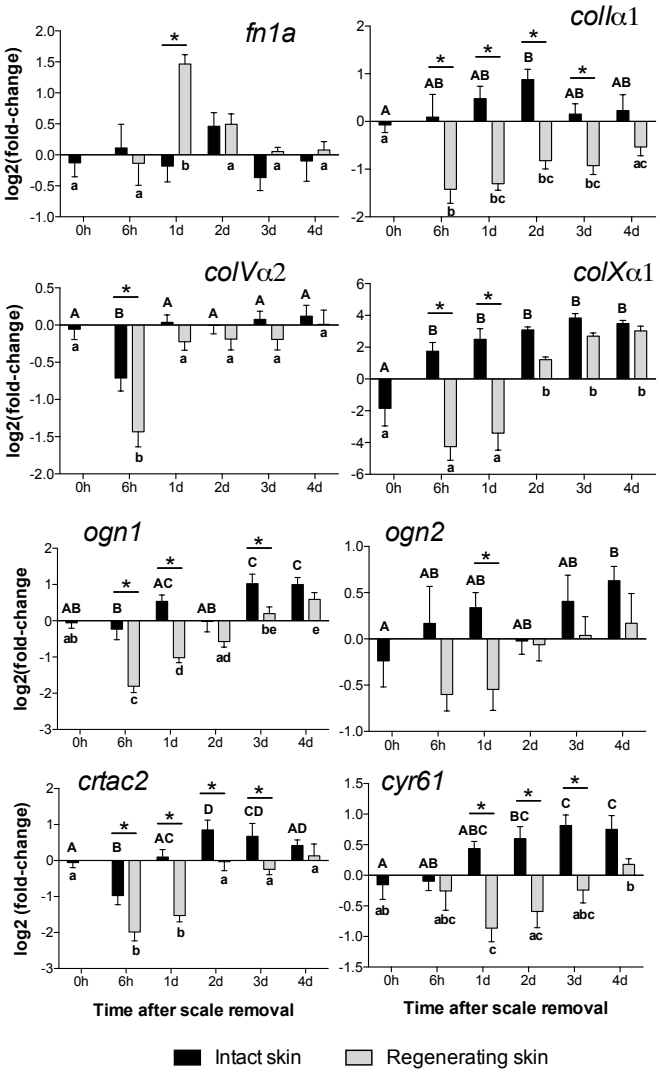


**B**

| Genes | *collα1* | *colVα2* | *ogn1* | *ogn2* | *colXα1* | *cyr61* | *crtac2* |
|---|---|---|---|---|---|---|---|
| *fn1a* | 0.145 | 0.233 | -0.169 | -0.134 | -0.081 | -0.110 | -0.032 |
| *collα1* | | 0.526 | 0.584 | 0.373 | 0.543 | 0.635 | 0.602 |
| *colVα2* | | | 0.648 | 0.459 | 0.497 | 0.482 | 0.598 |
| *ogn1* | | | | 0.591 | 0.746 | 0.560 | 0.645 |
| *ogn2* | | | | | 0.445 | 0.382 | 0.450 |
| *colXα1* | | | | | | 0.557 | 0.585 |
| *cyr61* | | | | | | | 0.501 |

**Supplementary figure 2. 3 - Relative expression obtained by qPCR of cell proliferation, remodelling and epithelial-mesenchymal interactions related genes during sea bream healing after scale removal in intact and regenerating skin. A:** Relative expression levels of *pcna*, *krt2*, *mmp9*, *edar* and *shh* was estimated in log2(fold-change) using the geometric mean of *rps18* and ß-*actin* as reference genes. Results are presented as mean ± sem of 4-6 individuals. Statistical significance ($p < 0.05$) between groups was assessed using two-way ANOVA followed by the Fisher`s Least Significant Difference (LSD) post-test. Differences in intact and regenerating skin during the experimental trial are annotated with different letters and comparisons between intact and regenerating skin at the same time point are indicated with an *asterisk*. **B:** Spearman correlation analysis (r) between the group of genes ($p < 0.05$).

**A**

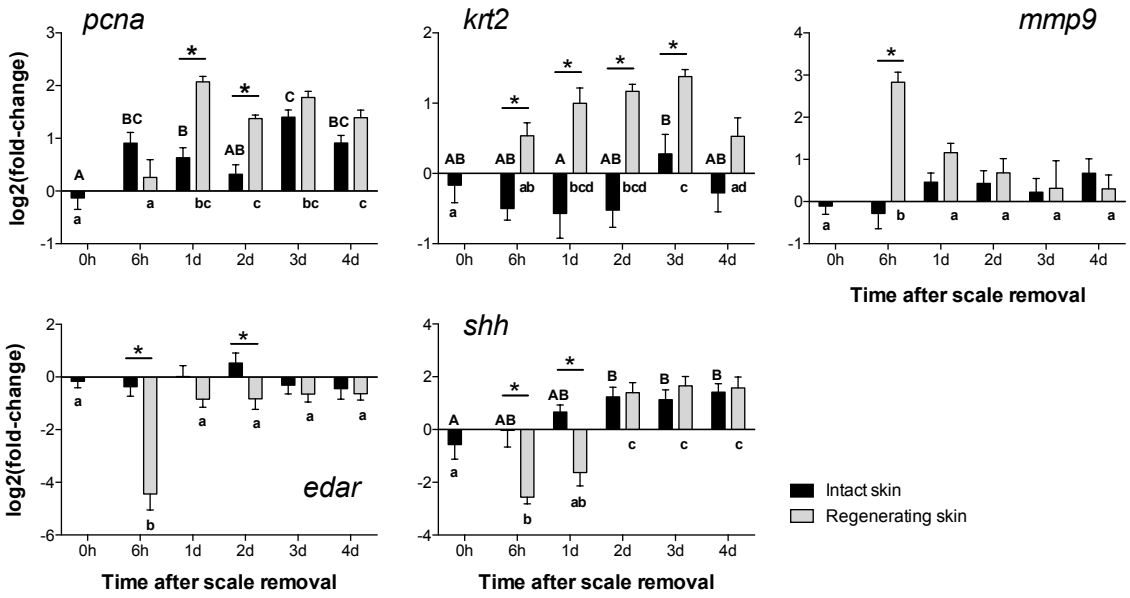


**B**

| Genes | *mmp9* | *shh* | *krt2* | *edar* |
|---|---|---|---|---|
| *pcna* | 0.107 | 0.260 | 0.696 | -0.149 |
| *mmp9* | | -0.141 | 0.197 | 0.297 |
| *shh* | | | 0.062 | 0.478 |
| *krt2* | | | | 0.352 |

**Supplementary figure 2. 4 - Relative expression obtained by qPCR of immune-related genes during sea bream healing after scale removal in intact and regenerating skin. A:** Relative expression levels of *mpo*, *csf1r*, *cdk1*, *cd48* and *cd200* was estimated in log2(fold-change) using the geometric mean of *rps18* and ß-*actin* as reference genes. Results are presented as mean ± sem of 4-6 individuals. Statistical significance ($p < 0.05$) between groups was assessed using two-way ANOVA followed by the Fisher`s Least Significant Difference (LSD) post-test. Differences in intact and regenerating skin during the experimental trial are annotated with different letters and comparisons between intact and regenerating skin at the same time point are indicated with an *asterisk*. **B:** Spearman correlation analysis (r) between the group of genes ($p < 0.05$).

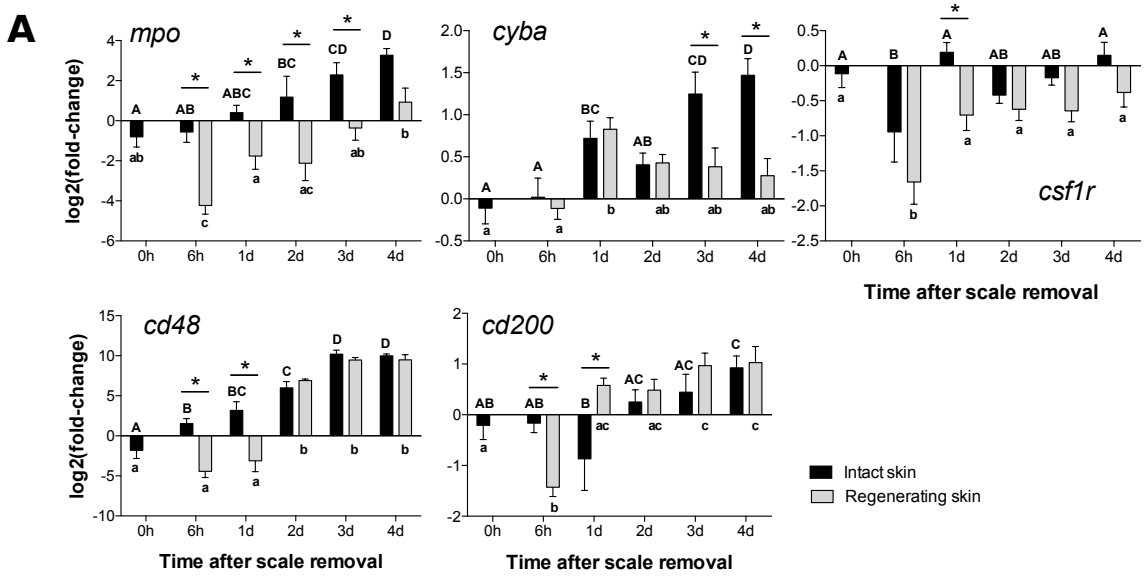


**B**

| Genes | *cyba* | *csf1r* | *cd48* | *cd200* |
|---|---|---|---|---|
| *mpo* | 0.476 | 0.419 | 0.615 | 0.377 |
| *cyba* | | 0.459 | 0.462 | 0.465 |
| *csf1r* | | | 0.346 | 0.170 |
| *cd48* | | | | 0.592 |

# 3

*Manuscript in preparation*

# Angiopoietin-like family in skin regeneration of the teleost gilthead sea bream (*Sparus aurata*)

Rita A Costa, João CR Cardoso & Deborah M Power*

Comparative Endocrinology and Integrative Biology, Centre of Marine Sciences, Universidade do Algarve, Campus de Gambelas, 8005-139 Faro, Portugal.

**Authors contributions:**
DMP conceived the project; DMP and RAC devised the experimental design and conducted laboratory based experiments; JCRC devised the in silico analysis; all authors were involved in the analysis and interpretation of the results; DMP, JCRC and RAC wrote the manuscript. All author critically revised the manuscript.

### 3.1. Abstract

The angiopoietin-like (ANGPTL) family is a group of eight (ANGPTL 1 to 8) secreted proteins structurally similar to angiopoietins that are recognized angiogenic factors in vertebrates. In mammals, ANGPTL have been involved in many functions and are important in tissue repair, cell proliferation and blood vessel formation, a process that remains largely unknown in other vertebrates. In teleost fish, the orthologue of human *ANGPTL2* promotes regeneration of zebrafish fin, in sea bream the expression of the putative *ANGPTL4* in skin is modified by feeding and in the trout embryos the human orthologue *ANGPTL7* is expressed in the dermomyotome, suggesting a putative conserved role in vertebrate skin homeostasis. The present study explores the ANGPTL family in fish and their role in teleost skin regeneration. Homologues of human *ANGPTL1 – 7* were identified in teleosts and gene family expansion occurred. A novel gene member *angptl9* was found in fish and also in *Xenopus*, lizard and chicken genomes but is absent in mammals. Orthologues of the human *ANGPTL8* were only found in mammals. The teleost Angptls share conserved sequence and structure with the human members and *angptl1b*, *angptl2b*, *angptl4a*, *angptl4b* and *angptl7* were successfully amplified from sea bream skin. To investigate their role in fish skin regeneration process, a superficial damage was induced in sea bream by scale removal and transcript expression in regenerating skin was accessed during a 4-day healing process and compared to intact skin taken from the same animal. Re-establishment of the physical barrier occurred in the first two days when an increase of epidermis thickness and basement membrane and an increase of the number of blood vessels were observed. During this period expression of *angptl1b* and *angptl2b* were significantly increased ($p < 0.05$) but *angptl7* was significantly down-regulated ($p < 0.05$) relative to intact skin suggesting that they play antagonic effects during fish wound healing. Expression of *angptl4a* and *angptl4b* did not differ between regenerating and intact skin. The results suggest that in teleosts Angptls maintained their conserved role in the regulation of skin healing and epidermis matrix structure and that their members, like in mammals, seem to contribute differently during skin healing process. Exploitation of the fish *angptl* members in skin sheds new light on the molecular understanding of tissue regeneration and scale formation and will enable the identification of new candidates as targets for the treatment of diseases that affect fish skin in aquaculture.

**Keywords**: Angptls, teleost, evolution, expression, skin regeneration

## 3.2. Introduction

The skin is the largest organ in the body and its role in innate immunity as a barrier between the external and internal environment makes it of major importance for the maintenance of homeostasis. This organ is well supplied with blood vessels and nerve endings that receive tactile and thermal stimuli from the environment (Hildebrand 1974). The skin has evolved from a simple respiratory epithelium in the amphioxus (Olson 1961) to a complex multicellular and multipurpose tissue in vertebrates (Seifert and Maden 2014; Chernova 2009). The general structure of skin in all vertebrates has been conserved and it is composed of an upper epidermal layer that interfaces with the exterior, an intermediate dermal layer and the basal hypodermic layer. Fish skin differs in several aspects from mammalian skin and the functional divergence between skin in a terrestrial and aquatic environment is presumably underpinned by significant divergence in molecular and cellular processes. While in human skin the primary physical barrier that confers protection is the stratified epidermis that is composed of dead keratinized cells, in fish the epidermis is composed of metabolically active cells with little keratinization (Fast et al. 2002; Elliot 2011a, 2011b; Vieira et al. 2011). Goblet cells and club cells produce mucous rich in proteases, mucins, immunoglobulins and antimicrobial peptides (AMPs) that protect the living epidermis of the fish integument (Gomez et al. 2013). The most pronounced difference between the skin in terrestrial and aquatic vertebrates is the presence in fish skin of scales that are mineralized structures of dermal origin, that protect the underlying dermis from abrasion and damage caused by predation (Bereiter-Hahn and Zylberberg 1993).

The importance of the skin as a protective barrier and in the maintenance of internal homeostasis means that any damage has to be rapidly repaired. The process of skin repair in vertebrates is complex and involves a cascade of local and systemic responses to restore tissue integrity. In mammals the outcome of injury to skin is repair and scaring but in amphibians and fish regeneration occurs and the disrupted tissue is replaced by skin with the original tissue architecture (Seifert and Maden 2014). In fish, scale removal provokes skin wounds and the loss of epidermal cells, scales and the superficial dermis. Removal of scales damages a key barrier of the innate immune system and consequently provokes an inflammatory response and activation of the processes associated with healing and skin and scale re-growth (Fast et al. 2002). Fish skin heals rapidly and the wound surface is rapidly covered in mucus and re-epithelialization occurs from the wound margin (Quilhac and Sire 1999; Iger and Abraham 1990). Skin and scale regeneration in the fish in which it has been studied involves, re-epithelialization and differentiation of scale-forming cells (day 1-2), production of the external

layer matrix (days 3-5), production of the basal-plate matrix (days 6-14) and finally partial mineralization of the basal plate (days 14-28) (Guerreiro et al. 2013). Wound repair and skin regeneration studies are numerous in mammals (Seifert et al. 2012a; Philips et al. 2011) and amphibians (Godwin and Rosenthal 2014; Seifert et al. 2012b), but are much less frequent in the fishes, the largest group of extant vertebrates (Nelson et al. 2001) and the molecular basis of skin repair is generally restricted to single gene studies (de Vrieze et al. 2011; Harris et al. 2008; Sire and Akimenko 2004; Monnot et al. 1999).

In mammals, the ANGPTLs family is composed of 8 secreted glycoproteins (ANGPTL1 to 8) that regulate a plethora of physiological and pathophysiological processes and in the skin they are involved in tissue repair and cell proliferation (Santulli 2014). Members of this family are characterised by the presence of an amino-terminal coiled-coil domain (CCD), a linker region and a carboxyl-terminal fibrinogen-related domain (FReD). The exception is ANGPTL8 that is an atypical shorter member that has lost the FReD domain and has only been described in mammals (Fu et al. 2013). ANGPTLs are structurally similar to Angiopoietins (ANGPT), an important family of vascular growth factors (Fagiani and Christofori 2013; Thomas and Augustin 2009; Ward and Dumont 2002; Suri et al. 1996; Maisonpierre et al. 1997). Recently it was demonstrated that some of the actions of ANGPTL are mediated by receptors that belong to the immunoglobulin-like superfamily (Zheng et al. 2012).

In humans, ANGPTL4 induces keratinocyte migration during wound healing (Goh et al. 2010a; Goh et al. 2010b) and epidermal differentiation post-healing (Pal et al. 2011). In mouse, overexpression of *ANGPTL6* in skin promotes epidermal hyperplasia and enlargement of dermal lymphatic and blood vessels to favour wound healing (Okazaki et al. 2012; Oike et al. 2003). ANGPTL7 regulates extracellular matrix (ECM) formation (Comes et al. 2011) and is highly expressed in keratinocytes and a potent anti-angiogenic factor in the cornea (Toyono et al. 2015). This protein was also described to inhibit tumour growth in a mouse xenograph model (Peek et al. 2002) and is required for the regeneration of human hematopoietic stem and progenitor cells (HSPCs) (Xiao et al. 2015a; Xiao et al. 2015b).

The functional importance of ANGPTL in mammalian skin makes them interesting candidates in the context of skin regeneration in fish. Homologues of several mammalian ANGPTL members have been described in teleosts. In particular, orthologues of human *ANGPTL2*, human *ANGPTL7* and human *ANGPTL4* have been described respectively, in fin repair (Kadomatsu et al. 2014; Kubota et al. 2005b), in the dermatome (Bricard et al. 2014), and in metabolically modified skin (Vieira et al. 2011) in fish. The preceding observation together with the reported role of ANGPTL in mammalian skin repair led us to hypothesize that

some functions are conserved between fish and mammals and that they may underpin skin regeneration in fish. The existence of multiple members of the ANGPTL family in vertebrates and the deficit of knowledge about this gene family in fish made it necessary to first characterize the evolution of the *ANGPTL* gene family and gene synteny in order to categorically identify the candidate genes targeted in this study. To assist in designation of putative function we identified the motifs in the deduced piscine *ANGPTL* proteins that have been conserved during evolution. We then mapped the tissue distribution of gene family members using *in silico* molecular resources (EST and microarray probes) and confirmed the association of ANGPTL family members with the integument by qPCR in sea bream intact skin and skin regenerating after scale removal. Taking into consideration the role of ANGPTL in tissue repair, cell proliferation and angiogenesis in mammals we correlated the expression patterns of *angptl1b*, *angptl2b*, *angptl4a*, *angptl4b* and *angptl7* with the initial phases of piscine skin regeneration to test if the function of ANGPTLs has been conserved during the evolution of the vertebrates.

## 3.3. Materials and Methods

### 3.3.1. Genome and EST database searches

Homologues of human angiopoietin-like (ANGPTL) family members were procured in 15 fish genome assemblies (supplementary table 3.1). Using as queries the deduced mature protein sequences of human ANGPTLs, ten teleost genomes were explored of which nine were available from Ensembl (www.ensembl.org/, accessed in May 2015) and included: two puffer fishes (*Tetraodon nigroviridis*, *Takifugu rubripes*), stickleback (*Gasterosteus aculeatus*), Nile tilapia (*Oreochromis niloticus*), medaka (*Oryzias latipes*), platyfish (*Xiphophorus maculatus*), Atlantic cod (*Gadus morhua*), cavefish *(Astyanax mexicanus*) and zebrafish (*Danio rerio)* and the sea bass (*Dicentrarchus labrax*) assessed from the sea bass genome assembly (http://seabass.mpipz.de). Searches were complemented by mining additional fish genomes at ENSEMBL (www.ensembl.org/, accessed in May 2015); a basal ray-finned fish, the spotted gar (*Lepisosteus oculatus*), the coelacanth (*Latimeria chalumnae*) that is basal to the tetrapod lineage, and a jawless fish, the marine lamprey (*Petromyzon marinus*). The genome of two cartilaginous fishes the elephant shark (*Callorhinchus milii*, http://esharkgenome.imcb.a-star.edu.sg/) and little skate (*Leucoraja erinacea*, http://skatebase.org/) were also analysed.

To assess *angptl* gene family evolution, searches were extended to genomes of terrestrial vertebrates and invertebrates (early deuterostomes, protostomes and early metazoan).

This included 4 terrestrial vertebrates (the amphibian *Xenopus tropicalis*, the reptile the Anole lizard, *Anolis carolinensis*, the chicken, *Gallus gallus* and two mammalians: the marsupial opossum *Monodelphis domestica* and the placental the mouse, *Mus musculus* available from ENSEMBL and accessed in May 2015); 4 early deuterostomes (the hemichordate acorn worm, *Saccoglossus kowalevskii*, (www.hgsc.bcm.edu, accessed in May 2015); the echinoderm sea urchin, *Strongylocentrotus purpuratus* (metazoa.ensembl.org/index.html, accessed in May 2015); the cephalochordate amphioxus, *Branchiostoma floridae* (http://genome.jgi.doe.gov/Brafl1/Brafl1.home.html), accessed in May 2015; and the urochordate Ciona, *Ciona intestinalis* (www.ensembl.org/, accessed in May 2015); 11 protostomes (two annelids, *Capitela teleta* and *Helobdella robusta*; two molluscs *Crassostrea gigas* and *Lottia gigantea*; 5 arthropods the *Daphnia pulex*, *Ixodes scapularis*, *Tribolium castaneum, Drosophila melanogaster*, *Anopheles gambiae*, the nematode *Caernohabditis elegans* and the platyhelminth *Schistosoma mansoni*) and 2 early metazoans (the cnidarian, *Nematostella vectensis* and the porifera, *Amphimedon queenslandica*) were accessed from the Ensembl genomes database (www.ensemblgenomes.org, accessed in May 2015). Searches for putative *angptl-like* transcripts for the target invertebrate species were also performed at the NCBI (http://www.ncbi.nlm.nih.gov) database using the deduced protein of the human ANGPTL against the species-specific nucleotide collections (nr/nt).

To aid in the identification of *angptl* candidates with a putative functional role in the fish skin, the deduced sea bass *angptl* protein sequences were used to identify *angptl* transcripts isolated from skin EST libraries using a tblastn query against the teleost EST collection (http://www.ncbi.nlm.nih.gov, taxid:32443). The sequence hits with e < -70 were retained and their identity was confirmed against human orthologues. Microarray probes modified in a sea bream skin/scale regeneration experiment (Vieira et al. 2011) and a transcriptome assembly of sea bass skin (Pinto et al., unpublished data) were also analysed for skin *angptl* candidates. For the skin expression studies, the *angptl* family members from the gilthead sea bream (*Sparus aurata*) were identified from the species-specific NCBI EST database subset (taxid:8175, http://www.ncbi.nlm.nih.gov) and a sea bream transcriptome assembly prepared "in house" from multiple tissues (Louro et al. *unpublished results*).

### 3.3.2. Phylogenetic analysis

Phylogenetic analysis of fish and other metazoan ANGPTL family members was performed using the deduced mature protein sequences. Two hundred and twenty-six sequences including the ANGPTL1 to 9 and also ANGPT 1, 2 and 4 sequences from 23 vertebrates

including the 15 fish species and the cephalochordate representatives were used to construct the phylogenetic trees. The deduced mature protein sequences were aligned using ClustalW (v2) (www.genome.jp/tools/clustalw/). Gaps that resulted from the sequence alignment were removed using the AliView v 1.17.1 (Larsson 2014) and the edited ANGPT/ ANGPTL protein alignment was submitted to the ProtTest 2.4 server (http://darwin.uvigo.es/software/prottest2_server.html) to identify the best model to study ANGPTL protein evolution using the Akaike Information Criterion (AIC) statistical model (Abascal et al. 2005).

Phylogenetic analysis was performed using two approaches: Bayesian interference (BI) and maximum likelihood (ML). The BI was built in MrBayes 3.2 (Ronquist et al. 2012) using the substitution model JTT (Aamodel=Jones, (Jones et al. 1992)) and 1.000.000 generations sampling request and probability values to support tree branching. The ML method was performed with 100 bootstrap replicates to test the robustness of the phylogenetic clades in the ATGC interface PhyML 3.0 (Guindon et al. 2010). The ML tree was built with a JTT substitution model with a fixed proportion of invariable sites value (0.008) and 4 gamma-distributed rate categories (1.272). Both BI and ML phylogenetic trees were rooted using the metazoan ANGPT clade and had similar branch topologies.

### 3.3.3. Multiple sequence comparisons and analysis

The deduced mature proteins of the fish Angptl were compared with human homologues to identify conserved motifs that were maintained across vertebrates or that were characteristic of each family cluster identified by phylogenetic analysis. Alignments were performed in ClustalW (v2) and then manually edited using Genedoc (iubio.bio.indiana.edu/) software that was also used to calculate the percent of sequence identity/similarity between fish, terrestrial vertebrates and cephalochordate homologues. Conserved domains in the fish sequences were identified using Smart (smart.embl-heidelberg.de/) and UniProt (www.uniprot.org) software. The mature protein sequences of the sea bream *angptl* transcripts were deduced using the ExPASy Translate Tool (web.expasy.org/translate/).

### 3.3.4. Short-range gene linkage

To further confirm gene identification and to establish an evolutionary model for the metazoan *angptl* genes, the gene environment of the chromosomes or genome fragments that host the *angptl9* and *angptl8* genes was characterized and compared across vertebrates. Short-

range gene linkage comparisons included human, chicken (*angptl9*) or lizard (*angptl8,* as the chicken lacks a conserved gene environment), coelacanth, spotted gar and elephant shark and also two teleosts the tilapia and the zebrafish. The vertebrate neighbouring gene environment was retrieved from the Genomicus database (http://www.genomicus.biologie.ens.fr/) using the gene environment of human *angptl8* and spotted gar *angptl9* as a reference. The homologue genome regions in elephant shark and lamprey were characterized by querying their specific genome assemblies with the conserved flanking genes of *angptl8* and *angptl9* identified in teleosts and tetrapods. The gene environment of vertebrate *angptl7*, the Angptl member clustering to *angptl9*, was also investigated to establish if a homologue genome region exists in the cephalochordate genome. The identity of genes from the *angptl7* homologue genome region in the cephalochordate assembly was confirmed against the vertebrate protein databases.

### 3.3.5. Sea bream skin regeneration challenge

A stock of adult sea bream of the same age class (1-year-old) were purchased from a commercial supplier (CUPIMAR SA, Cádiz, Spain) and transferred to Ramalhete, the marine station of the Centre of Marine Sciences (CCMAR, University of the Algarve, Faro, Portugal). Fish were maintained in 1000 L tanks supplied with a continuous flow of aerated sea water at 18-20ºC, pH 7.8-8.1, 37 ppt salinity, > 80% oxygen saturation and at a density of < 5 kg $m^{-3}$. For maintenance, fish were fed at 2% (total kg fish/tank) *ad libitum* twice daily with a commercial feed (Excel; Skretting, Burgos, Spain).

For the skin regeneration challenge, adult sea bream (n = 48, length = 34 ± 1.3 cm) were divided randomly between five 500 L tanks (n = 8 per tank) supplied with a continuous flow of aerated seawater at 20 ± 2ºC and maintained under the conditions described above. For the skin regeneration challenge, fish were anesthetised with 2-phenoxyethanol in seawater (1:10,000; Sigma-Aldrich) and scales were removed from the left flank of the body by gently stroking the skin with forceps to minimise damage to the dermis. A group of fish (n = 8) were killed immediately (zero time) after scale removal and samples of intact skin (untouched right hand flank) and damaged skin (left hand flank) were snap frozen in liquid nitrogen and subsequently stored at -80$^{o}$C for molecular analysis or were fixed in 4% paraformaldehyde (4% PFA, pH 7.4) for histology. In this way the same fish provided control and regenerating skin samples and they could be directly compared. To minimize undue stress to the fish the 5 tanks represented the different time points of the sample time series after scale removal: 6 h and day 1, 2, 3 and 4. Intact and regenerating skin samples (n = 8/ time point) were collected from fish anaesthetised in 2-phenoxyethanol (1:10,000, Sigma-Aldrich), and were weighted, length

measured and a photograph taken. Fish were killed by decapitation and skin below the dorsal fin on the left (regenerating skin) and right hand flank (intact skin) of the same fish was collected and a portion frozen in liquid nitrogen and the other portion fixed for histological examination.

Fish maintenance and subsequent experiments complied with the Guidelines of the European Union Council (86/609/EU) and was covered by a group 1 license (Direção-Geral de Veterinária, Portugal). The behaviour and health of animals was visually monitored each day and no evidence of skin infection, modified behaviour or mortality occurred during the experiment.

### 3.3.5.1. Skin histological and morphometric analysis

Intact and regenerating skin samples from sea bream (0h, 6h, 1, 2, 3 and 4 days after scale removal) were fixed in 4% PFA, decalcified overnight in 0.5 M ethylenediaminetetraacetic acid (EDTA, pH 8) and dehydrated in ethanol (70%, 90% and 100%), saturated in xylene and impregnated and embedded in low melting point paraffin wax (Histosec, Merck). Serial 5 µm sections of skin were mounted on 3-aminopropyltriethoxysilane (APES) coated glass slides, dried overnight at 37ºC, cooled to room temperature and stored until required. Masson`s trichrome staining was used to distinguish between collagen rich and/or mineralized and non-mineralized tissue as previously described (Vieira et al. 2011). Stained sections were analysed using a microscope (Leica DM2000) coupled to a digital camera (Leica DFC480) linked to a computer for digital image analysis. Digital images were used to quantify the thickness of the epidermis, basement membrane and dermis as well as the number and diameter (20 vessels per section) of blood vessels in intact (n = 3, 1 section per fish) and regenerating (n = 3, 1 section per fish) skin using the ImageJ v1.44o software (Abramoff et al. 2004).

### 3.3.5.2. RNA extraction and cDNA synthesis

Total RNA was extracted from sea bream intact and regenerating skin using a Maxwell® 16 MDx Instrument (Promega) and a Maxwell 16 Total RNA Purification Kit (Promega), according to the manufacturer`s instructions. Quality and integrity of total RNA was verified using a NanoDrop 1000 Spectrophotometer (Thermo Scientific). Purified total RNA (1-3 µg) was treated with 1.5 U DNAse (Ambion DNA-*free*™ kit) following the manufacturer`s instructions. DNA free total RNA (100 or 250 ng) was used for first strand cDNA synthesis in

a 20 µl reaction volume containing 100 mM p6 random hexamers (GE Healthcare, UK), 100 U of RevertAid™ Reverse Transcriptase (Fermentas) and 8 U of RiboLock™ RNase Inhibitor (Fermentas). cDNA was synthesized by incubating for 10 minutes at 20°C, followed by 50 minutes at 42°C and 5 minutes at 72°C. The quality of cDNA was checked by PCR amplification of *rps18* with specific primers (table 3.1) using the following cycle: 10 minutes at 95°C, followed by 25 cycles of 95°C for 30 seconds, 60°C for 30 seconds and 72°C for 30 seconds and a final 5 minutes at 72°C. The PCR products were run on a 1% agarose gel to confirm amplicon size and the absence of contamination with genomic DNA.

### 3.3.5.3. Quantitative expression analysis (QRT-PCR)

The expression of *angptl1b*, *angptl2b*, *angptl3b*, *angptl4a*, *angptl4b*, *angptl7* and *angptl9b* was confirmed in sea bream skin and the abundance of the amplified transcripts were subsequently characterised in intact and regenerating skin by quantitative real-time PCR. Transcript specific primers were designed using the sea bream sequences as templates (table 3.1) and QRT-PCR was carried out in duplicate 10 µl reactions of 1x SsoFast-Evagreen Supermix (Biorad) containing cDNA (≈ 16.7 ng) and 300 nM of forward and reverse primers. Quantification was performed in a StepOnePlus thermocycler (Applied Biosystems, UK) using the standard-curve method (software StepOne$^{TM}$ Real-Time PCR Software v2.2) and the following program: 30 seconds at 95°C, 45 cycles of 5 seconds at 95°C and 15 seconds at 60°C. A standard curve was included to permit the initial quantity of target template to be related to amplification cycle. A final melting curve was carried out between 60°C and 95°C and produced a single product dissociation curve for each gene. Relative expression (log2 (fold-change)) was estimated using the geometric mean of two-reference transcripts *rps18* and *ß-actin* that did not vary significantly ($p > 0.05$) between the control and regenerating skin samples. Pearson correlation analysis was performed for the *angptl* family members and *vegfab*, a mediator of vascular development in zebrafish (Bahary et al. 2007).

**Table 3. 1 - List of the primers used for gene expression analysis by quantitative RT-PCR in sea bream (*Sparus aurata*) skin.** Accession number/reference, primer sequence, amplicon length (bp), annealing temperature (T °C) and qPCR efficiency (%) and $R^2$ are indicated for each pair of primers. F: forward and R: reverse primer.

| | Accession Number | Primer sequences (5`to 3`) | Amplicon (bp) | T (ºC) | Efficiency (%) | $R^2$ |
|---|---|---|---|---|---|---|
| *angptl1b* | | F: GCATGCAGGTCTACAGTCG<br>R: CAAAGGCTCGGGTGTTGTC | 135 | 58 | 96 | 0.99 |
| *angptl2b* | | F: TGCTGCACGAGATCATCAGGAA<br>R: GTACTTGTGCTCGAGATCTTT | 128 | 60 | 89 | 0.99 |
| *angptl4a* | | F: AGATACAGAAGGCTGATGCT<br>R: CTGGTCGTTGTCTTGGTC | 101 | 60 | 99 | 0.99 |
| *angptl4b* | | F: AAATAATGTCGACCGAAGAG<br>R: CGAGTTACCACAGCTGTTG | 128 | 60 | 81 | 0.99 |
| *angptl7* | | F: CAGTACGCTCAGGATCGAGATGG<br>R: ATGGTGCTGAAGTTGGTGTTGTT | 171 | 60 | 97 | 0.99 |
| *vegfab* | | F: ACGTCCAGCTATAACATTACAA<br>R: CTTTCTTTAACCTACACTCA | 115 | 58 | 90 | 0.99 |
| *rps18* | AM490061 | F: AGGGTGTTGGCAGACGTTAC<br>R: CTTCTGCCTGTTGAGGAACC | 164 | 60 | 88 | 0.99 |
| *ß-actin* | X89920 | F: CCCTGCCCCACGCCATCC<br>R:TCTCGGCTGTGGTGGTGAAGG | 94 | 60 | 92 | 0.99 |

### 3.3.6. Statistical analysis

Significant changes in relative transcripts expression in intact and regenerating skin during the wound healing process were assessed using a two-way ANOVA followed by the Fisher`s Least Significant Difference (LSD) post-test using the StatPlus:mac LE v5 2015 (AnalystSoft Inc., USA). Relative expression data are presented as mean ± standard error of the mean (Gilkes et al. 2013). Statistical significance was considered at $p < 0.05$. Significant differences in intact or regenerating skin at different time points during the experiment are annotated with different letters and significant differences between intact and regenerating skin at the same time point are annotated with an asterisk.

## 3.4. Results

### 3.4.1. Angptls in fish and other metazoans

Sequence homologues of human ANGPTL family members were identified in several fish. A previously undescribed member of this family was identified in fish genomes and also in *Xenopus*, lizard and chicken genomes and was designated *angptl9*. The new ANGPTL family member was absent from mammalian genomes. In contrast, orthologues of human *ANGPTL8* were absent from fish and other non-mammalian vertebrate genomes (supplementary table 3.1 and figure 3.1). Ten teleost fish genomes were analysed and the total *angptl* gene number

retrieved per genome varied from 10 to 13 depending on retention or not of duplicate gene copies of *angptl1*, *angptl2*, *angptl3* and *angptl4* and the new *angptl9* gene identified in this study. Duplicates of human *ANGPTL1* gene homologues were identified in all teleost genomes analysed but the persistence of paralogues for the other family members was species-dependent and it was not possible in some species to establish if the full complement of genes was present in the genome because of the incompleteness of the assemblies.

In the slowly evolving fish genome of the spotted gar (*Lepisosteus oculatus*), which diverged prior to the teleost radiation, a single *angptl* gene copy was found. The lobe-finned coelacanth, a fish basal to tetrapods, had a similar gene repertoire to the spotted gar with the exception of the duplicate *angptl5* genes. In the cartilaginous fish the elephant shark (*Callorhinchus milii*) and the little skate (*Leucoraja erinacea*), 5 and 4 *angptl* genes, respectively were retrieved and orthologues of the teleost *angptl5*, *angptl6* and *angptl9* remain to be identified. Searches in the jawless fish, the marine lamprey (*Petromyzon marinus*), recovered putative *angptl2* and *angptl5* genes but the incomplete nature of its genome assembly means that the existence of other members remains to be established. In the gilthead sea bream (*Sparus aurata*) that does not have a sequenced genome, 10 *angptl* transcripts were retrieved but the orthologues of *angptl3a* and *angptl6* were not identified.

Terrestrial vertebrates including, the amphibian (*Xenopus tropicalis*), the anole lizard (*Anolis carolinensis*), the chicken (*Gallus gallus*), the opossum (*Monodelphis domestica*) and the mouse *(Mus musculus*) had a similar gene repertoire to human but in non-mammalian genomes an orthologue of the fish *angptl9* gene also existed. Orthologues of human *ANGPTL8* were only identified in mammals and were absent from other vertebrates.

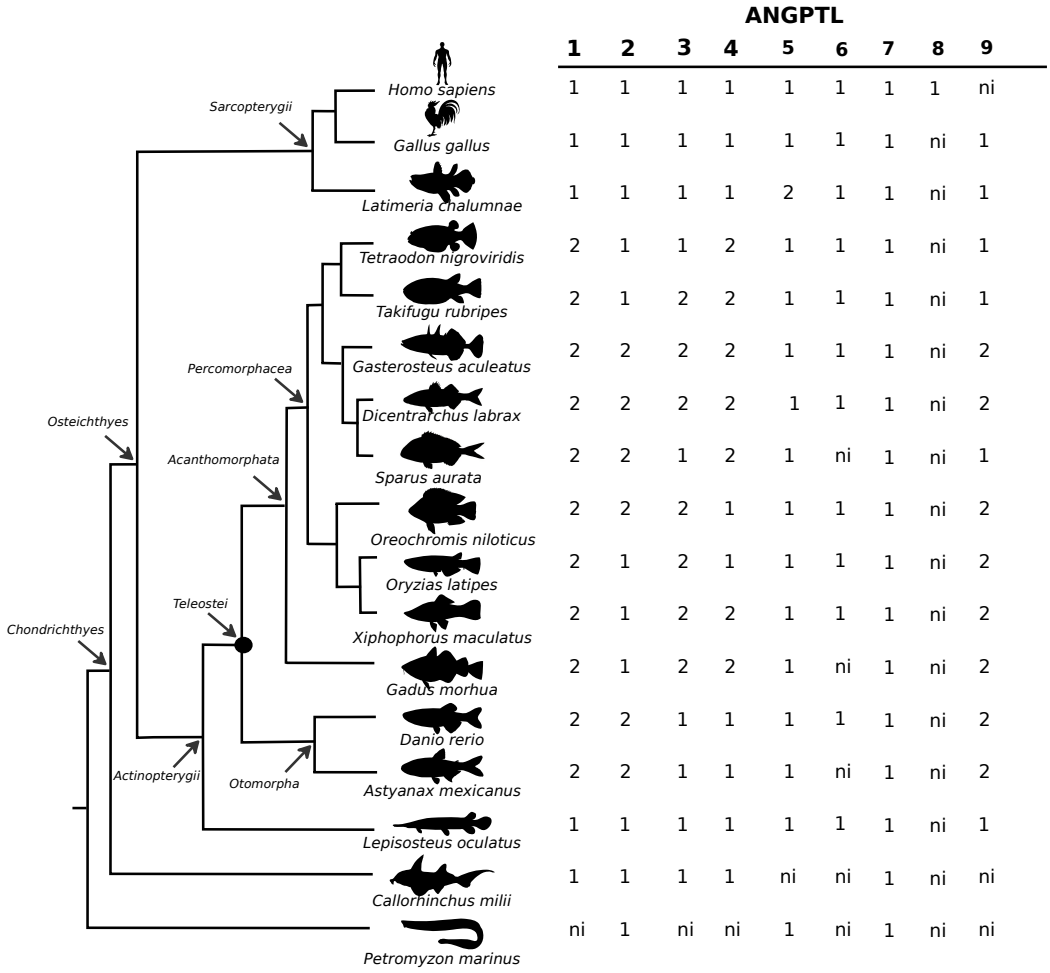


**Figure 3. 1 - ANGPTL family gene members in fish.** The number of predicted *angptl* genes identified is indicated. The chicken and human genes are also indicated to allow comparisons with the fish homologues. *ni*: not identified

In the cephalochordate (*Branchiostoma floridae*) at least 5 putative *angptl-like* genes were identified (supplementary table 3.1) indicating that this gene family is ancient and arose prior to the vertebrate radiation. Data mining of other early deuterostome genomes failed to retrieve annotated genes although predicted transcripts orthologous to human ANGPTL1 were identified in a urochordate, the sea squirt (*Ciona intestinalis*, XM_002126240), in an echinoderm, the sea urchin (*Strongylocentrotus purpuratus*, XM_781185, XM_003727342), and in a hemichordate, the acorn worm (*Saccoglossus kowalevskii*, XM_002739547 and XM_006819919). An orthologue of human ANGPTL2 (XM_001178311) was also identified in the sea urchin, although the deduced transcripts were much longer and only part of the transcript shared homology with the human ANGPTLs (< 20% aa sequence similarity) and this sequence was not considered for further analysis. In protostome and early deuterostome

genomes sequence hits for proteins related to the vertebrate ANGPTLs such as tenascins, ficolins, fibrinogen and others were obtained but were not subsequently considered in this study.

### 3.4.2. Phylogeny of the fish Angptls

Phylogenetic analysis of vertebrate and cephalochordate ANGPTLs revealed the genes shared a common origin and that the family members emerged early during the deuterostome radiation (figure 3.2, supplementary figure 3.1 and 3.2). According to the tree topology, four main protein clusters that contain distinct members of the ANGPTL family exist: the ANGPTL1-2-6 cluster (ANGPTL1, ANGPTL2, ANGPTL6), the ANGPTL3-4 cluster (ANGPTL3, ANGPTL4), the ANGPTL5 cluster (ANGPTL5) and the ANGPTL7-9 cluster (ANGPTL7, ANGPTL9). According to the tree topology, the ANGPTL3-4 cluster diverged early after the gene duplication event that gave rise to the ancestral gene from which the ANGPTL1-2-6, ANGPTL5 and ANGPTL7-9 subsequently emerged. This suggests that the ancestral ANGPTL gene duplicated prior to the radiation of vertebrates and that the family members arose from different ancestral genes.

In teleosts, duplicate copies of *angptl1*, *angptl2*, *angptl3, angptl4* and *angptl9* arose from the whole genome duplication event reported for this lineage (Jaillon et al. 2004). The teleost *angptl* gene duplicates were differentiated using the letter *a* and *b* and the gene environment of paralogue *a* shared the greatest conservation with the homologue chromosome regions in human and the spotted gar (http://www.genomicus.biologie.ens.fr). In other fish single gene family members existed with the exception of *angptl5* that was duplicated in the coelacanth genome.

The five cephalochordate *angptl-like* genes clustered with the vertebrate ANGPTLs (figure 3.2). Four of which group within the vertebrate ANGPTL7 clade and three of which (Amphioxus_ii, Amphioxus_iii and Amphioxus_iv) seem to have resulted from species-specific gene duplications. The fifth ANGPTL (Amphioxus_v) sits prior to the emergence of the vertebrate ANGPTL1-2-6 and ANGPTL7-9 clades. The existence of other ANGPTL family members in amphioxus was not established due to the incompleteness of its genome assembly.

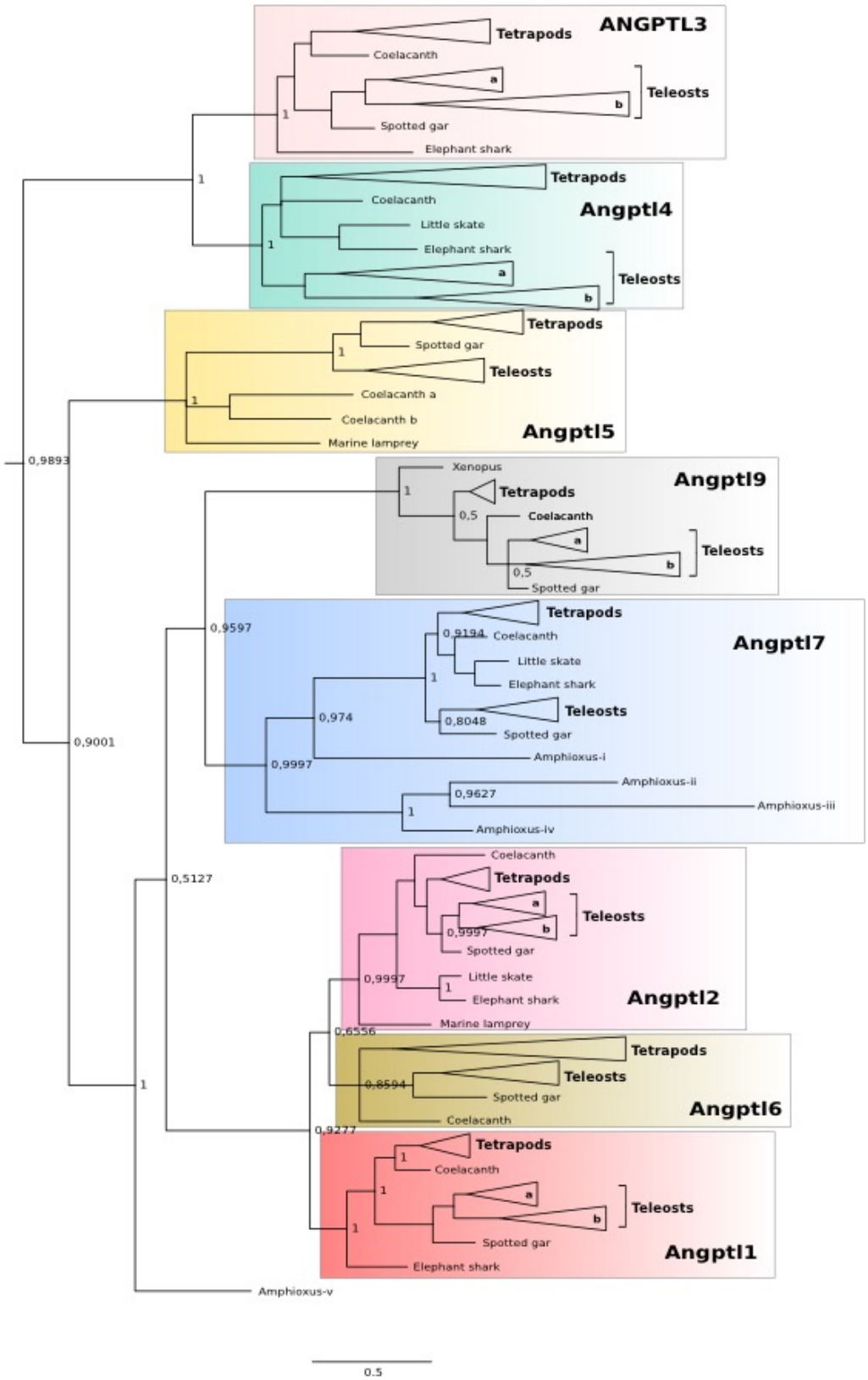


**Figure 3. 2 - Phylogenetic tree of the fish and other metazoan ANGPTL family members constructed with the Maximum-likelihood (ML) algorithm.** The Phylogenetic analysis was performed with the deduced amino acid sequences in ATGC (http://www.atgc-montpellier.fr/phyml/) with a fixed value for the proportion of invariable sites 0.008, 4 gamma-distributed rate categories (1.272) and 100 bootstrap replicates. Tree was rooted with the metazoan ANGPT clade (ANGPT1, 2 and 4). Accession numbers available in supplementary tables 3.1 and 3.4.

### 3.4.3. Sequence conservation of the fish Angptls with human and cephalochordate

Amino acid (aa) sequence alignment of the fish ANGPTLs with the human orthologues revealed that they are highly conserved and protein domains and sequence motifs are shared by teleost and tetrapod sequences (figure 3.3 and supplementary figures 3.3a - d). This includes an N-terminal coiled-coil domain (CCD) and a highly conserved fibrinogen-related domain (FReD) in the C-terminal region that is also present in ANGPT proteins (Santulli 2014). Within the FReD motif, four highly conserved cysteine residues predicted to establish two intramolecular disulphide bonds were conserved in human and fish, however their importance in protein structure and function still remain to be established (Shan et al. 2009) (figure 3.3). Human and fish ANGPTL1, 2 and 7 were the most highly conserved members and the deduced mature proteins shared 76%, 80% and 82% aa sequence similarity, respectively (supplementary table 3.2). The deduced sequence of ANGPTL9 was also highly conserved between the vertebrates that possess it and across the teleosts shared 75-78% aa similarity. The most divergent forms of ANGPTL between fish and human were ANGPTL4 and ANGPTL6 that shared 47% and 54% aa sequence similarity, respectively (supplementary table 3.2).

Although overall all the vertebrate ANGPTL family members shared relatively high sequence conservation some specific amino acid sequences that have been linked to protein processing or protein structural configuration/function were also common across fish and human (figure 3.3 and supplementary figure 3.3). This included the three cysteine residues and two glycosylation sites within the CCD of ANGPTL1, ANGPTL2 and ANGPTL6; an N-glycosylation site (CCD motif) and a C-glycosylation site (FReD) in ANGPTL3; an N-glycosylation site in the CCD of vertebrate ANGPTL4 and the amino acids $His^{46}$, $Gln^{50}$ and $Gln^{53}$ that were important for the regulation of lipoprotein lipase (LPL) in humans and the elevation of plasma triglyceride levels in mice (Yau et al. 2009); and three glycosylation sites, one within the CCD and two in the FReD domains, in ANGPTL7. A unique glycosylation site within the CCD was predicted in the deduced protein of ANGPTL9 from teleosts and the spotted gar.

The deduced cephalochordate *angptls-like* (i to iv) proteins shared the highest sequence similarity (29-37% aa) with vertebrate ANGPTL7 and within the deduced protein the FReD domain was most highly conserved (supplementary figure 3.4).

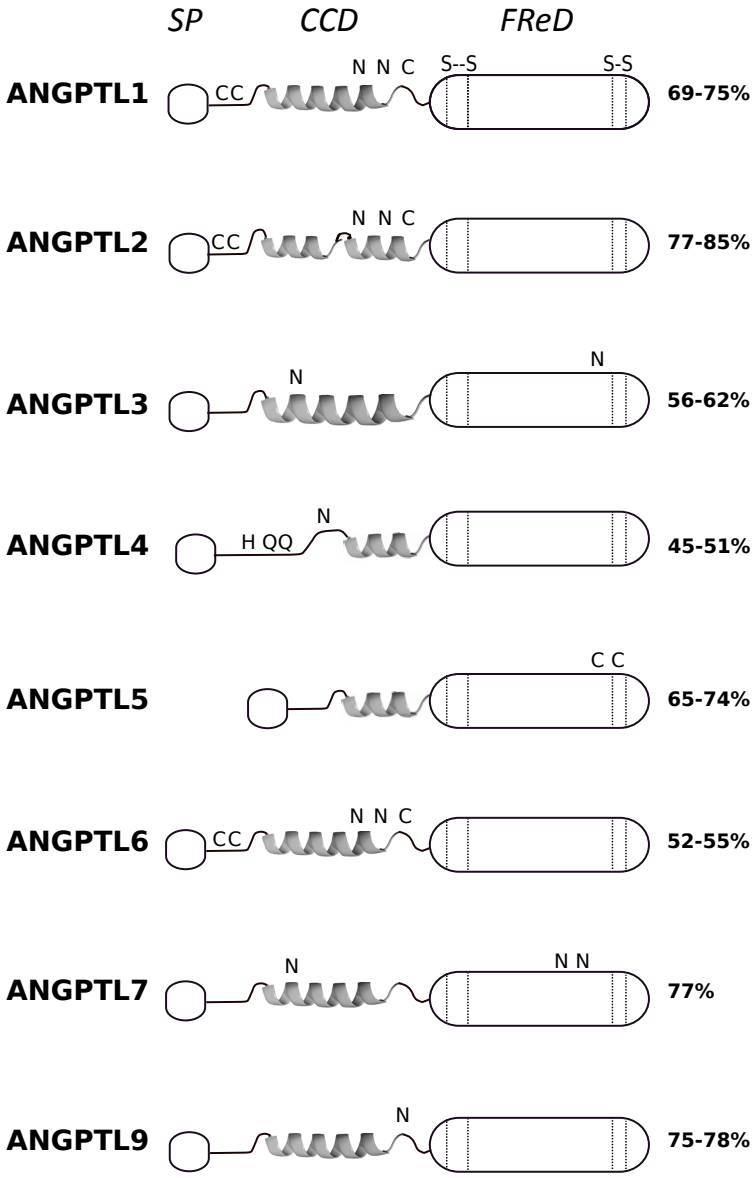


**Figure 3. 3 - Schematic representation of the deduced structure and conserved consensus motifs of the fish and human ANGPTLs.** The signal peptide region (SP), the coiled-coil domain (CCD) and the highly conserved fibrinogen-related domain (FReD) are annotated. The four conserved cysteine residues within the FReD motif that are potentially involved in the establishment of two intramolecular disulphide bonds are indicated by "S-S", other conserved cysteine residues are represented by "C" and predicted glycosylation (N-x-T/S) motifs are annotated with "N". Across fish, the amino acid residues that regulate the activity of the human ANGPTL4 ($His^{46}$, $Gln^{50}$ and $Gln^{53}$ (Yau et al. 2009) are also conserved. Figure is not drawn to scale and the percent of amino acid sequence similarity between the fish and the human orthologues is indicated. The complete sequence alignments of the human with the spotted gar and teleost (zebrafish, sea bass and sea bream) are available in supplementary figure 3.

### 3.4.4. Neighbouring gene analysis

To better understand the evolution of the *ANGPTL* gene during the vertebrate radiation, the neighbouring gene environment of mammalian *ANGPTL 8* and non-mammalian *Angptl 9* were compared between fish and tetrapods. In human, the *ANGPTL8* gene mapped to

chromosome 19 and orthologues of the flanking genes were found in other vertebrate genomes. A chromosome region with a similar gene repertoire to that flanking human *ANGPTL8* was found in the lizard and in the fish (coelacanth, spotted gar and elephant shark, figure 3.4) even through the *ANGPTL8* gene was absent from their genomes. Of the nine genes that flank human *ANGPTL8*, eight retain linkage in chromosome 2 of the lizard and in scaffold LG6 of the spotted gar genome suggesting the loss of this gene in these species is potentially a consequence of lineage specific gene deletions (figure 3.4).

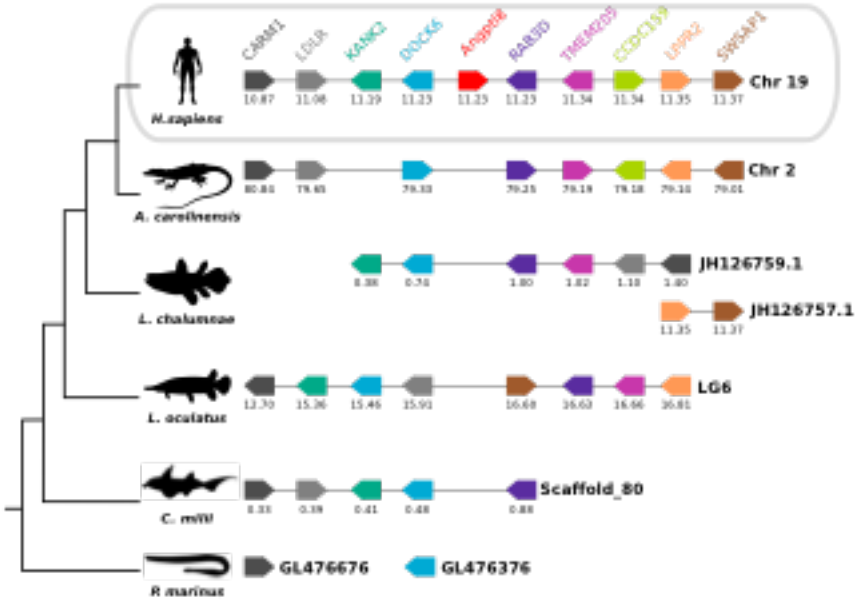


**Figure 3. 4 - Comparison of the homologous genome regions harbouring the human ANGPTL8 with fish.** The gene environment of the human ANGPTL8 gene was characterised and compared with the Anole lizard, the coelacanth (lobed-finned fish), the spotted gar (ray-finned fish), the elephant shark (cartilaginous fish) and the marine lamprey (jawless fish) homologue regions. Horizontal lines represent the chromosome fragments and arrow boxes indicate genes and arrowhead point to the direction of the predicted gene transcription. Gene names are indicated according to the human annotation and the same colours represent gene homologues and they are represented according to their order in the chromosome. The size of the genome fragments analysed and the predicted location of the gene in the chromosome is indicated in Megabase pairs (Mb). Gene names and symbols are: Coactivator-Associated Arginine Methyltransferase 1 (*CARM1*), Low Density Lipoprotein Receptor (*LDLR*), KN Motif And Ankyrin Repeat Domains 2 (*KANK2*), Dedicator Of Cytokinesis 6 (*DOCK6*), Member RAS Oncogene Family (RAB3D), Transmembrane Protein 205 (*TMEM205*), Coiled-Coil Domain Containing 159 (*CCDC159*), Lipid Phosphate Phosphatase-Related Protein Type 2 (*LPPR2*) and SWIM-Type Zinc Finger 7 Associated Protein 1 (*SWSAP1*).

In the spotted gar, the *angptl9* gene maps to LG1 and in the chicken to chromosome 3 and eight genes in linkage were identified. In the human genome a chromosome region was identified that was homologous to the gene environment flanking the fish *angptl9* gene even though the gene has been lost from mammalian genomes (figure 3.5). The genes that flank the *angptl9* gene in fish and in chicken are shared between two human chromosomes (chromosome

2 and 6) indicating reorganisation of this genome region during the radiation of mammals. Characterisation of the neighbouring gene environment of the duplicate teleost *angptl9* genes revealed that they map to genome regions that share a similar gene complement confirming that they emerged from the teleost genome tetraploidization.

The gene environment of the cephalochordate *angptl7* orthologue was also characterised (supplementary figure 3.4). Comparison of the gene environment of *angptl7* in fish (elephant shark, spotted gar, teleost and coelacanth) and tetrapods revealed similarity with cephalochordate scaffold_150 that houses amphioxus *angptl-like*_ii, iii and iv and suggests that vertebrate and cephalochordate *angptl7* shared a common ancestral origin. The neighbourhood of amphioxus *angptl-like*_i that maps to scaffold_598 shared no gene linkage with any of the vertebrate chromosomes/ scaffolds containing *ANGPTL* genes.

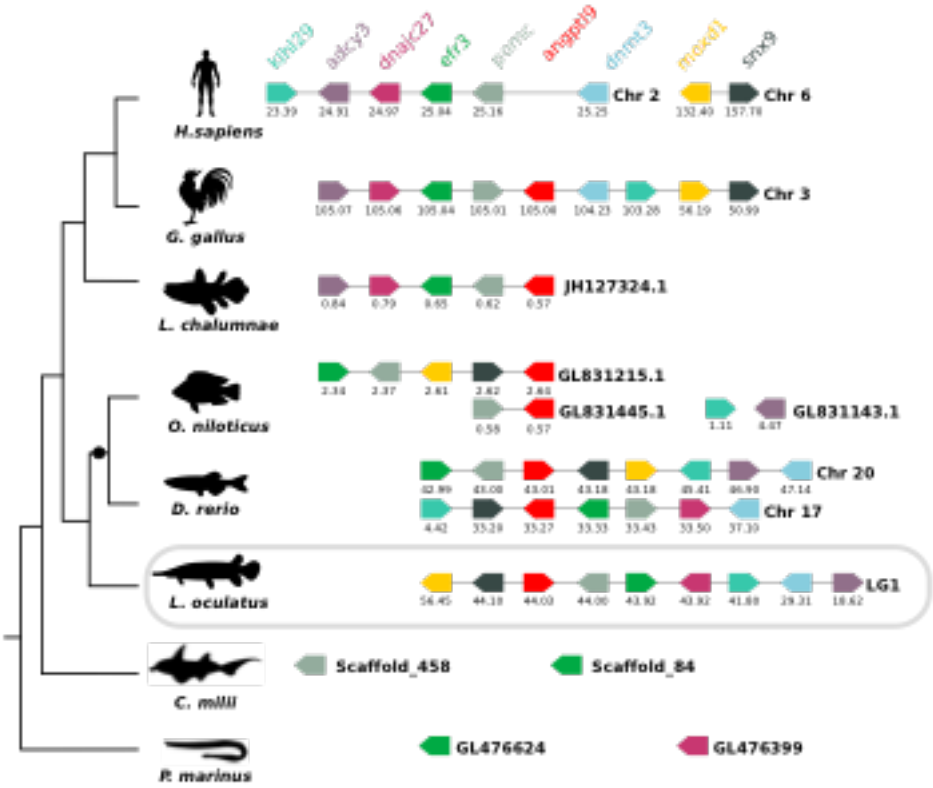


**Figure 3. 5 - Comparison of the homologous genome regions harbouring the fish *angptl9* with human.** The gene environment of the spotted gar *angptl9* gene was compared with the teleost (zebrafish and tilapia), coelacanth (lobe-finned fish), the elephant shark (cartilaginous fish) and the marine lamprey (jawless fish) and with the tetrapods chicken and human. Horizontal lines represent the chromosome fragments and arrow boxes indicate genes and arrowhead points to the orientation of the predicted gene transcription. Gene symbols are indicated and homologue genes are represented by the same colour and they are represented according to their order in the chromosome. The size of the genome fragments analysed and the location of the gene in the chromosome is indicated in Megabase pairs (Mb). are indicated in Megabase pairs (Mb). "●" represents the teleosts specific genome duplication (TSGD). Gene names and symbols are: kelch-like family member 29 (*klhl29*), adenylate cyclase 3 (*adcy3*), DnaJ (Hsp40) homolog, subfamily C member 27 (*dnajc27*), EFR3 (*efr3*), proopiomelanocortin (*pomc*), DNA(cytosine-5)-methyltransferase 3 (*dnmt3*), monooxygenase, DBH-like 1 (*moxd1*) and sorting nexin 9 (*snx9*).

### 3.4.5. Morphological and morphometric evaluation of sea bream intact and regenerating skin

Longitudinal transverse sections of intact and regenerating sea bream skin samples were used to characterize the ontogeny of the tissue regenerative response after scale removal (figure 3.6). The three typical layers, the epidermis, dermis and hypodermis were observed in histological sections of intact sea bream skin. The scales sat in individual scale pockets, inserted in the dermis and several layers of mineralized collagen were visible (figure 3.6A). The removal of scales tears and damages the epidermis, dermis and scale pocket and 1 day after scale removal (figure 3.6B) the torn edges of the ruptured epidermis although still attached to the skin left the dermis and scale pocket exposed directly to the aquatic milieu. Blood vessels were observed in the loose dermis but not in the compact dermis. Fast re-epithelialization of the epidermis occurred and two days after scale removal a new epidermis covered the dermis (figure 3.6C). A continuous basal layer and basal membrane were observed and formed an interface between the epidermis and the loose dermis. The scale papilla was also evident in the loose dermis two days after scale removal and delineated the location of the future scale pocket and new scale. Establishment of the external barrier was completed two days after scale removal (figure 3.6D) and numerous blood vessels were observed in the loose dermis. A thin layer of non-mineralized tissue was visible inside the scale pocket three days after scale removal and corresponded to the forming scale. By day 4 after scale removal (figure 3.6E) the structure of the regenerating skin already resembled that of the intact skin, although the mineralized scale was very thin and still did not correspond in thickness or size to the ontogenetic scale.

Morphometric evaluation of the sea bream skin (figure 3.7) revealed the most dramatic changes in the regenerating skin, where a marked increase in the thickness of the basement membrane ($p = 0.04$) was observed from 6h onwards and a progressive increase in the thickness of the epidermis ($p = 0.04$) was observed from 1 day onwards when compared to time 0. No changes in the thickness of the dermis were observed during the experiment ($p > 0.05$). In the intact skin the thickness of the epidermis ($22.87 \pm 1.151\mu m$), basement membrane ($2.53 \pm 0.121\mu m$) and dermis ($185.4 \pm 9.431\mu m$) remained constant throughout the healing period.

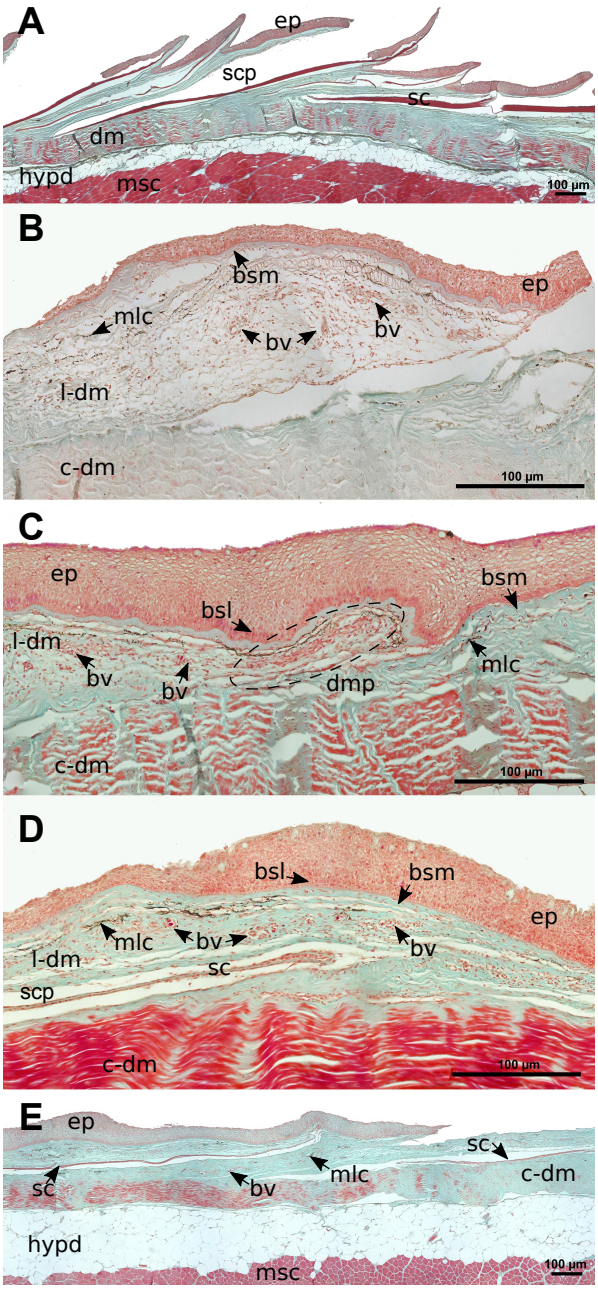


**Figure 3. 6 - Morphological evaluation of sea bream intact and regenerating skin (1, 2, 3 and 4 days after wounding) stained with Masson`s trichrome**. The posterior region of the scale is orientated to the right. Connective tissue is stained green and mineralized and collagen-rich tissues are stained bright red. **A**: Intact skin before scale removal. **B**, **C**, **D** and **E**: Regenerating skin at 1, 2, 3 and 4 days after wounding, respectively. ep: epidermis; dm: dermis; l-dm: loose dermis; c-dm: compact dermis; hypd: hypodermis; sc: scale: scp: scale pocket; msc: muscle; bsm: basement membrane; bsl: basal layer; dmp: dermal papilla; mlc: melanocytes; bv: blood vessel.

In order to access the recovery of the vascular system in regenerating skin during the healing process the number and diameter of the blood vessels in the different periods analysed were determined (figure 3.8). An increase in the number of blood vessels was observed at 6h after wounding in both regenerating ($p = 0.026$) and intact ($p = 0.033$) skin compared to time 0 (figure 3.8A). This was subsequently followed by a decrease in the number of blood vessels to

similar levels to that observed at time 0 and remained relatively constant ($p < 0.05$) during the 4-day recovery period analysed. Analysis of the blood vessel diameter (figure 3.8B) revealed that an increase in diameter was progressively observed during the first 24h post-wounding in regenerating skin. Blood vessel diameter was relatively constant in intact skin ($p > 0.05$). This revealed that the increase in blood vessel number 6h after wounding in both intact and damaged skin was not the consequence of vasodilation and suggests that new blood vessels were formed.

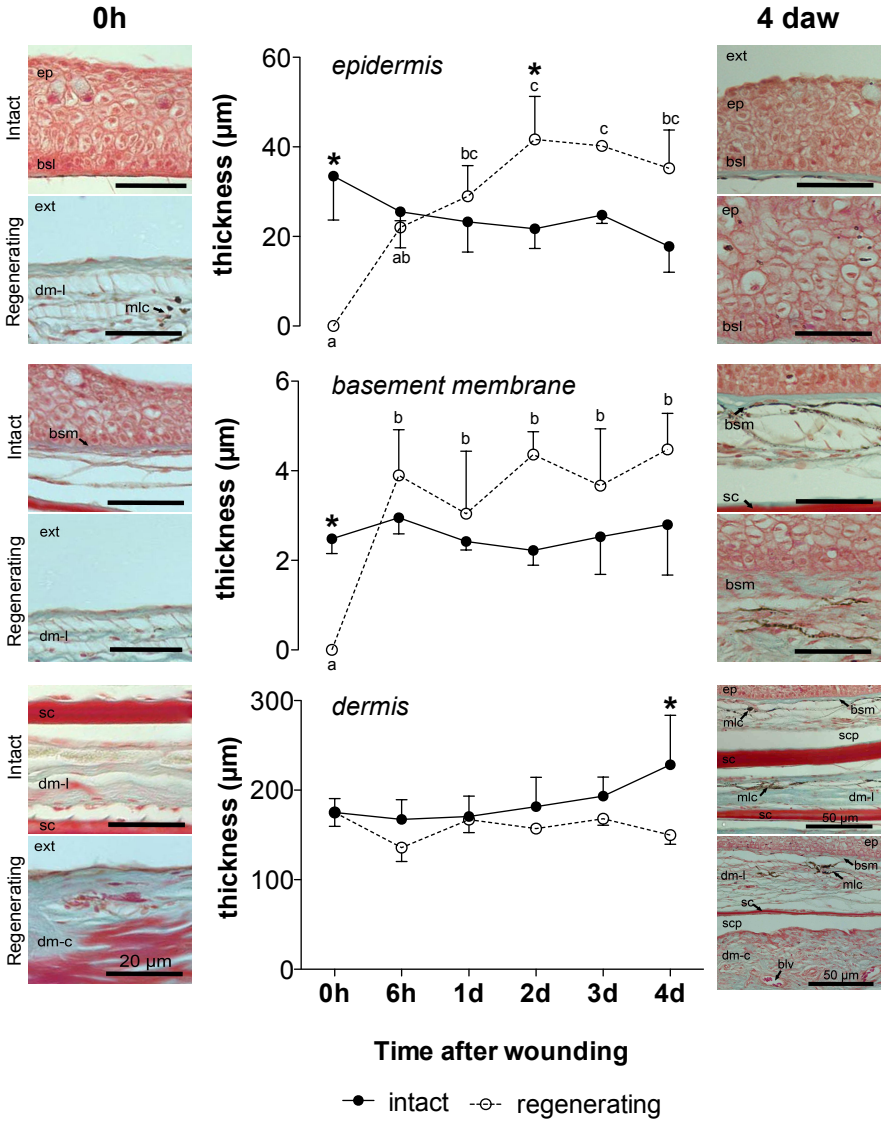


**Figure 3. 7 - Morphometric evaluation of sea bream skin during wound healing after scale removal.** The thickness of the epidermis, basement membrane and dermis during sea bream skin recovery after scale removal is represented. Each value represents the mean ± sem (n = 3). Statistical significance between groups was assessed using a two-way ANOVA followed by Fisher`s Least Significance Difference (LSD) post-test. Statistical significances were considered at $p < 0.05$ and differences in intact and regenerating skin during the experimental trial are annotated with different letters and comparisons between intact and regenerating skin at the same time point are signalled with an asterisk. A histological image of the skin layers at the start (0h) and end (4 days after wounding, daw) of the experimental trial is represented aside each graphs in order to illustrate the induced tissue aggression and the respective recovery with time. Ep: epidermis; bsl: basal layer; bsm: basement membrane; dm-l: loose dermis; dm-c: compact dermis; sc: scale; scp: scale pocket; mlc: melanocytes; blc: blood vessel; ext: exterior. Scale bars: 20 µm (scale bars alone) and 50 µm.

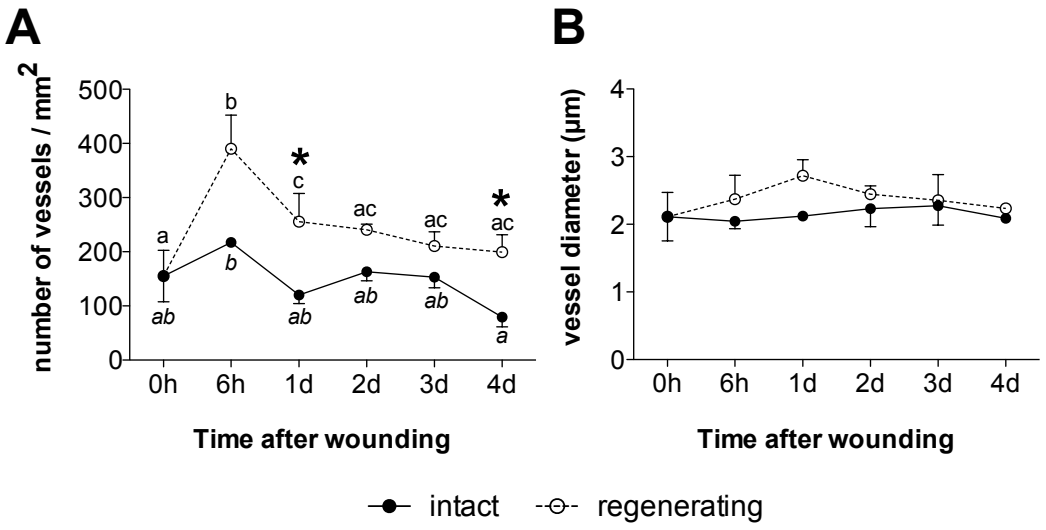


**Figure 3. 8 - Number of blood vessels (A) and blood vessel diameter (B) during skin wound healing in sea bream.** Each value represents the mean ± sem (n = 3). Statistical significance between groups was assessed using two-way ANOVA followed by Fisher`s Least Significance Difference (LSD) post-test. Statistical significances were considered at $p < 0.05$ and differences in intact and regenerating skin during the experimental trial are annotated with different letters and comparisons between intact and regenerating skin at the same time point are signalled with an asterisk

### 3.4.6. Expression of angptl family members during sea bream skin regeneration

Analysis of *angptl* transcript distribution in fish by analysing ESTs in NCBI revealed that they have a widespread tissue distribution (supplementary table 3.3). The results of *in silico* analysis indicated that *angptl2b*, *angptl3b*, *angptl4a*, *angptl4b*, *angptl7* and *angptl9b* transcripts are expressed in fish skin (table 3.2, supplementary table 3.3). Verification by qPCR using cDNA from sea bream skin confirmed the presence of *angptl1b*, *angptl2b*, *angptl4a*, *angptl4b* and *angptl7* transcripts but not *angptl3b* and *angptl9b* that were therefore excluded from further analysis.

The abundance of *angptl1b*, *angptl2b*, *angptl4a*, *angptl4b* and *angptl7* transcripts was evaluated during sea bream skin regeneration along with *vegfab*, a mediator of vascular development in zebrafish (Bahary et al. 2007) (figure 3.9). The transcript abundance of *angptl1b* and *angptl2b* was significantly increased (6h and 1d, $p < 0.05$) at initial stages of skin regeneration compared to the undamaged skin (from the other flank of the same fish) and subsequently decreased significantly (3d and 4d, $p < 0.05$). Correlation analysis revealed that the expression of both transcripts was correlated ($r = 0.55957$, $p < 0.001$) and suggests that they may regulate similar processes during the sea bream skin regeneration process.

**Table 3. 2 - Digital expression data of *angptls* in the teleost skin.** Searches were performed against the teleost NCBI database, sea bass skin transcriptome library (unpublished) and sea bream skin scale microarray probes (Vieira et al. 2011).

| | Teleost EST from skin | Seabass skin transcriptome | Sea bream skin microarray probes |
|---|---|---|---|
| *angptl1a* | ni | ni | ni |
| *angptl1b* | ni | ni | ni |
| *angptl2a* | ni | ni | ni |
| *angptl2b* | ni | 1050028/1053154 | ni |
| *angptl3a* | ni | ni | ni |
| *angptl3b* | ni | ni | SAPD06471_1/ SAPD06461_1 |
| *angptl4a* | ni | 1054686 | SAPD06461_2 |
| *angptl4b* | GH688340 | 1076279/1094540 | ni |
| *angptl5* | ni | ni | ni |
| *angptl6* | ni | ni | ni |
| *angptl7* | AM979347/DT055381 | 1091792 | SAPD09662_2 |
| *angptl9a* | ni | ni | ni |
| *angptl9b* | ni | 1099452 | ni |

In contrast, *angptl7* was significantly down-regulated from 6h to 4d ($p < 0.05$) in regenerating skin relative to intact skin at 0 time. The transcription of *angptl4a* and *angptl4b* was similar and was significantly down-regulated from 6h to 4d ($p < 0.05$) in regenerating skin relative to intact skin at 0 time. The change in transcript abundance over time of *angptl4a* and *angptl4b* were highly correlated ($r = 0.88358$, $p < 0.001$) and no significant differences in transcript abundance existed between intact and regenerating skin. Overall, the variable expression pattern of *angptls* in regenerating sea bream skin suggests they have different roles during skin regeneration in teleosts.

The relative expression of *angptl1b* (figure 3.9A) in intact skin taken from the undamaged flank of sea bream, decreased significantly from day 1 ($p = 0.00353$), 3 ($p = 0.01061$) to 4 ($p = 0.0087$) relative to the start of the experiment time 0. In regenerating skin, the relative abundance of *angptl1b* transcripts relative to skin at time 0 was significantly increased at 6h ($p = 0.01028$) up until day 2 and subsequently decreased at day 3 and 4 when it was significantly lower ($p = 0.00083$) than intact skin at time 0. Pair wise comparisons of *angptl1b* transcript abundance in intact and regenerating skin at each time point revealed significant up-regulation in regenerating skin at 6 hours ($p = 0.00053$) and 1 day ($p = 0.00015$) after scale removal.

*Angptl2b* (figure 3.9B) transcripts in intact skin were significantly decreased at 6h ($p = 0.00005$) and day 4 ($p = 0.01823$) when compared to 0 time. In contrast, in regenerating skin

*angptl2b* transcripts were significantly up-regulated ($p < 0.05$) at days 1, 2 and 3 and then strongly and significantly down-regulated at day 4 ($p = 0.01908$) compared to skin at time 0. Pair wise comparisons of intact and regenerating skin at each time point revealed that *angptl2b* transcripts were significantly up-regulated in the regenerating skin relative to intact skin at 6 hours ($p = 0.00069$) and 1 day ($p = 0.00011$) after scale removal (time 0).

*Angptl4a* and *angptl4b* (figure 3.9C and D) transcripts had a similar pattern of expression and their abundance decreased progressively after scale removal and were significantly down-regulated ($p < 0.001$) 1 day after scale removal in both intact and regenerating ($p < 0.001$) skin. Pair wise comparisons of intact and regenerating skin in the same individual at each time point did not reveal any significant differences in *angptl4a* and *angptl4b* transcript abundance.

Expression of *angptl7* was variable in both intact and regenerating skin samples over the 4 days of the experiment (figure 3.9E). In intact skin, a*ngptl7* transcripts were significantly down-regulated ($p = 0.002$) 6h after the start of the experiment, then significantly up-regulated at day 1 ($p < 0.001$) and day 3 ($p < 0.001$) relative to 6h. By day 4, a*ngptl7* transcript abundance in intact skin was similar to time 0. In regenerating skin, *angptl7* was significantly down-regulated ($p < 0.001$) at 6 h and day 1, 2 and 4 after scale removal relative to time 0. Comparison of a*ngptl7* transcripts in intact and regenerating skin of the same individual at each time point analysed revealed significant down-regulation ($p < 0.001$) of *angptl7* in regenerating skin 1 and 3 days after scale removal.

Expression of *vegfab* in intact skin increased progressively and was significantly up-regulated ($p = 0.0015$) from day 3 onwards when compared to skin at time 0 (figure 3.9F). In the regenerating skin, *vegfab* transcript abundance was not significantly different at any time point analysed. Pair wise comparison of *vegfab* transcripts in intact and regenerating skin of the same individual at each time point analysed did not reveal any significant differences. No significant correlation between *vegfab* and *angptl* transcript expression was found.

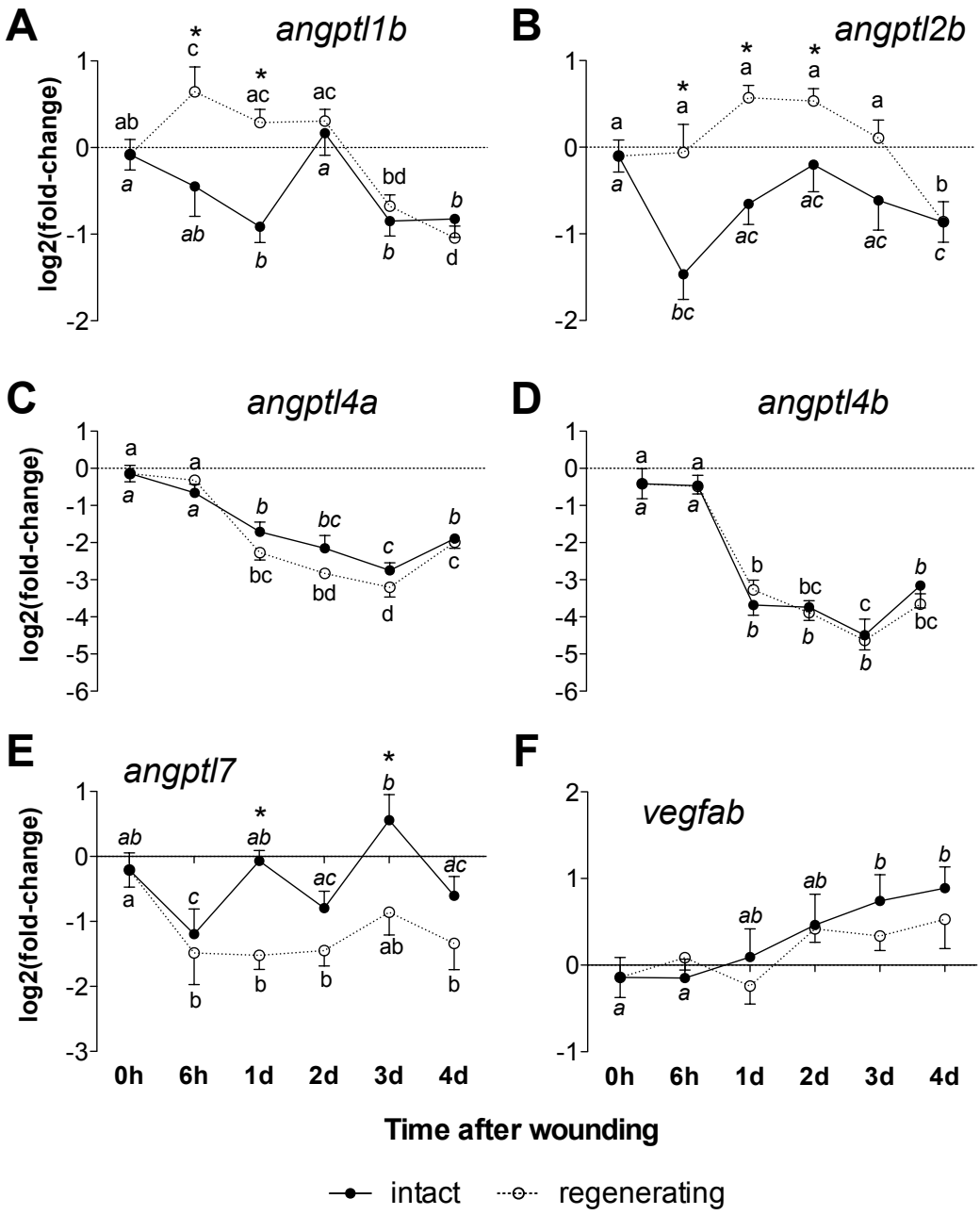


**Figure 3. 9 - Relative expression of the sea bream *angptl1b*, *angptl2b*, *angptl4a*, *angptl4b*, *angptl7* and *vegfab* in intact and regenerating skin.** Expression levels were obtained by qPCR and each value, that represents the mean ± sem (n = 6) of the relative expression (log2 (fold-change)), was estimated using the geometric mean of *rps18* and *ß-actin* in intact and regenerating skin at time 0 h, 6 h and days 1, 2, 3 and 4 after scales removal. Statistical significance between groups was assessed using two-way ANOVA followed by the Fisher`s Least Significant Difference (LSD) post-test. Statistical significances were considered at $p < 0.05$ and differences in intact and regenerating skin during the experimental trial are annotated with different letters and comparisons between intact and regenerating skin at the same time point are signalled with an asterisk.

## 3.5. Discussion

The Angptl family is a large family of multifunctional proteins that are involved in skin regeneration and regulate angiogenesis in mammals. In the present study we characterised for the first time fish Angptl gene repertoire and study their evolution in metazoans. In fish a new Angptl family member was found, Angptl9 that is absent from mammals but also present in non-mammalian genomes. The orthologues of the human Angptl8 was lost from fish and other vertebrate genomes and is exclusive to mammals. Duplicates of the human orthologues persisted in teleost genomes and were identified in the cephalochordate genome suggesting that they have emerged early prior to the vertebrate radiation.

We generated experimental data confirming the expression of Angptl family members in the integument of fish skin and conducted a skin regeneration experiment in the teleost sea bream to demonstrate the role of ANGPTL family members in skin regeneration has been conserved during evolution. In sea bream *angptl1b*, *angptl2b*, *angptl4a*, *angptl4b* and *angptl7* are expressed in skin and the abundance of *angptl1b*, *angptl2b* and *angptl7* was modified during skin regeneration. Their conserved role in skin function highlights their probable importance in tissue regeneration across the vertebrate.

### 3.5.1. *Angptl* members in fish

Homologues of the mammalian ANGPTLs exist in fish. In the teleost they have duplicated and phylogenetic analysis and gene synteny confirmed that they were the result of the lineage specific genome duplication (Jaillon et al. 2004). Some of the gene duplicates have persisted and the distinct number of ESTs retrieved for the *angptl* paralogues and their differential *in silico* distribution in skin suggests that after genome duplication functional specialization has occurred suggesting that they may have acquired a range of different physiological functions. ANGPTL genes were found from lamprey (a jawless fish and representative of the vertebrate ancestral genome) to coelacanth (a lobe-finned fish that diverged subsequently to the teleosts and is basal to the tetrapods) to mammals. The ANGPTL family members from fishes share highly conserved sequence and structure motifs with the human homologues and some of the residues of functional importance in the human protein have been maintained (Yau et al. 2009). The fish in common to the human homologues share two highly conserved and characteristic signature motifs of this family: the N-terminal coiled-coil domain (CCD), which likely contributes to protein oligomerization, and the C-terminal fibrinogen-like domain (FReD) that in the related ANGPT protein family are thought to be the receptor-binding domain (Brindle et al. 2006; Procopio et al. 1999). In fish ANGPTL the

presence of a conserved N-terminus signal peptide suggest that they are also secreted and the identification of conserved potential glycosylation consensus sites in the predicted proteins suggests that like the mammalian orthologues they are glycosylated proteins and may function as pleotropic endocrine/autocrine factors (Hato et al. 2008). In common with the human ANGPTLs, the fish members possess four conserved cysteine residues within the C-terminus FReD motif that potentially form two intramolecular disulphide bonds. However the importance in ANGPTL protein structure and function of the four conserved cysteine residues remains to be discovered as in the human ANGPTL4 alanine replacement studies failed to reveal functional modification (Shan et al. 2009). ANGPT proteins possess a further two conserved cysteine residues compared to ANGPTL and the resulting conformational difference between the two sets of proteins was proposed to be the basis of protein selectivity for distinct receptor families, although this remains to be confirmed (Hato et al. 2008).

A number of changes have occurred during the evolution of the ANGPTL family and a new vertebrate member, ANGPTL9 was found in the present study in non-mammalian vertebrates such as, fish, the *Xenopus*, Anole lizard and chicken. Gene synteny analysis suggests that the loss of ANGPTL9 from mammals was probably the result of chromosome rearrangements that occurred early during their radiation. Similarly, orthologues of the mammalian ANGPTL8 gene were absent from the sequenced genomes of fish and other non-mammalian vertebrates. ANGPTL8 is an atypical family member as it lacks the FReD domain, the glycosylation sites and the amino acids forming the intramolecular disulphide bonds but has an overlapping function with ANGPTL3 and 4 inhibiting lipoprotein lipase activity (Fu et al. 2013; Lee et al. 2009). The absence of a ANGPTL8 gene from non-mammalian vertebrates but the existence of a conserved homologue ANGPTL8 gene environment across the vertebrates suggests that the subsequent gene loss may be due to lineage specific gene deletions.

In mammals the FReD is essential for the angiogenic activity of the ANGPTL protein while the CCD domain seems to be more important for other physiological functions that include regulation of lipid metabolism by inhibition of lipoprotein lipase (Ono et al. 2003). The functional importance of ANGPTL proteins and their duplicates in fish physiology is unknown but given their higher sequence homology with mammalian orthologues we hypothesize that depending on the physiological context they may share conserved roles. In fact, in the zebrafish, the only teleost where members of this family were previously been described, the human orthologues ANGPTL1, 2 and 6 are ubiquitously expressed and overlapping expression in tissues in which they are expressed in human and the zebrafish ANGPTL1 and 2 seemed to have a conserved role with the human orthologues in vertebrate vascular development (Kubota

et al. 2005a; Kubota et al. 2005b). Although care needs to be taken as the number of transcripts retrieved is conditioned to the tissue libraries available, the *in silico* identification in this study of many teleost Angptl EST transcripts from many tissue origins confirmed their widespread distribution and the distinct number of ESTs identified for each family member may be suggestive of their relative abundance.

Recently, ANGPTLs were found to activate immune inhibitory receptors of the leukocyte immunoglobulin (Ig)-like family a group of innate immune receptors that are expressed on the immune cells and involved in the control of the inflammatory responses and cytotoxicity (Zheng et al. 2012). Studies on the human ANGPTL2 and its receptor (LILRB2) found that neither the CCD nor the FReD binds to LILRB2. The authors suggested that ligand-receptor interaction occurs via the receptor immunoglobulin domain and that ANGPTL2 protein multimerization was essential for downstream signalling (Deng et al. 2014). Receptors for the fish ANGPTL are currently unknown, although potential immunoglobulin-like receptor transcripts have been described in fish and it will be important to establish if they have similar roles to those found in mammals (Stet et al. 2005).

### 3.5.2. ANGPTL emerged early and evolved via gene duplications and deletions

In vertebrates, ANGPTL evolved via gene duplication and deletions events and they are proposed to have shared common evolutionary origin with ANGPT, with which they share sequence and structure similarities. Four main ANGPTL vertebrate protein clusters that are suggested to have emerged from gene precursors that derived from duplications of the ancestral ANGPTL gene exist. The vertebrate ANGPTL1/2/6, ANGPTL3/4 and ANGPTL7/9 members arose from subsequent gene duplication events that likely occurred during the two rounds of genome doubling events early during the vertebrate radiation (Putnam et al. 2008; Dehal and Boore 2005; Ohno 1970). The teleost is by far the most successful and diverse group of vertebrates and more than 23.000 species have been identified (Venkatesh 2003). An explanation for this success is linked to the teleost specific genome duplication that is proposed to have provided the raw material for evolutionary adaptation and innovation (Glasauer and Neuhauss 2014). The phylogenetic analysis indicates that the ANGPTL genes duplicated early in the teleost radiation and was followed by gene loss so that in extant teleost genomes only a few paralogues persisted (Brunet et al. 2006). In the coelacanth species-specific gene duplication affected ANGPTL5 and the duplicates maps in tandem to the same genome fragment and their clustering in the phylogenetic tree suggests that their sequence has diverged

considerably from the other vertebrates. The identification of only two ANGPTLs (ANGPTL2 and 5) in lamprey and the non-identification of ANGPTL5, 6 and 9 in the cartilaginous fish genomes may be a consequence of their incomplete genome assemblies or linked to their unique physiological adaptations (skeleton, metabolism, ion regulation) to the aquatic environment and the associated gene deletions after their divergence from the common vertebrate ancestor.

Members of the ANGPTL family were suggested to have emerged prior to the vertebrate radiation and a sea squirt (*Ciona intestinalis*) gene homologue was found to be equally similar to the different vertebrate members (Doolitlle et al. 2012). We have also found other predicted ANGPTL-like genes in the genomes of several other early deuterostome species but their similarity with vertebrate ANGPTL family members were very low. The exception was the cephalochordate (*Branchiostoma floridae*) genome where 5 ANGPTL-like genes were found. The cephalochordate ANGPTL-like clustering revealed four of the genes were orthologues of the vertebrate ANGPTL7 gene cluster. Furthermore, the conserved gene environment flanking the cephalochordate ANGPTL-like genes and the vertebrate ANGPTL7 suggests that the ancestral gene emerged prior to the vertebrate radiation. The appearance of the ancestral ANGPTL family in the gene precursors of the cephalochordate suggests they may be a functional innovation linked with changes in organism complexity and physiology.

Proteins with FReD domain, such as Fibronectins, Ficolins and Tenascin are found in a variety of animal genomes and they are considered to have been one of the first groups of proteins to appear (Doolitlle et al. 2012). Putative proteins that share sequence similarity for the vertebrate ANGPTLs were found when screening protostome genomes but their identity as real ANGPTL was not confirmed and they may be part of other containing FReD protein families. We found a putative ANGPT in a cephalochordate, the amphioxus, even though these genes were previously proposed to be absent from urochordates based on genomic studies of a tunicate, the sea squirt (*C. intestinalis*) (Doolitlle et al. 2012). The present results reveal genome diversity, no doubt linked to organism biology, between urochordates (amphioxus and tunicate) commonly used as a proxy to better comprehend chordate genome evolution and our observations of the ANGPTL family confirms the notion that the tunicates have undergone higher gene loss and genome rearrangements (Louis et al. 2012).

### 3.5.3. Wound healing and Angptls expression in sea bream skin

In mammals wound healing is a complex and highly coordinated sequence of events triggered by blood clotting, followed by inflammation, vascularization, formation of granulation tissue and remodelling (Olczyk et al. 2014). In fish re-epithelialization of damaged

skin from the wound margins is independent of inflammatory signals from the blood clot or increased vascularization and starts immediately after wounding (Richardson et al. 2013; Quilhac and Sire 1999). Nonetheless, the formation of new blood vessels (vascularization) is critical to the initial stages of wound healing in all vertebrates and the inflammatory signals of TGFß and FGFR1 are necessary for fibroblast recruitment, granular tissue formation and vascularization and play a significant role in each stage of the healing process (Olczyk et al. 2014; Richardson et al. 2013). In this study, tissue re-epithelialization of the epidermis and organization of the dermal papillae to define the new scale pockets are the main morphological events that are induced. The re-establishment of the epithelial barrier was totally complete 2 days after trauma when epidermis thickness progressively increases in regenerating skin. The scale papilla was formed and the location of the future scale pocket and new scale is established.

To ensure correct recovery of the damaged tissue new blood vessels are formed from pre-existing vessels in the dermis. Endothelial cell migration is essential for angiogenesis and requires the activation of several signalling pathways and involves degradation of the extracellular matrix to enable progression of the migrating cells and cytoskeletal remodelling (Lamalice et al. 2007). In mammalians the formation of new blood vessels initiates 3 days after wounding (Olczyk et al. 2014) but in the fish skin this process initiates earlier. In a zebrafish skin recovery model the formation of blood vessels were initiated 1 day after wounding after a full thickness wound where epidermis and dermis were lost (Richardson et al. 2013). In our model of fish skin regeneration, a larger and superficial damaged was induced and only the loose dermis was affected. An increase in the number of blood vessels was observed 6h after wounding in both regenerating and intact skins suggesting that new blood vessels are formed soon after wounding nonetheless the increase in expression of the *vegfab* blood vessel maker was observed 24h onwards. In teleost two *vegfa* genes exist resulting from the teleost tetraploidization (Jaillon et al. 2004) and remains to be establish the role of the *vegfa* paralogue in our sea bream skin healing model. In the future characterisation of this and of other angiogenic factors such as angiotensins should be carried out to investigate their relative importance in the remodelling of the fish skin vasculature during the initial stages of tissue recovery.

The existence and expression in both mammalian and fish skins of some of the ANGPTL family members, their link with integument repair and specifically in the sea bream their co-ordinated appearance with key steps of the repair program suggests they are of

physiological importance during regeneration and their role in vertebrate skin homeostasis is conserved. The variable pattern of expression of *angptl* family members during wound healing and the significant differences between regenerating and intact skins within the initial 48h post-wounding suggests they may play important and distinct roles in tissue re-epithelisation and angiogenesis. In zebrafish and mice *angptl1* and *angptl2* cooperate to induce apoptosis of endothelial cells and regulate vascular development (Kubota et al. 2005a; Kadomatsu et al. 2014). In mice *angptl2* induces a pro-inflammatory response and activates resident murine peritoneal monocytes and macrophages (Umikawa et al. 2015). It was not possible to directly establish the role of *angptl1b* and *angptl2b* in sea bream wound healing but their up-regulation early in tissue regeneration and subsequent decreased be linked to both angiogenic and pro-inflammatory effects.

In mammals, ANGPTL4 has a range of attributed biological roles. In the skin of ANGPTL4-knockout mice there is consistent down-regulation of numerous genes involved in epidermal differentiation and proliferation (Pal et al. 2011) and this protein was found to modulate cell-matrix protein communication during the murine wound healing. Furthermore, when *Angptl4* was expressed under the control of the keratinocyte promoter (K14) the K14-Angptl4 transgenic mice no increased vascularity in skin was observed when compared to control (Ito et al. 2003). The up-regulation of *angptl4* previously reported in regenerating sea bream skin 3 days after scale removal was associated with fasting rather than skin repair (Vieira et al. 2011) suggesting a functional link with control of lipoprotein and glucose metabolism as described for mammals (Oike et al. 2005). In our model, expression of both paralogues were strongly down-regulated in both intact and regenerating skin from 1 – 3 days' post damage suggesting that the initial re-epithelisation and increase of blood vessels is probably followed by inhibition of epidermal differentiation and proliferation as tissue rebuilding occurs.

In humans *Angptl7* was recently demonstrated to be an anti-angiogenic factor. In the cornea *in vitro* using HUVECs co-cultured with human corneal keratocytes (HCKs) and *in vivo* using mouse corneas (Toyono et al. 2015) indicated that ANGPTL7 might be responsible for maintaining the avascularity of the cornea in human eye (Comes et al. 2011). Our results suggest that the function of *angptl7* in sea bream skin seems to be conserved with that of the human and the decreased expression during the healing period in regenerating skin might favour angiogenesis and/or increased leakage from the blood vessels.

Scale removal had not only a local but also a systemic effect, reflected by the differential responses between the intact and regenerating skin of the same individual. The combination of both effects (local and systemic) eventually culminates with skin and scale recovery to the

ontogenetic shape and size. During the sea bream wound healing process expression of *angptl1b*, *2b* and *7* were distinct in both intact and regenerating skin and in the future it will be important to determine which cells are actively producing and secreting angptl members in fish skin and their distinct contributions to the maintenance of skin homeostasis.

### 3.6. Conclusion

The present study provides a comprehensive description of the evolution of the ANGPTLs genes in vertebrates and provides evidence for their conserved role in the regulation of skin regeneration using a sea bream regeneration skin model. ANGPTLs are a large conserved protein family in vertebrates that expanded in the teleosts. Mining vertebrate genomes revealed the existence of a novel family member (ANGPTL9) that was subsequently eliminated from the mammalian genomes and that ANGPTL8 only exist in mammals. In teleost *angptl* gene duplicated and some persisted in their genome. In sea bream, *angptl1b*, *angptl2b*, *angptl4a*, *angptl4b* and *angptl7* are expressed in skin and they seem to participate in skin recovery and to play a conserved role in the regulation of tissue re-epithelialization and angiogenesis in vertebrates. Their distinct expression during the healing period and between intact and regenerating skins, the potential involvement of other ANGPTL family members and other angiogenic factors suggests that as in mammals skin wound healing in fish is a complex process that remains to be fully understood. A*ngptl* expression in sea bream intact skin suggesting that they are also involved not only in the local response to damage but may also play an important role in the systemic skin response which remained to be further studied in the future.

### 3.7. Acknowledgements

This study was supported by Lifecycle EU-FP7 222719 and by national funds from FCT - Foundation for Science and Technology through project UID/Multi/04326/2013. RAC is funded by FCT SFRH/BD/81625/2011 grant and JCRC is supported by an auxiliary research contract under the project UID/Multi/04326/2013.

## 3.8. Supplementary material

**Supplementary table 3. 1 - Accession numbers of the fish, tetrapod and cephalochordate Angptl genes and transcripts.** * eliminated from tree as they were very incomplete; ni-not identified (*continuous in the next page*)

| | *angptl1* | *angptl2* | *angptl3* | *angptl4* | *angptl5* | *angptl6* | *angptl7* | *angptl8* | *angptl9* |
|---|---|---|---|---|---|---|---|---|---|
| ***Lepisosteus oculatus*** | ENSLOCG0000001 0528 | ENSLOCG0000000 1221 | ENSLOCG0000000 6610 | ENSLOCG0000000 2629 | ENSLOCG0000000055 94 | ENSLOCG00000007 369 | ENSLOCG0000000 6427 | ni | ENSLOCG00000 016685 |
| ***Leucoraja erinacea*** | Contig765 * | Contig17088 | ni | Contig63247 | ni | ni | Contig20369 | | |
| ***Callorhinchus milii*** | SINCAMG0000000 1650 | SINCAMG0000000 8104 | SINCAMG0000001 3226 | SINCAMG0000000 1584 | ni | ni | SINCAMG0000000 6852 | ni | ni |
| ***Petromyzon marinus*** | | ENSPMAG0000000 7297 | | | ENSPMAG000000006 563 | | | | |
| ***angptl-like Branchiostoma floridae*** | **Amphioxus_i** fgenesh2_pg.scaffol d_598000005 | **Amphioxus_ii** estExt_fgenesh2_pg. C_1500064 | **Amphioxus_iii** fgenesh2_pg.scaffol d_150000064 | **Amphioxus_iv** fgenesh2_pg.scaffol d_150000065 | **Amphioxus_v** fgenesh2_pg.scaffold_ 18000225 | | | | |

| | *angptl1* | *angptl2* | *angptl3* | *angptl4* | *angptl5* | *angptl6* | *angptl7* | *angptl8* | *angptl9* |
|---|---|---|---|---|---|---|---|---|---|
| ***Homo sapiens*** | ENSG00000116194 | ENSG00000136859 | ENSG00000132855 | ENSG00000167772 | ENSG00000187151 | ENSG00000130812 | ENSG00000171819 | ENSG00000130173 | ni |
| ***Mus musculus*** | ENSMUSG00000033544 | ENSMUSG00000004105 | ENSMUSG00000028553 | ENSMUSG00000002289 | ni | ENSMUSG00000038742 | ENSMUSG00000028989 | ENSMUSG00000047822 | ni |
| ***Monodelphis domestica*** | ENSMODG00000006041 | ENSMODG00000019796 | ENSMODG00000001506 | ENSMODG00000003801 | ENSMODG00000000550 | ENSMODG00000005137 | ENSMODG00000011148 | | ni |
| ***Gallus gallus*** | ENSGALG00000004290 | ENSGALG00000000927 | ENSGALG00000010978 | ENSGALG00000000619 | ENSGALG00000017191 | ENSGALG00000026633 * | ENSGALG00000003179 | ni | ENSGALG00000016599 |
| ***Xenopus tropicalis*** | ENSXETG00000030481 | ENSXETG00000021762 | ENSXETG00000010849 | ENSXETG00000021893 | ENSXETG00000005480 | ENSXETG00000030201 | ENSXETG00000017425 | ni | ENSXETG00000030926 |
| ***Anolis carolinensis*** | ENSACAG00000013089 | ENSACAG00000004716 | ENSACAG00000022908 | ni | ENSACAG00000012817 | ENSACAG00000003753 | ENSACAG00000000578 | ni | ENSACAG00000011446 |
| ***Latimeria chalumnae*** | ENSLACG00000010805 | ENSLACG00000014379 | ENSLACG00000005221 | ENSLACG00000017018 | a: ENSLACG00000016680<br>b: ENSLACG00000016758 | ENSLACG00000001623 | ENSLACG00000016342 | ni | ENSLACG00000011131 |
| ***Tetraodon nigroviridis*** | a: ENSTNIG00000010854<br>b: ENSTNIG00000007861 | ni<br>b: ENSTNIG00000019518 | ni<br>b: ENSTNIG00000007852 | a: ENSTNIG00000011062<br>b: ENSTNIG00000010200 | ENSTNIG00000009987 | ENSTNIG00000018563 | ENSTNIG00000005716 | ni | a: ENSTNIG00000016374<br>ni |
| ***Takifugu rubripes*** | a: ENSTRUG00000018466<br>b: ENSTRUG00000009057 | ni<br>b: ENSTRUG00000009281 | a: ENSTRUG00000018512<br>b: ENSTRUG00000002130 | a: ENSTRUG00000009245<br>b: ENSTRUG00000007525 | ENSTRUG00000017085 | ENSTRUG00000007516 | ENSTRUG00000009793 | ni | a: ENSTRUG00000013428<br>ni |
| ***Gasterosteus aculeatus*** | a: ENSGACG00000014590<br>b: ENSGACG00000016264 | a: ENSGACG00000018304<br>b: ENSGACG00000012019 | a: ENSGACG00000006902<br>b: ENSGACG00000016212 | a: ENSGACG00000015561<br>b: ENSGACG00000008217 | ENSGACG00000020628 | ENSGACG00000009845 | ENSGACG00000004901 | ni | a: ENSGACG00000010188<br>b: ENSGACG00000009530 |
| ***Dicentrarchus labrax*** | a: DLAgn00151810<br>b: DLAgn00245390 | a: DLAgn00080000<br>b: DLAgn00115210 | a: DLAg00146540<br>b: DLAgn00002570 | a: DLAgn00003870<br>b: DLAgn00147460 | DLAgn00042700 | DLAgn00191570 | DLAgn00134200 | ni | a: DLAgn00069630<br>b: DLAgn00197180 |
| ***Sparus aurata*** | a: Contig4701<br>b: SRR278741_isotig41953_Contig8996 | a: contig_SRR278741_isotig12348<br>b: contig_Contig12895_Contig8692 | ni<br>b: gi\|207963140 | a: Contig17088<br>b: Contig2898 | Contig9187 * | ni | Contig8383 | ni | a: SRR278741_isotig81803<br>ni |
| ***Oreochromis niloticus*** | a: ENSONIG00000002729<br>b: ENSONIG00000018643 | a: ENSONIG00000011544<br>b: ENSONIG00000010908 | a: ENSONIG00000008833<br>b: ENSONIG00000018623 | a: ENSONIG00000010501<br>ni | ENSONIG00000004892 | ENSONIG00000001601 | ENSONIG00000009286 | ni | a: ENSONIG00000013537<br>b: ENSONIG00000007236 |
| ***Oryzias latipes*** | a: ENSORLG00000014624<br>b: ENSORLG00000010138 | ni<br>b: ENSORLG00000013351 | a: ENSORLG00000010477 | a: ENSORLG00000005296<br>ni | ENSORLG00000005584 | ENSORLG00000005649 | ENSORLG00000000502 | ni | a: ENSORLG00000017323<br>b: ENSORLG00000000631 |
| ***Xiphophorus maculatus*** | a: ENSXMAG00000011442<br>b: ENSXMAG00000018324 | ni<br>b: ENSXMAG00000000203 | a: ENSXMAG00000010042<br>b: ENSXMAG00000000947 | a: ENSXMAG00000013934<br>b: ENSXMAG00000002569 | ENSXMAG00000010840 | ENSXMAG00000018050 | ENSXMAG00000001358 | ni | a: ENSXMAG00000003752<br>b: ENSXAM00000001233 |
| ***Gadus morhua*** | a: ENSGMOG00000016021<br>b: ENSGMOG00000016921 | ni<br>b: ENSGMOG00000006472 | a: ENSGMOG00000018204<br>b: ENSGMOG00000005911 | a: ENSGMOG00000010268<br>b: ENSGMOG00000001102 | ENSGMOG00000002183 | ni | ENSGMOG00000009770 | ni | a: ENSGMOG00000013023<br>b: ENSGMOG00000009664 |
| ***Danio rerio*** | a: ENSDARG00000012071<br>b: ENSDARG00000100159 | a: ENSDARG00000024030<br>b: ENSDARG00000068369 | a: ENSDARG00000044365<br>ni | a: ENSDARG00000035859<br>ni | ENSDARG00000056630 | ENSDARG00000020265 | ENSDARG00000027582 | ni | a: ENSDARG00000069305<br>b: ENSDARG00000012581 |
| ***Astyanax mexicanus*** | a: ENSAMXG00000005069<br>b: ENSAMXG00000009072 | a: ENSAMXG00000008131<br>b: ENSAMXG00000014684 | a: ENSAMXG00000010542<br>ni | a: ENSAMXG00000004641<br>ni | ENSAMXG00000004821 | | ENSAMXG00000014537 | ni | a: ENSAMXG00000006528<br>b: ENSAMXG00000011865 |

**Supplementary table 3. 2 - Percent of sequence identity/similarity of the fish Angptl members with the human orthologues.** Proteins are grouped according to the family clustering given by the phylogenetic analysis (figure 3.2).

| | ANGPTL1 | ANGPTL2 | ANGPTL3 | ANGPTL4 | ANGPTL5 | ANGPTL6 | ANGPTL7 |
|---|---|---|---|---|---|---|---|
| Coelacanth | 72 /85 | 69 /82 | 52 /72 | 34 /53 | a: 21 /28<br>b: 25 /37 | 38 /53 | 70 /84 |
| Seabass | a: 59 /74<br>b: 59 /74 | a: 67 /77<br>b: 73 /81 | a: 40 /59<br>b: 37 /56 | a: 35 /49<br>b: 31 /45 | 47 /65 | 40 /55 | 62 /77 |
| Zebrafish | a: 59 /73<br>b: 49 /69 | a: 69 /77<br>b: 73 /81 | 40 /61 | 34 /49 | 47 /67 | 39 /53 | 64 /77 |
| Spotted gar | 61 /75 | 80 /87 | 43 /62 | 35 /51 | 55 /74 | 41 /52 | 63 /77 |
| Elephant shark | 61 /76 | 69 /80 | 39 /58 | 26 /39 | | | 65 /82 |

**Supplementary table 3. 3 - List of the teleost *angptl* ESTs and their origin.** Data was retrieved from NCBI database using the sea bass members as queries. ESTs isolated from skin and also from teleost fins, bony structure covered with skin.

| | *SPECIES* | *EST* | *ORIGIN* |
|---|---|---|---|
| ***angptl1*** | | | |
| ***a*** | *Fundulus heteroclitus* | EV457512 | mixed |
| | *Gasterosteus aculeatus* | DN679836 | eyes |
| | *Haplochromis sp.* | BJ690922 | jaw |
| | *Osmerus mordax* | EL545667 | brain, kidney, spleen |
| | *Pimephales promelas* | DT207144 | brain |
| | *Danio rerio* | DY556787 | whole body |
| | *Oncorhynchus mykiss* | BX880889 | multi tissues |
| | | GR631620 | juveniles |
| ***b*** | *Solea senegalensis* | FF289610 | larva |
| ***angptl2*** | | | |
| ***a*** | *Astyanax mexicanus* | FO240466 | embryo |
| ***b*** | *Astyanax mexicanus* | FO240466 | embryo |
| | *Danio rerio* | EV758705 | fin blastema |
| | *Astyanax mexicanus* | FO292812 | embryo |
| | | FO261668 | embryo |
| | *Danio rerio* | EH447322 | brain |
| | | GW710929 | liver |
| | | GW711475 | liver |
| | | EH594391 | embryo |
| | | CK017217 | whole |
| | | AI497474 | liver |
| | *Fundulus heteroclitus* | DR441996 | gill, epithelium, liver, kidney, intestine, brain, muscle |
| | | DR441921 | gill, epithelium, liver, kidney, intestine, brain, muscle |
| | | CN982795 | liver |
| | *Gasterosteus aculeatus* | DW623632 | larva |
| | | DW623633 | larva |
| | *Nothobranchius furzeri* | DW623632 | larva |
| | | JZ205315 | whole |
| | *Salmo salar* | CK877205 | gills |
| | | DY739459 | brain, kidney, spleen |
| ***angptl3*** | | | |
| ***a*** | *Dicentrarchus labrax* | AM985545 | corpuscles of stannius |
| | | FM023639 | spleen |
| | *Gasterosteus aculeatus* | DW650503 | whole larva |
| | | DN678953 | eyes |
| | | DN661953 | gill |
| | *Ictalurus punctatus* | FD330641 | liver, pituitary, ovary and testes |
| | | FD354173 | liver, pituitary, ovary and testes |
| | *Oncorhynchus mykiss* | BX859662 | multi tissues |
| | *Osmerus mordax* | EL550631 | brain, kidney, spleen |
| | | EL546937 | brain, kidney, spleen |
| | | EL541764 | brain, kidney, spleen |
| | *Osmerus mordax* | EL550631 | brain, kidney, spleen |
| | | EL546937 | brain, kidney, spleen |
| | | EL541764 | brain, kidney, spleen |
| | *Perca flavescens* | GO572899 | brain |
| | *Pimephales promelas* | DT101316 | whole |
| | | DT361649 | liver |
| | | DT250496 | brain |
| | | DT233776 | brain |
| | | DT121688 | whole |
| | | DT156280 | whole |
| | | DT183404 | whole |

| | | | |
|---|---|---|---|
| ***b*** | none | none | none |
| ***angptl4*** | | | |
| ***a*** | *Carassius auratus* | AM925464 | olfactory epithelium |
| | *Danio rerio* | CK704410 | embryo |
| | | DT081717 | whole |
| | | CA470959 | kidney |
| | | CN323884 | whole |
| | | EE712569 | whole |
| | | CA470970 | kidney |
| | | DR720443 | whole |
| | | AW421268 | kidney |
| | | EE684289 | whole |
| | *Dicentrarchus labrax* | FM015083 | adipose tissue |
| | *Gasterosteus aculeatus* | DW642206 | larva |
| | | DT967252 | larva |
| | | DN714238 | larva |
| | | DV008747 | brain |
| | | DV004396 | brain |
| | | DT979570 | larva |
| | | DT967559 | larva |
| | *Ictalurus punctatus* | FD337910 | liver, pituitary, ovary and testes |
| | | CK419825 | ovary |
| | | FD366593 | liver, pituitary, ovary and testes |
| | | FD337313 | liver, pituitary, ovary and testes |
| | | FD321694 | liver, pituitary, ovary and testes |
| | | FD363847 | liver, pituitary, ovary and testes |
| | | GH688340 | head kidney, gill, intestine, spleen, skin and liver |
| | *Nothobranchius furzeri* | JZ281985 | whole |
| | *Oncorhynchus mykiss* | BX878049 | multi-tissues |
| | *Oryzias latipes* | AM374053 | embryo |
| | *Osmerus mordax* | EL529931 | brain, kidney, spleen |
| | *Perca flavescens* | GO654217 | ovary |
| | *Pimephales promelas* | GH715226 | kidney |
| | | DT085020 | whole |
| | *Rutilus rutilus* | EG548328 | gonads |
| | *Salmo salar* | DY707303 | brain, kidney, spleen |
| | | GE772875 | brain, kidney, spleen |
| ***b*** | *Gasterosteus aculeatus* | DW634900 | whole |
| | *Osmerus mordax* | EL529931 | brain, kidney, spleen |
| ***angptl5*** | *Danio rerio* | BM316886 | testis |
| | *Gasterosteus aculeatus* | DN699831 | larva |
| | | DN665907 | gills |
| | | DW596554 | eyes |
| | | DN665908 | gills |
| | | DN699832 | larva |
| | *Ictalurus punctatus* | FD272202 | whole |
| | | FD168715 | stomach, muscle, olfactory tissue and trunk kidney |
| | *Osmerus mordax* | EL537133 | brain, kidney, spleen |
| ***angptl6*** | none | none | none |
| ***angptl7*** | *Astyanax mexicanus* | FO365467 | embryo |
| | *Cyprinus carpio* | AU301661 | barbel |

| | | | |
|---|---|---|---|
| | *Danio rerio* | CT607729 | myoblast |
| | | EH593212 | embryo |
| | | DV594748 | olfactory epithelium |
| | | CT607380 | myoblast |
| | | CT638984 | myoblast |
| | | CK705286 | embryo |
| | | CN024346 | olfactory epithelium |
| | | CT617645 | myoblast |
| | | CN328568 | larvae |
| | | CK681510 | embryo |
| | | CT727753 | myoblast |
| | | CK714214 | embryo |
| | | BQ260309 | fin regeneration |
| | | CT641693 | myoblast |
| | | DV591176 | olfactory epithelium |
| | | EV758402 | fin |
| | | BF938099 | fin |
| | | CT619072 | myoblast |
| | | CK676887 | embryo |
| | | DV584729 | olfactory epithelium |
| | | CT696769 | myoblast |
| | | DT055381 | skin |
| | | CN017697 | olfactory epithelium |
| | | K700210 | embryo |
| | *Dicentrarchus labrax* | FM026002 | muscle |
| | *Gadus morhua* | GW856161 | eye |
| | *Gasterosteus aculeatus* | DN707956 | whole larva |
| | | DW609887 | whole larva |
| | | DT953523 | gills |
| | | DN692607 | eyes |
| | | DN702547 | whole larva |
| | | DT960268 | gills |
| | | DN678934 | eyes |
| | | DN702546 | whole larva |
| | *Ictalurus punctatus* | FD082683 | stomach, muscle, olfactory tissue, trunk kidney |
| | | FD280203 | whole fish |
| | *Oncorhynchus mykiss* | BX083906 | multi-tissues |
| | *Oreochromis niloticus* | GR652150 | heart |
| | *Oryzias latipes* | DK162082 | embryo |
| | | AM298930 | whole embryo |
| | | AM299515 | whole embryo |
| | *Paralichthys olivaceus* | FE042867 | gill |
| | *Poecilia reticulata* | ES385841 | embryo |
| | *Salmo-salar* | DY728205 | brain, kidney, spleen |
| | | EG783580 | thymus |
| | | EG844413 | thyroid |
| | | CK876680 | eye |
| | | EG840288 | thyroid |
| | | EG879077 | thyroid |
| | *Sparus aurata* | DY728205 | skin |
| | *Gadus morhua* | GW856677 | eye |
| ***angptl9*** | | | |
| ***a*** | *Gasterosteus aculeatus* | DW655560 | larva |
| | | DW639541 | larva |
| | *Oreochromis niloticus* | GR674400 | ovary |
| ***b*** | *none* | none | none |

**Supplementary table 3. 4 - Accession numbers of the fish, tetrapod and cephalochordate Angpt genes and transcripts**. ni-not identified

| | ***angpt1*** | ***angpt2*** | ***angpt4*** |
|---|---|---|---|
| *Homo sapiens* | ENSG00000154188 | ENSG00000091879 | ENSG00000101280 |
| *Mus musculus* | ENSMUSG00000022309 | ENSMUSG00000031465 | ENSMUSG00000027460 |
| *Monodelphis domestica* | ENSMODG00000005283 | ENSMODG00000012086 | ENSMODG00000019535 |
| *Gallus gallus* | ENSGALG00000016083 | ENSGALG00000016330 | ENSGALG00000026890 |
| *Anolis carolinensis* | ENSACAG00000010050 | ENSACAG00000009115 | ENSACAG00000010893 |
| *Takifugu rubripes* | ENSTRUG00000003523 | a: ENSTRUG00000014844<br>b: ENSTRUG00000015237 | ENSTRUG00000001096 |
| *Sparus aurata* | SRR278741_isotig78148 | SRR278741_isotig28682 | ni |
| *Oreochromis niloticus* | ENSONIG00000013548 | a: ENSONIG00000009668<br>b: ENSONIG00000004681 | ENSONIG00000005320 |
| *Oryzias latipes* | ENSORLG00000010226 | a: ENSORLG00000009631<br>b: ENSORLG00000005397 | ENSORLG00000020331 |
| *Astyanax mexicanus* | ENSAMXG00000021217 | a: ENSAMXG00000003812<br>b: ENSAMXG00000002649 | ENSAMXG00000009654 |
| *Lepisosteus oculatus* | ENSLOCG00000003157 | a: ENSLOCG00000016861<br>b: ENSLOCG00000001647 | ENSLOCG00000007459 |
| *Leucoraja erinacea* | Contig64192 | Contig18175 | ni |
| *Callorhinchus milii* | ni | SINCAMG00000013167 | SINCAMG00000000964 |
| *Petromyzon marinus* | | ENSPMAG00000000222 | |
| ***angptl-like*** | | | |
| *Branchiostoma floridae* | | fgenesh2680000014 | |

**Supplementary figure 3. 1 - Expanded phylogenetic tree of the fish and other metazoan ANGPTL family members using Bayesian Interference (BI).** Details are available from figure 3.2. Accession numbers available in supplementary tables 3.1 and 3.4.

Bayesian interference expanded phylogenetic tree

**Supplementary figure 3. 2 - Phylogenetic tree of the fish and other metazoan ANGPTL family members constructed with the Maximum-likelihood (ML) algorithm.** The Phylogenetic analysis was performed with the deduced amino acid sequences in ATGC (http://www.atgc-montpellier.fr/phyml/) with a fixed value for the proportion of invariable sites 0.008, 4 gamma-distributed rate categories (1.272) and 100 bootstrap replicates. Tree was rooted with the metazoan ANGPT clade (ANGPT1, 2 and 4). Accession numbers available in supplementary tables 3.1 and 3.4.

**Supplementary figure 3. 3 - Sequence alignments of the human, spotted gar, zebrafish, sea bass and sea bream Angptls.** Sequences were compared according to the protein phylogenetic clustering given by the phylogenetic analysis (Figure 2, Supplementary Figure 2 and 3). **A**: ANGPTL1-2-6; **B**: ANGPTL3-4; **C**: ANGPTL5 and **D**: ANGPTL7-9. Amino acid conservation is shaded and dark grey represent 80% and black 100% conservation. The signal peptide and the coiled-coil domain (CCD) in human sequences are underlined and highlighted in bold, respectively. The conserved fibrinogen-related domain (FReD) in human and in fish is boxed and the four conserved cysteine residues within this motif that are involved in two intramolecular disulphide bonds are highlighted in red and predicted glycosylation (N-x-T/S) motifs are underlined.

**A**

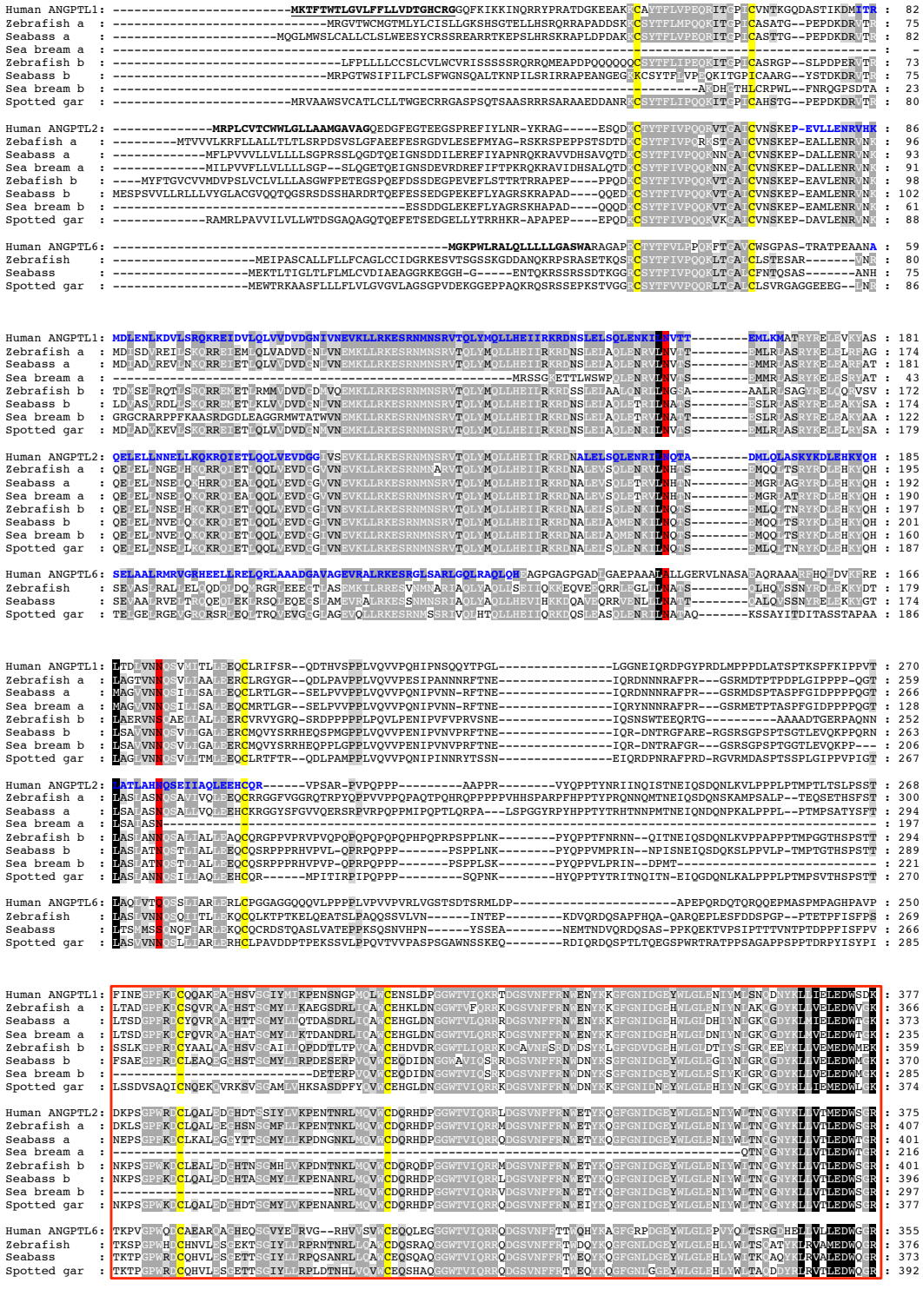

# B

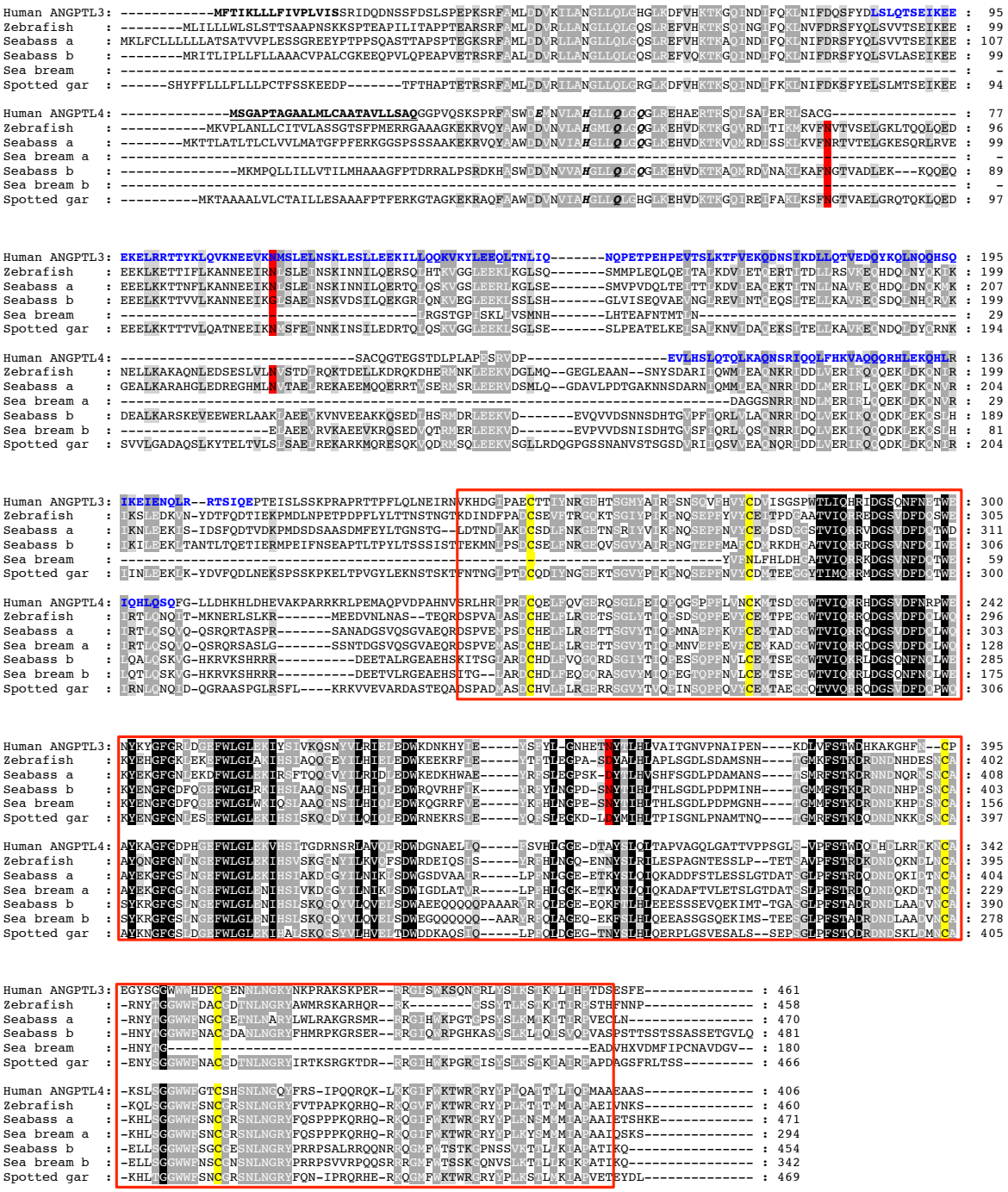
Human ANGPTL3:
Zebrafish
Seabass a
Seabass b
Sea bream
Spotted gar
Human ANGPTL4:
Zebrafish
Seabass a
Sea bream a
Seabass b
Sea bream b
Spotted gar

# C

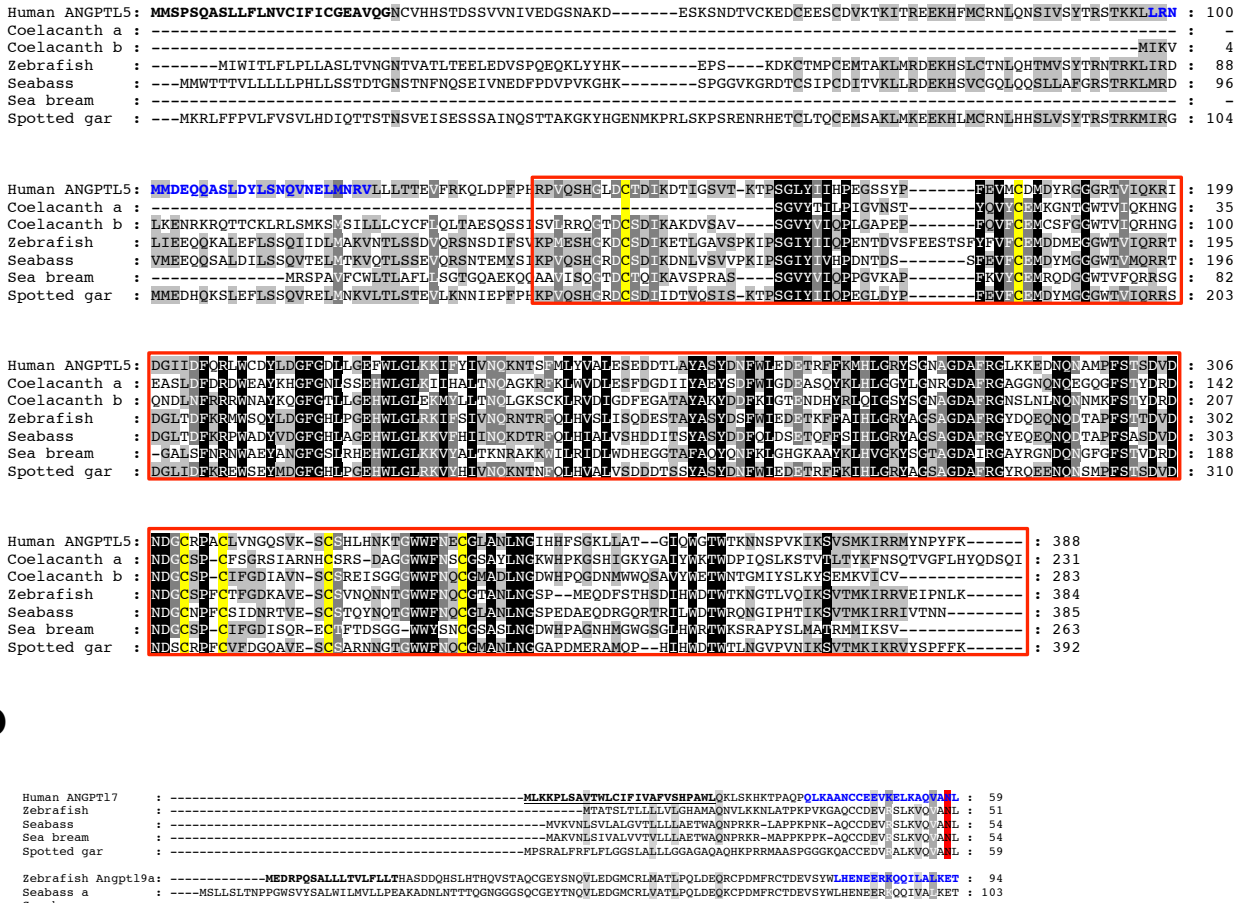
Human ANGPTL5: MMSPSQASLLFLNVCIFICGEAVQGNCVHHSTDSSVVNIVEDGSNAKD-------ESKSNDTVCKEDCEESCDVKTKITREEKHFMCRNLQNSIVSYTRSTKKLLRN : 100
Coelacanth a : ---------- : -
Coelacanth b : ---------- MIKV : 4
Zebrafish : -------MIWITLFLPLLASLTVNGNTVATLTEELEDVSPQEQKLYYHK--------EPS----KDKCTMPCEMTAKLMRDEKHSLCTNLQHTMVSYTRNTRKLIRD : 88
Seabass : ---MMWTTTVLLLLLPHLLSSTDTGNSTNFNQSEIVNEDFPDVPVKGHK--------SPGGVKGRDTCSIPCDITVKLLRDEKHSVCGQLQQSLLAFGRSTRKLMRD : 96
Sea bream : ---------- : -
Spotted gar : ---MKRLFFPVLFVSVLHDIQTTSTNSVEISESSSAINQSTTAKGKYHGENMKPRLSKPSRENRHETCLTQCEMSAKLMKEEKHLMCRNLHHSLVSYTRSTRKMIRG : 104
Human ANGPTL5: MMDEQQASLDYLSNQVNELMNRVLLLTTEVFRKQLDPFPHRPVQSHCLDCTDIKDTIGSVT-KTPSGLYIIHPEGSSYP-------FEVMCDMDYRGGGRTVIQKRI : 199
Coelacanth a : ---------- SGVYTIIPIGVNST-------YCVYCEMKGNTGWTVLQKHNG : 35
Coelacanth b : LKENRKRQTTCKLRLSMKSVSILLLCYCFIQLTAESQSSISVERRQCTDCSDIKAKDVSAV----SGVYVIQPLGAPEP-------FQVFCEMCSFGGWTVLQRHNG : 100
Zebrafish : LIEEQQKALEFLSSQIIDLMAKVNTLSSDVQRSNSDIFSVKPVESHCKDCSDIKETLGAVSPKIPSGIYIIQPENTDVSFEESTSFYFVFCEMDMEGGWTVIQRRT : 195
Seabass : VMEEQQSALDILSSQVTELMTKVQTLSSEVQRSNTEMYSIKPVQSHCRDCSDIKDNLVSVVPKIPSGIYIVPPDNTDS-------SFEVFCEMDYMGGWTVMQRRT : 196
Sea bream : ---------- MRSPAVFCWLTLAFLISGTGQAEKQCAAVISQCTQCTQIKAVSPRAS----SGVYVIQPGVKAP-------FKVVCEMRQDGGWTVFQRRSG : 82
Spotted gar : MMEDHQKSLEFLSSQVRELVNKVLTLSTEVLKNNIEPFPHKPVQSHCRDCSDIIDTVQSIS-KTPSGIYIIQPEGLDYP-------FEVFCEMDYMGGWTVIQRRS : 203
Human ANGPTL5: DGIIDFQRLWCDYLDGFGDLLGEFWLGLKKIFYIVNQKNTSFMLYVALESEDDTLAYASYDNFWIEDETRFFKMHLGRYSGNAGDAFRGLKKEDNQLAMPFSTSDVD : 306
Coelacanth a : EASLDFDRDWEAYKHGFGNISSEFWLGLKIIHALTNQAGKRFKLWVDLESFDGDIIYAEYSDFWIGDEASQYKLHLCGYLGNRGDAFRGAGGNQNQEGQGFSFYDRD : 142
Coelacanth b : QNDLNFRRRWNAYKQGFGTLLGEFWLGLEKMYLITNQLGKSCKLRVDIGDFEGATAYAKYDLDFKIGTGNDHYRLQIGSYSGNAGDAFRGNSLNLNQNNMKFSFYDRD : 207
Zebrafish : DGLTDFKRMWSQYLDGFGHLPGEFWLGLRKIFSHVNQRNTREQLHYSLISQDESTAYASYDSEWIEDETKFFAIHLGRYASSAGDAFRGYDQECNQETAPFSTTDVD : 302
Seabass : DGLTDFKRPWADYVDGFGHLAGEFWLGLKKVFHIINQKDTREQLHIALVSHDDITSYASYDDFQLDSETQFFSIHLGRYAGSAGDAFRGYEQEQNQETAPFSASDVD : 303
Sea bream : -GALSFNRNWAEYANGFGSLRHEFWLGLKKVYALTKNRAKKWILRIDLWDHEGGTAFAQYQNFKLGHGKAAYKLHVGKYSGTAGDAIRGAYRGNDQNGFGFSTVDRD : 188
Spotted gar : DGLIDFKRPWSEYMDGFGHLPGEFWLGLRKVYHIVNQKNTNFQLHYALVSDDDTSSYASYDNFWIEDETRFFKIHLGRYASSAGDAFRGYRQEENQNLSMPFSTSDVD : 310
Human ANGPTL5: NDGCRPACLVNGQSVK-SCSHLHNKTGWWFNECGLANLNGIHHFSGKLLAT--GIQWGTWTKNNSPVKIKSVSMKIRRMYNPYFK------ : 388
Coelacanth a : NDCCSP-CFSGRSIARNHCSRS-DAGGWWFNSCGSAYLNGKWHPKGSHIGKYGAIYWKTWDPIQSLKSTVLLTYKFNSQTVGFLHYQDSQI : 231
Coelacanth b : NDGCSP-CIFGDIAVN-SCSREISGGGWWFNQCGMADLNGDWHPQGDNMWWQSAVYMETWNTGMIYSLKYSEMKVICV-------------- : 283
Zebrafish : NDGCSPFCTFGDKAVE-SCSVNQNNTGWWFNQCGTANLNGSP--MEQDFSTHSDIHWDTWTKNGTLVQIKSVTMKIRRVEIPNLK------ : 384
Seabass : NDGCNPFCSIDNRTVE-SCSTQYNQTGWWFNQCGLANLNGSPEDAEQDRGQRTRILWDTWRQNGIPHTIKSVTMKIRRIVTNN------- : 385
Sea bream : NDCCSP-CIFGDISQR-ECNFTDSGG-WWYSNCGSASLNGDWHPAGNHMGWGSGLHWRTWKSRAPYSLMAIRMMIKSV-------------- : 263
Spotted gar : NDSCRPFCVFDGQAVE-SCSARNNGTGWWFNQCGMANLNGGAPDMERAMQP--HHHMDTWTLNGVPVNIKSVTMKIKRVYSPFFK------ : 392

# D

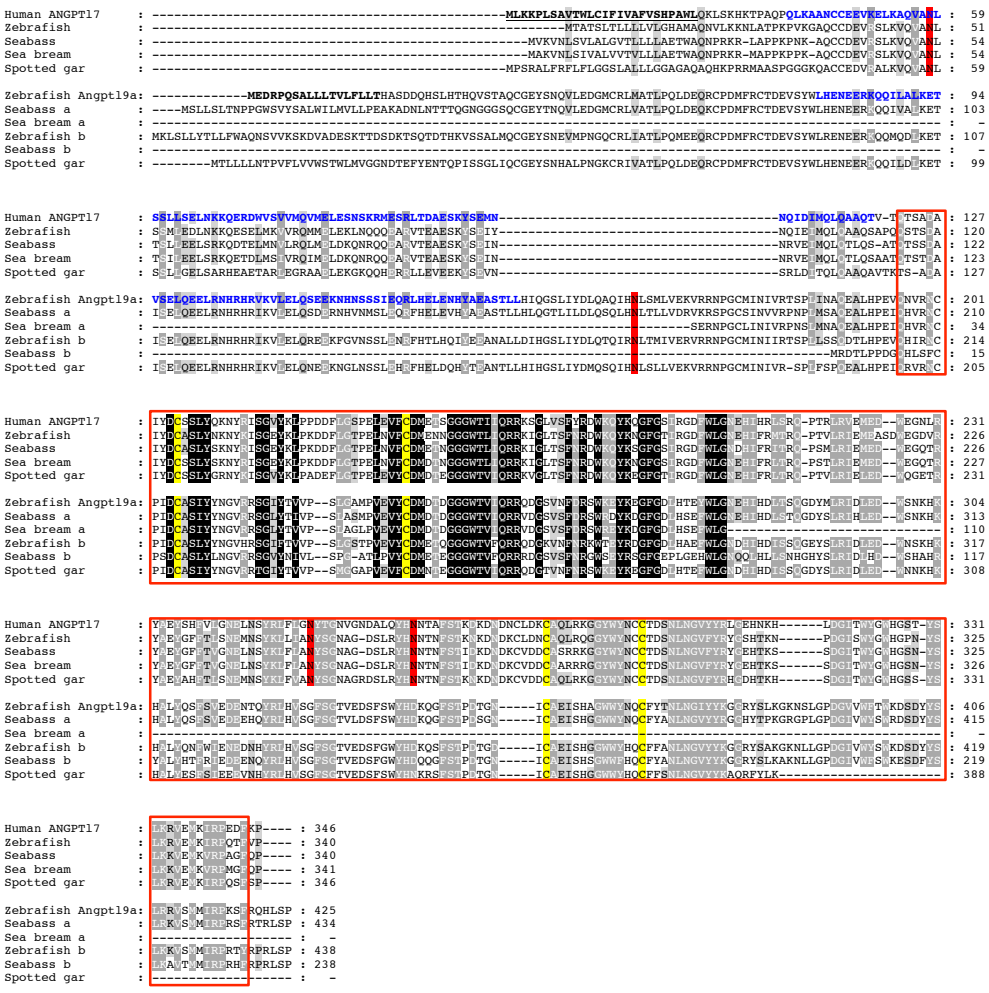
Human ANGPTl7 : MLKKPLSAVTWLCIFIVAFVSHPAWLQKLSKHKTPAQPQLKAANCCEEVKELKAQVAAL : 59
Zebrafish : MTATSLTLLLLVLGHAMAQNVLKKNLATPKPVKGAQCCDEVSLKVQAAL : 51
Seabass : MVKVNLSVLALGVTLLLLAETWAQNPRKR-LAPPKPNK-AQCCDEVSLKVQAAL : 54
Sea bream : MAKVNLSIVALVVTVLLLAETWAQNPRKR-MAPPKPPK-AQCCDEVSLKVQAAL : 54
Spotted gar : MPSRALFRFLFLGGSLALLLGGAGAQAQHKPRRMAASPGGGKQACCEDVSLKVQAAL : 59
Zebrafish Angptl9a: MEDRPQSALLLTVLFLLTHASDDQHSLHTHQVSTAQCGEYSNQVLEDGMCRLMATLPQLDEQRCPDMFRCTDEVSYWLHENEERKQQILALKET : 94
Seabass a : MSLLSLTNPPGWSVYSALWILMVLLPEAKADNLNTTTQGNGGGSQCGEYTNQVLEDGMCRLVATLPQLDEQKCPDMFRCTDEVSYWLHENEERQQIVALKET : 103
Sea bream a : ---------- : -
Zebrafish b : MKLSLLYTLLFWAQNSVVKSKDVADESKTTDSDKTSQTDTHKVSSALMQCGEYSNEVMPNGQCRLIATLPQMEEQRCPDMFRCTDEVSYWLRENEERQQMQDLKET : 107
Seabass b : ---------- : -
Spotted gar : --------MTLLLLNTPVFLVVWSTWLMVGGNDTEFYENTQPISSGLIQCGEYSNHALPNGKCRIVATLPQLDEQRCPDMFRCTDEVSYWLHENEERQQILDLKET : 99
Human ANGPTl7 : SSLLSELNKKQERDWVSVVMQVMELESNSKRMESRLTDAESKYSEMN----------NQIDIMQLQAAQTV-TTSTAIA : 127
Zebrafish : SIMEDLNKKQESELMKVRQMMLEKLNQQQAVTEAESKSLIY----------NQIEMQLAAQSAPQSTSLA : 120
Seabass : TLLEELSRKQDTELMNLRQLMLDKQNRQQAVTEAESKSLIN----------NRVEMQLTLQS-ATTSSLA : 122
Sea bream : TLIEELSRKQETDLMSVRQIMLDKQNRQQAVTEAESKSLIN----------NRVEMQLTLQSAATTSTLA : 123
Spotted gar : SLLGELSARHEAETARLEGRAALEKGKQQHLRLLEVEEKLSVN----------SRLDLTQLAAQAVTKTS-ALA : 127
Zebrafish Angptl9a: VEELQEELRNHRHRVKVLELQSEEKHNNSSSIEQRLHELENHVAEASTLLHIQGSLIYDLQAQIHNLSMLVEKVRRNPGCMINIVRTSPLINAEALHPEVVNVRLC : 201
Seabass a : IEELQEELRNHRHRIKVLELQSDLRNHVNMSLLQLPHELEVHLAASTLLHLQGTLILDLQSQLHNLTLLVDRVKRSPGCSINVVRPNPLMSAEALHPEIVHVRLC : 210
Sea bream a : ---------- SERNPGCLINIVRPNSLMNAEALHPEIVHVRLC : 34
Zebrafish b : IEELQEELRNHRHRIKVLELQREEKFGVNSSLLNLFHTLHQIEELANALLDIHGSLIYDLQTQIRNLTMIVERVRRNPGCMINIIRTSPLLSSLDTLHPEVVHIRLC : 214
Seabass b : ---------- MRDTLPPDGLHLSFC : 15
Spotted gar : IEELQEELRNHRHRIKVLELQNELKNGLNSSLLHLFHELDQHLTLANTLLHIHGSLIYDMQSQIHNLSLLVEKVRRNPGCMINIVR-SPLFSPLEALHPEILRVRLC : 205
Human ANGPTl7 : IYDCSSLYQKNYLISGVMKPPDDFLCSPELEVECDMESSGGWTLQRRKSGLVSEVRSWMYKQGFGSLRGDLNLGLELIHRLRL-PTRLRVEMELL-LEGNLR : 231
Zebrafish : IYDCASLYNKNYLISGEMKPKDDFLCTPELNVECDMENNGGWTLLQRRKICLTSEIRSWMYKNGFGTLRGDLNLGLELIHFLRL-PTVLRLEMEASDLEGDVR : 226
Seabass : IYDCASLYSKNYLISGEMKPKDDFLCTPELNVECDMENGGGWTLLQRRKICLTSEIRSWMYKSGFGSLRGDLNLGLDLIHFLRL-PSMLRLEMELL-LEGQTR : 226
Sea bream : IYDCSSLYSKNYLISGEMKPKDDFLCTPELNVECDMDNGGGWTLLQRRKICLTSEIRSWMYKNGFGSLRGDLNLGLELIHFLRL-PSTLRLEMELL-LEGQTR : 227
Spotted gar : IYDCSSLYGRNYLISGVMKPADEFLCTPELEVECDMDLPGGGWTVLQRRKVCLTSEIRSWMYKEGFGTLRGDLNLGLELIHFLRL-PTVLRLELEL--WQGETR : 231
Zebrafish Angptl9a: PIDCASIYYNGVLRSGVMKVPV--SLAMPVEVECDMDLPGGWTVLQRRQDGSVNSIRSWMYKDGFGDLHTELNLGLELIHDLLSLGDYMLRLDLEL--WSNKHR : 304
Seabass a : PIDCASIYYNGVLRSGVMKVPV--SLASMPVEVECDMDLPGGWTVLQRRVDGSVSSIRSWMYKDGFGDLHSELNLGLELIHDLLTLGDYSLRLHLEL--WSNKHR : 313
Sea bream a : PIDCASIYYNGVLRSGVMKVPV--SLAGLPVEVECDMDLPGGWTVLQRRVDGSVSSIRSWMYKDGFGDLHSELNLG---------------------------- : 110
Zebrafish b : PIDCASLYYNGVHRSGFMKVPV--SLSTPVEVECDMELPGGWTVLQRRQDGKVNSIRSWMYRDGFGDLHAELNLGLDLIHDLLSLGEYSLRLDLEL--WNSKHR : 317
Seabass b : PSDCASLYLNGVLRSGVMNHVL--SP-ATLPVEVECDMELPGGWTVLQRRRDGSVSSIRSWMYKGGFGEPLGEHNLGLQQLHLLNHGHYSLRLDLH--WSHAHR : 317
Spotted gar : PIDCASIYYNGVLRSGVMKVPV--SLTGAPVEVECDMNLPGGWTVLQRRQDGTVNSIRSWMYKEGFGDLHTELNLGLDLIHDLLSLGDYSLRLDLEL--WNNKHR : 308
Human ANGPTl7 : YLESHVVGLLNSYFLGMYTNVGNDALQLHNNTASFSLKLKDLDNCLDKCQLRKGYWYNCCTDSNLNGVYFLLEHNKH------LDGLTWYGLHGST-MS : 331
Zebrafish : YLEGFTLSLMNSYILAMYSNAG-DSLRLHNNTNPSFSIKLKDLCDLNCQLRQGGYWYNCCTDSNLNGVYFLYLSHTKN------PDGLSWYGLHGPN-MS : 325
Seabass : YLEGFTVGLLNSYILAMYSNAG-DSLRLHNNTNPSFSIKLKDKCVDDCSRRKGYWYNCCTDSNLNGVYFLYLEHTKS------SDGLTWYGLHGSN-MS : 325
Sea bream : YLEGFTVGLLNSYILAMYSNAG-DSLRLHNNTNPSFSIKLKDCVDDCARRRGYWYNCCTDSNLNGVYFLYLEHTKS------SDGLTWYGLHGSN-MS : 326
Spotted gar : YLEAHTLSLMNSYILAMYSNAGRDSLRLHNNTNPSFSIKLKDKCVDDCQLRKGYWYNCCTDSNLNGVYFLHLDHTKH------SDGLTWYGLHGSS-MS : 331
Zebrafish Angptl9a: HLLQSSVEFNTQYFLHSGFSSTVEDSFSWVHEKQGFSSPLTGLTGLEISHAGWWYNQCFYTNLNGIYYLGRYSLKGKNSLGPDGVWETLKDSDYMS : 406
Seabass a : HLLQSSVEFEHQYFLHSGFSSTVLDSFSWVHEKQGFSSPLSGLTGLEISHSGWWYNQCFYANLNGVYYLGRYTPKGRGPLGPDGIVWSSLKDSDYMS : 415
Sea bream a : ---------- : -
Zebrafish b : HLLQNSWEFNDHYFLHSGFSSTVEDSFGWVHEKQSFSSPLTGLTGLEISHSGWWYHQCFFANLNGVYYLGRYSAKGKNLLGPDGVWNSLKDSDYMS : 419
Seabass b : YLLHTSREFNEQYFLHSGFSSTVEDSFGWVHEQQGFSSPLTGLTGLEISHSGWWFHQCFYANLNGVYYLGRYSLKAKNLLGPDGIVWESLKESDFMS : 419
Spotted gar : HLLESSIEFVNHYFLHSGFSSTVEDSFSWVHKRSFSSPLTGLTGLEISHSGWWYHQCFFSANLNGVYYLAQRFYLK---------- : 388
Human ANGPTl7 : LLRELKIREDLKP---- : 346
Zebrafish : LLRELKIRQTLVP---- : 340
Seabass : LLKELKVREAGLQP---- : 340
Sea bream : LLKELKVRDMGLQP---- : 341
Spotted gar : LLRELKIRQSLSP---- : 346
Zebrafish Angptl9a: LLRSLMIRKKSLRQHLSP : 425
Seabass a : LLKSLMIRERSLRTRLSP : 434
Sea bream a : ---------- : -
Zebrafish b : LLKSLMIRRTLRPRLSP : 438
Seabass b : LLATLMIRRRHLRPRLSP : 238
Spotted gar : ---------- : -

**Supplementary figure 3. 4 - Comparison of the homologous genome regions harbouring the vertebrate *angptl7* with the cephalochordate**. The gene environment of 2 tetrapods (human and chicken), the lobed-finned fish (coelacanth), 3 ray-finned fish (tilapia, zebrafish and spotted-gar), the cartilaginous elephant shark, the lamprey and the amphioxus are compared. Horizontal lines represent chromosome fragments and its names and genome fragments are indicated at the right side; coloured block arrows represent genes according to the order in the chromosome and the arrowhead points to the predicted gene transcription. The location of the gene in the chromosome is indicated below each arrow, in Megabase pairs (Mb). ■: Whole Genome Duplication (WGD).●: Teleosts Specific Genome Duplication (TSGD). Gene names and gene symbols are: TAR DNA binding protein (*tardbp*), mannan-binding lectin serine protease 2 (*masp2*), spermidine synthase (*srm*), exosome component 10 (*exosc10*), mechanistic target of rapamicin (serine/threonine kinase) (*mtor*) and UbiA prenyltransferase domain containing 1 (*ubiad1*).

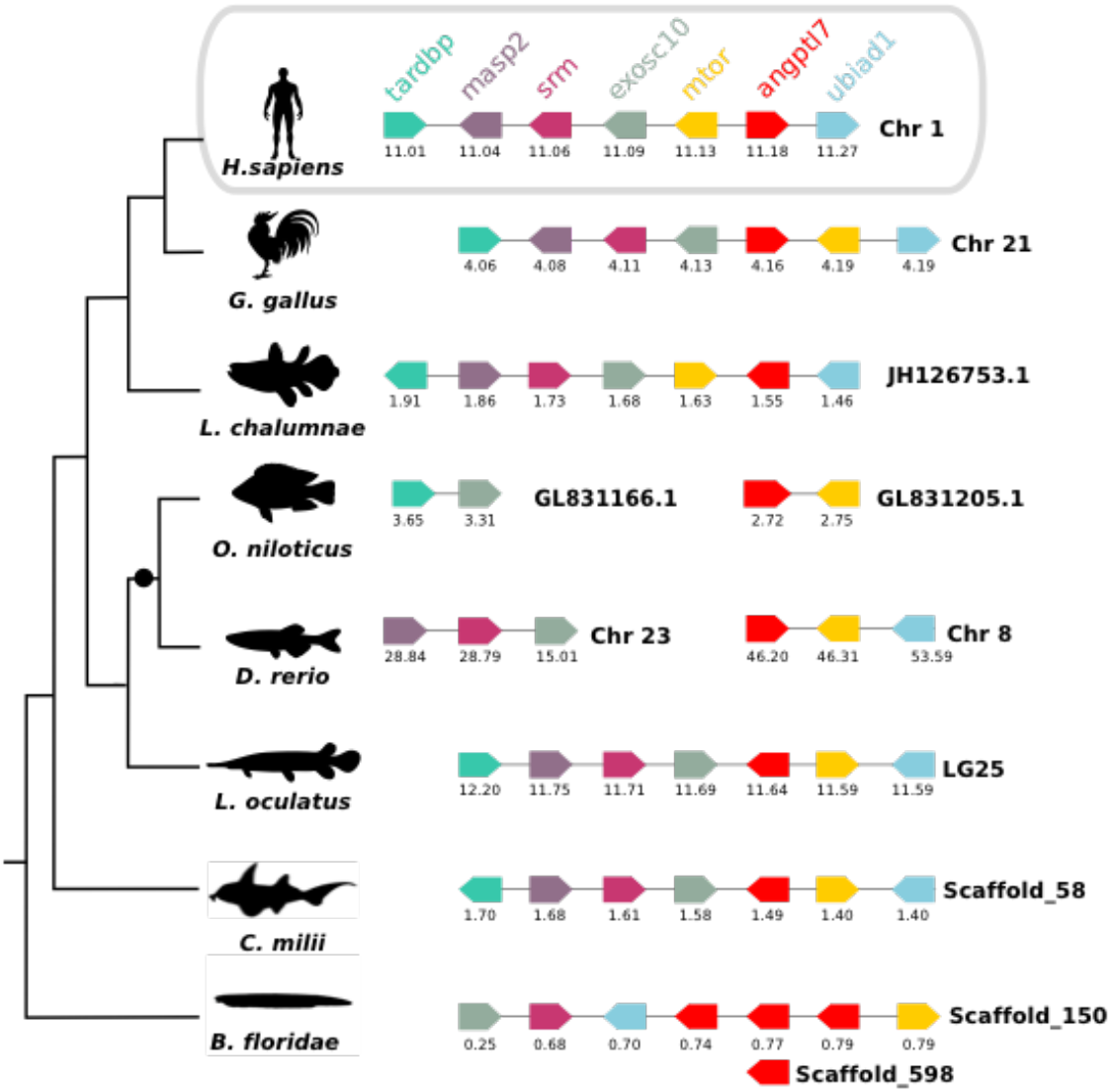

**Supplementary figure 3. 5 - Amino acid sequence alignment of the cephalochordate Angptl-like 7 with the human and spotted gar ANGPTL7.** Amino acid conservation is shaded and dark grey represent 80% and black 100% conservation. The signal peptide and the coiled-coil domain (CCD) in human sequences are underlined and highlighted in bold, respectively. The conserved fibrinogen-related domain (FReD) is boxed and the four conserved cysteine residues within this motif that are involved in two intramolecular disulphide bonds of the vertebrate proteins are highlighted in red.

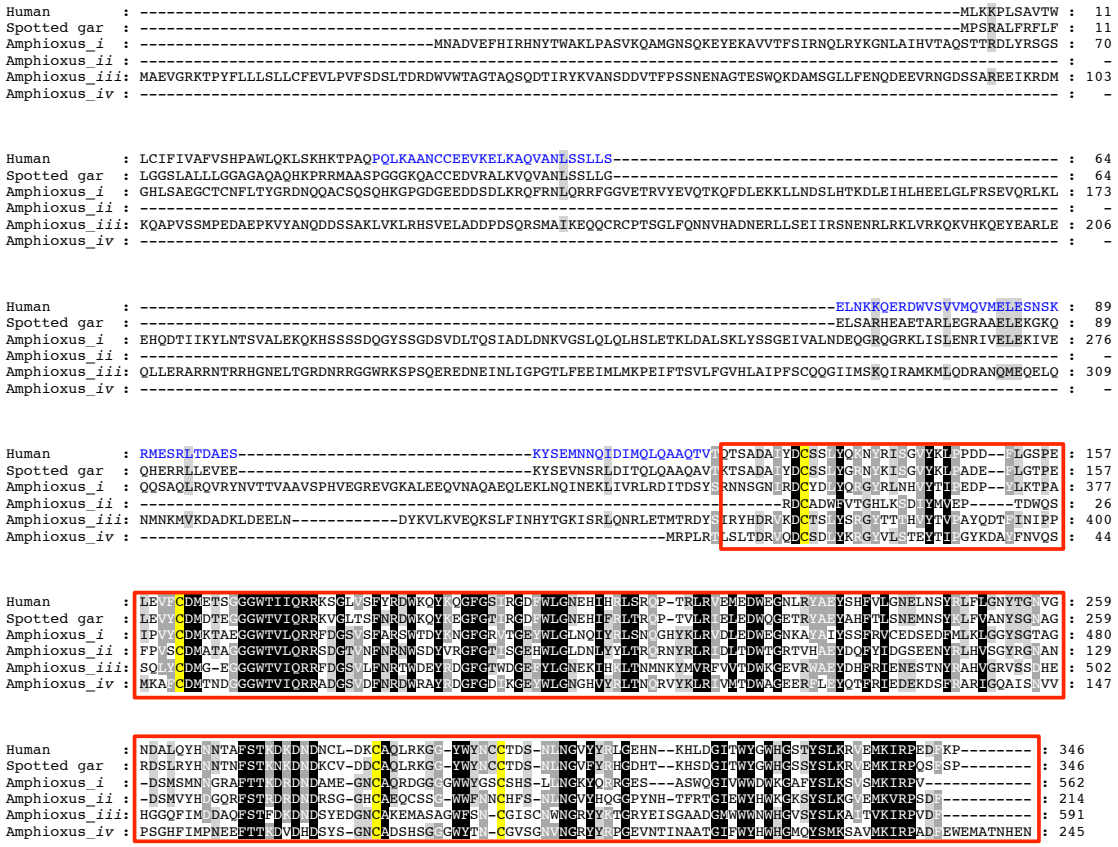

# 4

*Manuscript in preparation*

# Teleost osteoglycin duplicates are highly expressed in muscle and skin and involved in late-phase regeneration of skin

R.A. Costa[1]*, E. Capilla[2]*, R. Martins[1], L. Anjos[1], and D.M. Power[1]

[1]Comparative Endocrinology and Integrative Biology Group, Centre of Marine Sciences, University of Algarve, Campus of Gambelas, 8005-139 Faro, Portugal.

[2]Department of Physiology and Immunology, Faculty of Biology, University of Barcelona, Barcelona 08028, Spain.

**Authors contributions:**
DMP conceived the project; DMP, EC and RAC devised the experimental design and conducted laboratory based experiments; RM and LA conducted the in silico analysis; all authors were involved in the analysis and interpretation of the results; DMP, RC and EC drafted the manuscript; RM and LA contributed to preparation of figures and critically revised the manuscript.

## 4.1. Abstract

Osteoglycin (OGN) is a member of the small leucine-rich proteoglycan family and is a multifunctional protein that is largely uncharacterized in teleosts. A proteomic study has shown it clusters with proteins enriched during anatomical repair and immune activation in the gilthead sea bream. In the present study we assessed how life in an aquatic environment shaped Ogn evolution, structure and function in teleosts. The duplicate *ogn* genes encode proteins that share 66-72% amino acid sequence similarity and possess the characteristic seven leucine-rich repeats of the vertebrate class III SLRP family. Bone- and muscle-derived primary cell cultures were highly enriched in *ogn2* transcripts and it had an osteoinductive association and was also linked with myotube formation. *Ogn1* in bone derived primary cultures was far less abundant and its expression was induced in adipogenic conditions and increased as trans-differentiation progressed. A teleost skin/scale regeneration model revealed *ogn1* and *ogn2* were down-regulated during re-epithelialization and up-regulated when the scale increased in thickness during the phase of collagen fibre deposition and mineralization. Overall, our study suggests *ogn1* and *ogn2* are multifunctional in teleost fish and have retained common roles with the mammalian protein in matrix repair, although the duplicates have also acquired unique teleost specific functions.

**Keywords**: duplicate genes; subfunctionalization; extracellular matrix; regeneration; small leucine-rich proteoglycan (SLRP) family

## 4.2. Introduction

The extracellular matrix (ECM) is a characteristic of multicellular organisms and is of primary importance in establishing the basic characteristics of each tissue. ECM complexity increases from simple extant multicellular organisms to vertebrates, although its function in structure, organization and orientation of tissue is conserved (Huxley-Jones et al. 2007). The essential building blocks of the ECM are ubiquitous across organisms and include collagens, glycoproteins and proteoglycans (Bosman and Stamenkovic 2003; Iozzo and Schaefer 2015; Schaefer and Iozzo 2008). The increased ECM complexity in vertebrates, both terrestrial and aquatic, in relation to chordates is associated with gene family expansion through duplication of ancestral metazoan genes, and also through a small number of vertebrate specific gene innovations (Huxley-Jones et al. 2007). Knowledge about the ECM in the fishes is very patchy despite their unique adaptations and their evolutionary success (there are over 28,000 extant species) (Nelson et al. 2001). Furthermore, the teleost specific whole genome duplication increased gene number and the scope for gene innovations (Glasauer and Neuhauss 2014; Venkatesh 2003) and this coupled to the diversity of body forms and physiological adaptations to aquatic life modified ECM organisation as revealed by a recent study of teleost bone (Vieira et al. 2013).

The proteoglycans are grouped into 4 major classes when cellular and subcellular location, overall gene/ protein homology, and the presence of specific protein modules are taken into account (Iozzo and Schaefer 2015). The small leucine-rich proteoglycan (SLRP) family comprises the largest class of proteoglycans in the ECM and are proteins with a relatively small protein core (36-42 KDa), harbouring tandem leucine-rich repeats (LRRs) that may contain one or more glycosaminoglycan side chain, although there are some exceptions (Iozzo 1997; Iozzo and Murdoch 1996). The SLRP family is clustered into 5 main groups when protein and gene homology, chromosome localization and the presence and spacing of the classical N-terminal cysteine-rich repeat is taken into account (Henry et al. 2001; Huxley-Jones et al. 2007; McEwan et al. 2006; Iozzo 1999). The SLRPs have a diversity of functions and in addition to their role as structural constituents of the ECM they also interact with receptor tyrosine kinases (RTKs) and Toll-like receptors and regulate migration, proliferation, innate immunity, apoptosis and angiogenesis. The function of the SLRPs is suggested to be dependent on tissue context and organism. Functional compensation can occur between SLRPs and one form may substitute the loss of another and an example of this is the up-regulation of decorin when biglycan is lost in humans (Young et al. 2003).

The present study is focused on osteoglycin (OGN, a.k.a. mimecan) that belongs to cluster III of the SLRPs along with epiphycan (EPYC) and opticin (OPTC) (Henry et al. 2001). This group is characterized by a relatively low number of LRRs relative to other SLRP classes, and an N-terminal consensus sequence for tyrosine sulphation (Corpuz et al. 1996). The function of OGN has mainly been studied in mammals and it is a multifunctional protein in which its best characterized function is the regulation of collagen fibrillogenesis, the efficiency of which is increased when it is processed by BMP-1/Tolloid-like metalloproteinases (Vadon-Le Goff et al. 2015). OGN KO-mice are viable, fertile and grow normally but the skin has a modified tensile strength due to abnormalities in the collagen fibrils, which are on average thicker (Tasheva et al. 2002). OGN has a role in wound healing in the cornea (Sundarraj et al. 1998; Tasheva et al. 2002) and is a normal component of the vascular matrix, is associated with atherosclerotic lesions in rabbits and also modulates myocardial integrity and remodelling together with other ECM glycoproteins (Fernandez et al. 2003; Shanahan et al. 1997; Tasheva et al. 2002). Neurite outgrowth promoted by insulin-like growth factor-2 (IGF2) and IGF binding protein-2 (IGFBP2) is enhanced by OGN (Jeong et al. 2013). The recent identification of OGN in the mouse and human pituitary gland co-expressed with proopiomelanocortin (POMC) and its up-regulation by glucocorticoids in mouse and regulation of adrenocorticotropic hormone (ACTH) secretion reveals a novel function for OGN in the hypothalamic-pituitary-adrenal axis (HPAA) in mammals (Ma et al. 2010; Ma et al. 2011). An emerging role for OGN is that of a hormone that is liberated from adipose tissue and it acts as a satiety factor and inhibits food intake by inducing interleukin (IL)-1β and IL-6 expression in the hypothalamus (Cao et al. 2015). OGN is also implicated in a number of pathologies and during inflammation in humans OGN increases in the circulation and is down-regulated in tissues derived from colorectal adenomas and cancers compared to normal mucosa (Wang et al. 2007). The multifunctional characteristics of OGN may be indicative of a new axis of previously unsuspected actions for other SLRPs.

Proteomics has revealed different forms of OGN (splice variants) in tetrapod tissues including, subcutaneous adipose tissue and visceral adipose tissue from obese humans (Insenser et al. 2012), the reticular dermis of human skin (Mikesh et al. 2013), and the avian cortical and medullary bone (Wang et al. 2005). Far less is known about OGN in teleosts, although in a proteomics study of skin and scale regeneration in the teleost, gilthead sea bream (*Sparus aurata*), OGN was identified and was up-regulated along with 34 other proteins 5 days after regeneration when compared to intact, undamaged skin (Ibarz et al. 2013). The increase in OGN was in the context of a general enrichment of proteins associated with anatomical repair and

immune activation. In contrast, in a microarray study of the skin of Atlantic salmon (*Salmo salar*) exposed to increased cortisol for 18 days, OGN was among the most significantly down-regulated transcripts along with others associated with bone, the ECM, steroid metabolism, contraction and the immune response (Krasnov et al. 2012).

The present study focuses on OGN in teleosts and provides novel insight into OGN evolution and function. We analyse OGN evolution in teleosts and map the evolution of the duplicate forms resulting from the teleost specific whole genome duplication using comparative genomics and question how the challenge of an aquatic environment shaped OGN evolution; we identify the unique characteristics of the deduced protein in teleosts and use *in vitro* culture of fish primary cell lines to reveal *ogn2* has an osteoinductive association but also a link with myotube formation and that *ogn1* has an adipogenic-related expression; using a teleost skin/scale regeneration model we evaluate through transcript analysis the involvement of *ogn* in scale regeneration and skin repair. Overall the results indicate gene conservation during evolution, subfunctionalization of the duplicate teleost Ogns and conservation of the multi-functional nature of OGN in vertebrates.

## 4.3. Materials and Methods

### 4.3.1. Identification and characterization of osteoglycin (ogn) gene(s) in gilthead sea bream

To identify homologue(s) of *ogn* in the gilthead sea bream (*S. aurata*) available transcriptome data from vertebra, gill arch (Vieira et al. 2013) and white muscle (Garcia de la serrana et al. 2012) were interrogated by BLAST using a human *OGN* cDNA (NP_054776) as bait. *Ogn* homologues were extracted from genomes of terrestrial vertebrates (placental mammals, ungulates, birds and amphibians) and aquatic vertebrates (turtles, marine mammals and fish) using sequence similarity searches (BLASTX and TBLASTN) in NCBI (http://www.ncbi.nlm.nih.gov/), Ensembl (http://www.ensembl.org) and the European sea bass genome (http://seabass.mpipz.de/ version dicLab v1.0c) databases. OGN sequences were aligned using ClustalX (v2.0.11) (Larkin et al. 2007) and the alignments edited and the percentage of protein sequence similarity between OGN homologues determined using GeneDoc version 2.7.0 (Nicholas KB et al. 1997). The accession numbers of all the sequences used in this study are indicated in supplementary table 4.1. Preliminary data about *ogn* tissue distribution in teleosts was obtained by carrying out sequence similarity searches (BLASTX

and TBLASTN) against the Expressed Sequence Tags (ESTs) database (http://www.ncbi.nlm.nih.gov/genbank/).

### 4.3.2. Phylogenetic analysis and gene environment

To confirm the identity of OGNs retrieved by database searches, orthologues of SLRPs from group I, II and III were retrieved from cephalochordates and vertebrates and used to generate preliminary phylogenetic trees. Clustering of SLRPs was used to confirm putative Ogn sequences and these were then used for in depth phylogenetic analysis using human epiphycan (EPYC) as the out-group. The full-length, deduced protein sequences were used in multiple sequence alignments (using ClustalW v.2.0 (Larkin et al. 2007)) and analysed with ProtTEST (v2.4) (Abascal et al. 2005) to select the model of protein evolution that best fitted the dataset. Phylogenetic trees were generatedusing Maximum Likelihood (Corpuz et al. 1996) (PhyML 3.0 aLRT) (Guindon et al. 2010) and Neighbour Joining (NJ) methods with a JTT substitution model and a discrete gamma distribution of rates among sites with 4 categories and 100 or 1000 bootstrap replicates (ML and NJ, respectively). The accession numbers of all sequences used to generate phylogenetic trees are indicated in supplementary table 4.1.

A branch-specific test for positive selection, was used to assess the presence of significantly divergent branches in the ML gene tree (Branch Site REL (Pond et al. 2011)). The full-length, vertebrate *ogn* nucleotide coding sequences aligned in ClustalX v2.0.11 (Larkin et al. 2007) (see supplementary table 4.1 for accession numbers) were transferred into Translator X (Abascal et al. 2010) to obtain a codon-based alignment. The user tree option for analysis in Data Monkey (http://www.datamonkey.org/) of branch- and site-specific codon evolution was the vertebrate OGN ML tree.

To identify the chromosome harbouring the teleost *ogn* gene most like the ancestral form short range linkage maps of fish *ogn* genes were compared with Human *OGN*. The genes that flank *ogn1* (LG1A: 25953681-25958751) and *ogn2* (LG22-25: 8776719-8778287) in the European sea bass (*Dicentrarchus labrax*), Japanese puffer fish (*Takifugu rubripes*) (*ogn1* scaffold_192: 347893-352120 and *ogn2* scaffold_75: 1027406-1028311), zebrafish (*Danio rerio*) (*ogn1* Chr.22: 10564753-10570030 and *ogn2* Chr.23: 19968107-19971521), spotted gar (*Lepisosteus oculatus*) (*ogn1* LG5: 46192316-46202415), coelacanth (*Latimeria chalumnae*) (*ogn1* JH126569.1: 5130733-5135069) and Human *OGN* (Chr. 9: 92389641-92393152) were retrieved.

### 4.3.3. Promoter analysis

Coparison of the promoter sequences of *ogn1* and *ogn2* from sea bass (http://seabass.mpipz.de/ version dicLab v1.0c), which shares evolutionary proximity with the sea bream, and has a fully sequenced genome was used to identify potential differences in gene regulation. A 2 Kb sequence upstream of sea bass *ogn1* (DLAgn_00097140, LG1A: 25958752-25960751) and *ogn2* (DLAgn_00129310, LG22-25:8774557-8776556) was used to identify the transcription start site for each gene and putative transcription factor binding sites using MatInspector (www.genomatix.de). Position weight matrices were used to represent the TFBSs using default parameters. The matrix family library Version 9.1 of the genomatix suite (www.genomatix.de) was used for the analysis.

### 4.3.4. Multiple sequence alignments and protein characterization

A multiple sequence alignment (ClustalX v2.0.11 (Larkin et al. 2007)) of the deduced amino acid sequences for fish (*Lepisosteus oculatus, Sparus aurata, Oreochromis niloticus, Gadus morhua, Danio rerio, Latimeria chalumnae*) and terrestrial vertebrate (*Xenopus tropicalis, Gallus gallus, Homo sapiens*) OGNs was used to identify conserved motifs and domains using UniProt (http://www.uniprot.org), PROSITE (http://prosite.expasy.org/cgi-bin/prosite/) InterPro (http://www.ebi.ac.uk/ interpro/) and Pfam (http://pfam.xfam.org/) databases.

The consensus sequence for LRR repeat motifs characteristic of class III SLRP family members were identified manually (LXXLXLXXN/CXL, where L is a hydrophobic amino acid, N is Asn and C is Cys, and X is any amino acid). The characteristic N-terminal ($CX_2CXCX_6C$) and C-terminal ($CX_{33}C$) cysteine-rich clusters and disulfide bonds were identified by sequence similarity with annotated OGN sequences using DISULFIND software v.4. (http://disulfind.dsi.unifi.it, (Ceroni et al. 2006)). The signal peptide, molecular weight and isoelectric point of predicted proteins were determined using SignalP v.4.1 (http://www.cbs.dtu.dk/services/SignalP/) (Petersen et al. 2011)) and ProtParam (http://web.expasy.org/protparam/) (Gasteiger E et al. 2005). Post-translational modification (Lauter et al. 2011) sites such as: *N*-linked (GlcNAc, D-N-acetylglucosamine) and *O*-linked glycosylation (GalNAc, D-N-acetylgalactosamine), phosphorylation, YinOYang sites, leucine-rich nuclear exporting signals (http://www.cbs.dtu.dk/services) (Blom et al. 2004; Steentoft et al. 2013; Gupta and Brunak 2002; Cour et al. 2004), tyrosine sulfation (http://sulfosite.mbc.nctu.edu.tw (Chang et al. 2009)) and acetylation (http://bdmpail.biocuckoo.org) (Li et al. 2006) were identified. PROSITE MyDomains image

creator software (http://prosite.expasy.org/prosite.html) was used to build representative OGN structures.

### 4.3.5. Animal experiments

#### 4.3.5.1.Ethics Statement

The maintenance of the fish and subsequent experiments carried out at the Ramalhete`s experimental station of the Centre of Marine Sciences (CCMAR, University of Algarve, Faro, Portugal) and at the University of Barcelona (UB, Barcelona, Spain) complied with the Guidelines of the European Union Council (86/609/EU) and were covered by a group 1 license (Direção-Geral de Veterinária, Portugal) or approved by the corresponding Ethics and Animal Care Committee of Barcelona (permit numbers CEEA 243/12 and DAAM 6759).

The behaviour and health of all animals was monitored visually each day and no evidence of infection, modified behaviour or mortality was observed during the experiments.

#### 4.3.5.2. Tissue sampling

Gilthead sea bream juveniles (n = 3; 94-140 g) maintained under standard conditions (500 L open circuit sea water tanks, see below for details) at CCMAR, were anesthetized with 2-phenoxyethanol (1:10,000; Sigma-Aldrich, Tres Cantos, Spain) and nine tissues (fast-twitch/white skeletal muscle, visceral adipose tissue, vertebra, kidney, gill arches, gill filaments, skin, heart and liver) were collected and immediately snap-frozen in liquid nitrogen. The tissue panel was used to assess the distribution of *ogn* using quantitative real-time PCR (QRT-PCR).

#### 4.3.5.3.Tissue culture experiments

Gilthead sea bream juveniles were obtained from a hatchery in Northern Spain and maintained in the animal facility of the Faculty of Biology at UB in 200 L fiberglass tanks at 21 ± 1ºC, pH 7.5-8, 31-38‰ salinity and > 80% oxygen saturation under 12 h light/12 h dark photoperiod and fed *ad libitum* twice daily with a commercial feed (Excel; Skretting, Burgos, Spain).

##### 4.3.5.3.1. Bone-derived gilthead sea bream primary culture

Primary cultures (n = 5) derived from vertebra of gilthead sea bream juveniles (8-38 g) were performed using an established protocol (Capilla et al. 2011). Briefly, the vertebral

columns of 6 fish per culture were removed and washed, and small fragments were obtained mechanically using a scalpel. Then, two enzymatic digestions were performed in gentle agitation at 18ºC with 0.125% collagenase type II (Sigma-Aldrich, Spain). The fragments obtained were washed, plated in 10 cm plates with growth medium (GM) composed of Dulbecco's Modified Eagle Medium (DMEM) supplemented with 10% fetal bovine serum (FBS) and 1% antibiotic/antimycotic solution (A/A) and incubated at 23ºC and 2.5% $CO_2$. After a week, the fragments were removed and the cells collected by treating with 0.25% trypsin-EDTA (Invitrogen, Alcobendas, Spain) and used to generate several subcultures; cells were maintained for a maximum of 10 passages.

For the experiments, cells were trypsinised, suspended in GM, counted and plated in 6-well plates at a density of $10^5$ cells per well. The next day (day 0), the media was changed and cells were grown either under control (GM) or mineralizing conditions, using an osteogenic medium (OM; GM supplemented with 50 μg/ml of L-ascorbic acid, 10 mM β-glycerophosphate and 4 mM $CaCl_2$) or were induced to trans-differentiate with adipogenic medium (AM, GM supplemented with 10 μg/ml insulin, 0.25 μM dexamethasone, 0.5 mM 1-methyl-3-isobutylxanthine (IBMX) and 5 μl/ml lipid mixture (containing cholesterol and fatty acids from cod liver oil). Cultures were maintained for up to 20 days and media was replaced every 3-4 days. Samples consisted of a pool of 2 wells/primary culture (n = 5) and were collected into 1 ml of TRI reagent (Applied Biosystems, Alcobendas, Spain) at days 5, 10, 15 and 20 and stored at -80ºC until gene expression analysis. Development of the cells under GM, OM and AM conditions was followed using an Axiovert 40C inverted microscope (Zeiss, Germany) and images were captured with a Canon EOS 1000D digital camera. Three samples were collected at each time point and cultures were repeated in 5-8 independent experiments.

#### 4.3.5.3.2. Myocyte gilthead sea bream primary culture

Primary cultures (n = 4) of gilthead sea bream muscle satellite cells were performed as previously described (Montserrat et al. 2007). In brief, the epaxial fast-twitch/white skeletal musculature of juvenile fish (11-23 g) was collected and mechanically disrupted before enzymatic digestion at 18ºC with 0.2% collagenase type Ia (Sigma-Aldrich, Spain), followed by 0.1% trypsin (Sigma-Aldrich, Spain). Cells were washed in phosphate buffered saline (PBS), resuspended in GM, counted and plated at a density of 1.5-2 x $10^6$ cells per well in 6-well plates and incubated at 23ºC and 2.5% $CO_2$.

For characterisation, images of the cultures were captured with an Axiovert 40C inverted microscope (Zeiss) coupled to a Canon EOS 1000D digital camera and samples were

collected into 1 ml of TRI reagent (Applied Biosystems) at days 2, 4, 8 and 12 of each culture (n = 4) and stored at -80ºC until gene expression analysis. Individual samples consisted of a pool of 2 wells and three samples were collected at each time point.

#### 4.3.5.4. OGN in a scale regeneration model

Adult gilthead sea bream (1-year-old) were obtained from a commercial supplier and transferred to CCMAR. Fish (n = 30) were acclimated to a 500 L tank supplied with a continuous flow of aerated sea water at 19 ± 1ºC, 35 - 36‰ salinity and > 80% oxygen saturation under a standard 12 h light/12 h dark photoperiod for 3 weeks prior to the start of the experiment. The fish were fed twice daily (2% of fish weight) with a commercial diet (Provimi, Portugal).

On day 0 of the trial, fish were anaesthetized with 2-phenoxyethanol in seawater (1:10,000; Sigma-Aldrich), photographed (for measurement of length) and weighed. The scales were removed from the left side of the body below the dorsal fin by stroking the skin with forceps to minimise damage to the dermis. Fish were then rinsed in several changes of filtered seawater and returned to the experimental circuit. The whole procedure took approximately 2 min per fish.

On days 0, 5, 10 and 28 after scale removal a subset of fish (n = 6 / time point) were killed and skin repair and scale regrowth monitored using samples collected for molecular biology, biochemistry and histology from both flanks of each individual: the descaled side of the fish (called the regenerating sample / scales) and from the undamaged side (called the intact sample / scales). Fish (n = 6) were anesthetized with 2-phenoxyethanol (1:10,000; Sigma-Aldrich), photographed, weighed and length measured. A blood sample was collected by caudal puncture, centrifuged (10,000 rpm for 5 min) and the plasma transferred to a micro-centrifuge tube, frozen in liquid nitrogen and stored at -80ºC until analysis. Fish were killed by severing the spinal cord and intact and regenerating skin samples were taken. Samples (1.5 $cm^2$) were either frozen in liquid nitrogen or fixed in 4% paraformaldehyde (PFA; pH 7.4) at 4ºC for histology. Scales were also collected individually (n = 15 scales per fish) using a pair of forceps and put in enzyme buffer for alkaline phosphatase (ALP, n = 5 scales per fish, n = 6 fish) and tartrate-resistant acid phosphatase (TRAP, n = 5 scales per fish, n = 6 fish) assays, or placed in physiological saline (n = 5 scales per fish, n = 6) for histomorphometric analysis. In order to better monitor the regeneration / growth of scales, samples (n = 10 scales) were also collected from anesthetized fish (n = 2) at day 20 of the experiment for enzymatic and histomorphometric

analysis. These fish were not sacrificed and were allowed to recover in clean and aerated seawater before returning to the experimental tanks.

#### 4.3.5.4.1. Plasma analysis

The influence of scale removal on plasma biochemistry was assessed. The concentration of plasma calcium (Ca) and phosphorus (P) was determined in duplicate tubes of heat denatured pre-diluted plasma collected in the scale regeneration experiment using an endpoint colorimetric assay (Calcium-o-C v/v and Phorphorus v/v; Spinreact, Sant Esteve d'En Bas, Spain). Results were expressed as $mmol \cdot L^{-1}$. The plasma ions sodium (Na) and potassium (K) were determined using a flame photometer (BWB Technologies) according to the manufacturer`s instructions. Plasma osmolality was determined using a vapour pressure osmometer (Vapro Wescor 5520, South Logan, Utah, USA) and expressed in $mOsmol \cdot kg^{-1}$. Total plasma protein was measured in diluted samples (1:100) with the BioRad Protein Assay Dye Reagent (Cat.no. 500-0006; BioRad, El Prat de Llobregat, Spain) and results were expressed in $mg \cdot ml^{-1}$. Bovine serum albumin (BSA; Sigma-Aldrich) was used as the standard. Plasma aspartate-aminotransferase (AST; EC.2.6.1.1) and alanine-aminotransferase (ALT; EC 2.6.1.2), indicators of tissue inflamation, were determined using a spectrophotometric method with aspartate and alanine as the substrate, respectively (Gallardo et al. 2003) and activity was expressed as $mIU \cdot ml^{-1}$ of plasma.

#### 4.3.5.4.2. Scale TRAP and ALP activities

TRAP and ALP are markers of bone turnover and indicators of tissue demineralization and mineralization, respectively. Enzyme activity was measured in scales as described by Guerreiro *et al.* (2013). Briefly, individual scales were incubated with agitation in 200 µl of 10 mM paranitrophenyl (pNPP) in 0.1 mM Na-acetate buffer for 20 min at 24°C. In the case of TRAP 10 mM tartrate was included in the incubation buffer. The reaction was stopped with 2 M NaOH and the absorbance measured at 405 nm using a microplate reader (Benchmark; BioRad). The amount of pNPP converted into paranitrophenol (pNP) was calculated using a pNP standard curve. Individual scales were rinsed in distilled water and dried at 65°C to a constant weight. Results were expressed in nmol pNP $min^{-1}$ $mg^{-1}$.

#### 4.3.5.4.3. Calculation of scale area and regeneration rate

Scales were collected at 0, 5, 10, 20 and 28 days after scale removal (n = 21 - 30 scales for days 0, 5, 10 and 28; n = 10 for day 20) and stored in a saline solution at 4°C until analysis. The regrowth of scales was used to give a measure of the ontogeny of tissue recovery after damage. Intact and regenerating scales were photographed (Leica DFC480) and the software ImageJ 1.440 (Abramoff et al. 2004) used to measure the scale area ($mm^2$). The scale regeneration rate was calculated as previously described by Ohira *et al*. (2007). Briefly, the scale area of each regenerating scale was related to the average scale area of intact scales at time 0. The scale regeneration rate was obtained using the following equation: $RR_{area}\% = R_{area} / O_{area} \times 100$, (where $RR_{area}$ = increase in scale area, $R_{area}$ = the area of the regenerating scales and $O_{area}$ = the average area of scales at the start of the experiment, day 0). The increase in scale area ($mm^2$) was determined as the difference in area of the growing scales (from the intact and regenerating flanks) relative to the total area of the scales at the start of the experiment (time 0), assuming in the case of the regenerating scales that the area was 0.

#### 4.3.5.4.4. RNA extraction and cDNA synthesis

Total RNA from sea bream tissues snap frozen in liquid nitrogen was extracted using a Maxwell® 16 MDx Instrument (Promega, Madrid, Spain) with a Maxwell 16 Total RNA Purification Kit (Promega). RNA from cell culture samples was extracted with TRI reagent (Applied Biosystems) according to the manufacturer`s instructions. Quality and integrity of total RNA was verified using a NanoDrop1000 Spectrophotometer (Thermo Scientific, Alcobendas, Spain) and by running it on a 1.5% (m/v) agarose gel before treatment with 1.5 U DNAse (Ambion DNA-*free*™ kit, Austin, Texas, USA). DNA free, total RNA (500-1000 ng) was used for first strand cDNA synthesis in a 20 µl reaction volume containing 100 mM p6 random hexamers (GE Healthcare, UK), 100 U of RevertAid™ Reverse Transcriptase (Fermentas, Lithuania) and 8 U of RiboLock™ RNase Inhibitor (Fermentas). cDNA was synthesized for 10 min at 20°C, followed by 50 min at 42°C and 5 min at 72°C and the quality was checked by amplifying the ribosomal protein S18 (*rps18*) using the following cycle: 10 min at 95°C, followed by 25 rounds of amplification of 30 s at 95°C, 30 s at 60°C and 30 s at 72°C and finally one cycle of 5 min at 72°C. The PCR products were run on a 1% (m/v) agarose gel to confirm amplicon size.

#### 4.3.5.4.5. Quantitative real-time PCR (QRT-PCR)

QRT-PCR was carried out in duplicate 10 µl reactions of 1x SsoFast-Evagreen Supermix (BioRad) containing cDNA (≈ 16.7 ng) and 300 nM of forward and reverse primers. Specific PCR primers were designed for gilthead sea bream *ogn* transcripts using Primer premier (Biosoft, Palo Alto California, USA) and those for *ef1α*, *rps18* and *ß-actin* have previously been reported (table 4.1) (Vieira et al. 2012). Quantification was performed in a StepOnePlus thermocycler (Applied Biosystems) using the standard-curve method (software StepOne™ Real-Time PCR Software v2.2) and the following program: 30 s at 95°C, 45 cycles of 5 s at 95°C and 15 s at 60°C. Negative controls were also run and included a no template control (NTC, cDNA was substituted with water in PCR reactions) and a no reverse transcriptase control (RTC, RT was omitted from the cDNA synthesis reaction). A standard curve relating initial template quantity to amplification cycle was generated using serial dilutions of known concentrations of the target template. The templates for the standard curves were generated by conventional PCR using standard conditions, 10 ng cDNA, 1.5 U of Taq polymerase (Readymix Taq PCR Reaction Mix, Sigma-Aldrich) and 200 nM of long-forward and long-reverse primers (table 4.1) in a final volume of 50 µl. PCR products for standards were column purified (Illustra™ GFX™ PCR DNA and Gel Band Purification Kit, GE Healthcare) and quantified (NanoDrop1000; Thermo Scientific).

The relative expression of the analysed genes was estimated using the geometric mean of the reference transcripts *ef1α* and *rps18* in the case of cell cultures or *rps18* and *ß-actin* in the skin regeneration experiment, since their expression did not vary significantly ($p > 0.05$) between samples. The results of gene expression analysis was expressed as relative expression (copy number) for cell culture and as log2(fold-change) for the skin regeneration experiment.

**Table 4. 1 - List of primers used for gene expression analysis by quantitative real-time PCR (qPCR).** Gene name, primer sequence, amplicon length (base pairs, bp), annealing temperature (Ta, ºC) and efficiency (%) and $R^2$ are indicated for each primer pair. F: forward, R: reverse. na: not applicable

| Gene name | Primer sequence (5`➔3`) | Amplicon (bp) | Ta (ºC) | Efficiency | $R^2$ |
|---|---|---|---|---|---|
| *ogn1* | F: GAAGTCTCTCTTATTCACCTGT | 138 | 60 | 92.4 | 0.99 |
| | R: CAAAGGGTCACTGAAGTATCCA | | | | |
| *ogn2* | F: TGTTATTCTCCCATGGATCCTG | 125 | 60 | 100 | 0.99 |
| | R: GATCCCCCGCTGCATCTGTGG | | | | |
| *ogn1* | F: GAAGTCTCTCTTATTCACCTGT | 544 | 60 | na | na |
| | R: GTTGTTGGCATTGAAGGAT | | | | |
| *ogn2* | F: ATGATGCAACTGAGGACTTTAA | 392 | 60 | na | na |
| | R: GCTCCATCTTCAATCTCAG | | | | |

### 4.3.6. Statistical analyses

Significant changes in transcript abundance in the sea bream tissue panel were tested using a One-way ANOVA with a Bonferroni multiple comparison post-test. A Two-way ANOVA followed by a Fisher`s least significant difference (LSD) post-test was performed using StatPlus:mac LE v5 2015 (AnalystSoft Inc., USA). This revealed significant differences between experimental groups in gene transcript abundance, both in cell cultures and in the skin regeneration challenge, TRAP and ALP activity and scale growth during skin regeneration. The significance cut-off was set at $p < 0.05$ for all the statistical analysis performed. Data are presented as the mean ± standard error of the mean (sem).

## 4.4. Results

### 4.4.1. OGN phylogenetic analysis

Duplicate genes for *ogn* only existed in teleost genomes and presumably arose during the teleost specific whole genome duplication (figure 4.1 and supplementary table 4.1 for accession numbers). The ML and NJ phylogenetic trees were routed with human EPYC and had the same general topology (figure 4.1 and supplementary figure 4.1). The ML tree generated two major OGN clusters with very strong bootstrap support, one cluster contained the ray-finned fish Ogns and the other contained OGN from the terrestrial vertebrates and the coelacanth (figure 4.1). The teleost Ogns clustered into an Ogn1 and Ogn2 specific cluster and confirmed the identity of the isolated sea bream Ogn1 and 2. The Ogn from the gar (*Lepisosteus*

*oculatus*) was outside the teleost specific clades for Ogn1 and 2. A single *ogn* homologue was identified in placental mammals, ungulates, rodents, birds, reptiles and amphibians, and also in the extant ancestral fish in the tetrapod lineage, the coelacanth (*Latimeria chalumnae*). The *ogn1* gene from marine organisms (teleost fish, coelacanth and turtles) was under positive selection at several amino acid positions (table 4.2).

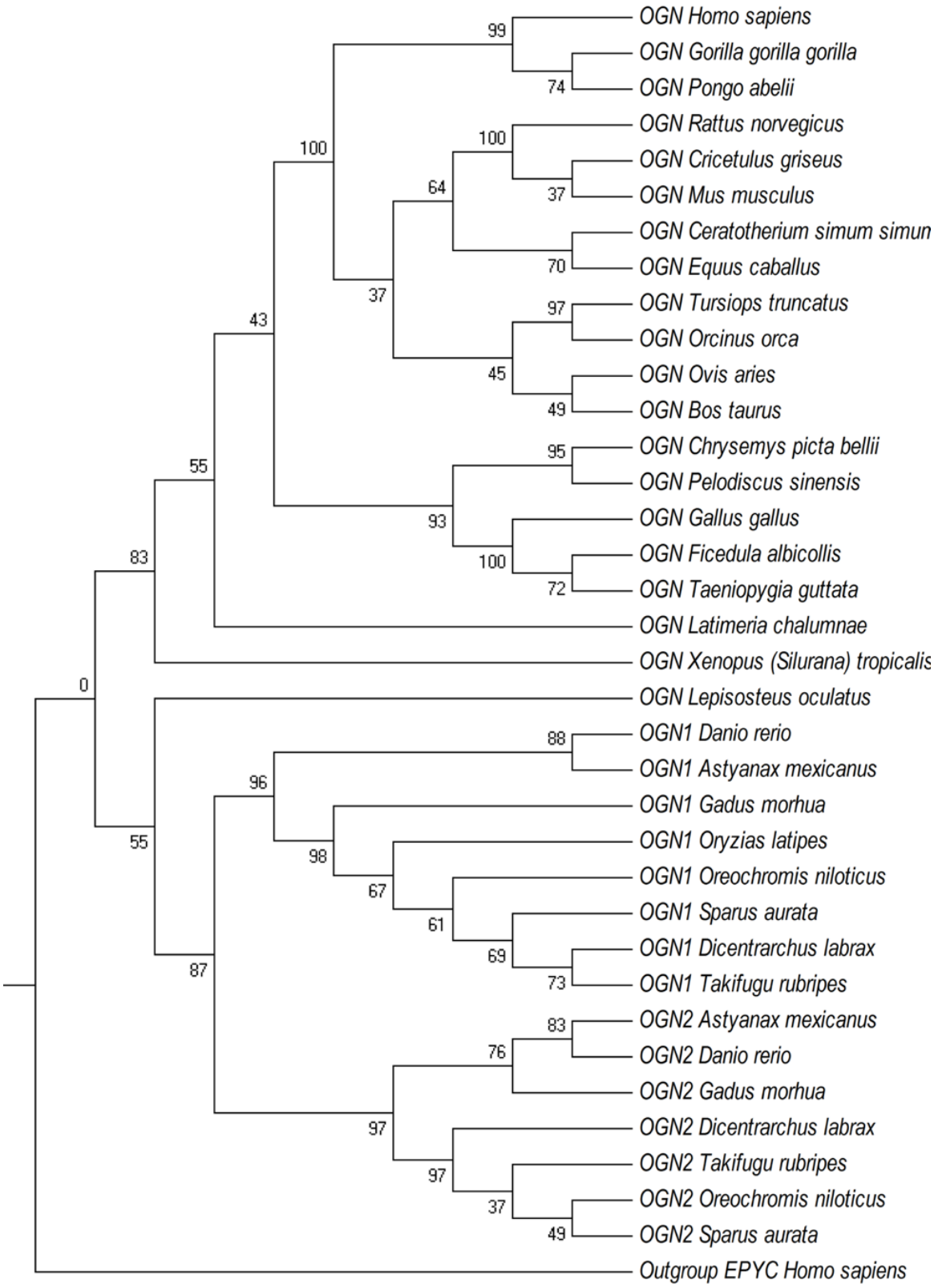


**Figure 4. 1 - Phylogenetic analysis of osteoglycins (OGNs) in vertebrates.** Phylogenetic analysis was performed using the Maximum Likelihood method with 100 bootstrap replicates and a JTT substitution model with a discrete gamma distribution of rates among sites with 4 categories. The supportive bootstrap values (%) are indicated at each node. To root the tree, the sequence of human epiphycan (EPYC) was used as the out-group. The accession numbers of all the sequences used in this phylogenetic tree are shown in supplementary table 4.1.

**Table 4. 2 - OGNs and positive selection**. Summary of tree branches exhibiting signatures of positive selection in gene-trees constructed for vertebrate osteoglycin genes. [a] Branch under episodic diversifying selection at $p \leq 0.05$. [b] The p-value for episodic selection at this branch corrected for multiple testing using the Holm-Bonferroni method. [c] The ω value inferred for positively selected sites long this branch. [d] The proportion of sites inferred to be evolving at ω+ along this branch. [e] Node 15 refers to the separation of *Takifugu rubripes* OGN1 with *Dicentrarchus labrax* and *Sparus aurata* OGN1.

| Branch[a] | Corrected p-value[b] | $\omega^{+c}$ | Pr $[\omega=\omega^{+}]^{d}$ |
|---|---|---|---|
| *D. labrax* OGN1 | <0.0001 | 74.07 | 0.16 |
| *T. rubripes* OGN1 | 0.000 | 16.40 | 0.15 |
| *O. latipes* OGN1 | 0.001 | 11.39 | 0.20 |
| *O. niloticus* OGN1 | 0.003 | 21.47 | 0.07 |
| Node 15[e] | 0.011 | 863.89 | 0.04 |
| *C. picta belii* OGN1 | 0.020 | 2785.35 | 0.02 |
| *A. mexicanus* OGN1 | 0.030 | 654.36 | 0.09 |
| *L. chalumnae* OGN1 | 0.043 | 12.91 | 0.19 |

The gene environment of *ogn* revealed high synteny between fish *ogn1* and tetrapod *OGNs* suggesting that it was the ancestral form (figure 4.2). In contrast, the gene environment of fish *ogn2* only shared synteny with fish homologues and in zebrafish *ogn1* and *ogn2* had a single common gene in linkage, the duplicated potassium channel tetramerisation domain containing 6 genes (*kctd6a* and *kctd6b*) (figure 4.2).

### 4.4.2. OGN sequence conservation

Analysis of available teleost genomes revealed that they possess duplicate genes and the deduced proteins shared between 66-72% aa sequence similarity (table 4.3). In the ray-finned fish lineage lepisosteiformes, the spotted gar contained a single *ogn* gene that encoded a protein that shared 68% sequence similarity with teleost Ogn1 and 2 suggesting that the teleost specific whole genome duplication generated the 2 teleost *ogn* genes. Searches in the genome of the elephant shark (*C. millii*; esharkgenome.imcb.a-star.edu.sg), lamprey (*Petromyzon marinus*) and the tunicate, *Ciona intestinalis*, revealed several putative members of the SLRP gene family but no homologue of *ogn*, suggesting that although it emerged in the ancestral organism of the fishes it was only retained in the bony fish.

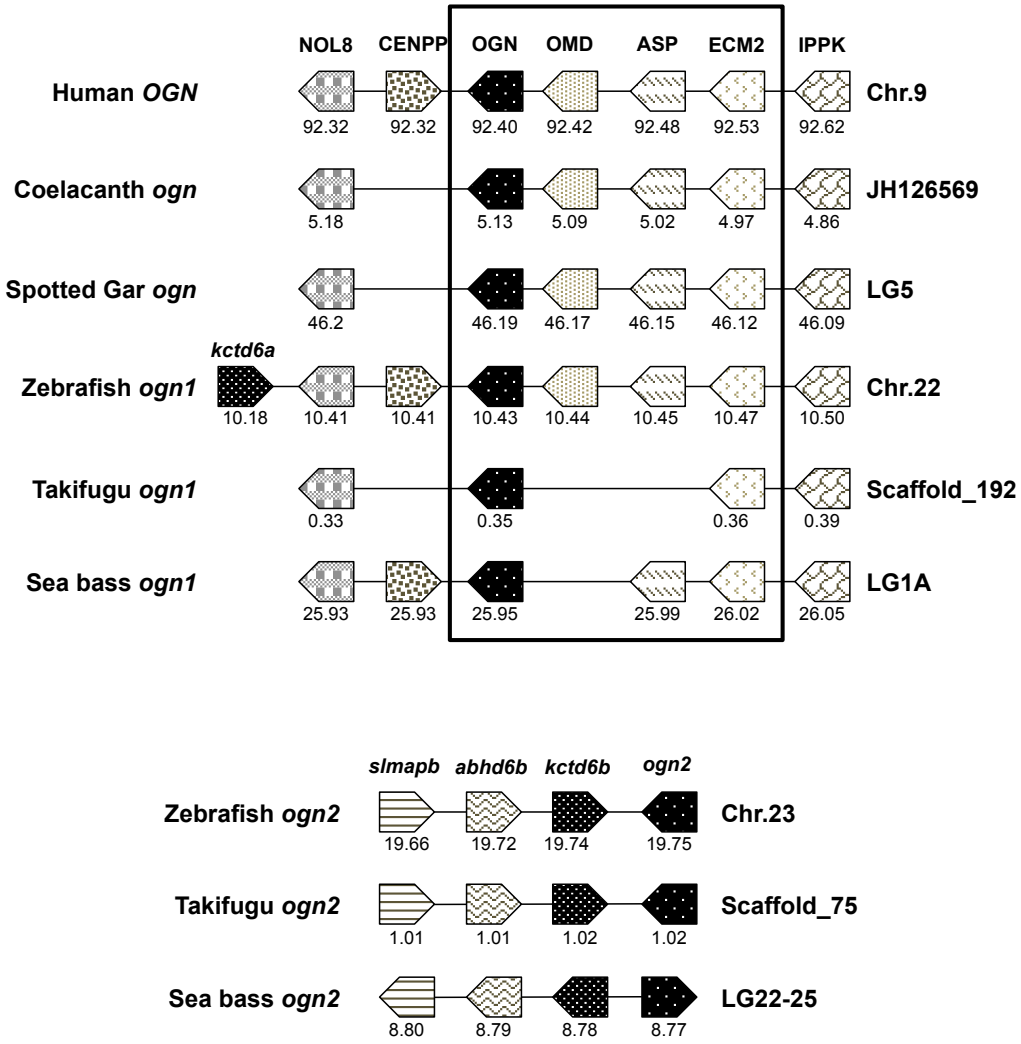


**Figure 4. 2 - Conserved synteny in vertebrate osteoglycins (*ogn*).** The gene environment of *ogn* genes was obtained from the Ensembl Genome Browser and from the UCSC genome browser of the sea bass genome at http://seabass.mpipz.mpg.de. Horizontal lines represent the chromosome fragments and arrow boxes indicate genes and arrowhead point to the direction of the predicted gene transcription. Homologue genes between species are given the same colour (shading) to facilitate perception of conservation. The predicted location of the gene in the chromosome is indicated in Megabase pairs. Note the higher conserved synteny between *OGN* in terrestrial vertebrates and teleost *ogn1*. NOL8 – Nucleolar protein 8; CENPP – Centromere protein P; OGN – Osteoglycin; OMD – Osteomodulin; ASP – Asporin; ECM2 – Extracellular matrix protein 2; IPPK – Inositol 1,3,4,5,6-pentakisphosphate 2-kinase; *kctd6* – Potassium channel tetramerisation domain containing 6; *Slmapb* – Sarcolemma associated protein b; *abhd6b* – Abhydrolase domain containing 6

**Table 4. 3 - Comparison of vertebrate OGNs and fish duplicates Ogn1 and 2**. The sequence identity and similarity (between brackets) are shown as percentages and the highest identities and similarities to the sea bream Ogn1 and 2 are shown in bold. Abbreviations: Sa – *Sparus aurata*, Dl – *Dicentrarchus labrax*, Dr – *Danio rerio*, Lo – *Lepisosteus oculatus*, Lc – *Latimeria chalumnae*, Xt – *Xenopus (silurana) tropicalis*, Gg – *Gallus gallus* and Hs – *Homo sapiens*.

| | Sa_Ogn1 | Dl_Ogn1 | Dr_Ogn1 | Sa_Ogn2 | Dl_Ogn2 | Dr_Ogn2 | Lo_Ogn | Lc_Ogn | Xt_OGN | Gg_OGN | Hs_OGN |
|---|---|---|---|---|---|---|---|---|---|---|---|
| Sa_Ogn1 | 0 | **71 (78)** | 59 (72) | 50 (68) | 54 (71) | 51 (67) | 52 (68) | 48 (62) | 47 (64) | 49 (67) | 47 (63) |
| Dl_Ogn1 | | 0 | 60 (72) | 50 (64) | 53 (68) | 51 (66) | 49 (65) | 47 (61) | 48 (64) | 47 (64) | 46 (62) |
| Dr_Ogn1 | | | 0 | 49 (64) | 52 (67) | 50 (65) | 55 (71) | 48 (61) | 49 (65) | 49 (64) | 49 (66) |
| Sa_Ogn2 | | | | 0 | **80 (91)** | 60 (75) | 54 (68) | 44 (60) | 47 (69) | 48 (60) | 47 (63) |
| Dl_Ogn2 | | | | | 0 | 61 (76) | 56 (69) | 44 (60) | 47 (64) | 48 (62) | 48 (64) |
| Dr_Ogn2 | | | | | | 0 | 52 (68) | 46 (58) | 45 (61) | 46 (60) | 46 (63) |
| Lo_Ogn | | | | | | | 0 | 51 (66) | 53 (69) | 53 (66) | 54 (70) |
| Lc_Ogn | | | | | | | | 0 | 52 (65) | 52 (63) | 54 (68) |
| Xt_OGN | | | | | | | | | 0 | 53 (68) | 54 (70) |
| Gg_OGN | | | | | | | | | | 0 | 63 (78) |
| Hs_OGN | | | | | | | | | | | 0 |

### 4.4.3. Multiple sequence alignments and protein characterization

Duplicate *ogn* transcripts were identified in the gilthead sea bream muscle, vertebra and gill arch transcriptomes (Genbank accession numbers: KM603667 and KM603668 for *ogn1* and *ogn2*, respectively) (supplementary figure 4.2). A multiple sequence alignment of sea bream Ogn1 and 2 with OGN from other teleosts, non-teleost fish, amphibians, birds and human revealed a conserved signal peptide sequence and seven characteristic LRR motifs typical of class III SLRP family members (figure 4.3 and supplementary figure 4.3). The consensus sequence for LRR (LXXLXLXXNXL, where L is a hydrophobic amino acid, N is Asn, and X is any amino acid) was found in LRRs 2, 3, 4, 5, 6, 7 while LRR1 was incomplete and the first consensus site lacked a hydrophobic amino acid. The central LRR domain was flanked by an N-terminal leucine rich repeat that incorporated a cysteine-rich cluster ($CX_2CXCX_6C$), see figure 4.3. The C-terminus contained two cysteine residues ($CX_{33}C$) with an LRR consensus sequence between them (figure 4.3 and supplementary figure 4.3). Additional features shared with other vertebrate class III SLRPs were also identified in fish Ogn1 and 2 proteins (figure 4.3 and supplementary figure 4.3). Consensus sites for disulphide bonds, that in human OGN form capping motifs (McEwan et al. 2006), were present in the N-terminus (C1 - C3 and C2 - C4, *aka* LRRNT capping motif) and C-terminus (C5 - C6, *aka* LRRCE capping motif (Park et al. 2008)) of fish Ogn. The conserved N-terminal consensus sequence for tyrosine sulphation in vertebrate OGN was absent from teleost Ogn1 (with the exception of cod, *Gadus morhua*). One to three leucine-rich nuclear export signals (NES) were identified in the OGNs analysed (figure 4.3) and a teleost specific NES localized in LRR5 was identified in both Ogn1 and 2. Teleost Ogns had a similar molecular weight (MW) but tended to be more basic than OGN in terrestrial vertebrates and other non-teleost fish.

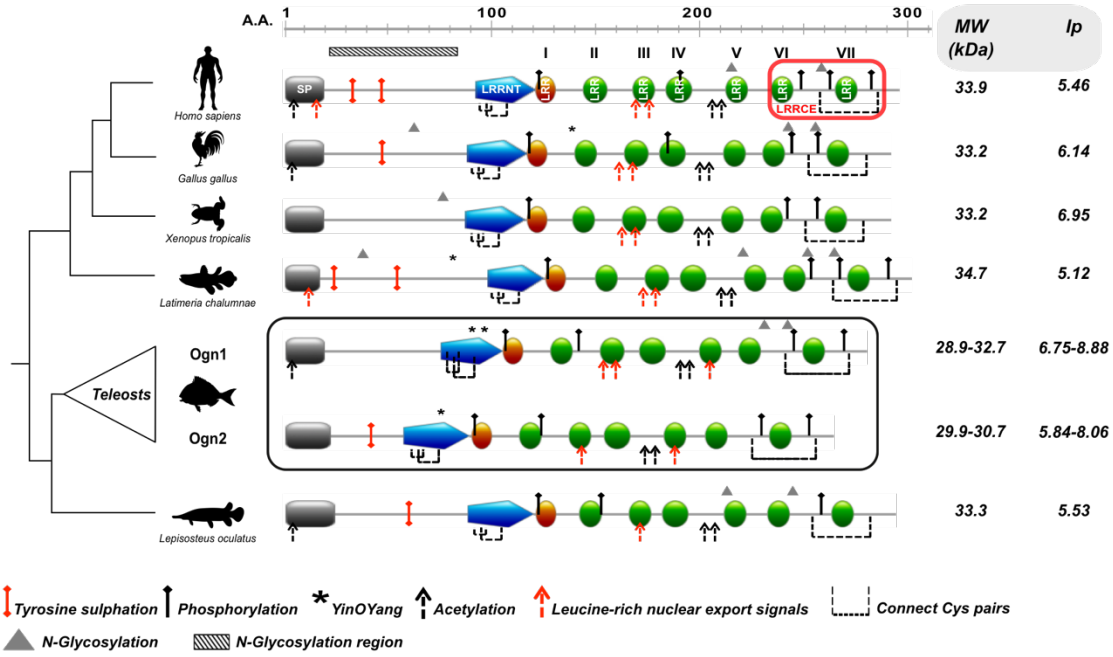


**Figure 4. 3 - Dendrogram comparing OGN structural features from representative organisms of the main vertebrate lineages.** Structural domains/motifs present in the amino acid sequences of OGNs from representative organisms are indicated as coloured blocks using the human OGN sequence as the reference. SP: signal peptide; LRRNT: leucine rich repeat N-terminal motif (blue); LRR: leucine rich repeated motif (green and orange and numbered I-VII); LRRCE: ear-containing leucine-rich repeat C-terminal motif (red box). LRRNT is the N-terminal cysteine flanked capping motif rich in hydrophobic amino acids. Green blocks represent the consensus region for LRR (LXXLXLXXNXL, where L is a hydrophobic amino acid, N is Asn, and X is any amino acid) and orange block is incomplete LRR in which the first consensus site is not a hydrophobic amino acid. LRRCE is the C-terminal cysteine flanked capping motif. The predicted consensus sites for post-translational modifications (PTMs) are indicated and described in the legend as: tyrosine sulphation (red pin); phosphorylation (black pin); N-linked glycosylation (triangle); *O*-linked glycosylation region (horizontal bar with black blades oblique); YinOYang sites (asterisks); acetylation (black dashed arrow). Broken lines connect adjacent cysteine pairs and leucine-rich nuclear export signals are indicated (red dashed arrow). The rule on the top indicates the number of amino acids (A.A). The *in silico* analysis of the molecular weight (MW, in kilodaltons, kDa) and the isolelectric point (Ip) of analysed OGNs are indicated on the right hand side of the figure. *Sparus aurata*, *Oreochromis niloticus*, *Gadus morhua* and *Danio rerio* Ogn1 and Ogn2 were chosen as the representative amino acid sequence for teleosts and are represented in the back box. Note: the MW/Ip (not given in the figure) of *S. aurata*, *O. niloticus*, *G. morhua* and *D. rerio* were respectively for Ogn1, 29.5/8.36, 28.9/8.88, 32.7/6.75 and for Ogn2, 30.2/7, 30.7/8.06, 29.9/6.49. For simplicity the figure only reports the maximum and minimum predicted MW/Ip values. The accession numbers of the sequences used for structural analysis are given in supplementary table 4.1.

### 4.4.4. OGN promoter analysis

Analysis of the sea bass *ogn1* and *2* promoters identified common and gene specific transcription factor binding sites (TFBS). The identified TFBS in both the *ogn1* and *2* promoters suggests that both genes are likely to have a wide tissue distribution and are involved in the regulation of adipocyte (e.g. KLF, GATA and PPARG), myocyte (e.g. PAX3, MEF and SIX1) and chondrocyte (e.g. SOX5-6, SOX9 and RUNX3) differentiation (figure 4.4). The promoter of *ogn1* diverged from the promoter of *ogn2* in that it was enriched in TFBS associated with osteoblast differentiation (e.g. RUNX2, MSX and ATF4). In addition, in both the *ogn1* and *2*

promoters several putative ETS1 binding sites characteristic of UV responsive genes were present.

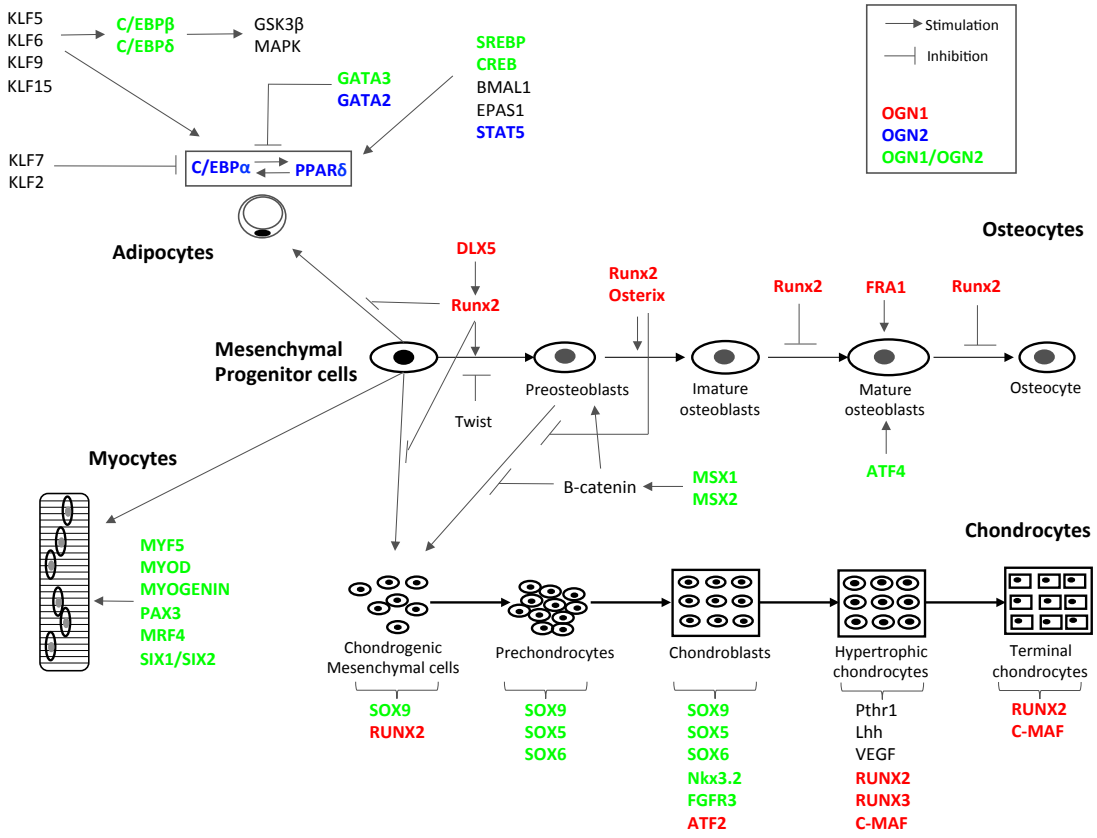


**Figure 4. 4 - Promoter analysis.** The promoter sequences (2 Kb upstream of) of *ogn1* and *ogn2* from sea bass (http://seabass.mpipz.de/ version dicLab v1.0c) were used to identify the transcription start site for each gene and putative transcription factor binding sites (TFBS) using MatInspector (www.genomatix.de). Several TFBS were identified in the promoters of sea bass *ogn1* (in red) and *ogn2* (in blue) and these were associated with different cell lineages derived from mesenchymal progenitor cells.

### 4.4.5. Tissue distributions of *ogn1* and *ogn2*

BLAST searches against the EST database in GeneBank (http://www.ncbi.nlm.nih.gov/genbank/) revealed that transcripts of *ogn1* were present in the olfactory epithelium, eye, muscle, thyroid, skin, bone, scales and digestive tissue while transcripts for *ogn2* were detected in jaw, thyroid, thymus, head kidney, spleen and skeletal muscle of several teleosts, *C. auratus*, *D. rerio*, *G. aculeatus*, *Salmo salar*, *G. morhua*, *O. niloticus*, *Haplochromis sp.* and *D. labrax* (table 4.4).

Analysis of *ogn1* and *ogn2* transcript distribution in gilthead sea bream tissues using qPCR corroborated the EST analysis and revealed that *ogn1* and *ogn2* were highly expressed in muscle, skin and gill arches but were low abundance in liver, gill filaments, kidney, heart,

vertebra and adipose tissue (figure 4.5). Head kidney, jaw, thyroid, thymus, spleen, olfactory epithelium, eye and digestive tissue were not analysed by qPCR.

**Table 4. 4 - Digital tissue distribution for ogn in teleost fish.** Sequence similarity searches (BLASTX and TBLASTN) were done using the sea bream *ogn1* and *2* sequences against the Expressed Sequence Tags (ESTs) database (http://www.ncbi.nlm.nih.gov/genbank/).

| Species | Tissue | Accession number | Identity | Reference |
|---|---|---|---|---|
| *Carassius auratus* | Olfactory epithelium | AM928511 | 77% *ogn1* | |
| *Danio rerio* | Myoblast | CT620959 | 75% *ogn1* | |
| *Gasterosteus aculeatus* | Eyes | DN691791 | 67% *ogn1* | |
| *Salmo salar* | Fast muscle | DY467584 | 81% *ogn1* | |
| *Salmo salar* | Thyroid | EG868446 | 63% *ogn1* | |
| *Salmo salar* | Skin | - | - | Krasnov et al. (2012) doi: 10.1186/1471-2164-13-130 |
| *Danio rerio* | Fin | EV761307 | 77% *ogn1* | |
| *Danio rerio* | Postcranial axial skeleton | - | - | Kessels et al. (2014) PubMed: 24608635 |
| *Danio rerio* | Pituitary | - | - | He et al. (2014) doi: 10.1530/JOE-13-0488 |
| *Sparus aurata* | Skin/scales | - | - | Ibarz et al. (2013) doi:10.1007/s10126-013- |
| *Gadus morhua* | Digestive tissue | FF416230 | 71% *ogn1* | |
| *Oreochromis niloticus* | Skin | GR683533 | 82% *ogn1* | |
| *Haplochromis sp.* | Jaw | BJ695864 | 75% *ogn2* | |
| *Salmo salar* | Thymus | EG772938 | 72% *ogn2* | |
| *Salmo salar* | Thyroid | EG869322 | 70% *ogn2* | |
| *Salmo salar* | Head kidney | EG900788 | 70% *ogn2* | |
| *Dicentrarchus labrax* | Spleen | FM024708 | 67% *ogn2* | |
| *Oreochromis niloticus* | Skeletal muscle | GR688606 | 83% *ogn2* | |

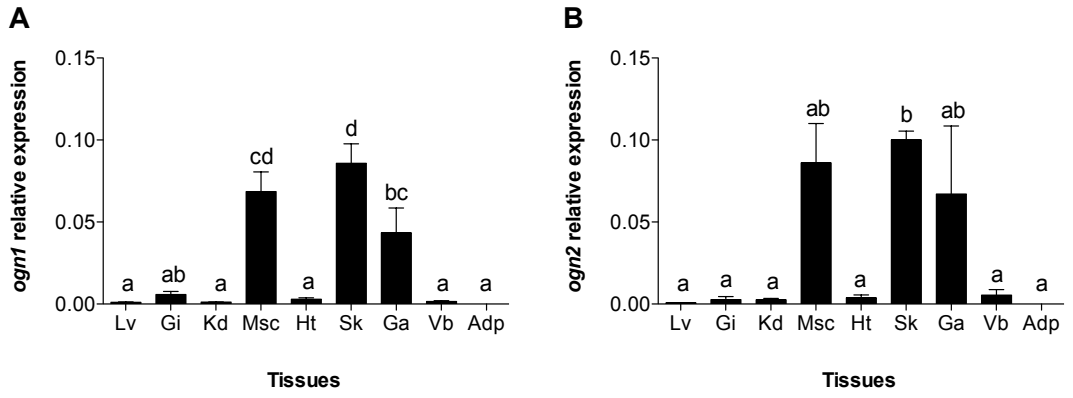


**Figure 4. 5 - Expression profile of gilthead sea bream osteoglycins (*ogn1* and *ogn2*) in adult tissues.** Quantitative relative expression of **A:** *ogn1* and **B:** *ogn2* in adult sea bream tissues. Lv: Liver; Gi: gill filaments; Kd: kidney; Ms: muscle; H: heart; Sk: skin; Ga: gill arches; Vb: vertebra; Ad: adipose**.** Results are presented as mean + sem (n = 3). Relative expression was determined using the geometric mean of *rps18* and *ß-actin* as references. A One-way ANOVA followed by a Tukey test was used to test for significant differences in transcript abundance between sea bream tissues and are indicated with letters (different letters denote significant differences, $p < 0.05$). Note that muscle, skin and gill arches have the highest relative expression of both *ogn1* and *2* in sea bream.

### 4.4.6. Expression of *ogn1* and *ogn2* during differentiation of bone-derived and myocyte primary cultures

The expression of the duplicated *ogn* genes was analysed in bone-derived primary cell cultures growing in GM, OM and AM conditions. The morphological analysis of the cells presented in figure 4.6A showed that cells incubated in GM were mostly shaped like fibroblasts, whereas those in OM had a cobblestone-like appearance, and by day 20 multiple nodules of mineralization existed (indicated by the arrowheads) (Capilla et al. 2011). To further determine the osteogenic lineage of cells grown in OM, the expression of the ECM molecule osteopontin (*op*) was determined (figure 4.6B). The expression of *op* in cells growing in OM was significantly higher than in cells grown in GM at 5 and 20 days of culture ($p < 0.001$). *Op* expression in cells growing in GM was very low and remained stable at 5 and 20 days of culture. In this model system of vertebra-derived cells, the relative expression of *ogn2* was on average 150-fold higher than that of *ogn1* irrespective of the incubation media or time (figures 4.6C and D). The expression of *ogn1* increased significantly in cells growing in GM with higher levels of expression observed in cells at days 15 ($p = 0.0008$) and 20 ($p = 0.045$) in comparison with cells at day 5 (figure 4.6C) or cells in OM at days 15 ($p = 0.0002$) and 20 ($p = 0.0035$) (figure 4.6C). *Ogn2* expression did not change in cell cultures in GM or OM (figure 4.5) but was significantly up-regulated ($p = 0.024$) by 20 days of culture in cells in OM relative to those in GM.

Morphological analysis of cells incubated in AM (figure 4.7A) revealed that by day 10 they were round and had an enlarged cytoplasm and that by day 20 of culture contained some lipid droplets. In this cell model system, the relative expression of *ogn2* was 5-fold higher than *ogn1*. *Ogn1* transcript expression in GM was significantly up-regulated at 15 ($p = 0.010$) days of culture when compared to day 5 (figure 4.7B). The expression of *ogn1* increased significantly from 10 to 20 days of culture in AM ($p = 0.012$). The expression of *ogn2* in cells incubated in GM (figure 4.7C) was significantly up-regulated on day 20 relative to days 5 ($p = 0.024$) and 10 (0.002) but did not change in AM as the culture progressed.

Representative images of early myoblasts (day 2) and small myotubes (day 8) are shown in figure 4.8A. In common with osteoblast cultures, the relative expression of *ogn2* was 4 to 6-fold higher than *ogn1* in myocyte cultures at all the time points analysed (figures 4.8B and C). *Ogn1* expression increased as the cultures progressed and was significantly ($p < 0.001$) higher at day 8 relative to days 2 and 4 and the increase coincided with the time that myocyte cells start to fuse and form small myotubes (figure 4.8A and B). *Ogn2* was significantly more expressed at day 12 of the culture relative to day 2 ($p = 0.023$) (figure 4.8C).

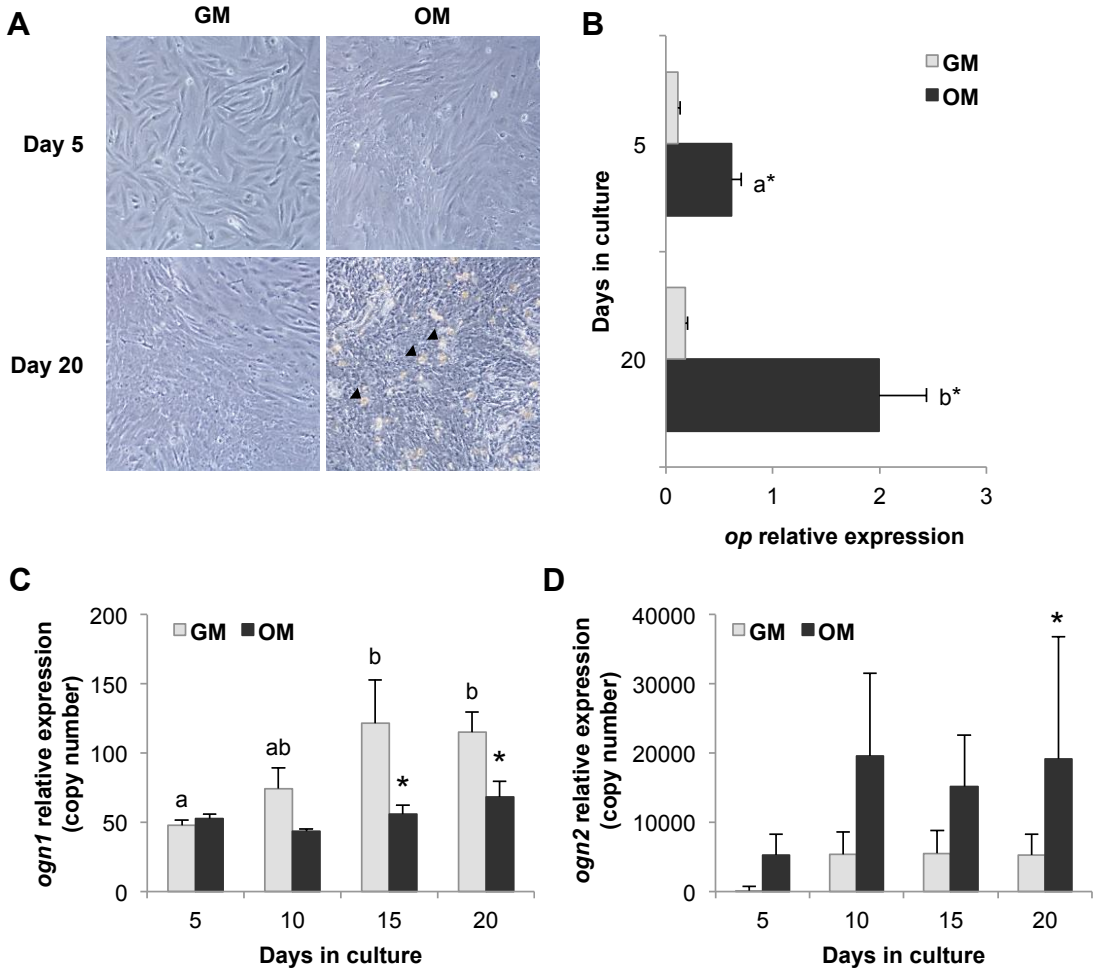


**Figure 4. 6 - Expression profile of osteoglycins (*ogn1* and *ogn2*) in gilthead sea bream bone-derived primary cell cultures in osteogenic medium. A:** Representative images of gilthead sea bream cells derived from vertebra growing in control (GM) or osteogenic (OM) conditions at days 5 and 20 of culture development. The arrowheads indicate nodules of mineralization. Images at 20x magnification. Normalized expression of **B:** *op*; **C:** *ogn1* and **D:** *ogn2* in bone-derived cells growing in GM or OM at different days of the culture (5 to 20). Results are shown as mean + sem (n = 5-8 independent cultures). Normalized expression was determined using the geometric mean of *ef1α* and *rps18* as reference. A two-way ANOVA followed by the Fisher`s Least Significant Difference (LSD) post-test was performed to identify differences in gene expression among the experimental groups. Significant differences ($p < 0.05$) within each culture are represented with different letters and the asterisk indicates differences between the cultures media.

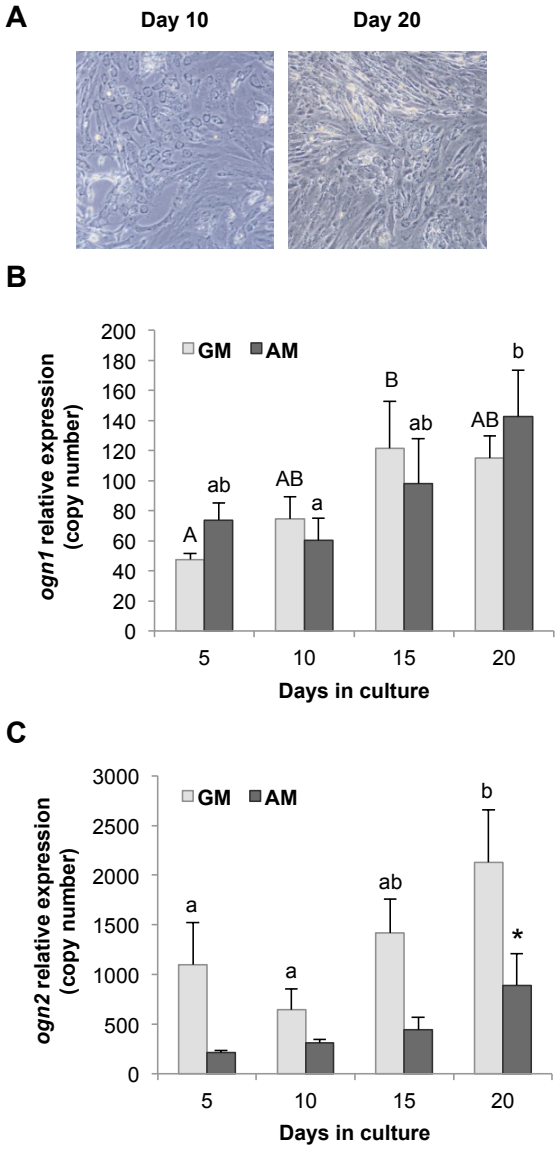


**Figure 4. 7 - Expression profile of osteoglycins (*ogn1* and *ogn2*) in gilthead sea bream bone-derived primary cell cultures in adipogenic medium. A**: Representative images of gilthead sea bream cells from vertebra growing in adipogenic medium (AM) at days 10 and 20 of culture development. Images at 20x magnification. Normalized expression (copy number) of **B**: *ogn1* and **C**: *ogn2* in bone-derived cells growing in AM at different days of the culture (5 to 20) determined using the geometric mean of *ef1α* and *rps18* as reference. Results are shown as mean ± sem (n = 5-6 independent cultures). A two-way ANOVA followed by the Fisher`s Least Significant Difference (LSD) post-test was performed to identify differences in gene expression among the experimental groups. Significant differences ($p < 0.05$) within each culture are represented with different letters and the asterisk indicates differences between the cultures media. Upper case letters are for cells in GM and lower case letters are for cell in AM.

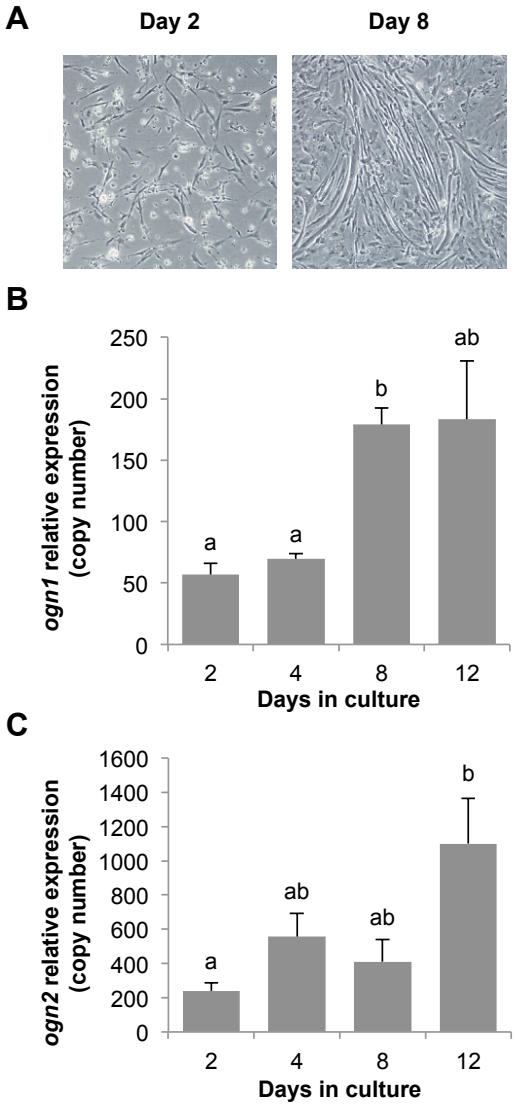


**Figure 4. 8 - Expression profile of osteoglycins (*ogn1* and *ogn2*) in gilthead sea bream myocyte primary cultured cells. A**: Representative images of gilthead sea bream muscle cells at days 2 and 8 of culture development. Images at 20x magnification. Normalized expression (copy number) of **B**: *ogn1* and **C**: *ogn2* in the myocyte cells at different culture days (2 to 12) determined using the geometric mean of *ef1α* and *rps18* as reference. Results are shown as mean + sem (n = 4 independent cultures). A One-way ANOVA followed by a Tukey test was used to test for significant differences in gene expression through time and are indicated with letters (different letters denote significant differences, $p < 0.05$).

### 4.4.7. Characterisation of OGN in a scale regeneration model

#### 4.4.7.1. Plasma parameters

Plasma Ca (figure 4.9) varied between 2.30 and 2.94 mmol·$L^{-1}$ and was significantly higher ($p = 0.01$) 28 days after scale removal compared to days 0 and 10; whereas plasma P remained constant throughout. Ionic levels of Na and K in plasma were not affected by scale removal. Plasma osmolality was not affected by scale removal but the levels of total protein

were significantly higher ($p = 0.001$) 28 days after scale removal (26.12 $mg \cdot ml^{-1}$) compared to days 0 and 5. Plasma concentrations of AST and ALT did not change significantly during the experimental trial (figure 9).

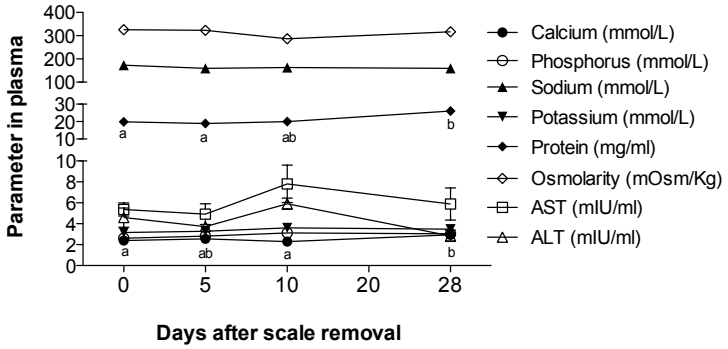


**Figure 4. 9 - Changes in plasma calcium, phosphorus, sodium, potassium, proteins, osmolality, aspartate-aminotransferase (AST) and alanine-aminotransferase (ALT) during scale recovery in gilthead sea bream.** Each value represents the mean ± sem (n=6). A One-way ANOVA followed by Bonferroni test tested significant differences in each parameter and differences are indicated with letters (different letters denote significant differences, $p < 0.05$). Scale removal did not affect plasma parameters since these were fairly constant during the experimental trial with the exception of plasma calcium and total protein that significantly increased at day 28.

### 4.4.7.2. Scale biochemistry and histomorphology

#### 4.4.7.2.1. Scale growth

The progression of scale growth was monitored by measuring the scale area (figure 4.10A). Twenty days after removal of the original scales the regenerating scales were the same size as the intact scales. The most significant increase in scale area occurred over the first 5 days when the regenerating scales achieved 60% of the area of the intact scale. The area of regenerating scales was significantly ($p = 0.004$) smaller (3.58 ± 0.227 $mm^2$) than that of the scales from the undamaged flank (5.03 ± 0.174 $mm^2$) at days 5 and 10 of the experiment ($p < 0.001$) (figure 4.10A). At day 28 the area of the scales in the intact and regenerating flanks were both significantly higher ($p < 0.001$) than the area of scales at the start of the experiment (time 0).

The increase in scale area at day 5 was significantly ($p = 0.007$) higher in regenerating scales (2.35 ± 0.20 $mm^2$) relative to scales (1.06 ± 0.13 $mm^2$) from the intact flank (figure 4.10D). At this time the regenerating scales attained 60.87 ± 3.86% of the size of the scales from the intact flank. By day 20 the regenerating scales were already larger ($p < 0.05$, 114.2 ± 6.89%) than the original scales at time 0 (figure 4.10A). A pause in the growth of the

regenerating scales occurred between days 5 – 10 but the growth rate then increased significantly ($p < 0.05$) again from day 10 to 28.

#### 4.4.7.2.2. Enzyme activity

TRAP activity in scales (figure 4.10B) sampled from the intact flank of fish was significantly ($p = 0.03$) higher at day 5 ($10.31 \pm 0.774$ nmol·min$^{-1}$·mg$^{-1}$) after scale removal compared to day 0 ($4.09 \pm 0.301$ nmol·min$^{-1}$·mg$^{-1}$) and decreased back to initial levels by day 10. TRAP activity in the scales removed from the regenerating flank of the fish relative to those at 0 time was significantly higher ($p < 0.0001$) at days 5 ($43.72 \pm 10.289$ nmol·min$^{-1}$·mg$^{-1}$) and 10 ($17.15 \pm 1.135$ nmol·min$^{-1}$·mg$^{-1}$) after scale removal, and returned to initial levels by day 20 ($p = 0.58$) and remained low thereafter. TRAP activity in scales from the regenerating flank of fish was significantly higher ($p < 0.0001$) at days 5 and 10 than in scales from the intact flank of the same fish.

ALP activity in scales from the intact flank of fish (figure 4.10C) remained constant throughout the experimental trial whilst in the scales from the regenerating flank reached a maximum at day 5 ($p < 0.0001$, $26.35 \pm 4.79$ nmol·min$^{-1}$·mg$^{-1}$) relative to other time points. ALP activity in regenerating scales at day 10 significantly ($p < 0.0001$) decreased ($8.88 \pm 0.609$ nmol·min$^{-1}$·mg$^{-1}$) relative to day 5 and by day 20 ALP activity was similar ($p = 0.53$, $3.97 \pm 0.52$ nmol·min$^{-1}$·mg$^{-1}$) to time 0.

The TRAP/ALP ratio in scales (figure 4.10E) taken from the intact flank of fish was significantly higher at day 5 ($p < 0.0001$, ratio 7) compared to days 0, 10, 20 or 28 after scales were removed from the regenerating flank. In the scales taken from the regenerating flank of fish, the TRAP/ALP ratio was similar (ratio 1-2.2) until day 28 when it increased significantly ($p < 0.0001$, ratio 5.3).

#### 4.4.7.2.3. Expression profile of ogn1, ogn2 and op during sea bream scale / skin regeneration

The expression of *ogn* transcripts during scale / skin regeneration was determined in skin samples from the intact and regenerating flank using qPCR (figures 4.10F-H). Five days after scale removal, the transcript abundance of *ogn1* (figure 4.10F) and *ogn2* (figure 10G) was significantly ($p < 0.05$) down-regulated in the regenerating skin but by the end of the experimental trial (day 28) when the TRAP/ALP ration was high (indicative of matrix deposition) they were both significantly ($p < 0.05$) up-regulated.

The relative abundance of *ogn1* transcripts in skin from the intact and regenerating flank (figure 4.10F) was not significantly different at 0 or 10 days after scale removal. However, the transcript abundance of *ogn1* in regenerating skin was significantly up-regulated relative to intact skin at days 5 ($p = 0.014$) and 28 ($p=0.015$) ($p < 0.01$). Comparison of *ogn2* transcript abundance between intact and regenerating skin revealed it was significantly down-regulated in regenerating skin at day 5 ($p = 0.037$) and 10 ($p = 0.024$) and up-regulated in regenerating skin at day 28 ($p < 0.001$) (figure 4.10G).

The transcript abundance of *op* (an extracellular structural protein of bone) in the skin from the regenerating flank did not vary significantly ($p > 0.05$) during the experiment. Although a significant up-regulation ($p < 0.001$) of *op* transcripts occurred in regenerating skin relative to intact skin at days 5 and 10 (figure 4.9H), which coincides with a period of rapid scale growth (figure 4.10A and D).

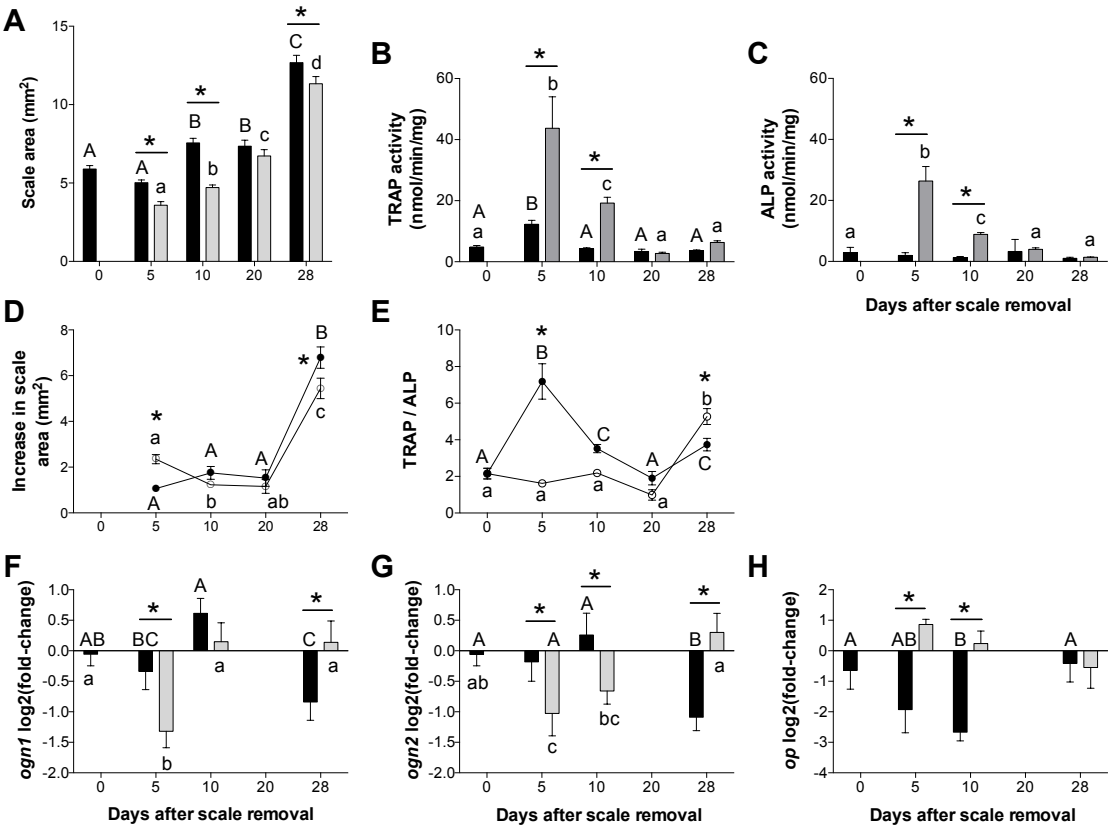


**Figure 4. 10 - Scale growth and enzymatic activities of TRAP and ALP in sea bream scales and gene expression in the skin of sea bream. A:** Area of the scales ($mm^2$) and **D:** Increase in scale area ($mm^2$). Changes in **B:** tartrate-resistant acid phosphatase, **C:** alkaline phosphatase (ALP) activities (nmol $pNP \cdot min^{-1} mg^{-1}$) and **E**: Ratio TRAP/ALP. Results are presented as mean ± sem. Expression profile of **F**: osteoglycin 1(*ogn1*), **G**: osteoglycin 2 (*ogn2*) and **H**: osteopontin (*op*). Results are presented as the relative expression in log2(fold-change) ± sem. A two-way ANOVA followed by the Fishers' Least Significant Difference (LSD) post-test was performed to identify differences in each of the parameters and statistical significance was considered at $p < 0.05$. Upper case letters are for intact scales and skin, lower case letters for regenerating scales and skin and *asterisk* identifies differences between the intact and regenerating flanks of the experimental animals.

## 4.5. Discussion

Ogn is present in the sea bream and other teleosts and duplicate forms arose during the teleost specific whole genome duplication and were maintained in the genome through subfunctionalization as revealed by the divergent *ogn1* and *2* promoters, protein motifs and tissue distribution. The teleost specific Ogn1 and 2 share 66-72% amino acid sequence similarity and possess all the characteristic motifs of the vertebrate SLRP family, although the absence of some motifs from one or other form of the teleost Ogn duplicates suggests that the proteins have both shared and specific functions. The defining protein motifs of the SLRP family were conserved across all the vertebrate OGNs analysed and this suggests that functional conservation probably exists for this protein from mammals to teleosts. The overlapping tissue distribution of *ogn* transcripts in teleosts and mammals further supports the notion that they may have common functions. However, the specific evolution of fish and their physiology that diverges from mammals plus the existence of duplicate genes and divergence of the sequence and domains in their protein products suggests Ogn has also acquired fish specific functions. Specific functions for the duplicate *ogn*s are suggested by their different behaviour in differentiating primary cell cultures. A surprising observation from the primary cell culture of muscle, bone, and trans-differentiating adipocytes was the notably higher levels of expression (as much as five fold higher) of *ogn1* and *ogn2* transcripts and this may suggest that tissue maturation is important for their regulation. In normal skin *ogn1* and *ogn2* transcripts are low abundance and we propose this reflects a role in normal skin homeostasis. In contrast, in regenerating fish skin *ogn1* and *ogn2* transcripts are strongly down-regulated until re-establishment of the tissue has occurred and their up-regulation is coincident with the timing of increased mineralization of the scales (day 28). An intriguing observation for which we have no explanation was the change in *ogn* transcript abundance in the skin from the undamaged flank of fish undergoing skin regeneration in the other flank.

### 4.5.1. OGN evolution and structure

Phylogenetic analysis of teleost *ogn* confirms that it belongs to the SLRP family, members of which have been identified from bacteria to man (Kobe and Deisenhofer 1995; Buchanan and Gay 1996). Furthermore, teleost Ogn duplicates possess most of the key structural motifs that characterize the proteoglycans: a central domain with a variable number of LRRs and a C-terminal domain of poorly defined function. However, teleost Ogn1 unlike Ogn2 lacks an N-terminal tyrosine sulphate and in Ogn2 the characteristic C-terminal *N*-linked glycosylation in the ear-extension of the last LRR (LRR 7, (Park et al. 2008) is absent and only

one YinOYang site ($Ser_{77}$ in *S. aurata*) exists and is suggestive of divergent functions. Nonetheless, the characteristic modular structure and typical 7 LRRs of class III proteoglycans (Matsushima et al. 2000) were conserved in teleost Ogn1 and 2. Analysis of the LRRs in teleost Ogn1 and 2 revealed the two main repeat units, S (1, 4 and 6) and T (2, 3, 5 and 7) were organised into 4 super-repeats (ST_TSTST) as found in mammalian class III proteoglycans (Matsushima et al. 2000). Conserved clusters of cysteine residues in the N- and C-termini flanked the LRR domains in teleost Ogn1 and 2. The C-terminal leucine-rich repeat cysteine capping motif is a typical LRRCE motif (Park et al. 2008) and was present in both Ogn1 and 2 and it presumably forms 2 disulphide bridges as has been observed in the crystal structure of decorin and biglycan from mammals (Park et al. 2008; Scott et al. 2006; Scott et al. 2004). The conservation of the LRRs in teleost Ogns suggest it probably has the curved, solenoid structure modelled from the crystal structure of bovine decorin (Scott et al. 2004), which is a site of protein/protein interaction. The general conservation of teleost Ogns with mammalian type III proteoglycans supports the notion that their basic functions are conserved and suggests as occurs in mammals a potential role in collagen fibril assembly, bone mineral deposition and cellular growth (Ameye and Young 2002; Schaefer and Iozzo 2008; Waddington et al. 2003). The significant rise in *ogn1* and *2* in regenerating skin conincides with the increased mineralization of the scales (as indicated by the 5-fold rise in the ALP/TRAP ratio) and we speculate suggests an ancient origin for its function in ectopic bone formation.

The persistence of duplicate genes in metazoa genomes is quite common (Force et al. 1999; Hughes 2002) and it is assumed to be either a consequence of gain of novel function (neofunctionalization) or partitioning of the function of the ancestral molecule (subfunctionalization). Phylogenetic and synteny analysis support the notion that the 2 teleost *ogn* genes arose during the teleost specific whole genome duplication as only a single gene occurs in the spotted gar and other vertebrate lineages. The synteny analysis of *ogn1* and *2* from the puffer fish, sea bass and zebrafish suggests the duplicates arose by tandem gene duplication and gene migration as the linkage groups of *ogn1* and *2* have little in common. Analysis of phylogenetic trees revealed that *ogn1* is evolving under positive selection in the teleosts, which is coherent with a neofunctionalization model for preservation of gene duplicates (Conant and Wolfe 2008). The loss of the N-terminal tyrosine sulphate motif in Ogn1 may be symptomatic of neofunctionalization and suggests the post-translational addition of keratan sulphate (Corpuz et al. 1996) is unlikely to occur and so some of its functions will divergefrom Ogn2. A keratan sulphate form of OGN is abundant in the cornea and sclera in mammals (Funderburgh et al.

1997) and it remains to be established if keratan sulphate is added to teleost Ogn2 *in vivo* and if this form occurs in the cornea and sclera. In general the distribution of *ogn* transcripts in teleosts overlaps with that in mammals and *ogn1* and *2* are present in bone (Tasheva et al. 1999), the pituitary gland, muscle, vascular system, heart, lung and adipose tissue (Cao et al. 2015; Hu et al. 2005; Kampmann et al. 2009).

Data about the mammalian *OGN* promoter is limited and one study identified Oct-1, a metal response element (MRE) and an NF-KB recognition sites in the promoter and an interferon-stimulated response element (ISRE) and p53 DNA-binding site in the first intron (Tasheva et al. 2002). A subsequent study in the context of *OGN* in the eye identified elements responsible for UV activation of transcription (Tasheva and Conrad 2003). The human and bovine mimecan (*OGN*) promoters are both responsive to UV and contain conserved UV responsive regulatory elements including the p53 DNA-binding site in the first intron, the E box in the proximal promoter and a responsive region between nucleotides -1314 and -1907. Although no experimental analysis of the sea bass promoter was performed in this study comparative analysis in Genomatix of the human and fish *OGN* promoters indicates that regulation between these organisms is likely to diverge, as relatively few common conserved regulatory elements exist. In contrast, the promoter regions of the duplicate fish *ogns* have a large number of overlapping TFBS (figure 4). The nature and context of the regulatory modules suggests they are involved in adipocytes, myocytes and chondrocytes differentiation. However, the *ogn1* promoter has a unique content of response elements associated with bone osteoblasts. The cell culture assays reveal that a significant rise in both *ogn1* and *ogn2* transcripts is associated with myotube fusion. However, results are less clear cut in relation to the association of *ogn1* and *ogn2* with adipocyte trans-differentiation or osteoblast differentiation but this may be related to the heterogeneous nature of the cell cultures after OM or AM is added and further experiments are required. Nonetheless, the significant increase in *ogn1* in adipocyte cells is congruent with observations that *OGN* transcripts occur in mammalian adipose tissue (Cao et al. 2015). Overall, the divergent expression pattern of *ogn1* and *2* in differentiating muscle and bone (both in OM and AM) cell cultures suggests that the duplicate teleost *ogn* genes may have been maintained during evolution via subfunctionalization rather than neofunctionalization. A striking observation was the high abundance of *ogn1* and *2* in cell cultures compared to tissues, which we speculate suggests in tissues containing fully differentiated cells gene expression is repressed. This idea supports the ectopic osteoinductive role first identified for *OGN* in

mammals (Bentz et al. 1989). Furthermore, it seems likely that as occurs in mammals functional compensation can occur between thefish duplicate Ogn proteins (Young et al. 2003).

### 4.5.2. OGN function

The overlapping tissue distribution of *ogn*s in fish and mammals is unsurprising taking into account their well conserved protein structure that suggests they are likely to share conserved function. This means that in the absence of studies of Ogn function in fish the results from mammals may provide clues about shared and unique functions of the protein. The *in vitro* studies using gilthead sea bream primary cell cultures from muscle and bone using selective medium (Capilla et al. 2011; Montserrat et al. 2007) provided insight into possible functions of *ogn1* and *2* in cell differentiation. In sea bream myogenic cells in primary culture *ogn2* transcripts are highly abundant compared to *ogn1* and both transcripts are up-regulated after myotubes form. The results in sea bream parallel those in mammals in which OGN is up-regulated in the secretome during skeletal myogenesis of C2C12 cells (Chan et al. 2007) and also when myoblastic cells differentiate into myotubes (Tanaka et al. 2012). *Ogn2* transcripts are also highly abundant in sea bream bone cell cultures maintained in growth media. The change of sea bream osteoblast cultures to osteogenic media (OM) causes the appearance of occasional mineralized cell clusters among non-mineralized cells. In mammals it has been proposed that OGN only enhances mineralization in well-differentiated osteoblasts (Tanaka et al. 2012), this also appears to be the case in sea bream although the heterogeneous cell phenotype in the sea bream mineralizing osteoblast cultures in OM probably explains the extremely variable transcript expression of *ogn2*. In a recent proteomics study on humans, OGN was identified in the subcutaneous and visceral fat of normal and morbidly obese individuals (Insenser et al. 2012). Subsequently, it was demonstrated in mice that OGN is present in high concentrations in adipose and is secreted into the circulation and acts as an anorexic hormone (Cao et al. 2015). In line with this, teleost *ogn1* and *ogn2* transcripts are abundant in cultures of sea bream bone-cells in AM and the increase in *ogn1* transcript abundance is co-incident with adipocyte differentiation and it will be of interest in the future to explore the role of *ogn* in adipose tissue and as a regulatory factor of appetite in fish. Overall, the results from the sea bream primary cell culture reveal a 5-fold increase in *ogn2* transcripts relative to its tissue abundance that we cannot explain. The divergent pattern of expression of *ogn1* and *2* in differentiating primary cell cultures and in tissues further supports the notion that subfunctionalization of the duplicated genes occurred. Further studies will be required to

establish the regulation of *ogn1* and *ogn2* expression in fish tissue and if the duplicate genes and their protein products interact.

We have previously identified Ogn in a proteomics study of the regenerating marine teleost fish skin model (Ibarz et al. 2013) and for this reason we focussed on the same model in this study. Ogn is significantly up-regulated in regenerating skin 5 days after scale removal along with other proteins of relevance for ECM and tissue structure such as Lamin, keratins, actins, collagen type I and annexins (Ibarz et al. 2013). In the same study Ogn is not up-regulated when fish were exposed to estradiol (E2) but this is most likely linked to the acceleration in the regenerative process as there is no evidence that E2 down-regulates OGN (Pinto et al., personal communication). Normally after scale loss in fish re-epithelialization and differentiation of scale-forming cells is completed within 1- 2 days and subsequently at 3 - 5 days the bony matrix of the scale is produced, followed by production of basal-plate matrix at days 6 -14 and calcification at days 14 - 28. The increase in Ogn detected in the previous proteomics study coincides with the time at which new scales are formed in the scale pocket at 3-5 days in the medaka and sea bass (Ibarz et al. 2013; Ohira et al. 2007a; Guerreiro et al. 2013). What therefore is the explanation for the strong down-regulation of OGN transcripts at day 5 in our study? This we propose is linked to the rate of scale growth, which after a preliminary growth spurt as the new scale forms (up to 3 days) stops increasing in area from day 5 - 20 (figure 4.10A); this coincides with a strong down-regulation of *ogn1* and *2* transcripts. Between day 20-28 a significant increase in scale area occurs (figure 4.10A) and the ALP/TRAP ratio (an indicator of osteoblast activity, figure 4.10E) increase five-fold and *ogn1* and *2* transcripts are significantly up-regulated. Future studies will be required to discriminate between the function of Ogn in fish skin matrix assembly during regeneration and the formation of the ectopic mineralized structures, the scales.

SLRP are key regulators of matrix assembly and their low levels of expression in the provisional matrix of healing skin promotes endothelial cell migration and the formation of new blood vessels (Merline et al. 2009; Iozzo and Schaefer 2010). In fact, the matricellular components of mammalian skin impacts resident cells causing them to produce specific matrix elements that control the outcome of healing, promoting either complete repair or dysfunctional healing (Wells et al. 2016). Teleost skin regeneration after scale removal involves reorganization of the dermis to form the new scale pocket as well as the rapid increase in scale area and thickness (Bereiter-Hahn and Zylberberg 1993) to re-establish its protective functions. These processes are accompanied by a rearrangement of the ECM and the progressive increase in collagen production (collagens I and V), especially by hyposquamal scleroblasts to deposit

the thick collagen fibrils that form the basal plate of the new scales (Guellec and Zylberberg 1998). In early stages of skin repair in sea bream *ogn1* and *ogn2* are down-regulated but at later stages they are up-regulated and we propose that these matricellular proteins in addition to their role in scales may contribute to the organization of collagen fibre assembly and for this reason increase significantly during the late-phase of fish skin regeneration. Further studies are required to establish the basis for the divergent results between protein abundance (previous study) and transcript abundance (present study) and to establish if *ogn1* and *ogn2* have specific functions in regeneration and if in common with what occurs during mammalian skin repair, OGN regulates collagen fibrillogenesis after processing by BMP-1/Tolloid-like metalloproteinases (Ge et al. 2004).

## 4.6. Conclusion

We identified duplicate genes for *ogn* in fish and revealed that the structure of the genes has been well conserved during vertebrate evolution. The maintenance of two *ogn* genes in teleost genomes is associated with divergence of their promoter structure and tissue transcript expression together with differences in the functional motifs of the deduced proteins. We hypothesize that subfunctionalization explains the retention of the duplicate genes. The high levels and regulated expression of *ogn1* and *ogn2* in fish cell cultures during myotube formation and the significant increase in *ogn1* and *ogn2* transcripts in cells induced to differentiate into adipocytes or bone, respectively suggests that in fish *ogn* has pleiotropic inductive effects. We also infer from the fish skin regeneration model the involvement of fish *ogns* in the formation of scale ectopic mineralized structures. We propose based upon the results of the evolutionary and molecular analysis and primary cell culture and skin regeneration model that the role of OGN in ectopic bone formation is an ancient and conserved function in vertebrates.

## 4.7. Acknowledgements

The authors would like to thank Emilio J. Vélez and Natàlia Riera-Heredia for their help with the cell cultures. This study was financed by Lifecycle EU-FP7 222719 and by Portuguese funds through Foundation for Science and Technology (FCT). RAC is funded by FCT SFRH/BD/81625/2011 grant. RM and LA were in receipt of Post-doctoral fellowships (SFRH/BPD/66742/2009 and SFRH/BPD/79105/2011) from FCT. EC was supported by funds from the MICINN AGL2010-17324 and Generalitat de Catalunya 2014SGR-01371.

## 4.8. Supporting material

**Supplementary table 4. 1 - Accession numbers of all proteins and nucleotides sequences used in this study.**

| Scientific name | Proteins | | | Nucleotides | |
|---|---|---|---|---|---|
| | Epiphycan (EPYC) | Osteoglycin 1 (OGN1) | Osteoglycin 2 (OGN2) | Osteoglycin 1 (OGN1) | Osteoglycin 2 (OGN2) |
| *Homo sapiens* | NP_004941 | NP_054776 | | KJ891722 | |
| *Gorilla gorilla gorilla* | | XP_004048314 | | XM_004048267 | |
| *Pongo abelii* | | NP_001125484 | | NM_001132012 | |
| *Bos taurus* | | AAI02527 | | BC102526 | |
| *Equus caballus* | | XP_001918010 | | XM_001917975 | |
| *Ovis aries* | | XP_004004124 | | XM_004004076 | |
| *Ceratotherium simum simum* | | XP_004442782 | | XM_004442726 | |
| *Tursiops truncatus* | | XP_004313640 | | XM_004313593 | |
| *Orcinus orca* | | XP_004284166 | | XM_004284119 | |
| *Mus musculus* | | NP_032786 | | NM_008760 | |
| *Cricetulus griseus* | | XP_003505386 | | XM_003505338 | |
| *Rattus norvegicus* | | NP_001099573 | | XM_006253696 | |
| *Gallus gallus* | | NP_989540 | | NM_204209 | |
| *Taeniopygia guttata* | | XP_002193114 | | XM_002193078 | |
| *Ficedula albicollis* | | XP_005052963 | | XM_005052906 | |
| *Xenopus (Silurana) tropicalis* | | ENSXETP00000045198 | | ENSXETT00000045198 | |
| *Pelodiscus sinensis* | | XP_006127625 | | XM_006127563 | |
| *Chrysemys picta bellii* | | XP_005279975 | | XM_008165394 | |
| *Latimeria chalumnae* | | XP_005987115 | | XM_005987054 | |
| *Lepisosteus oculatus* | | XP_006631165 | | XM_006631102 | |
| *Gadus morhua* | | ENSGMOP00000003044 | ENSGMOP00000004605 | ENSGMOT00000003141 | ENSGMOT00000004743 |
| *Astyanax mexicanus* | | ENSAMXP00000005237 | ENSAMXP00000013872 | ENSAMXT00000005237 | ENSAMXT00000013872 |
| *Danio rerio* | | NP_001013588 | ENSDARP00000048890 | NM_001013570 | ENSDARG00000031489 |
| *Salmo salar* | | ACI68238 | ACM08413 | BT056541 | BT048437 |
| *Oryzias latipes* | | XP_004086171 | | XM_004086123 | |
| *Dicentrarchus labrax* | | DLAgn_00097140 | DLAgn_00129310 | DLAgn_00097140 | DLAgn_00129310 |
| *Oreochromis niloticus* | | ENSONIP00000000621 | XP_003438910 | ENSONIT00000000620 | XM_003438862 |
| *Takifugu rubripes* | | ENSTRUP00000023699 | ENSTRUP00000027803 | ENSTRUT00000023797 | ENSTRUT00000027913 |
| *Sparus aurata* | | KM603667 | KM603668 | KM603667 | KM603668 |
| *Callorhinchus milii* | | XP_007907071 | | | |

**Supplementary figure 4. 1 - Phylogenetic analysis of osteoglycins (OGNs) in vertebrates performed with the Neighbour Joining (NJ) method.** Phylogenetic analysis was performed with 1000 bootstrap replicates and a JTT substitution model with a discrete gamma distribution of rates among sites with 4 categories. The supportive bootstrap values (%) are indicated at each node. To root the tree, the sequence of human epiphycan (EPYC) was used as the out-group. The accession numbers of all the sequences used in this phylogenetic tree are shown in supplementary table 4.1.

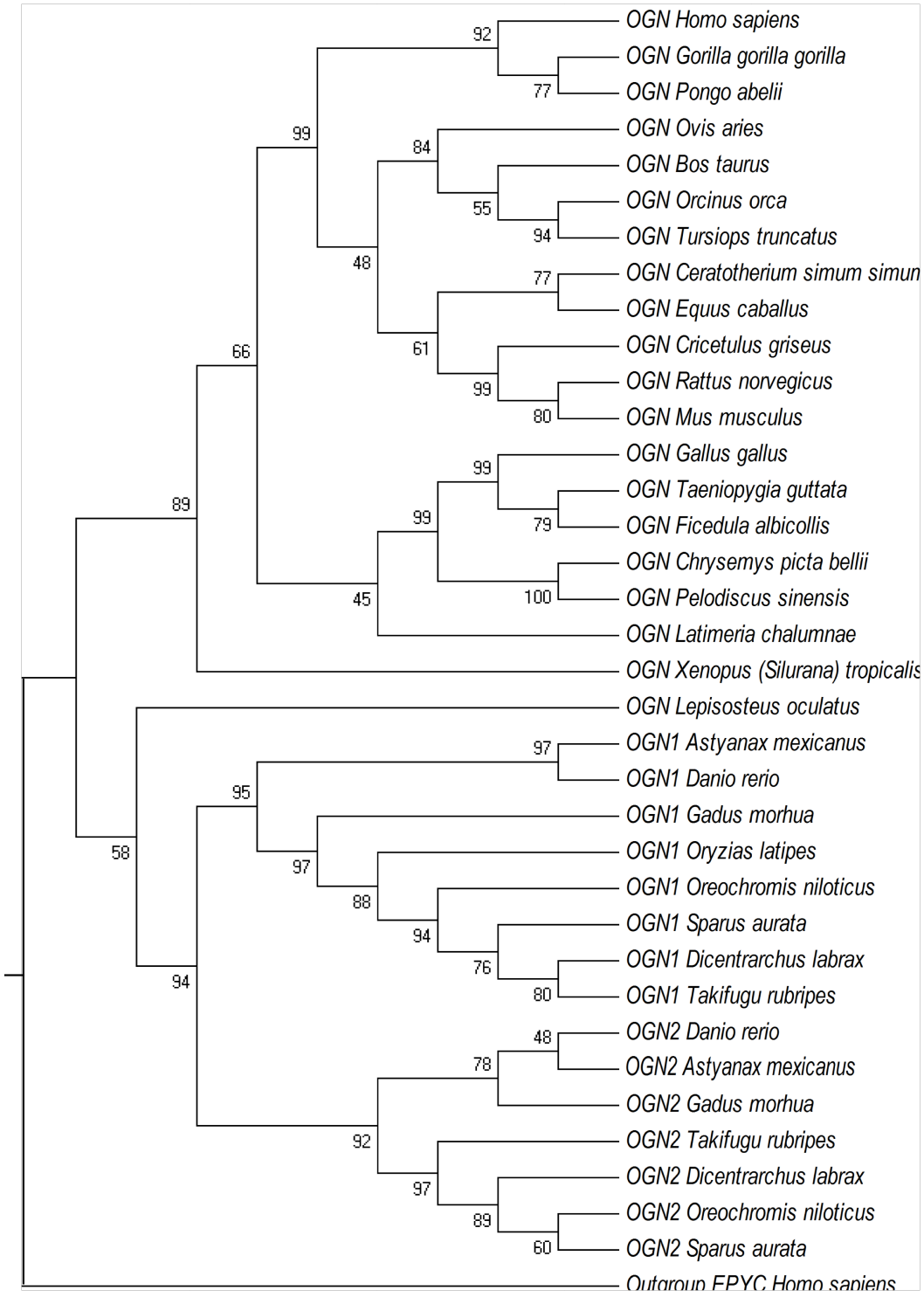

**Supplementary figure 4. 2 - Gilthead sea bream osteoglycins 1 and 2 (*ogn1 and ogn2*) nucleotide sequences and encoding proteins.** *Asterisk* signals the stop codon of the open reading frame.

***Sparus aurata ogn1***

```
   1 - ATGAAGTCTCTCTTATTCACCTGTATGCTGGTGCCGTGGCTGGTGGCAGCCTCAGCCAGGAAGTCTGACCAGGATTCACAGCTGATAGTG - 90
   1 - M  K  S  L  L  F  T  C  M  L  V  P  W  L  V  A  A  S  A  R  K  S  D  Q  D  S  Q  L  I  V  - 30

  91 - GGAATTCTACCTGGCAGGGAGCTGAATGGATACTTCAGTGACCCTTTGAATTCAAGAAGGGCTCGGAGAGCAGTGTCTCTTGCTGATGAA - 180
  31 - G  I  L  P  G  R  E  L  N  G  Y  F  S  D  P  L  N  S  R  R  A  R  R  A  V  S  L  A  D  E  - 60

 181 - CCTGATGACAGCCCAGTCTCAGAAGGAGGAGACGCATCTGACCTGCCCACCTGCCTTCTGTGTGTGTGTCTGACGGGTTCAGTGTATTGT - 270
  61 - P  D  D  S  P  V  S  E  G  G  D  A  S  D  L  P  T  C  L  L  C  V  C  L  T  G  S  V  Y  C  - 90

 271 - GAGGAAGTCAGCCCAGACATGACCAGTGTACCCACCCTGCCTAAAGAGACGGCCTATCTGTATGCCCGCTTCAACAAGATCAAGAAGATC - 360
  91 - E  E  V  S  P  D  M  T  S  V  P  T  L  P  K  E  T  A  Y  L  Y  A  R  F  N  K  I  K  K  I  - 120

 361 - AGCACCAAAGATTTTGCTGGCATTTTGACTCTGAAGAGGATTGATCTGACAGGGAACCTGATCTCAGAGATTGAAGACGGGGCATTTTCT - 450
 121 - S  T  K  D  F  A  G  I  L  T  L  K  R  I  D  L  T  G  N  L  I  S  E  I  E  D  G  A  F  S  - 150

 451 - AAACTTGCCCTCCTGGAGTCATTATCTCTGGCTGAGAACAGACTGGTCAAACTTCCAATGCTCCCTGCCAAACTCACATCCTTCAATGCC - 540
 151 - K  L  A  L  L  E  S  L  S  L  A  E  N  R  L  V  K  L  P  M  L  P  A  K  L  T  S  F  N  A  - 180

 541 - AACAACAACTTCCTTAAAACCAGGGGTGTCAAGGCCAATGCTTTCAAGAAATTGACCAAGCTGACCCACCTGTACCTGGCTGACAACCAG - 630
 181 - N  N  N  F  L  K  T  R  G  V  K  A  N  A  F  K  K  L  T  K  L  T  H  L  Y  L  A  D  N  Q  - 210

 631 - TTGGAAGCTGTTCCACAAATCCCTGACAGTGTTCAGATCTTACATCTACAGAACAACAACATCACTGAGGTCAACGTAGATACCTTCTGC - 720
 211 - L  E  A  V  P  Q  I  P  D  S  V  Q  I  L  H  L  Q  N  N  N  I  T  E  V  N  V  D  T  F  C  - 240

 721 - AGGTCCAATGACACCTACTACCTACGACCAAGCCTCAATGAGGTCCGTCTGGATGGCAACCCTGTGGTGCTGTCGAAGAACCCTGACAGC - 810
 241 - R  S  N  D  T  Y  Y  L  R  P  S  L  N  E  V  R  L  D  G  N  P  V  V  L  S  K  N  P  D  S  - 270

 811 - TTCACCTGTATGAAGGTACTGCCTAGTGGACGGTACCGCTGA                                                - 852
 271 - F  T  C  M  K  V  L  P  S  G  R  Y  R  *                                                - 300
```

***Sparus aurata ogn2***

```
   1 - ATGATGCAACTGAGGACTTTAATCTTCACATATGTTATTCTCCCATGGATCCTGTCTTCTGCAGCAAAGGATGAATTCATGGAAGCGAGA - 90
   1 - M  M  Q  L  R  T  L  I  F  T  Y  V  I  L  P  W  I  L  S  S  A  A  K  D  E  F  M  E  A  R  - 30

  91 - AAACCCAAGCCAGGCGTTGTAACCTATCCAGACTATGAAGAACCAGCCACAGATGCAGCGGGGGATCCAAAAGCTGATGAGCTGCCGACT - 180
  31 - K  P  K  P  G  V  V  T  Y  P  D  Y  E  E  P  A  T  D  A  A  G  D  P  K  A  D  E  L  P  T  - 60

 181 - TGTCTGCTGTGTGTTTGCCTGAGTGGATCCGTTTACTGTGAGGAGGTGTCCCCTGAAATGTCAGCTGTCCCAGCACTGCCAAAGGAAACG - 270
  61 - C  L  L  C  V  C  L  S  G  S  V  Y  C  E  E  V  S  P  E  M  S  A  V  P  A  L  P  K  E  T  - 90

 271 - GCATACCTCTACGCACGTTTCAACAAAATCACAAGAATACGCAACAGCGACTTTGCGGACATGGCCCCATTAAGAAGAATTGACCTCAGT - 360
  91 - A  Y  L  Y  A  R  F  N  K  I  T  R  I  R  N  S  D  F  A  D  M  A  P  L  R  R  I  D  L  S  - 120

 361 - GGGAATCTCATCTCTGAGATTGAAGATGGAGCTTTTTCAAAACTTCCCGATCTCGAGGAGCTCATTCTTGCAGAAAACAAACTGACTAGA - 450
 121 - G  N  L  I  S  E  I  E  D  G  A  F  S  K  L  P  D  L  E  E  L  I  L  A  E  N  K  L  T  R  - 150

 451 - CTTCCCATCATGCCCACCAAACTAGTGACATTTAATGCTAATTTCAACAAGCTAAAAACCCAGGGTGTAAAGGCAACTGCTTTTAAGAAA - 540
 151 - L  P  I  M  P  T  K  L  V  T  F  N  A  N  F  N  K  L  K  T  Q  G  V  K  A  T  A  F  K  K  - 180

 541 - CTTACGAGACTGTCGTATCTGTACCTTGGAAACAATGAACTCACAGCAGTGCCCCAACTTCCAGAGTCCCTTAATGTTGTGCACCTGCAA - 630
 181 - L  T  R  L  S  Y  L  Y  L  G  N  N  E  L  T  A  V  P  Q  L  P  E  S  L  N  V  V  H  L  Q  - 210

 631 - AACAACAAGATCTCAACTATAACAGATGAGACATTCTGCAAAGGTAACACCAGTTACTACATCCGGACCAACTTGTACCAGGTGAGACTG - 720
 211 - N  N  K  I  S  T  I  T  D  E  T  F  C  K  G  N  T  S  Y  Y  I  R  T  N  L  Y  Q  V  R  L  - 240

 721 - GACGGGAATCCCATCCAGCTTTCGAAGCACCCCAACAGCTTCATTTGTCTGGAGACTCTCCCTATTGGATGGTACAACTGA          - 801
 241 - D  G  N  P  I  Q  L  S  K  H  P  N  S  F  I  C  L  E  T  L  P  I  G  W  Y  N  *           - 270
```

**Supplementary figure 4. 3 - Amino acid sequence alignments of human and fish osteoglycins (Ogn).** The conserved amino acid residues are shaded. The numbers on the right hand side indicate the position of the amino acid residues. The predicted signal sequences are boxed. The * mark the N-terminal ($CX_2CXCX_6C$) and C-terminal ($CX_{33}C$) cysteine-rich clusters characteristic of OGN proteins and family members. The seven LRR motifs characteristic of class III SLRP family members are marked as L-motif 1-7. The putative glycosaminoglycan-attachment sites (φ) are also marked. The accession numbers of all the sequences used in this alignment are shown in supplementary table 4.1.

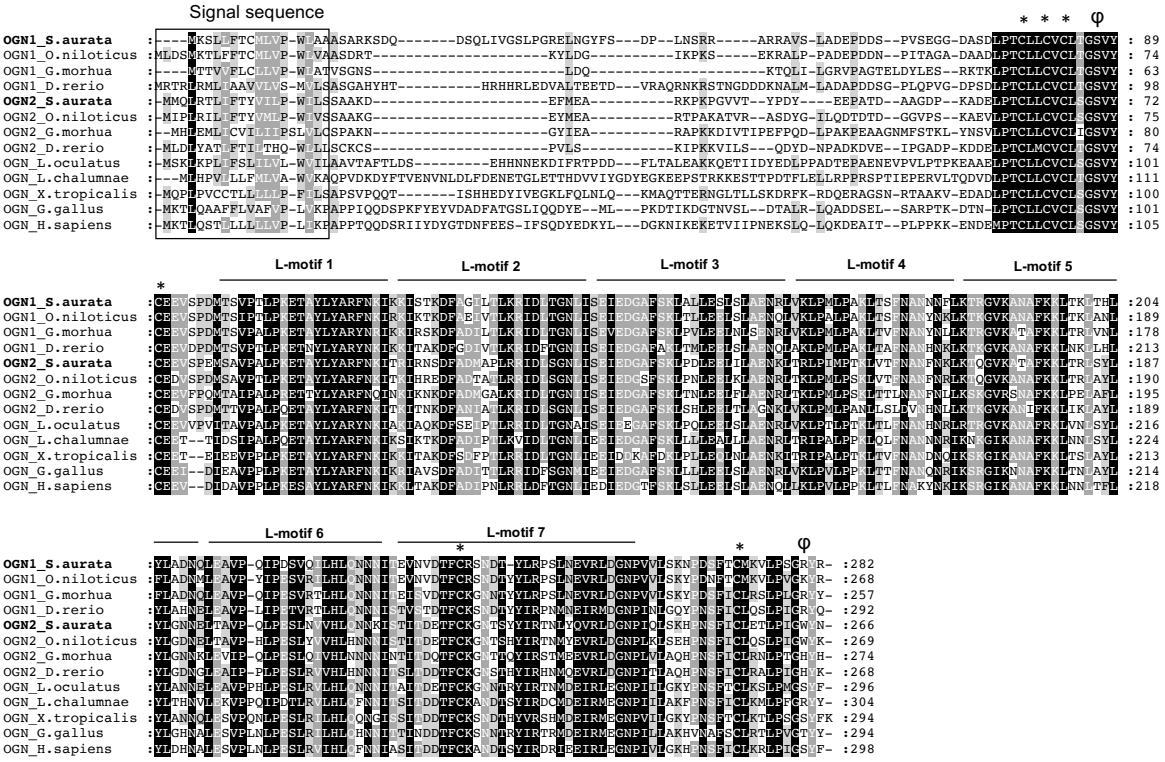

# 5

# The effect of the intermediate metabolite alpha-ketoglutarate (AKG) on skin integrity, function and repair in the teleost sea bream (*Sparus aurata*)

R.A. Costa[1], A.P. Harrison[2] and D.M. Power[1]

[1]Comparative Endocrinology and Integrative Biology Group, Centre of Marine Sciences, University of Algarve, Campus of Gambelas, 8005-139 Faro, Portugal.

[2] Department of Animal and Veterinary Basic Sciences, Faculty of Life Sciences, Copenhagen University, Gronnegaardsvej 7, 1870 Frederiskberg C, Denmark.

## 5.1. Abstract

Alpha-ketoglutarate (AKG) is a key intermediate metabolite in the Tricarboxylic Acid cycle (TCA cycle) with known roles in amino acid metabolism and collagen synthesis. The beneficial effects of the oral administration of AKG in improving bone mineralization, renal function and protein anabolism have been well demonstrated in birds and mammals but few studies exist on its effect in teleost fish. The present study tested the effect of the oral administration of AKG on the regeneration of the integument in sea bream (*Sparus aurata*) after scale removal. AKG was administrated in the diet to adult sea bream at a concentration of $0.1 g \cdot Kg \cdot day^{-1}$ for 4 weeks and then the scales were removed from the left flank of the fish and the recovery followed at 0, 2, 5, 10 and 28 days after scale removal. Plasma biochemistry was not significantly altered by AKG treatment compared to the controls but the enzymatic activity of TRAP and ALP was significantly up-regulated ($p < 0.001$) and the regeneration of scales was faster ($p < 0.05$) in the treated fish indicating that AKG treatment favoured scale mineralization. The epithelial outgrowth from the intact scales evaluated with the scale-skin assay was significantly higher ($p < 0.05$) in the treated group 28 days after scale removal providing further evidence that in sea bream skin after scale removal AKG treatment favours the re-epithelialization process and scale growth.

**Keywords**: skin, alpha-ketoglutarate (AKG), metabolism, regeneration, teleost

## 5.2. Introduction

Alpha-ketoglutarate (AKG) is a multifunctional biological substance that plays an important role in cell metabolism and physiology. AKG is a rate-determining intermediate of the tricarboxylic-acid cycle (Gilkes et al. 2013) where it regulates the oxidation of fatty acids, amino acids and glucose for energy production (figure 5.1; (Wu et al. 2016)). In addition to its role in the TCA cycle, AKG is an important detoxifying molecule and a nitrogen scavenger that removes toxic metabolites from cells and plays a key regulatory role in gene expression and cellular signalling. In mammals and birds, dietary AKG has been shown to stimulate cell growth and to improve tissue recovery and repair and is an attractive supplement to improve cellular energy status, immunity and health in animals and humans (Harrison and Pierzynowski 2008). AKG promotes protein synthesis since it is an intermediate in the oxidation of glutamate and glutamine figure 5.1; (Harrison and Pierzynowski 2008; Lambert et al. 2006; Rutten et al. 2005). Furthermore, AKG is a co-factor of prolyl 4-hydroxylase (P4H) that is essential for the synthesis of collagen (Wu et al. 2016) and elastin, essential extracellular matrix (ECM) protein that confers resistance to deformity and compliance (Siddiq et al. 2008; Rosenbloom and Cywinski 1976).

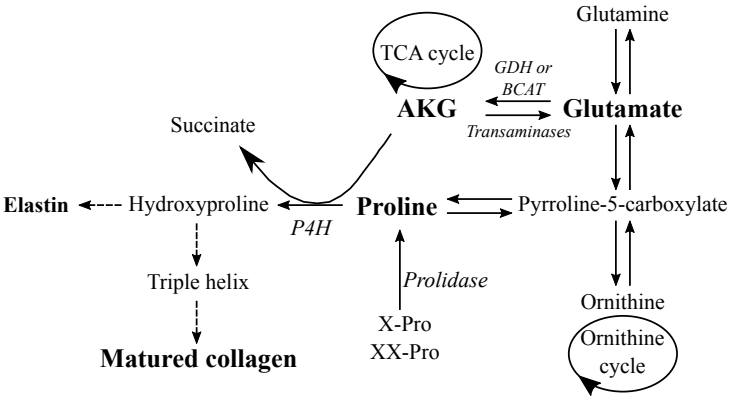


**Figure 5. 1 - Role of AKG in the production of collagen and elastin.** *P4H*: prolyl 4-hydroxylase; *GDH*: glutamate dehydrogenase; *BCAT*: Branch-chained amino acid transferase. Adapted from Son et al. 2007.

If AKG is not in surplus then proline is produced from glutamate by the cytosolic proline recycling exopeptidases, pyrroline 5-carboxylase (P5C) and prolidase that hydrolyse di or tri proline peptides from tissue matrix degradation or dietary protein (Karna et al. 2001; Palka 1996). When AKG is available it acts as an alternative metabolic/oxidative molecule to glutamate/glutamine for the production of the cell proline pool through its transamination into glutamate and subsequent conversion to proline (Son et al. 2007).

Several studies have addressed the effect of AKG on bone metabolism in vertebrates and demonstrated that AKG has an anabolic effect on bone synthesis and stimulates trabecullar collagen synthesis to improve bone mineralization (Harrison and Pierzynowski 2008; Rutten et al. 2005; Kowalik et al. 2005; Tatara et al. 2005; Tatara et al. 2004a; Tatara et al. 2004b; Harrison et al. 2004; Bienko et al. 2002). In postmenopausal women dietary AKG inhibits the development of osteoporosis (Tocaj et al. 2003) and in rats (Wistar) with induced osteopenia counteracts bone loss (Bienko et al. 2002). AKG also has a positive impact on soft tissue during healing in human and animals. In patients on haemodialysis AKG improved renal function by facilitating the uptake of organic anions by the renal tubules (Welborn et al. 1998). Administration of AKG to turkeys (*Meleagris gallopavo*) had positive effects on skeletal development and osteopenia since it improved bone mineral density and increased elastic strength in long bones like the tibia and femur (Tatara et al. 2004b). In humans, supplementation of AKG improved skeletal muscle catabolism in patients and was beneficial in postoperative scenarios (Wirén et al. 2002; Hammarqvist et al. 1991; Wernerman et al. 1990). In Sprague Dawley rats over 8 weeks' post-surgery AKG reversed the loss in body weight and reduction in the elasticity of the aorta typically associated with stomach-bypass (Harrison et al. 2011). In the skin, the topical application of AKG decreased wrinkle formation after UVB exposure by increasing the activity of the prolidase enzyme and in this way collagen production (Son et al. 2007).

In fish, relatively few studies have addressed the effect of AKG on metabolism but similar physiological effects to mammals and birds have been described. In Atlantic salmon (*Salmo salar*) treated with 17-β-estradiol AKG reduced urea emission (Olin et al. 1992) and in the proteome of the sea bream (*Sparus aurata*) pituitary treated with AKG somatolactin production was significantly down-regulated suggesting it may have an endocrine/metabolic role in fish (Ibarz et al. 2010). Preliminary studies in seabream revealed that dietary supplementation of AKG (calcium salt) increased the plasma levels of aspartate-aminotransferase (AST) an enzyme that is involved in protein synthesis and the re-establishment of the dermis after scale removal presumably due to increased synthesis of collagen and elastin (Costa 2009). Moreover, the identification of large TRAP positive cells surrounding scales in the absence of differences in scale thickness or inorganic content in AKG treated fish was taken to suggest that it affects scale turnover (Costa 2009). The present study aims to test the hypothesis that dietary AKG supplementation acting through its stimulatory effect on collagen synthesis modifies skin properties and improves scale regeneration in sea

bream (*Sparus aurata*). The long term effect of AKG supplementation ($0.1 g \cdot kg^{-1} \cdot day$) on the metabolism, integrity and function of the integumentary system of fish was studied.

## 5.3. Material and Methods

### 5.3.1. Ethics Statement

The maintenance of the fish and subsequent experiments carried out at the Ramalhete`s experimental station of the Centre of Marine Sciences (CCMAR, University of Algarve, Faro, Portugal) complied with the Guidelines of the European Union Council (86/609/EU) and were covered by a group 1 license (Direção-Geral de Veterinária, Portugal). The behaviour and health of all animals was monitored daily and no evidence of infection, modified behaviour or mortality was observed during the experiments.

### 5.3.2. Alpha-ketoglutarate treatment

Alpha-ketoglutarate (α-Ketoglutaric acid (AKG) or oxo-glutarate; $C_5H_6O_5$; Molecular mass = 146.11 $g \cdot mol^{-1}$) was administered to the experimental animals *via* the diet at a concentration of $0.1 g \cdot Kg \cdot day^{-1}$ AKG. An aqueous solution of AKG was prepared and pH was partially neutralized with NaOH (5M) to pH ~4. The solution was sprinkled on the commercial diet (Provimi, Portugal), dried overnight and was sprayed with cod liver oil to increase palatability. The control diet was sprayed with cod liver oil only.

### 5.3.3. Animals experiments

Adult gilthead sea bream (1-year-old) were obtained from a commercial supplier and transferred to Ramalhete experimental station at CCMAR (Universidade do Algarve, Faro). Prior to the start of the experiment, fish (n = 80) were acclimated to two 500 L tanks supplied with a continuous flow of aerated sea water at 19 ± 1ºC, 35 - 36‰ salinity and > 80% oxygen saturation under a standard 12h light/12h dark photoperiod for 3 weeks. Fish were fed twice a day (1.5% body weight, bw) with a commercial diet (Provimi, Portugal). Two experiments were performed to study the effect of AKG treatment: 1) on sea bream skin and scale metabolism (experiment 1, supplementary figure 5.1A), also with the objective of optimizing the techniques for posterior analysis, and 2) on skin and scale regeneration after damage preceded by 4 weeks of AKG treatment (experiment 2, supplementary figure 5.1B).

#### 5.3.3.1. Experiment 1 – Preliminary trial on the influence of AKG treatment in the integument of sea bream

Two experimental tanks (500 L) were considered for the Control (n = 16) and AKG (n = 16) treated sea bream and the experimental trial had a duration of 28 days (supplementary figure 5.1A). Control fish were fed (1.5% bw) with a commercial diet (Provimi, Portugal) coated with cod liver oil and AKG treated fish were fed (1.5% bw) with the same commercial diet supplemented with 0.1g · Kg · $day^{-1}$ AKG and coated with cod liver oil (March 2013). On days 0 and 14 (n = 4 / time point) fish were anaesthetized with 2-phenoxyethanol in seawater (1:10,000; Sigma-Aldrich), photographed and weight (g), standard length, total length and condition factor (K) recorded. A blood sample was collected by caudal puncture, centrifuged (10,000 rpm for 5 min) and the plasma transferred to a micro-centrifuge tube, frozen in liquid nitrogen and stored at -80ºC until analysis. Fish were killed by severing the spinal cord and skin (1.5 $cm^2$), muscle, liver and kidney samples were taken and frozen in liquid nitrogen and stored at -80ºC until analysis. Skin samples were also fixed in 4% paraformaldehyde (PFA; pH 7.4) at 4ºC for histology. Scales were also collected individually (n = 10 scales per fish) using a pair of forceps and put in enzyme buffer for alkaline phosphatase (ALP, n = 5 scales per fish, n = 4 fish) and tartrate-resistant acid phosphatase assays (TRAP, n = 5 scales per fish, n = 4 fish) or mounted in culture media for evaluation of the epithelial outgrowth (details given below).

To better monitor the effect of the AKG treatment, scales (n = 5 scales per fish) were more frequently collected during the experimental trial. Fish (n = 4) were anesthetized with 2-phenoxyethanol in seawater (1:10,000; Sigma-Aldrich) at days 7 and 21 for quantification of TRAP and ALP activity and to evaluate epithelial outgrowth from scales. These fish were allowed to recover in clean and aerated seawater before returning them to the experimental tanks.

#### 5.3.3.2. Experiment 2 – Influence of AKG treatment in sea bream skin regeneration after scale removal

##### 5.3.3.2.1. Power Analysis

A prospective power analysis was performed in order to estimate the minimum required number of experimental animals to achieve statistical significance for the experiment. The software GraphPad StatMate version 2.0a for Macintosh (San Diego, California, USA; www.graphpad.com) was used with parameters obtained from previous pilot experiments in the host laboratory. An unpaired t-test with an expected SD for each group of 0.13 and a

significance level (alpha) of 0.05 (two-tailed) were used. The minimum sampling size required was 6 experimental animals per treatment group (supplementary table 5.1).

A four-week period of AKG treatment was performed before the regeneration challenge (supplementary figure 5.1B) in order to evaluate the long term effect of AKG supplementation in the recovery of the integument. The regeneration experiment run for 28 days (April 2013) and control (n = 24) and AKG (n = 24) treated sea bream were fed as previously described. On day 0 of the trial (supplementary figure 5.1B), fish were anaesthetized with 2-phenoxyethanol in seawater (1:10,000; Sigma-Aldrich), photographed (for length measurements) and weight (g), standard length, total length and condition factor (K) recorded. Scales were removed from the left side of the body below the dorsal fin by stroking the skin with forceps taking care to minimise damage of the dermis. Fish were then rinsed in several changes of filtered seawater before returning them to the experimental circuit. The whole procedure took approximately 2 min per fish.

On days 0, 2, 5, 10 and 28 after scale removal a subset of fish (n = 6 / time point) were anesthetized with 2-phenoxyethanol (1:10,000; Sigma-Aldrich), photographed, weighed and length measured. A blood sample was also collected as previously described. Fish were killed by decapitation and skin and scales samples were collected from both flanks of the same individual: the descaled side of the fish (designated the regenerating sample) and from the undamaged side (designated the intact sample). Skin samples (1.5 $cm^2$) were either frozen in liquid nitrogen or fixed in 4% paraformaldehyde (PFA; pH 7.4) at 4ºC for histology. Samples of white muscle and liver were also collected and were frozen in liquid nitrogen and stored at -80ºC until analysis. The heart, including the conus and part of the dorsal aorta was sampled and preserved in physiological saline (0.9% NaCl with 0.01% $NaN_3$) and stored at 4ºC for elasticity analysis. Scales were collected individually (n = 15 scales per fish) using a pair of forceps. Collected scales were, a) transferred to buffer for alkaline and tartrate-resistant acid phosphatase analysis (ALP, n = 5 scales per fish, n = 6 fish; TRAP, n = 5 scales per fish of n = 6 fish); b) placed in physiological saline (n = 5 scales per fish of n = 6) for histomorphometric analysis; or c) mounted in culture media for evaluation of the epithelial outgrowth. Scales (n = 10) were also collected from anesthetized fish (n = 2) at 14, 20 and 25 days of the experimental trial. These fish were not sacrificed and were allowed to recover in clean and aerated seawater before returning to the experimental tanks.

### 5.3.3.3. Plasma biochemistry

To determine the initial status of experimental animals and if the administrated AKG modified the blood chemistry of fish (control and treated) from experiment 1 (day 0) and experiment 2 (days 0, 5, 10 and 28) several plasmatic parameters were analysed. The concentration ($mmol \cdot L^{-1}$) of plasma calcium (Ca) and phosphorus (P) was determined in duplicate in heat-denatured plasma using an endpoint colorimetric assay (Calcium-o-C v/v and Phosphorus v/v; Spinreact, Spain). The plasma ions sodium ($Na^{2+}$) and potassium ($K^{+}$) were determined using a flame photometer (BWB Technologies, UK) according to the manufacturer`s instructions. Plasma osmolality ($mOsmol \cdot kg^{-1}$) was determined using a vapour pressure osmometer (Vapro Wescor 5520, USA). Total plasma protein ($mg \cdot ml^{-1}$) was measured in diluted samples (1:100) with the Protein Assay Dye Reagent (BioRad, Spain) and bovine serum albumin (BSA; Sigma-Aldrich, Spain) was used as the standard. Plasma aspartate-aminotransferase (AST; EC.2.6.1.1) and alanine-aminotransferase (ALT; EC 2.6.1.2), indicators of tissue damage, were determined using a spectrophotometric method with aspartate and alanine respectively, as the substrate (Gallardo et al. 2003). In these assays, enzyme activities ($mIU \cdot ml^{-1}$ of plasma) were coupled, through the action of malic dehydrogenase (MDH), to the oxidation of NADH and measured at 340 nm.

To determine if the treatment regime modified the stress axis the circulating level of cortisol was measured by radioimmunoassay (RIA, (Rotllant et al. 2005a)). The concentration of cortisol (F) was determined using a 1/20 dilution (in 0.01M PBS, pH 7.6) of heat-denatured plasma with a specific F antisera and a radiotracer [1,2,6,7-3H] Cortisol (TRK407 Specific activity 50-90 Ci/mmol, Amersham Biosciences, UK). The assay characteristics and its validation for quantification of F in fish blood has previously been reported (Rotllant et al. 2005).

### 5.3.3.4. TRAP and ALP enzymatic assays

TRAP and ALP are markers of bone turnover and indicators of tissue demineralization and mineralization, respectively. The activity of TRAP and ALP was measured as described by Guerreiro et al. (2013) in intact and regenerating scales (n = 5 scales per fish per enzyme) from n = 4 fish from experiment 1 and 6 fish from experiment 2. Briefly, individual scales were incubated in 200 µl of 10 mM paranitrophenyl (pNPP) in 0.1 mM Na-acetate buffer for 20 min at 24°C. In the case of TRAP assays, 10 mM tartrate was included in the incubation buffer. The reaction was stopped with 2 M NaOH and the enzyme activity was measured at 405 nm using a microplate reader (Benchmark; BioRad). The amount of pNPP converted into paranitrophenol

(pNP) was calculated using a pNP standard curve. After assays, individual scales were rinsed in distilled water and dried to a constant weight at 65°C and cooled to room temperature in a desiccator. In the case of regenerating scales at 5 days (experiment 2) due to their small, fragile and soft character, they were dried and weighed as pools of several scales. Results for enzyme activity are expressed in nmol pNP $min^{-1}$ $mg^{-1}$.

#### 5.3.3.5. Epithelial outgrowth assay

An *in vitro* fish skin culture model for re-epithelialisation was used to characterise the initial process of wound healing in sea bream by measuring epidermal outgrowth (Matsumoto and Sugimoto 2007). Individual scales from control and AKG treated fish from the experiment 1 (days 0 and 7) and from experiment 2 (intact and regenerating scales, days 10, 14, 20, 25 and 28) were removed from the sea bream integument. Scales were washed in sterile water, followed by two changes of DMEM-high glucose medium (Sigma-Aldrich, Spain), one change of DMEM-high glucose medium with 1% antibiotics (penicillin-streptomycin, (P/S), Sigma-Aldrich) and then placed in DMEM-high glucose medium supplemented with 10% FBS (Sigma-Aldrich 2008) and 1% antibiotics (PS) on a glass slide coated with a Poly-L-lysine solution. The preparations were incubated for 24h at 24°C and then observed under a microscope with polarized light (Olympus BH-2). A photographic record of the epidermal outgrowth in control and AKG treated fish was recorded (Leica DFC480) and the software ImageJ 1.44o (Abramoff et al. 2004) was used to measure the outgrowth calculated as the outgrowth area / scale area ($mm^2$). At days 2 and 5 of regeneration the small size and fragile nature of the scales meant the regrowth assay was not performed (experiment 2). At day 0, when fish were descaled and sampled (n = 12 fish) it was not logistically possible to also run the outgrowth assay.

#### 5.3.3.6. Skin conductivity

Electric conductance of the skin depends on the moisture of the skin cells. When moistened, skin behaves like a high water content tissue when compared to dry skin (Gabriel et al. 2009). In this context, skin conductivity was measured to evaluate if the treatment modified this property in the control and AKG treated fish in experiment 1 and experiment 2. A piece of skin (2x3 $cm^2$) was mounted between two platinum plates connected to a power supply and to the amp meter by gold electrodes. A constant voltage of 3 V was applied to the tissue, and the voltage was registered before (basal) and after (final) turning on the amp meter. The difference

between the basal and final voltage was used to estimate the electric resistance of the skin using the Ohms law (I = V/R, where, V is the voltage, R is resistance and I is the current). Conductance is then given by the inverse of the resistance (1/R) and results expressed as Siemens per minute ($S \cdot m^{-1}$).

### 5.3.3.7. Calculation of scale area and regeneration rate

Scales were collected from the regenerating and intact flanks of control and AKG treated sea bream (experiment 2) at 0, 5, 10, 20 and 28 days after scale removal (n = 21 - 30 scales for days 0, 5, 10 and 28; n = 10 for day 20) and stored in a saline solution at 4°C until morphometric analysis. The regrowth of scales was used to measure ontogeny of tissue recovery after damage. Intact and regenerating scales were photographed (Leica DFC480) and the software ImageJ 1.440 (Abramoff et al. 2004) was used to measure the scale area ($mm^2$). The scale regeneration rate was calculated as previously described by Ohira et al. (2007). Briefly, the area of each regenerating scale was related to the average area of intact scales at time 0. The scale regeneration rate was obtained using the following equation: $RR_{area}\% = R_{area} / O_{area} \times 100$, (where $RR_{area}$ = increase in scale area, $R_{area}$ = the area of the regenerating scales and $O_{area}$ = the average area of scales at the start of the experiment, day 0). The increase in scale area ($mm^2$) was determined as the difference in area of the growing scales (from the intact and regenerating flanks) relative to the total area of the scales at the start of the experiment (time 0), assuming in the case of the regenerating scales that the area was 0.

### 5.3.3.8. Heart elasticity measurement

Cardiac muscle elasticity was measured for the heart samples collected during experiment 2. Determination of the elasticity of the heart was used as an indicator of modified protein synthesis and efficacy of the AKG treatment (Harrison et al. 2011; Harrison et al. 2009). Sections of the conus were attached between an FT03 force displacement transducer (Grass Instruments, West Warwick, RI, USA) and a fixed metal pin, and immersed into a 44 ml chamber, at 37ºC, containing PBS Ringer (0.15 M pH 7.4). Force was measured using a force transducer connected to a "home-built" bridge amplifier, interfaced with an 8S PowerLab A/D Converter (AD Instruments, Australia). The transducer had a functional range of 0 - 0.05 kg, with a reliable force of 2 mg, equivalent to 0.004 % of the functional range. The PowerLab 8S A/D converter was connected to an iBook G4 running LabChart v.5.4 Software (AD Instruments). The data recording was at a sampling speed of 40,000 data samples per second

(40 KHz), and the input impedance of the amplifier was 200 MΩ differential. Sections were exposed to a series of step-wise increases in tension.

#### 5.3.3.8.1. Force measurements

The recorded signal was adjusted to zero for un-tensioned conus sections with the aid of an offset dial mounted on the pre-amplifier unit. Each conus section was then exposed to approximate 3 step-wise increases in tension (each step being an increase of 0.09 Newtons, N), until a final maximal tension of 0.49 N (measured using the FT03 Grass Force transducer) was achieved. The conus sections were then allowed to relax totally before being exposed to repeated step-wise increases in tension two more times, in close succession. Conus sections were subsequently removed and weighed.

#### 5.3.3.8.2. Elastic recoil calculations

It was assumed that the tension in the wall of the conus sections was equivalent to that recorded by the force transducer as the result of a manual stretch. The fall in the recording trace that was seen immediately after a step-wise increase in tension was then measured and taken as the elastic recoil in the conus sections. The measurement of Average Slope ($g \cdot ms^{-1}$) obtained for each conus sample was subsequently converted into $N \cdot ms^{-1}$ before being adjusted for sample weight to give a final elastic recoil value in $N \cdot ms^{-1} \cdot mg^{-1}$ wet wt.

### 5.3.4. Statistical analysis

Significant changes between AKG treated and control groups were assessed using a two-way ANOVA followed by the Fisher`s Least Significant Difference (LSD) post-test using the StatPlus:mac LE v5 2015 (AnalystSoft Inc., USA). Data are presented as mean ± standard error of the mean (sem). Statistical significance was considered at $p < 0.05$. Significant differences at different time points during the experiment are annotated with different letters and significant differences between intact and regenerating samples at the same time point are annotated with an asterisk.

## 5.4. Results

### 5.4.1. Experiment 1 – Preliminary trial on the influence of AKG treatment in the integument of sea bream

#### 5.4.1.1. Plasma biochemistry

At the beginning of the experiment, before administering AKG no significant differences in plasma parameters (figure 5.2) were detected between the experimental groups (control and AKG treated fish), which means that fish were in a similar physiological state. Control fish plasma contained 2.05 ± 0.27 mmol·$L^{-1}$ of calcium and 3.25 ± 0.57 mmol·$L^{-1}$ of phosphorus compared to 2.30 ± 0.29 mmol·$L^{-1}$ and 3.33 ± 0.19 mmol·$L^{-1}$, respectively in AKG treated fish. Plasma sodium and potassium were 132.35 ± 27.59 mmol·$L^{-1}$ and 3.48 ± 0.85 mmol·$L^{-1}$ respectively, in the control group and 166.12 ± 28.64 mmol·$L^{-1}$ and 3.48 ± 0.83 mmol·$L^{-1}$ respectively, in the treated fish. The osmolality of control plasma (313.75 ± 28.2 mOsmol·$kg^{-1}$) and plasma from treated fish (335.5 ± 12.4 mOsmol·$kg^{-1}$) was not significantly different. Total protein in plasma was in the normal physiological range in all fish (control, 18.49 ± 2.79 mg·$ml^{-1}$ vs. 18.51 ± 1.54 mg·$ml^{-1}$, AKG, n = 6) as were the plasma transaminases, AST (control, 4.93 ± 2.79 mIU·$ml^{-1}$ vs. 4.9 1 ± 1.55 mIU·$ml^{-1}$, AKG, n = 2 due to low volume of the plasma samples) and ALT (control, 5.26 ± 0.39 mIU·$ml^{-1}$ vs. 3.26±0.53 mIU·$ml^{-1}$, AKG, n = 4). Indicating liver metabolism was unaffected by AKG. The concentration of plasma cortisol was in the normal physiological range in control and AKG treated animals.

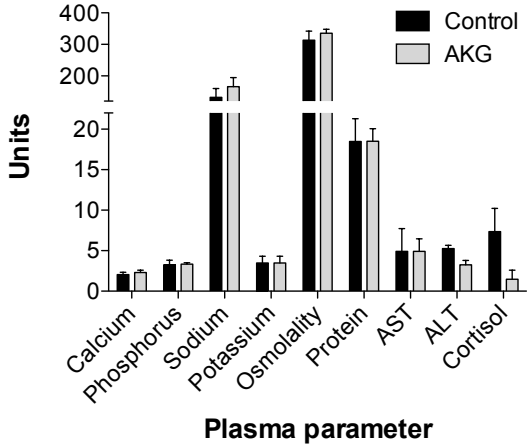


**Figure 5. 2 - Plasma parameters of Control and AKG treated sea bream at the beginning of the preliminary trial (Day 0).** Calcium (mmol·$L^{-1}$); Phosphorus (mmol·$L^{-1}$); Sodium (mmol·$L^{-1}$); Potassium (mmol·$L^{-1}$); Osmolality (mOsmol·$kg^{-1}$); Protein (mg·$ml^{-1}$); AST: aspartate-aminotransferase (IU·$ml^{-1}$); ALT: alanine-aminotransferase (IU·$ml^{-1}$) and Cortisol (ng·$ml^{-1}$). Results are presented as mean ± sem of n = 4 fish. A One-way ANOVA tested differences between experimental groups, and no significant differences were detected for any of the parameters quantified.

### 5.4.1.2. TRAP and ALP enzymatic activity in sea bream scales

Independent of the experimental group and sampling time, TRAP activity was always higher than ALP activity, suggesting that osteoblast activity is predominant in the process of scale mineral turnover. The activity of TRAP and ALP in ontogenetic sea bream scales (figure 5.3A and B, respectively) was not affected by the AKG treatment, and was similar during the experiment in both control, and treated scales. By the end of the experiment (end of March) the activity of TRAP and ALP in the scales of both control and AKG treated fish was significantly reduced ($p < 0.02$) relative to time 0. The ratio of TRAP/ALP, an indicator of mineral turnover in bony tissue, was not significantly different between scales from control and AKG treated fish and was constant throughout the experimental trial (figure 5.3C). This indicates that AKG treatment has no impact on the activity of TRAP and ALP.

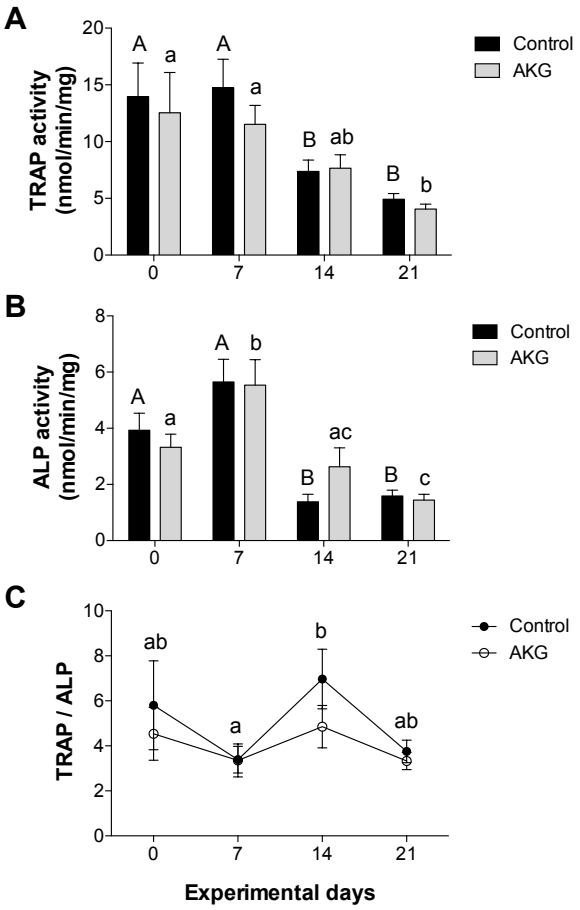


**Figure 5. 3 - Preliminary evaluation of the enzymatic activity of tartrate-resistant acid phosphatase and alkaline phosphatase (ALP) in sea bream scales of Control and AKG treated fish. A:** TRAP activity (nmol·pNP·min$^{-1}$·mg$^{-1}$) in Control and AKG treated sea bream scales. **B:** ALP activity (nmol·pNP·min$^{-1}$·mg$^{-1}$) in Control and AKG treated sea bream scales. Results are presented as mean + sem. **C:** TRAP/ALP ratio (arbitrary units) in Control and AKG treated sea bream scales. Results are presented as mean ± sem of 20 scales from 4 fish. Statistical significance between groups was assessed using a two-way ANOVA followed by the Fisher`s Least Significant Difference (LSD) post-test and significant differences considered at $p < 0.05$ and are annotated with different letters. Significant differences between control and treated scales at the same time point were not detected.

### 5.4.1.3. Epithelial outgrowth of sea bream scales-skin

The outgrowth of epithelial tissue from the scales in culture media (figure 5.4A) in AKG treated and control groups was similar in the beginning of the experiment (0 time). Two weeks after AKG treatment epithelial outgrowth increased significantly ($p = 0.01$) compared to the controls. The epidermal outgrowth was multi-layered in both the control and AKG treated fish (figure 5.4B).

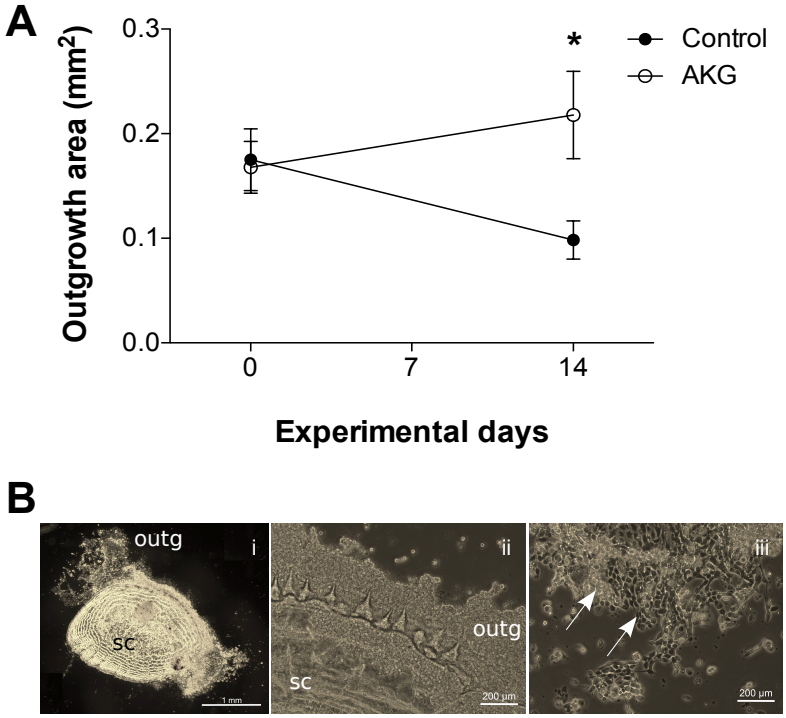


**Figure 5. 4 - Preliminary evaluation of the epithelial outgrowth of Control and AKG treated sea bream scales. A:** Epithelial outgrowth area after 24h of incubation at 24°C measured with ImageJ software. Control: n = 12-19 scales and AKG: n = 39-52 scales collected from 4 fish. Results are presented as mean ± sem and statistical differences between groups was assessed using a two-way ANOVA followed by the Fisher`s Least Significant Difference (LSD) post-test and statistical significance was considered at $p < 0.05$. Significant differences between experimental groups are indicated with an *asterisk*. **B:** Epithelial outgrowth within a fish scale-skin culture system. **i**: Outgrowth of an epidermal sheet from the anterior part of the scale-skin. **ii** and **iii:** Magnification of the epidermal sheet evidencing the multi-cellular layers, identified by the arrows heads. Sc: scale; outg: outgrowth.

### 5.4.1.4. Skin conductivity

The electric conductivity of the skin after 14 days AKG treatment (figure 5.5) was similar ($p = 0.90$) in control ($0.368 \pm 0.039$ $S \cdot m^{-1}$) and treated ($0.357 \pm 0.086$ $S \cdot m^{-1}$) skin, although it was more variable in the treated skin. These results indicate that the electrical properties of the skin were not affected by AKG treatment.

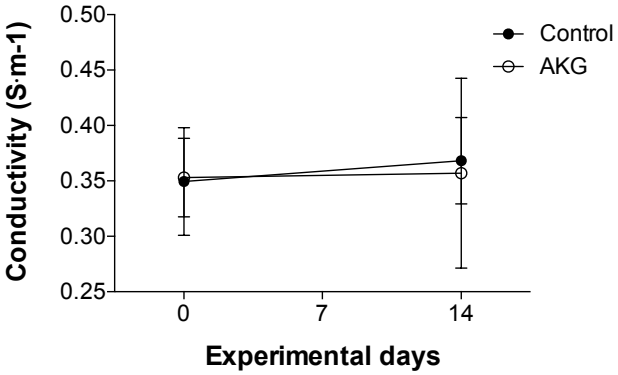


**Figure 5. 5 - Preliminary evaluation of skin conductivity in Control and AKG treated sea bream (n = 4) skin at the beginning (Day 0) and after two weeks (Day 14) of the experimental trial.** Results are presented as mean ± sem and statistical significance was assessed using a two-way ANOVA followed by the Fisher`s Least Significant Difference (LSD) post-test. Statistical significance was considered at $p < 0.05$ and no significant differences were detected between groups.

## 5.4.2. Experiment 2 – Influence of AKG treatment in sea bream skin regeneration after scale removal

### 5.4.2.1. Plasma biochemistry

The variation in plasma parameters was similar in both control and AKG treated groups during the experiment (figure 5.6), indicating that AKG does not significantly affect the blood chemistry of the experimental animals. In both control (2.94 ± 0.09; $p < 0.01$) and AKG (3.17 ± 0.18, $p < 0.01$) treated groups plasma calcium (figure 5.6A) increased significantly at day 28 after scale removal compared to all other sample points. Plasma phosphorus (figure 5.6B) in the control group remained constant throughout the experiment but in the AKG treated group it increased significantly ($p = 0.008$) at day 10 and 28 after scale removal. The ratio Ca/P also increased in the same period of time, though not significantly (figure 5.6C). Ionic levels of sodium (figure 5.6D) were significantly ($p = 0.02$) lower in the plasma of both control and AKG treated groups at day 28 after scale removal. Ionic levels of potassium (figure 5.6E) significantly ($p = 0.01$) increased at day 10 after scale removal in both experimental groups. Plasma osmolality (figure 5.6F) did not significantly change in either group during the experiment. In the control group, total protein in plasma increased significantly ($p < 0.01$) at day 28 after scale removal (26.25 ± 1.22 $mg \cdot ml^{-1}$) compared to all other days (18.8-19.9 $mg \cdot ml^{-1}$) but no significant changes occurred in the AKG treated fish (figure 5.6G). Plasma levels of AST (figure 5.6H) and ALT (figure 5.6I) did not change significantly in the AKG treated fish, although in the control fish ALT decreased significantly ($p = 0.02$) at day 28 (2.27 ± 0.70 $IU \cdot ml^{-1}$) compared to day 10 after scale removal. Cortisol (figure 5.6J) levels were not significantly different between the control and AKG treated fish during the experiment.

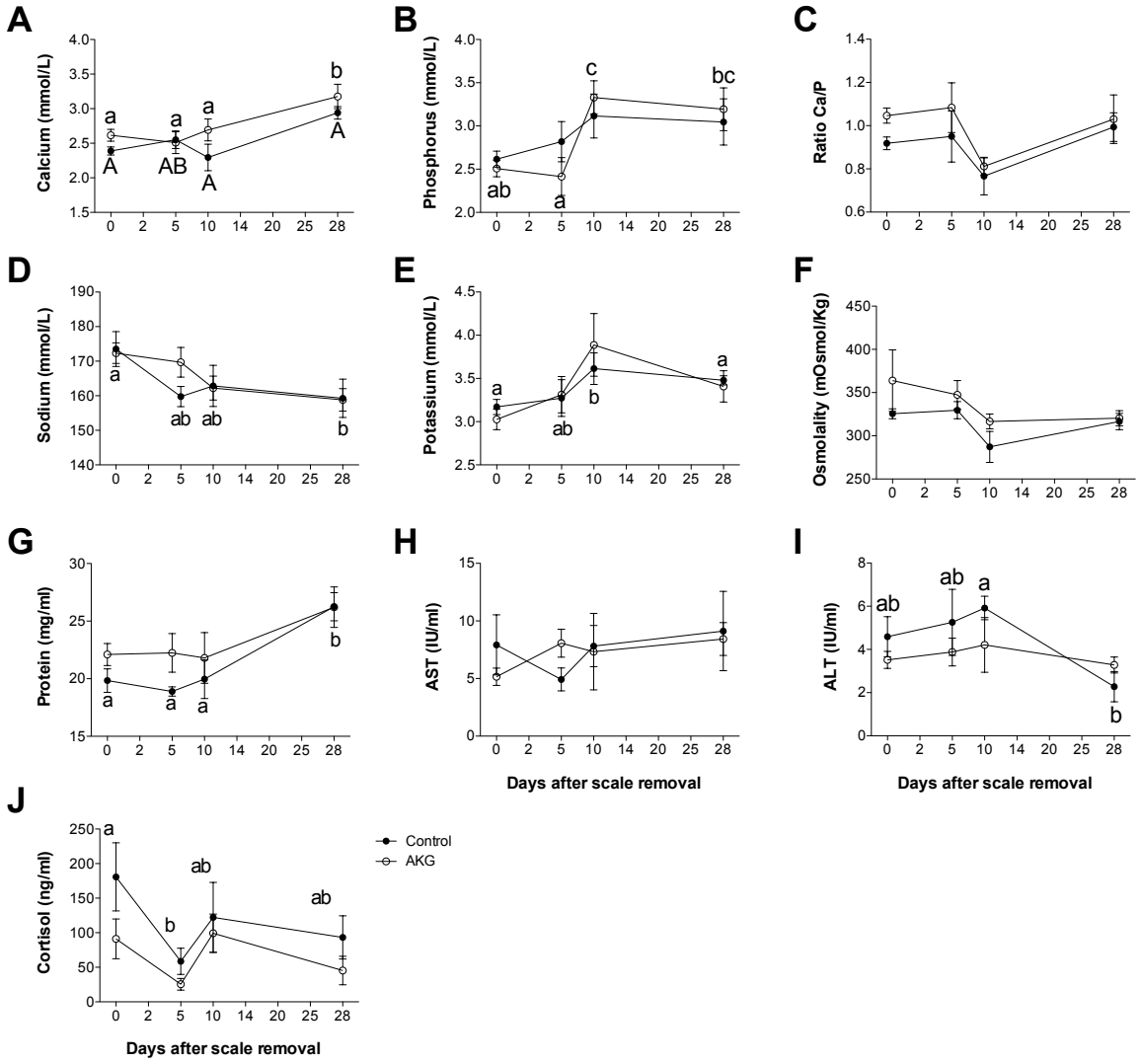


**Figure 5. 6 - Plasma parameters of Control and AKG treated sea bream (n = 6) during scale regeneration.** **A:** Calcium (mmol·$L^{-1}$) **B:** Phosphorus (mmol·$L^{-1}$) **C:** Ratio Ca/P (arbitrary units) **D:** Sodium (mmol·$L^{-1}$) **E:** Potassium (mmol·$L^{-1}$) **F:** Osmolality (mOsmol·$kg^{-1}$) **G:** Protein (mg·$ml^{-1}$) **H:** AST (aspartate-aminotransferase; IU·$ml^{-1}$) **I:** ALT (alanine-aminotransferase; IU·$ml^{-1}$) **J:** Cortisol (ng·$ml^{-1}$). Results are presented as mean ± sem and statistical differences between groups was assessed using a two-way ANOVA followed by the Fisher`s Least Significant Difference (LSD) post-test. Statistical significance was considered at $p < 0.05$ and significant differences are annotated with different letters. No statistical differences between control and treated plasmas at the same time point were detected.

### 5.4.2.2. Enzymatic activity and scale growth in intact and regenerating scales

In agreement with the observation made in experiment 1, TRAP activity was always higher than ALP activity, suggesting that osteoblast activity is predominant in scale mineral turnover in sea bream. In the AKG treated and control groups TRAP (figure 5.7A and B) and ALP (figure 5.7C and D) activities at days 5 and 10 after scale removal were significantly up-regulated ($p < 0.001$) in regenerating scales relative to intact scales. The increase in TRAP and ALP activity coincided with a significant increase ($p < 0.0001$) in the area of the regenerating

scales from day 0 to day 5 (figures 5.8A and B). The TRAP/ALP ratio (figure 5.7E and F) was significantly higher ($p \leq 0.01$) on day 5 and 14 in intact scales relative to regenerating scales in both AKG treated and control fish. A significant increase ($p < 0.05$) in scale area (figures 5.8A-D) occurred in both experimental groups from 20 to 28 days after scale removal and this coincided with a second significant increase ($p < 0.05$) in the TRAP/ALP ratio (figures 5.7E and F) and higher rate of scale regeneration (figures 5.8E and F).

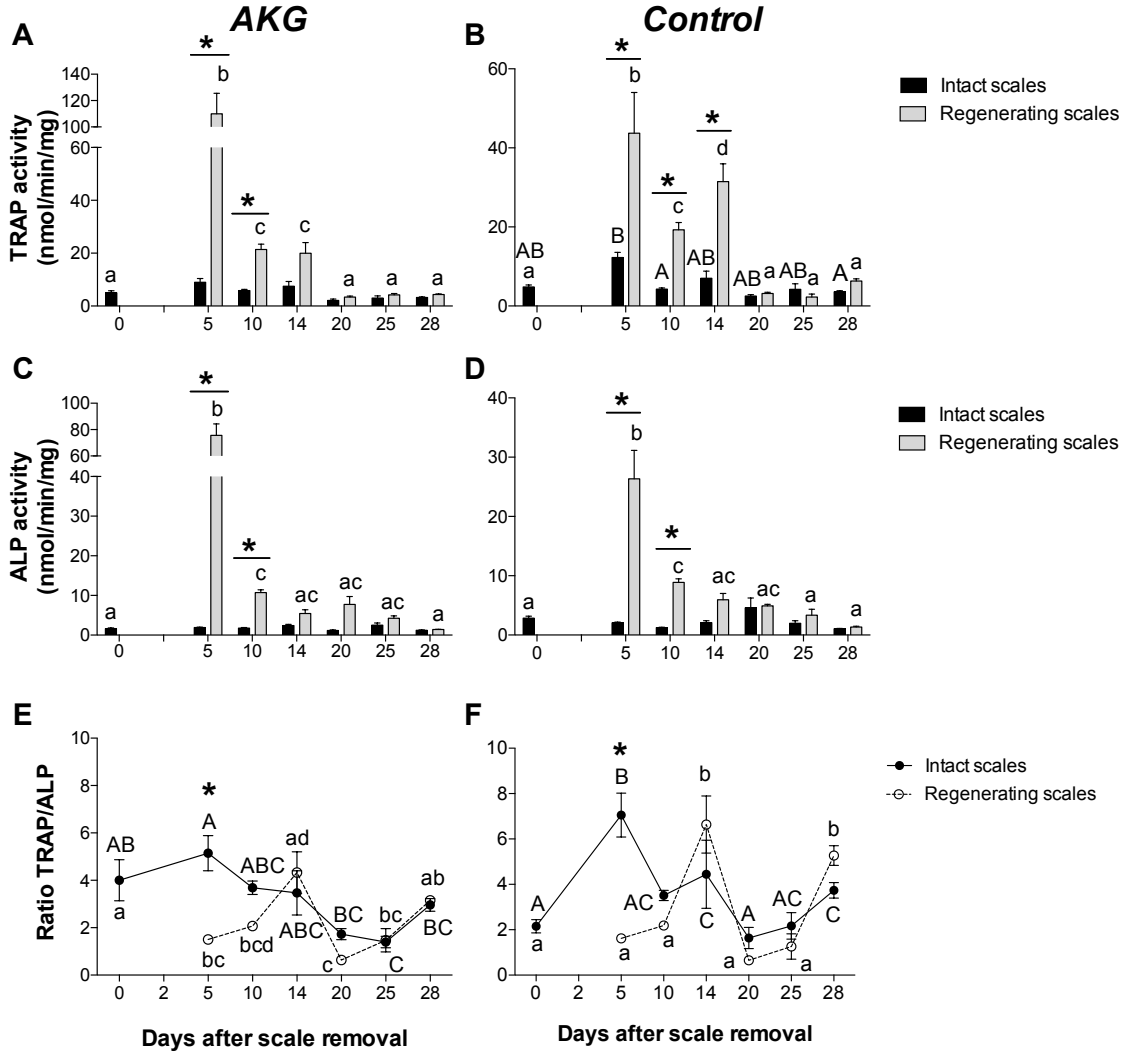


**Figure 5. 7 - Enzymatic activity of tartrate-resistant acid phosphatase and alkaline phosphatase (ALP) in sea bream during scale regeneration process.** Scales (n = 10-30) from the AKG treated and Control fish were used. **A and B:** TRAP activity (nmol·pNP·min$^{-1}$·mg$^{-1}$) **C and D:** ALP activity (nmol·pNP·min$^{-1}$·mg$^{-1}$). Results are presented as mean + sem. **E and F:** TRAP/ALP ratio (arbitrary units). Results are presented as mean ± sem. Statistical significance between groups was assessed using a two-way ANOVA followed by the Fisher`s Least Significant Difference (LSD) post-test. Statistical significance was considered at $p < 0.05$ and significant differences are annotated with different letters. Comparisons between intact and regenerating scales groups at the same time point are indicated with an *asterisk*.

Comparison of the two experimental groups at individual time points (non-parametric t-test with Mann-Whitney post-test) revealed a significant increase in the activity of TRAP ($p = 0.0021$) and ALP ($p < 0.0001$; figure 5.7) in the AKG treated group 5 days after scale removal. AKG also accelerated the increase in the area of the regenerating scales ($p = 0.0007$; figure 5.8) at 5 days relative to the controls. These results indicate that AKG promotes faster regrowth and constitution of the new scales over the first 5 days of integument regeneration.

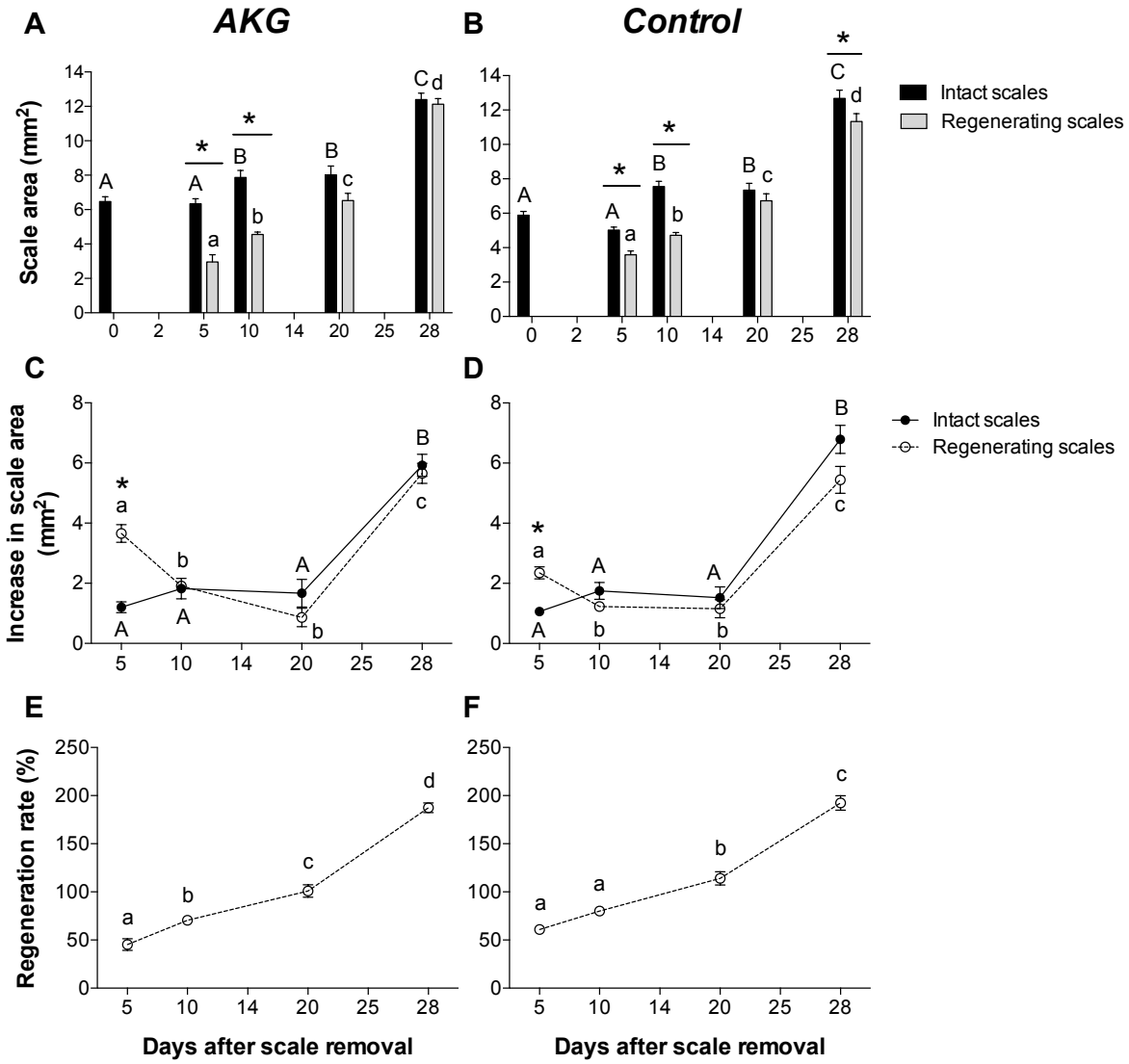


**Figure 5. 8 - Scale growth in AKG treated and Control sea bream. A and B:** Area of the scales (n = 10-30; $mm^2$) **C and D:** Increase in scale area (n = 10-30; $mm^2$), as determined by the difference between the area of the growing scales and the average area of the scales at time 0, and **E and F:** Regeneration rate (n = 10-30; %). Results are presented as mean ± sem and statistical significance between groups was assessed by two-way ANOVA followed by the Fisher`s Least Significant Difference (LSD) post-test. Statistical significance was considered at $p < 0.05$ and significant differences are indicated with different letters. Significant differences between intact and regenerating scales at the same time point are signalled with an *asterisk*.

### 5.4.2.3. Epithelial outgrowth of sea bream scales-skin

The epithelial outgrowth area 10 days after scale removal in regenerating scales was significantly higher ($p < 0.001$) than in intact scales, irrespective of the experimental group. The rate of expansion of the outgrowth area progressively decreased towards the end of the trial. Despite this tendency the outgrowth capacity of the intact scales of the AKG treated group was significantly higher (non-parametric t-test; $p = 0.048$) than the controls at the end of the experimental trial.

Epithelial outgrowth from the regenerating scales-skin in the AKG treated group (figure 5.9A) significantly decreased ($p < 0.03$) from day 20 ($0.117 \pm 0.014$ mm$^2$) onwards relative to day 10 after scale removal ($0.173 \pm 0.013$ mm$^2$). At days 14 ($0.139 \pm 0.011$ mm$^2$) and 20 after scale removal epithelial outgrowth was significantly higher in AKG treated regenerating scales-skin than in the intact skin.

In the control group (figure 5.9B) the outgrowth from the intact scales-skin increased significantly ($p = 0.004$) at day 14 ($0.129 \pm 0.015$ mm$^2$) compared to day 10 ($0.075 \pm 0.011$ mm$^2$) and then progressively decreased to day 28 after scale removal. In regenerating control scales-skin epithelial outgrowth significantly decreased ($p < 0.001$) from day 10 ($0.161 \pm 0.014$ mm$^2$) to 28 ($0.061 \pm 0.011$ mm$^2$) after scale removal.

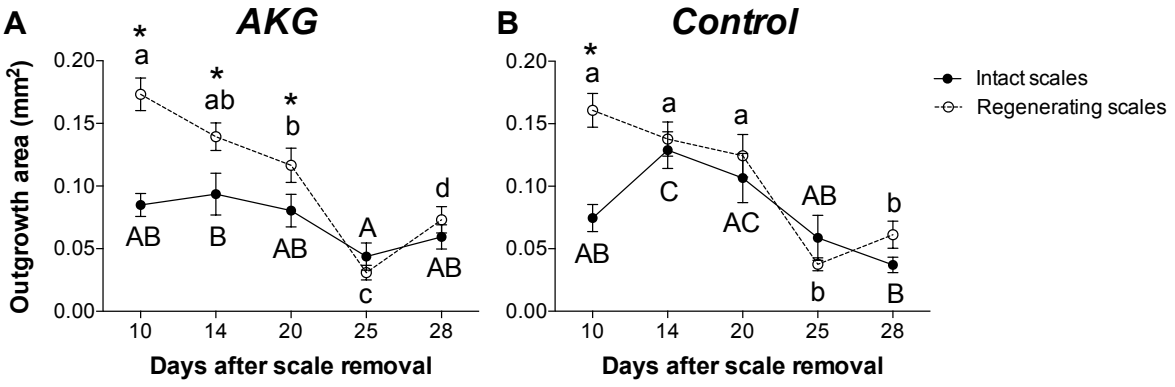


**Figure 5. 9 - Epithelial outgrowth in intact and regenerating sea bream skin.** The epithelial outgrowth area was measured after 24h of incubation at 24°C with the ImageJ software. The epithelial outgrowth was measured at 10, 14, 20, 25 and 28 days after scale removal using 22-52 scales from AKG treated (**A**) and Control (**B**) fish. Results are presented as mean ± sem and statistical significance between groups was assessed using a two-way ANOVA followed by the Fisher`s Least Significant Difference (LSD) post-test. Significant differences were considered at $p < 0.05$ and are annotated with different letters. Significant differences between intact and regenerating skin at the same time point are indicated with an *asterisk*.

### 5.4.2.4. Skin conductivity

Significant differences between experimental groups were not observed and this suggests that the electric properties of the skin were not affected by the long term treatment with AKG (figure 5.10). In the treated skin (figure 5.10A) a significant decrease ($p = 0.01$) in skin conductivity was observed at day 2 similarly in intact ($0.250 \pm 0.005$ $S \cdot m^{-1}$) and regenerating ($0.257 \pm 0.006$ $S \cdot m^{-1}$) skin samples and this was re-established by day 5 after scale removal (intact skin: $0.464 \pm 0.065$ $S \cdot m^{-1}$ and regenerating skin: $0.446 \pm 0.006$ $S \cdot m^{-1}$).The conductivity of the intact control skin (figure 5.10B) increased significantly ($p < 0.01$; $1.028 \pm 0.337$ $S \cdot m^{-1}$) at day 10 however this can be a consequence of the high variability of the measurements and needs to be further confirmed. The conductivity of the control regenerating skin remained constant over the experimental trial.

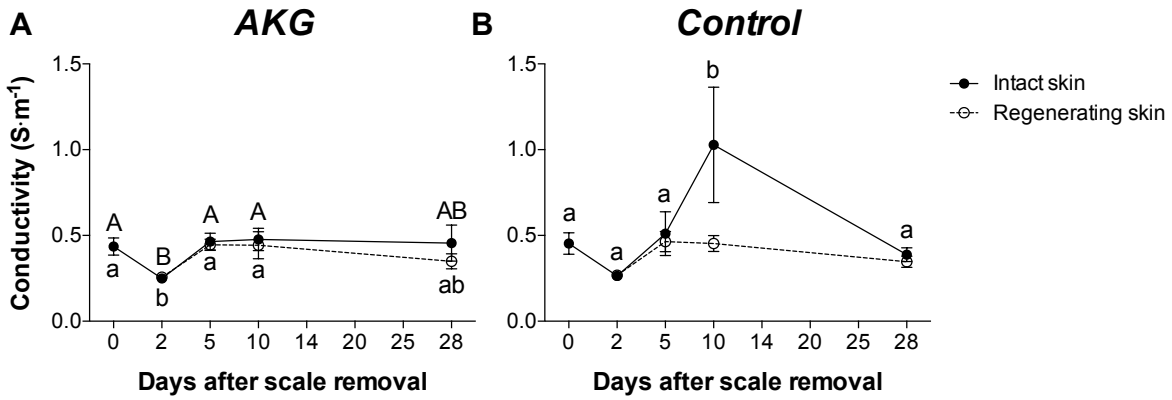


**Figure 5. 10 - Skin conductivity in intact and regenerating skin.** Results are presented as mean ± sem. Statistical significance between groups was assessed using a two-way ANOVA followed by the Fisher`s Least Significant Difference (LSD) post-test and significant differences were considered at $p < 0.05$ and are signalled with different letters. No significant differences between the intact and regenerating skin at the same time point were detected.

### 5.4.2.5. Elasticity of sea bream heart

AKG caused a significant increase ($p = 0.028$) from day 10 ($3e^{-6} \pm 1e^{-6}$ $N \cdot ms^{-1} \cdot mg^{-1}$ wet wt) onwards in the elasticity of the heart (figure 5.11) relative to day 0. Furthermore, 10 days after the removal of the scales the heart of AKG treated sea bream was significantly more elastic ($p = 0.013$) than the control tissue ($1e^{-6} \pm 2.18e^{-7}$ $N \cdot ms^{-1} \cdot mg^{-1}$ wet wt).

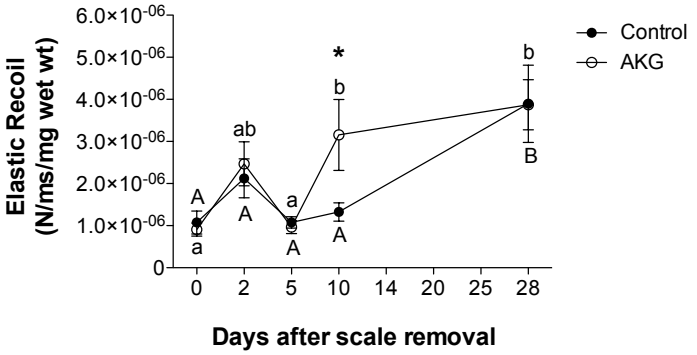


**Figure 5. 11 - Elastic recoil of AKG treated and Control sea bream (n = 6) heart (conus).** Results are presented as mean ± sem and statistical significance between groups was assessed using a two-way ANOVA followed by the Fisher`s Least Significant Difference (LSD) post-test and significant differences were considered at $p < 0.05$ and are signalled with different letters. No significant differences between the control and treated groups at the same time point were detected.

## 5.5. Discussion

In teleost fish the effect of AKG supplementation on physiology and metabolism has been poorly addressed. In this study we provide novel insights into the effect of AKG in the teleost sea bream. In common with terrestrial vertebrates, AKG enhanced epidermal cell proliferation, improved biomineralization of regenerating scales and increased cardiac muscle elasticity in fish.

### 5.5.1. AKG stimulates epithelial outgrowth of sea bream scale-skin

In cultured human dermal fibroblasts AKG supplementation increased cell proliferation (Son et al. 2007) and in the sea bream it accelerated skin epithelial outgrowth. The outgrowth of epidermal skin cells from sea bream treated with AKG for 2 weeks was 2.2 fold greater than control epidermal cell suggesting that as found in mammals and birds increased levels of AKG stimulate cell growth and tissue expansion. In teleost skin regeneration the major restructuring/reorganisation events after damage induced by scale removal occur during the first 5 days. The reorganisation of the epidermis in fish skin occurs during the first 24 hours and by day 3 the skin barrier is reconstituted and the epidermis covers the wounded area and the dermal papilla are already defined and by day 4 the ECM of the new scales is already being

secreted and mineralized (chapter 2). Epidermal outgrowth was not studied during the first 3 days (experiment 2) in the present study but is an important target for future studies. The stimulatory effect of AKG on epidermal outgrowth was still evident after 56 days treatment (total duration of experiment 2: pre-feeding followed by the regeneration challenge) and was significantly higher ($p < 0.05$) than the control.

The stimulation of other cell types by AKG was not established in the present study. However, considering that sea bream epidermal cells are highly proliferative and the plasma half-life of AKG in mammals is less than 5 minutes (Dabek et al. 2005), we hypothesise that its effect is probably more pronounced on rapidly dividing/proliferating cells. For example, humans with psoriasis have high levels of circulating AKG and this has been associated with the accelerated skin proliferation of this disease. Psoriasis lesions have been associated with increased collagen synthesis through increased activity of P4H (Armstrong et al. 2014). Psoriasis is characterized by general epidermal dysfunction with immune dysregulation (Palau et al. 2013; Nestle et al. 2009) and therefore the higher concentration of AKG may contribute to the structural and immune and inflammatory pathology characteristic of the disease (Armstrong et al. 2014). The same study also reported a reduction in plasma glutamine in psoriatic patients relative to healthy controls and the authors hypothesised that the high rates of cell proliferation characteristic of this disease is fuelled by increased rates of protein synthesis (Armstrong et al. 2014).

Overall, the results of this part of the study indicate that AKG has a determinant role in fish skin homeostasis and supports the idea that in teleost skin AKG supplementation accelerates tissue re-epithelialization after tissue injury as occurs in human skin. It will be of interest in the future to establish if AKG stimulates recovery of other lesions as this may be relevant for aquaculture.

### 5.5.2. AKG stimulates sea bream scale biomineralization

Treatment with AKG favoured mineral deposition in regenerating scales of sea bream. This was suggested by the increased activity during the first 5 days after scale removal of both TRAP (a marker of mineral mobilisation) and ALP (a marker of mineralization) in scales from fish treated with AKG. The increased activity of TRAP and ALP in the scales from AKG treated fish coincided with the formation of new scales and the initiation of mineralization (chapter 2). In mammals, AKG affects bone mineralization and lambs given AKG had improved cortical and trabecular bone mineral density (femur) as a consequence of increased proline synthesis and its conversion to hydroxyproline which stimulates the synthesis of collagen and therefore

bone mineralization (Harrison et al. 2004). Osteoblasts and osteoclasts, are the cells responsible for the deposition and remodelling of minerals in bony tissue in mammals, and the glutamate receptors (GluR) are expressed in bone and play an important role in bone cell activity and in the regulation of bone metabolism. AKG is a glutamate precursor and thus has an anabolic effect on bone metabolism via glutamate innervation (Taylor 2002). In fish, scales are mineralized elements imbricated in the integument and osteoblasts (or scleroclasts) and osteoclasts (or scleroclasts) are responsible for scale deposition and remodelling (Witten et al. 2001; Bereiter-Hahn and Zylberberg 1993; Sire et al. 1990). The existence of glutamate receptors in fish scale or bone remains to be established but considering that the cellular elements and the mechanisms of action responsible for mineral deposition and remodelling are conserved during evolution we hypothesise that in fish the effect of AKG supplementation on scale regrowth and mineralization may be mediated by glutamate receptors. In the future, it will be of interest to establish the mineral content of the scales from fish given AKG and to establish how it brings about its action to influence scale growth.

### 5.5.3. AKG seems to increase elasticity of the sea bream heart muscle

Arterial elasticity is dependent on connective tissue content and requires an appropriate supply of amino acids for remodelling and repair. In the present study, the conus and part of the aorta collected from control and AKG treated sea bream was used to measure tissue elasticity and served as a proxy for increased/ decreased collagen synthesis. In both control and AKG treated fish increased resistance to deformity and increased elastic recoil of the conus and aorta was observed 2 days after scale removal, although by 10 days the conus and aorta AKG treated fish was significantly more elastic.

In elderly mice administration of AKG increased collagen synthesis and significantly improved the elasticity of their aortas (Harrison et al. 2009). Moreover, in stomach-bypass operated rats, oral administration of AKG restored aortic elasticity to 60% in recovery animals compared to the controls, suggesting that the altered amino acid metabolism induced by the surgery was compensated by the dietary surplus of AKG (Harrison et al. 2011). In common with mammals, a previous study revealed dietary AKG (calcium salt) in fish also modified cardiac muscle performance as revealed by the improved elasticity of the aortas (Costa 2009). The difference between the present and previous results in fish and mammals may be linked to the use of pure AKG (and not the salt of calcium or sodium) and the analysis of the conus and part of the dorsal aorta in the present study. It is well established that different compartments of the vertebrate heart have different muscular properties (Icardo 2012). Overall, our data

suggest that tissue damage (caused by scale removal) and AKG supplementation modify heart muscle elasticity in sea bream, although the mechanism was not established and further studies will be required.

Elastic recoil values are estimated as a function of the wet weight of the tissue. In both experimental groups (control and treated) the heart weight decreased and was significantly lower ($p < 0.05$) at the end of the experimental trial (28 days after scale removal) relative to day 0. This observation was unexpected and the reason this occurred was not determined and this aspect requires further analysis. In the future, to better understand how AKG supplementation affect teleost vessel elasticity it will be pertinent to determine if the collagen and elastin content and structure in the experimental hearts was modified.

## 5.6. Conclusions

It has recently been demonstrated that AKG administered in the diet does not affect final body weight but can improve the daily-gain and gain:feed and improves glutamine metabolism and enhanced utilization of amino acids (He et al. 2016). In our experimental model, results

indicate that supplementation with AKG accelerates not only scale biomineralization but also stimulates cell proliferation and improves tissue elasticity and presumably formation of the structural building blocks that allow tissue recovery after injury without affecting the overall physiological status of the experimental animals. Our results suggest that in fish skin, as occurs in mammalian bone and muscle, AKG favours protein anabolism during wound healing and substantiates its use as a dietary supplement in post-surgical and post-burn conditions either in human as in animal health.

## 5.7. Supplementary material

**Supplementary table 5. 1 - Power analysis.** Table of tradeoffs given an unpaired t-test with an expected standard deviation (SD) for each group of 0.13 and a significance level (*alpha*) of 0.05 (two-tailed) performed with GraphPad StatMate version2.0a for Macintosh. The number of experimental fish was defined considering a minimum sampling size of 6 fish.

**Table of tradeoffs:**

For any combination of sample size (N) and power, this table shows the difference between means that can be detected.

| | Power | | | | |
|---|---|---|---|---|---|
| **N per group** | **99%** | **95%** | **90%** | **80%** | **50%** |
| 3 | 0.579 | 0.487 | 0.438 | 0.378 | 0.265 |
| 4 | 0.466 | 0.392 | 0.352 | 0.304 | 0.213 |
| 5 | 0.400 | 0.337 | 0.303 | 0.262 | 0.183 |
| 6 | 0.357 | **0.300** | 0.270 | 0.233 | 0.163 |
| 7 | 0.325 | 0.273 | 0.246 | 0.212 | 0.149 |
| 8 | 0.300 | 0.253 | 0.227 | 0.196 | 0.137 |
| 9 | 0.281 | 0.236 | 0.212 | 0.183 | 0.128 |
| 10 | 0.264 | 0.222 | 0.200 | 0.173 | 0.121 |
| 12 | 0.239 | 0.201 | 0.181 | 0.156 | 0.109 |
| 14 | 0.219 | 0.185 | 0.166 | 0.143 | 0.100 |
| 16 | 0.204 | 0.172 | 0.154 | 0.133 | 0.093 |
| 18 | 0.192 | 0.161 | 0.145 | 0.125 | 0.088 |
| 20 | 0.181 | 0.152 | 0.137 | 0.118 | 0.083 |
| 25 | 0.161 | 0.136 | 0.122 | 0.105 | 0.074 |

**Supplementary table 5. 2 - Biological parameters of the experimental fish.** The biological parameters of the experimental fish from both experiments is present: weight (g), standard length, total length, condition factor (*K*) and, only in experiment 2, the heart wet weight (mg).

## Experiment 1

| Experimental days | Experimental group | Fish # | Weight (g) | Standard Length | Total length | *K* |
|---|---|---|---|---|---|---|
| -4w | Control | 1 | 93 | 15,65 | 18,10 | 2,43 |
| | Control | 2 | 74 | 13,80 | 15,71 | 2,82 |
| | Control | 3 | 79 | 14,42 | 16,64 | 2,64 |
| | Control | 4 | 105 | 15,47 | 17,68 | 2,83 |
| | AKG | 5 | 80 | 14,40 | 16,98 | 2,68 |
| | AKG | 6 | 86 | 14,96 | 17,88 | 2,57 |
| | AKG | 7 | 76 | 13,68 | 16,09 | 2,97 |
| | AKG | 8 | 106 | 15,01 | 16,97 | 3,13 |
| -3w | Control | 9 | 70 | 13,93 | 16,00 | 2,59 |
| | Control | 10 | 67 | 13,60 | 15,70 | 2,67 |
| | Control | 11 | 104 | 16,12 | 18,35 | 2,48 |
| | Control | 12 | 88 | 15,28 | 17,57 | 2,47 |
| | AKG | 13 | 85 | 14,70 | 17,02 | 2,68 |
| | AKG | 14 | 95 | 15,75 | 17,93 | 2,43 |
| | AKG | 15 | 112 | 16,85 | 19,35 | 2,34 |
| | AKG | 16 | 99 | 16,69 | 18,88 | 2,13 |
| -2w | Control | 17 | 87 | 15,75 | 17,99 | 2,23 |
| | Control | 18 | 108 | 16,75 | 19,30 | 2,30 |
| | Control | 19 | 111 | 17,38 | 19,89 | 2,11 |
| | Control | 20 | 105 | 16,74 | 19,42 | 2,24 |
| | AKG | 21 | 94 | 17,29 | 19,67 | 1,82 |
| | AKG | 22 | 92 | 14,88 | 16,82 | 2,79 |
| | AKG | 23 | 60 | 15,52 | 17,65 | 1,60 |
| | AKG | 24 | 72 | 14,11 | 16,62 | 2,56 |
| -1w | Control | 25 | 89 | 15,03 | 17,30 | 2,62 |
| | Control | 26 | 66 | 13,63 | 15,81 | 2,61 |
| | Control | 27 | 89 | 15,03 | 17,34 | 2,62 |
| | Control | 28 | 110 | 16,36 | 19,08 | 2,51 |
| | AKG | 29 | 94 | 15,21 | 17,72 | 2,67 |
| | AKG | 30 | 82 | 15,03 | 17,31 | 2,41 |
| | AKG | 31 | 96 | 16,47 | 18,65 | 2,15 |
| | AKG | 32 | 70 | 14,22 | 16,34 | 2,43 |

## Experiment 2

| Experimental days | Experimental group | Fish # | Weight (g) | Standard Length | Total length | *K* | Heart wet wt (mg) |
|---|---|---|---|---|---|---|---|
| **Day 0** | Control | 33 | 75 | 15,17 | 17,33 | 2,15 | 12,8 |
| | Control | 34 | 103 | 16,86 | 19,30 | 2,15 | 15,5 |
| | Control | 35 | 92 | 16,13 | 18,02 | 2,19 | 13,8 |
| | Control | 36 | 70 | 14,50 | 16,60 | 2,30 | 11,1 |
| | Control | 37 | 89 | 16,32 | 18,28 | 2,05 | 13,6 |
| | Control | 38 | 90 | 16,66 | 19,18 | 1,95 | 10,2 |
| | AKG | 39 | 83 | 15,16 | 17,49 | 2,38 | 13,8 |
| | AKG | 40 | 90 | 16,44 | 18,69 | 2,03 | 22,3 |
| | AKG | 41 | 85 | 15,59 | 17,60 | 2,24 | 15,1 |
| | AKG | 42 | 104 | 16,47 | 18,56 | 2,33 | 21,3 |
| | AKG | 43 | 113 | 16,68 | 18,72 | 2,43 | 17,4 |
| | AKG | 44 | 97 | 15,63 | 17,60 | 2,54 | 14,8 |
| **Day 2** | Control | 45 | 67 | 15,39 | 17,19 | 1,84 | 8,4 |
| | Control | 46 | 65 | 14,23 | 16,15 | 2,26 | 11,1 |
| | Control | 47 | 92 | 15,88 | 18,23 | 2,30 | 4,2 |
| | Control | 48 | 66 | 14,96 | 16,82 | 1,97 | 9,6 |
| | Control | 49 | 84 | 15,63 | 17,52 | 2,20 | 6,4 |
| | Control | 50 | 94 | 16,04 | 18,33 | 2,28 | 10,7 |
| | AKG | 51 | 76 | 15,00 | 16,89 | 2,25 | 11,6 |
| | AKG | 52 | 64 | 13,99 | 16,30 | 2,34 | 4,5 |
| | AKG | 53 | 93 | 15,50 | 17,48 | 2,50 | 6,0 |
| | AKG | 54 | 110 | 16,80 | 18,78 | 2,32 | 15,9 |
| | AKG | 55 | 84 | 16,00 | 17,56 | 2,05 | 3,9 |
| | AKG | 56 | 97 | 16,91 | 18,71 | 2,01 | 15,5 |
| **Day 5** | Control | 57 | 89 | 15,48 | 18,09 | 2,40 | 17,8 |
| | Control | 58 | 94 | 16,62 | 18,83 | 2,05 | 20,4 |
| | Control | 59 | 103 | 17,39 | 19,14 | 1,96 | 19,9 |
| | Control | 60 | 86 | 15,93 | 17,72 | 2,13 | 12,0 |
| | Control | 61 | 89 | 16,54 | 18,37 | 1,97 | 20,2 |
| | Control | 62 | 69 | 15,20 | 17,12 | 1,96 | 5,7 |
| | AKG | 63 | 91 | 15,31 | 17,28 | 2,54 | 17,0 |
| | AKG | 64 | 100 | 16,46 | 18,62 | 2,24 | 17,1 |
| | AKG | 65 | 91 | 15,67 | 17,61 | 2,37 | 16,7 |
| | AKG | 66 | 95 | 16,60 | 18,62 | 2,08 | 13,9 |
| | AKG | 67 | 81 | 15,72 | 17,59 | 2,09 | 11,6 |
| | AKG | 68 | 92 | 16,27 | 18,38 | 2,14 | 18,0 |
| **Day 10** | Control | 69 | 81 | 15,23 | 17,06 | 2,29 | 2,3 |
| | Control | 70 | 93 | 17,01 | 19,02 | 1,89 | 8,6 |
| | Control | 71 | 96 | 16,17 | 18,25 | 2,27 | 12,6 |
| | Control | 72 | 105 | 17,28 | 19,30 | 2,04 | 16,8 |
| | Control | 73 | 107 | 18,06 | 20,17 | 1,82 | 15,2 |
| | Control | 74 | 104 | 16,97 | 19,03 | 2,13 | 10,7 |
| | AKG | 75 | 91 | 15,45 | 17,75 | 2,47 | 7,5 |
| | AKG | 76 | 70 | 14,98 | 16,81 | 2,08 | 4,6 |
| | AKG | 77 | 72 | 14,73 | 16,83 | 2,25 | 9,8 |
| | AKG | 78 | 76 | 15,91 | 18,04 | 1,89 | 3,8 |
| | AKG | 79 | 110 | 17,27 | 19,21 | 2,13 | 10,7 |
| | AKG | 80 | 68 | 15,67 | 17,71 | 1,77 | 11,1 |
| **Day 28** | Control | 81 | 110 | 17,50 | 19,26 | 2,05 | 5,0 |
| | Control | 82 | 108 | 16,61 | 18,99 | 2,36 | 10,0 |
| | Control | 83 | 66 | 14,48 | 16,58 | 2,17 | 4,2 |
| | Control | 84 | 99 | 15,03 | 17,58 | 2,92 | 9,6 |
| | Control | 85 | 118 | 16,96 | 19,47 | 2,42 | 13,0 |
| | Control | 86 | 92 | 15,53 | 17,54 | 2,46 | 5,8 |
| | AKG | 87 | 66 | 14,91 | 17,23 | 1,99 | 13,1 |
| | AKG | 88 | 118 | 17,39 | 19,79 | 2,24 | 8,4 |
| | AKG | 89 | 92 | 16,40 | 18,34 | 2,08 | 6,9 |
| | AKG | 90 | 114 | 17,15 | 19,01 | 2,26 | 6,8 |
| | AKG | 91 | 116 | 17,79 | 19,81 | 2,06 | 8,8 |
| | AKG | 92 | 94 | 16,34 | 19,05 | 2,16 | 8,7 |

**Supplementary figure 5. 1 - Diagram with the experimental design of the two experiments**. **A**: Experiment 1 – Preliminary trial on the influence of AKG treatment in the integument of sea bream. **B**: Experiment 2 – Influence of AKG treatment in sea bream skin regeneration after scale removal. Red *asterisk* indicates samplings in which the experimental animals were sacrificed. w: weeks

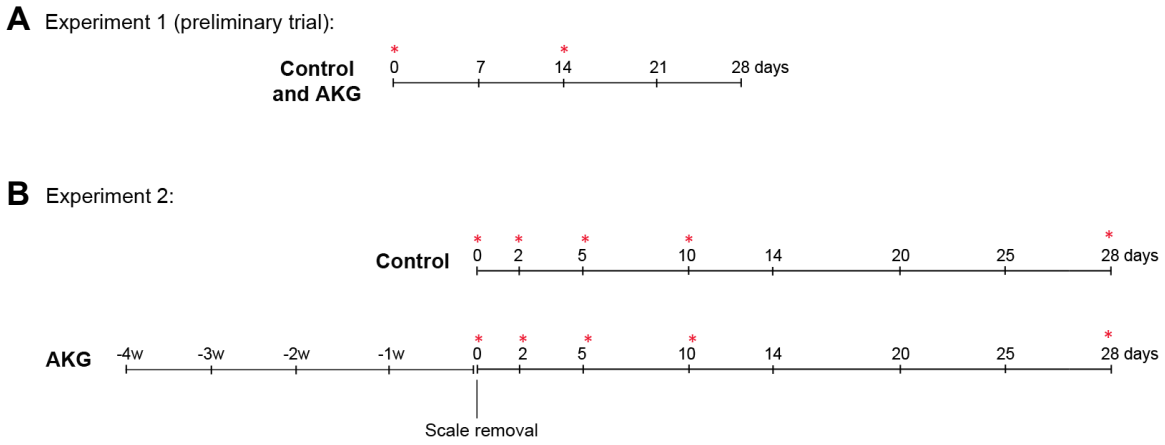

# 6

# General discussion and Future Perspectives

## 6.1. General discussion

The skin is a protective barrier and its maintenance is essential for survival so that when it is damaged it has to be rapidly repaired and in the majority of vertebrates skin repair involves the formation of a scar in the post-injured area. Although beneficial for maintaining tissue integrity, scaring often interferes with the complete recovery of injured tissues (Gowronska-Kozak et al. 2014). The process of skin repair in vertebrates is complex and involves a cascade of local and systemic responses to restore tissue integrity. Studies of skin in fish are of relevance for veterinary medicine, are essential for an important production sector, aquaculture and can also contribute as a biomedical model for regeneration. The advantages of fish skin as an experimental model is the ease of access and experimentation, the epidermis is living and not obscured by a layer of dead cornified cells, it has a high regenerative capacity, does not wrinkle or scar and physiological systems, including the immune system, tend to be less complex in fish, which facilitates interpretation of results. The overall aim of this thesis was to identify key factors involved in skin homeostasis and repair using a teleost to generate a simple comparative model for skin repair integrating metabolic, endocrine and immune considerations. The work started with the characterization of skin and scale regeneration in the sea bream and with it the

biological processes supressed during cutaneous regeneration were identified. The pattern of expression of a selection of transcripts related with ECM and matricellular proteins, proliferation, cytoskeletal remodelling, epithelial-mesenchymal interactions and the immune system revealed, using a detailed time course analysis of the cutaneous repair process in this species, which genes are involved in the early healing phase. The establishment of the histological and molecular pattern of cutaneous repair after superficial damage in sea bream then allowed the study of new genes and proteins with well described functions in repair in higher vertebrates but for which sparse information is available in teleosts, like the angiopoietin-like family and the matricellular protein osteoglycin. Also, by using the same fish to study intact and damaged skin it was possible to establish the direction of the locally inflicted injury independent of the systemic response. The results obtained provide for the first time a comprehensive description of the immune system behaviour and tissue reorganization after superficial damage in adult teleosts skin and identified and characterised key vertebrate gene families involved in tissue repair that share conserved structural and functional roles in the fish skin-scale regenerating model.

Studies of scales in fish have generally been focussed on their contribution to calcium balance and turnover and a few studies of their development and origin have been published. In the present study scale removal is placed in the context of tissue regeneration and the development of the scales is considered in a whole tissue perspective. Scale removal had not only a local but a systemic effect, reflected by the differential gene expression responses between the regenerating and intact skin of the same individual. In sea bream regenerating skin, new scales started to be deposited on the left damaged flank of fish by dermal osteoblasts from 3 days onwards and the deposited extracellular matrix started to calcify by day 4 and this pattern coincides with what has been previously reported in other teleosts (Guerreiro et al. 2013; Sire et al. 1990). New gene markers quantified in the present study may also be related to scale formation and growth, like collagen type X (*colXα1*) and cartilage acidic protein 2 (*crtac2*) and the study of these genes in sea bream wound repair should be further analysed in the future. The use of the same individual to study intact and regenerating skin overcome the problem of individual variation and offered the opportunity to compare samples with an identical genomic background. The changes in gene expression detected in the intact skin were triggered by the damaged inflicted on the other flank (regenerating flank) of the fish and represent the systemic consequence of a locally inflicted damage. The combination of both effects (local and systemic) eventually culminates with skin and scale recovery to the ontogenic shape and size

A baseline comparison of intact and regenerating sea bream skin and scales was studied. The logical connection between gene function and expression and changes in expression caused by a biotic or abiotic factors is a powerful tool to infer function and this approach has been used to gain insight into the wound repair process (Li et al. 2001). Most teleosts loose some of their scales at least once during their lifetime (Bereiter-Hahn an Zylberberg 1993) and when scales are lost, the epidermis is also lost and the superficial dermis and scale pocket are directly exposed to the aquatic environment (Guerreiro et al. 2013; Vieira et al. 2011; Quilhac and Sire 1999). Loss of scales creates a failure in a key barrier of the innate immune system and wounds caused by scale loss are rapidly repaired and re-epithelialization from the wound margins is triggered (Quilhac and Sire 1999; Iger and Abraham 1990). In the regenerating skin of sea bream, re-establishment of the physical barrier occurred in the first two days when an increase of epidermis thickness and basement membrane and an increase of the number of blood vessels were observed. The recovery of the epidermal coverage occurred in 2 days and was accompanied by an increase in the thickness of the epidermis (figure 2.3, 2.4, 3.6 and 3.7) and increased proliferation (*pcna*) and cytoskeletal remodelling (*krt2*) (figure 2.6 and supplementary figure 2.3) and is in accordance with the previous studies in teleosts and tetrapods.

The formation of new blood vessels (vascularization) is critical to the initial stages of wound healing in all vertebrates and the process of sea bream skin vascularization was briefly characterized in the present study (chapters 2 and 3). At the transcripts level, the down-regulation of vascular endothelial growth-factor A-like (SAPD14109, log-fold = -1.943; supplementary table 2.1) in sea bream skin 3 days after scale removal combined with the pattern of expression of the angiogenic factors *cyr61* (figure 2.5 and supplementary figure 2.2) and *vegfab* (figure 3.9), genes that were down-regulated during the early stages of skin repair, uncover the process of vascularization in sea bream cutaneous wounding revealing that it is supressed in the early stages of repair. However, at the morphological level, an increase in the number of blood vessels were observed in the regenerating dermis from 6h onwards (figure 3.8), earlier than previously described in the zebrafish (Richardson et al. 2013) and much earlier than in mammals, where the formation of new blood vessels initiates 3 days after wounding (Olczyk et al. 2014).

Several members of the angiopoietin-like family, which regulate a plethora of physiological and pathophysiological processes in mammals and in the skin are involved in

tissue repair and proliferation (Santulli 2014) are also expressed in the skin of sea bream. The involvement of the human orthologue of *ANGPTL2* had previously been demonstrated in fin repair in zebrafish (Kubota et al. 2005a) and the present study now identified more members of the same family with putative roles in tissue re-epithelialization and angiogenesis during regeneration processes in teleosts. The expression of *angptl1b* and *angptl2b* were increased in the regenerating sea bream skin relative to intact skin in the first 48h post-wounding but *angptl7* was significantly down-regulated relative to intact skin. The results suggest that in teleosts Angptls maintained their conserved role in the regulation of skin healing and epidermis matrix structure and that their members, like in mammals, seem to contribute differently during skin healing process.

In the present study the involvement of the matricellular protein osteoglycin in cutaneous repair was demonstrated for the first time. Osteoglycin is duplicated in teleosts and both *ogn1* and *ogn2* are involved in late-phase damage repair, and not in the early stages of repair, of sea bream skin. Additionally, their up-regulation is induced with selected culture medias in primary cell cultures of bone and muscle but not in the early phases of wound healing in sea bream after scale removal. In the latter, a down-regulation of ogns occurs initially in both intact and regenerating skin (figure 4.6 and 4.7), when re-epithelialization and scale patterning are defined and the barrier function that protects the animals from the external environment is re-established, and are only up-regulated (figure 4.10) when the skin tissue enters the remodelling phase and its topological structures (the scales) matures by increasing in thickness during the phase of collagen fibre deposition and mineralization.

The expression pattern of the collagens during sea bream skin healing after scale removal is similar to the one observed during wound healing in the nude mice (*FOXN1*-deficient), where the injury caused an immediate decline in collagen skin tissue content that was later recovered and stabilized 21 days after injury (Gawronska-Kozak 2011). Considering that the regenerative processes are associated with the slow deposition and progressive remodelling of collagen and that the present study in the skin of sea beam indicated a progressive deposition and remodelling of collagens may partially explain the teleosts ability to regenerate wounded skin and reinforces the use of teleosts has an important experimental animal in the field of regenerative medicine in the since that they can contribute with relevant information on the pathways that lead to scar-free healing. The comparative model of skin regeneration used in the present study provided new insights into functionality in relation to the

matrix, lack of wrinkles and scaring and are relevant from a biomedical perspective and also from a cosmetic perspective.

Components of the innate (*mpo*, *cyba*, *csf1r*) and acquired (*cd48*, *cd200*) immune system are supressed during the early stages of sea bream skin regeneration after superficial damage and only after the epidermal coverage is re-established and dermal reorganization has started are they progressively re-established to assure immune surveillance. The inflammatory signals of TGFß and FGFR1 are necessary for fibroblasts recruitment, granular tissue formation and vascularization and play a significant role in each of the healing process (Olczyk et al. 2014; Richardson et al. 2013). Though these molecules were not quantified in the present study, there is an indication that TGFß is supressed in the regenerating and intact sea bream cutaneous repair after scale removal (Mateus, *unpublished results*). Overall, the results of the study are in line with the active role of the skin in protection against pathogens and indicates that suppression of immune function appears to be an essential facet of tissue repair in teleosts.

The present study also provides new insights into the metabolic effect of AKG in teleosts. Based on the current knowledge about the biological effects of AKG supplementation and based on a preliminary study in sea bream (Costa 2009), it was initially hypothesized that the dietary supplementation of AKG, acting through its stimulatory effect on collagen synthesis, would modify skin properties and improve scale regeneration in sea bream. The use of the comparative skin regeneration model revealed that dietary AKG stimulated scales biomineralization, reflected by the increased activity of the enzymes TRAP and ALP in the early stages of repair (first 5 days) and accelerated growth of the treated scales from the regenerating flank of the experimental animals. Dietary AKG also stimulated epidermal cell proliferation which suggest that it has a determinant role in fish skin homeostasis and supports the idea that in teleosts skin AKG supplementation accelerates tissue re-epithelialization after injury as occurs in human skin.

The control of collagen metabolism could potentially be very useful in a variety of therapeutic and cosmetic applications since it has been demonstrated that the long-term topical application of alpha-ketoglutarate on the skin of hairless mice for twelve weeks (three times a week) stimulates procollagen production and decreases UVB-induced wrinkle formation (Son et al. 2007). Also, the process of ageing is associated with changes in skeletal, muscular, gastrointestinal, neural hormonal and metabolic processes that seriously affect an individual`s

performance and quality of life. Within an age range of 40-80 years, concentrations of AKG in the blood decrease by as much as 10-fold from mg/ml level to just a few ng/ml, making this a very realistic clinical parameter for use as an index of ageing (Harrison and Pierzynowski 2008).

## 6.2. Future perspectives

To complement the results from these studies on skin regeneration in teleosts, it would be necessary, in the near future, to clarify the role of the quantified angiogenic factors (*cyr61* and *vegfab*), of the angiopoietin-like family members with modified expression during sea bream skin regeneration (*angptl1a*, *angptl2b* and *angptl7*) and of the matricellular proteins *ogn1* and *ogn2* using immunolocalization techniques, such as *in situ* hybridization or immunohistochemistry with specific antibodies, in order to identify which cells are producing the proteins and where is it accumulated so that their relative importance in the remodelling of the fish skin vasculature and matrix proteins during the initial stages of tissue recovery can be clarified. The integration of these analyses would then facilitate the study of the endocrine factors in the regeneration of the skin.

The effect of AKG supplementation deserves further attention in the future. Mapping the proteome of the intact and regenerating sea bream skin treated with AKG through two-dimensional gel electrophoresis (2D-electrophoresis) would allow the identification of the proteins that are most affected by the treatment. The quantification of the enzyme prolyl-4-hydroxylase (*P4H*) in the RNA extracts and the level of hydroxyproline in the protein extracts would help to better characterize the effect of AKG in collagen synthesis in teleosts. It would also be of interest to establish the mineral content of the scales from fish given AKG and establish how it brings about its action to influence scale growth.

# 7

# References

**Abascal, F., Zardoya, R. and Posada, D.** (2005) ProtTest: selection of best-fit models of protein evolution. *Bioinformatics* 21, 2104-5

**Abascal, F., Zardoya, R. and Telford, M. J.** (2010) TranslatorX: multiple alignment of nucleotide sequences guided by amino acid translations. *Nucleic Acids Research* 38, W7-W13

**Abramoff, M., Magalhães, P. and Ram, S.** (2004) Image processing with ImageJ. *Biophotonics International* 11, 36-42

**Ameye, L. and Young, M. F.** (2002) Mice deficient in small leucine-rich proteoglycans: novel in vivo models for osteoporosis, osteoarthritis, Ehlers-Danlos syndrome, muscular dystrophy, and corneal diseases. *Glycobiology* 12, 107R-116R

**Anjos, L., Gomes, A. S., Melo, E. P., Canario, A. V. and Power, D. M.** (2013) Cartilage Acidic Protein 2 a hyperthermostable, high affinity calcium-binding protein. *Biochim Biophys Acta* 1834, 642-50

**Armstrong, A. W., Wu, J., Johnson, M. A., Grapov, D., Azizi, B., Dhillon, J. and Fiehn, O.** (2014) Metabolomics in psoriatic disease: pilot study reveals metabolite differences in psoriasis and psoriatic arthritis. *F1000Res* 3, 248

**Bahary, N., Goishi, K., Stuckenholz, C., Weber, G., Leblanc, J., Schafer, C. A., Berman, S. S., Klagsbrun, M. and Zon, L. I.** (2007) Duplicate VegfA genes and orthologues of the KDR receptor tyrosine kinase family mediate vascular development in the zebrafish. *Blood* 110, 3627-36

**Bangert, C., Brunner, P. M. and Stingl, G.** (2011) Immune functions of the skin. *Clin Dermatol* 29, 360-76

**Barton, B. A.** (2002) Stress in fishes: a diversity of responses with particular reference to changes in circulating corticosteroids. *Integr Comp Biol* 42, 517-25

**Bentley, P.** (1998). Hormones and the Integument. In *Comparative Vertebrate Endocrinology*, pp. 303-335: Cambridge University Press.

**Bentz, H., Nathan, R. M., Rosen, D. M., Armstrong, R. M., Thompson, A. Y., Segarini, P. R., Mathews, M. C., Dasch, J. R., Piez, K. A. and Seyedin, S. M.** (1989) Purification and characterization of a unique osteoinductive factor from bovine bone. *J Biol Chem* 264, 20805-10

**Bereiter-Hahn, J. and Zylberberg, L.** (1993) Regeneration of Teleost Fish Scales. *Comparative Biochemistry and Physiology* 105A, 625-641

**Berg, A.** (1968) Studies on the metabolism of calcium and strontium in freshwater fish. I. Relative contribution of direct and intestinal absorption. *Memorie dell'Istituto Italiano di Idrobiologia* 23, 161-196

**Bienko, M., Radzki, R. P., Puzio, I., Filip, R., Pierzynowski, S. G. and Studzinski, T.** (2002) The influence of alpha-ketoglutarate (AKG) on mineralization of femur in rats with established osteopenia. . *Acta Orthopaedica Scandinavica* 73, 52

**Birk, D. E.** (2001) Type V collagen: heterotypic type I/V collagen interactions in the regulation of fibril assembly. *Micron* 32, 223-37

**Blom, N., Sicheritz-Ponten, T., Gupta, R., Gammeltoft, S. and Brunak, S.** (2004) Prediction of post-translational glycosylation and phosphorylation of proteins from the amino acid sequence. *Proteomics* 4, 1633-49

**Bornstein, P. and Sage, E. H.** (2002) Matricellular proteins: extracellular modulators of cell function. *Curr Opin Cell Biol* 14, 608-16

**Bosman, F. T. and Stamenkovic, I.** (2003) Functional structure and composition of the extracellular matrix. *Journal of Pathology* 200, 423-428

**Bowden, P. E., Quinlan, R. A., Breitkreutz, D. and Fusenig, N. E.** (1984) Proteolytic modification of acidic and basic keratins during terminal differentiation of mouse and human epidermis. *Eur J Biochem* 142, 29-36

**Bragulla, H. H. and Homberger, D. G.** (2009) Structure and functions of keratin proteins in simple, stratified, keratinized and cornified epithelia. *J Anat* 214, 516-59

**Braiman-Wiksman, L., Solomonik, I., Spira, R. and Tennenbaum, T.** (2007) Novel insights into wound healing sequence of events. *Toxicol Pathol* 35, 767-79

**Bricard, Y., Ralliere, C., Lebret, V., Lefevre, F. and Rescan, P. Y.** (2014) Early fish myoseptal cells: insights from the trout and relationships with amniote axial tenocytes. *PloS One* 9, e91876

**Brindle, N. P. J., Saharinen, P. and Alitalo, K.** (2006) Signaling and functions of angiopoietin-1 in vascular protection. *Circ Res* 98, 1014-1023

**Brockes, J. P. and Kumar, A.** (2005) Appendage regeneration in adult vertebrates and implications for regenerative medicine. *Science* 310, 1919-23

**Brunet, F. G., Roest Crollius, H., Paris, M., Aury, J. M., Gibert, P., Jaillon, O., Laudet, V. and Robinson-Rechavi, M.** (2006) Gene loss and evolutionary rates following whole-genome duplication in teleost fishes. *Mol Biol Evol* 23, 1808-16

**Buchanan, S. G. S. and Gay, N. J.** (1996) Structural and functional diversity in the leucine rich repeat family of proteins. *Progress in Biophysics & Molecular Biology* 65, 1-44

**Busam, K. J.** (2010). Dermatophatology: Saunders Elsevier.

**Cao, H. M., Ye, X. P., Ma, J. H., Jiang, H., Li, S. X., Li, R. Y., Li, X. S., Guo, C. C., Wang, Z. Q., Zhan, M. et al.** (2015) Mimecan, a Hormone Abundantly Expressed in Adipose Tissue, Reduced Food Intake Independently of Leptin Signaling. *Ebiomedicine* 2, 1718-1724

**Capilla, E., Teles-Garcia, A., Acerete, L., Navarro, I. and Gutierrez, J.** (2011) Insulin and IGF-I effects on the proliferation of an osteoblast primary culture from sea bream (Sparus aurata). *Gen Comp Endocrinol* 172, 107-14

**Castillo-Briceno, P., Sepulcre, M. P., Chaves-Pozo, E., Meseguer, J., Garcia-Ayala, A. and Mulero, V.** (2009) Collagen regulates the activation of professional phagocytes of the teleost fish gilthead seabream. *Mol Immunol* 46, 1409-15

**Ceroni, A., Passerini, A., Vullo, A. and Frasconi, P.** (2006) DISULFIND: a disulfide bonding state and cysteine connectivity prediction server. *Nucleic Acids Res* 34, W177-81

**Cerutti, A. and Rescigno, M.** (2008) The biology of intestinal immunoglobulin A responses. *Immunity* 28, 740-50

**Chan, X. C. Y., McDermott, J. C. and Siu, K. W. M.** (2007) Identification of secreted proteins during skeletal muscle development. *Journal of Proteome Research* 6, 698-710

**Chang, W. C., Lee, T. Y., Shien, D. M., Hsu, J. B., Horng, J. T., Hsu, P. C., Wang, T. Y., Huang, H. D. and Pan, R. L.** (2009) Incorporating support vector machine for identifying protein tyrosine sulfation sites. *J Comput Chem* 30, 2526-37

**Chen, C. C., Mo, F. E. and Lau, L. F.** (2001) The angiogenic factor Cyr61 activates a genetic program for wound healing in human skin fibroblasts. *J Biol Chem* 276, 47329-37

**Chernova, O.** (2009) Skin Derivatives in Vertebrate Ontogeny and Phylogeny. *Biology Bulletin* 36, 175-183

**Christian, L. M., Graham, J. E., Padgett, D. A., Glaser, R. and Kiecolt-Glaser, J. K.** (2006) Stress and wound healing. *Neuroimmunomodulation* 13, 337-46

**Colgravea, M. L., Allinghama, P. G. and Jones, A.** (2008) Hydroxyproline quantification for the estimation of collagen in tissue using multiple reaction monitoring mass spectrometry. *Journal of Chromatography A* 1212, 150-153

**Comes, N., Buie, L. K. and Borrás, T.** (2011) Evidence for a role of angiopoietin-like 7 (ANGPTL7) in extracellular matrix formation of the human trabecular meshwork: implications for glaucoma. *Genes to Cells* 16, 243-259

**Conant, G. C. and Wolfe, K. H.** (2008) Probabilistic cross-species inference of orthologous genomic regions created by whole-genome duplication in yeast. *Genetics* 179, 1681-92

**Conesa, A., Gotz, S., Garcia-Gomez, J. M., Terol, J., Talon, M. and Robles, M.** (2005) Blast2GO: a universal tool for annotation, visualization and analysis in functional genomics research. *Bioinformatics* 21, 3674-6

**Corpuz, L. M., Funderburgh, J. L., Funderburgh, M. L., Bottomley, G. S., Prakash, S. and Conrad, G. W.** (1996) Molecular cloning and tissue distribution of keratocan. Bovine corneal keratan sulfate proteoglycan 37A. *J Biol Chem* 271, 9759-63

**Costa, R. A.** (2009). The effect of alpha-ketoglutarate on a piscine skin model: a molecular and morphological study. In *Department of Biomedical Sciences and Medicine*, vol. MSc. Portugal: University of Algarve.

**Coulombe, P. A. and Wong, P.** (2004) Cytoplasmic intermediate filaments revealed as dynamic and multipurpose scaffolds. *Nat Cell Biol* 6, 699-706

**Cour, T. l., Kiemer, L., Molgaard, A., Gupta, R., Skriver, K. and Brunak, S.** (2004) Analysis and prediction of leucine-rich nuclear export signals. *Protein Eng Des Sel* 17, 527-36

**Cowin, A. J., Brosnan, M. P., Holmes, T. M. and Ferguson, M. W.** (1998) Endogenous inflammatory response to dermal wound healing in the fetal and adult mouse. *Dev Dyn* 212, 385-93

**Cui, C.-Y. and Schlessinger, D.** (2006) EDA Signaling and Skin Appendage Development. *Cell Cycle* 5, 2477-2483

**Cuttle, L., Nataatmadja, M., Fraser, J. F., Kempf, M., Kimble, R. M. and Hayes, M. T.** (2005) Collagen in the scarless fetal skin wound: detection with picrosirius-polarization. *Wound Repair Regen* 13, 198-204

**Dabek, M., Kruszewska, D., Filip, R., Hotowy, A., Pierzynowski, L., Wojtasz-Pajak, A., Szymanczyk, S., Valverde Piedra, J. L., Werpachowska, E. and Pierzynowski, S. G.** (2005) alpha-Ketoglutarate (AKG) absorption from pig intestine and plasma pharmacokinetics. *J Anim Physiol Anim Nutr (Berl)* 89, 419-26

**Dang, C. M., Beanes, S. R., Lee, H., Zhang, X., Soo, C. and Ting, K.** (2003) Scarless fetal wounds are associated with an increased matrix metalloproteinase-to-tissue-derived inhibitor of metalloproteinase ratio. *Plast Reconstr Surg* 111, 2273-85

**de Vrieze, E., Sharif, F., Metz, J. R., Flik, G. and Richardson, M. K.** (2011) Matrix metalloproteinases in osteoclasts of ontogenetic and regenerating zebrafish scales. *Bone* 48, 704-12

**Dehal, P. and Boore, J. L.** (2005) Two rounds of whole genome duplication in the ancestral vertebrate. *PLoS Biol* 3, e314

**Deng, M., Lu, Z. G., Zheng, J. K., Wan, X., Chen, X. L., Hirayasu, K., Sun, H. Z., Lam, Y., Chen, L. P., Wang, Q. H. et al.** (2014) A motif in LILRB2 critical for Angptl2 binding and activation. *Blood* 124, 924-935

**Ding, L., Kuhne, W. W., Hinton, D. E., Song, J. and Dynan, W. S.** (2010) Quantifiable Biomarkers of Normal Aging in the Japanese Medaka Fish (*Oryzias latipes*). *PloS One* 5

**Doolitlle, R. F., McNamara, K. and Lin, K.** (2012) Correlating structure and function during evolution of fibrinogen-related domains. *The Protein Society* 21, 1808-1823

**Elliot, D. G.** (2011a). Functional Morphology of the Integumentary System in Fishes. In *Encyclopedia of Fish Physiology: From Genome to Environment*, vol. 1 (ed. F. A.P.), pp. 476-488. San Diego Academic Press: Elsevier.

**Elliot, D. G.** (2011b). The many functions of fish integument. In *Encyclopedia of Fish Physiology: From Genome to Environment*, (ed. A. Farrel), pp. 471-475. San Diego Academic Press: Elsevier.

**Eming, S. A., Hammerschmidt, M., Krieg, T. and Roers, A.** (2009) Interrelation of immunity and tissue repair or regeneration. *Semin Cell Dev Biol* 20, 517-27

**Esteban, M. Á.** (2012) An Overview of the Immunological Defenses in Fish Skin. *ISRN Immunology*

**Esteban, M. Á. and Cerezuela, R.** (2015). Fish mucosal immunity: skin. In *Mucosal Health in Aquaculture*, pp. 67-92: Elsevier.

**Estêvão, M. D., Silva, N., Redruello, B., Costa, R., Gregório, S., Canário, A. V. M. and Power, D. M.** (2011) Cellular morphology and markers of cartilage and bone in the marine teleost *Sparus auratus*. *Cell & Tissue Research* 343, 619-635

**Fagiani, E. and Christofori, G.** (2013) Angiopoietins in angiogenesis. *Cancer Lett* 328, 18-26

**Fast, M. D., Sims, D. E., Burka, J. F., Mustafa, A. and Ross, N. W.** (2002) Skin morphology and humoral non-specific defence parameters of mucus and plasma in rainbow trout, coho and Atlantic salmon. *Comp Biochem Physiol A Mol Integr Physiol* 132, 645-57

**Fernandez, B., Kampmann, A., Pipp, F., Zimmermann, R. and Schaper, W.** (2003) Osteoglycin expression and localization in rabbit tissues and atherosclerotic plaques. *Molecular and Cellular Biochemistry* 246, 3-11

**Flik, G., Fenwick, J. C., Kolar, Z., Mayer-Gostan, N. and Bonga, S. E. W.** (1986) Effects of low ambient calcium levels on whole-body Ca2+ flux rates and internal calcium pools in the freshwater cichlid teleost, *Oreochromis mossambicus*. *J. Exp. Biol.* 120, 249-264

**Force, A., Lynch, M. and Postlethwait, J.** (1999) Preservation of duplicate genes by subfunctionalization. *American Zoologist* 39, 78A-78A

**Fu, Z., Yao, F., Abou-Samra, A. B. and Zhang, R.** (2013) Lipasin, thermoregulated in brown fat, is a novel but atypical member of the angiopoietin-like protein family. *Biochem Biophys Res Commun* 430, 1126-31

**Fuchs, E.** (1983) Evolution and complexity of the genes encoding the keratins of human epidermal cells. *J Invest Dermatol* 81, 141s-4s

**Funderburgh, J. L., Corpuz, L. M., Roth, M. R., Funderburgh, M. L., Tasheva, E. S. and Conrad, G. W.** (1997) Mimecan, the 25-kDa corneal keratan sulfate proteoglycan, is a product of the gene producing osteoglycin. *J Biol Chem* 272, 28089-95

**Gabriel, C., Peyman, A. and Grant, E. H.** (2009) Electrical conductivity of tissue at frequencies below 1 MHz. *Phys Med Biol* 54, 4863-78

**Gallardo, M. A., Sala-Rabanal, M., Ibarz, A., Padrós, F., Blasco, J., Fernández, J. and Sánchez, J.** (2003) Functional alterations associated with the 'winter syndrome' in gilthead sea bream (*Sparus aurata*). *Aquaculture* 223, 15-27

**Garcia de la serrana, D., Vieira, V. L., Andree, K. B., Darias, M., Estevez, A., Gisbert, E. and Johnston, I. A.** (2012) Development temperature has persistent effects on muscle growth responses in gilthead sea bream. *PloS One* 7, e51884

**Gasteiger E, Hoogland C, Gattiker A, Duvaud S, Wilkins MR, Appel RD and A, B.** (2005). Protein Identification and Analysis Tools on the ExPASy Server. In *The Proteomics Protocols Handbook*, (ed. J. M. Walker), pp. 571-607: Humana Press.

**Gawronska-Kozak, B.** (2011) Scarless skin wound healing in FOXN1 deficient (nude) mice is associated with distinctive matrix metalloproteinase expression. *Matrix Biol* 30, 290-300

**Gawronska-Kozak, B., Grabowska, A., Kopcewicz, M. and Kur, A.** (2014) Animal models of skin regeneration. *Reprod Biol* 14, 61-7

**Ge, G. X., Seo, N. S., Liang, X. W., Hopkins, D. R., Hook, M. and Greenspan, D. S.** (2004) Bone morphogenetic protein-1/Tolloid-related metalloproteinases process osteoglycin and enhance its ability to regulate collagen fibrillogenesis. *Journal of Biological Chemistry* 279, 41626-41633

**Gilkes, D. M., Chaturvedi, P., Bajpai, S., Wong, C. C., Wei, H., Pitcairn, S., Hubbi, M. E., Wirtz, D. and Semenza, G. L.** (2013) Collagen prolyl hydroxylases are essential for breast cancer metastasis. *Cancer Res* 73, 3285-96

**Gill, S. E. and Parks, W. C.** (2008) Metalloproteinases and their inhibitors: regulators of wound healing. *Int J Biochem Cell Biol* 40, 1334-47

**Gilliver, S. C., Ashworth, J. J. and Ashcroft, G. S.** (2007) The hormonal regulation of cutaneous wound healing. *Clinics in Dermatology* 25, 56-62

**Glasauer, S. M. and Neuhauss, S. C.** (2014) Whole-genome duplication in teleost fishes and its evolutionary consequences. *Molecular Genetics and Genomics* 289, 1045-60

**Godwin, J., Kuraitis, D. and Rosenthal, N.** (2014) Extracellular matrix considerations for scar-free repair and regeneration: insights from regenerative diversity among vertebrates. *Int J Biochem Cell Biol* 56, 47-55

**Godwin, J. W. and Rosenthal, N.** (2014) Scar-free wound healing and regeneration in amphibians: immunological influences on regenerative success. *Differentiation* 87, 66-75

**Goh, Y. Y., Pal, M., Chong, H. C., Zhu, P., Tan, M. J., Punugu, L., Lam, C. R., Yau, Y. H., Tan, C. K., Huang, R. L. et al.** (2010a) Angiopoietin-like 4 interacts with integrins beta1 and beta5 to modulate keratinocyte migration. *Am J Pathol* 177, 2791-803

**Goh, Y. Y., Pal, M., Chong, H. C., Zhu, P., Tan, M. J., Punugu, L., Tan, C. K., Huang, R. L., Sze, S. K., Tang, M. B. et al.** (2010b) Angiopoietin-like 4 interacts with matrix proteins to modulate wound healing. *J Biol Chem* 285, 32999-3009

**Gomez, D., Sunyer, J. O. and Salinas, I.** (2013) The mucosal immune system of fish: the evolution of tolerating commensals while fighting pathogens. *Fish Shellfish Immunol* 35, 1729-39

**Gorczynski, R. M., Chen, Z., Shivagnahnam, S., Taseva, A., Wong, K., Yu, K. and Khatri, I.** (2010) Potent immunosuppression by a bivalent molecule binding to CD200R and TGF-betaR. *Transplantation* 90, 150-9

**Grayfer, L., Hodgkinson, J. W. and Belosevic, M.** (2011) Analysis of the antimicrobial responses of primary phagocytes of the goldfish (Carassius auratus L.) against Mycobacterium marinum. *Dev Comp Immunol* 35, 1146-58

**Gu, L. H. and Coulombe, P. A.** (2007) Keratin function in skin epithelia: a broadening palette with surprising shades. *Curr Opin Cell Biol* 19, 13-23

**Guellec, D. L. and Zylberberg, L.** (1998) Expression of Type I and Type V Collagen mRNAs in the Elasmoid Scales of a Teleost Fish as Revealed by In Situ Hybridization. *Connective Tissue Research* 39, 257-267

**Guerra, R. R., Santos, N. P., Cecarelli, P., Silva, J. R. M. C. and Hernandez-Blazquez, F. J.** (2008) Healing of skin wounds in the African catfish Clarias gariepinus. *Journal of Fish Biology* 73, 572-583

**Guerreiro, P. M., Costa, R. and Power, D. M.** (2013) Dynamics of scale regeneration in seawater- and brackish water-acclimated sea bass, Dicentrarchus labrax. *Fish Physiol Biochem* 39, 917-30

**Guindon, S., Dufayard, J. F., Lefort, V., Anisimova, M., Hordijk, W. and Gascuel, O.** (2010) New algorithms and methods to estimate maximum-likelihood phylogenies: assessing the performance of PhyML 3.0. *Syst Biol* 59, 307-21

**Gupta, R. and Brunak, S.** (2002) Prediction of glycosylation across the human proteome and the correlation to protein function. *Pac Symp Biocomput*, 310-22

**Gurtner, G. C., Werner, S., Barrandon, Y. and Longaker, M. T.** (2008) Wound repair and regeneration. *Nature* 453, 314-21

**Hammarqvist, F., Wernerman, J., von der Decken, A. and Vinnars, E.** (1991) Alpha-ketoglutarate preserves protein synthesis and free glutamine in skeletal muscle after surgery. *Surgery* 109, 28-36

**Harris, M. P., Rohner, N., Schwarz, H., Perathoner, S., Konstantinidis, P. and Nusslein-Volhard, C.** (2008) Zebrafish eda and edar mutants reveal conserved and ancestral roles of ectodysplasin signaling in vertebrates. *PLoS Genet* 4, e1000206

**Harrison, A., Pawlowska, M., Bartels, E. M., Piedra, J. L. V., Skrzypek, H. and Pierzynowski, S.** (2011) The effects of oral administration of alpha ketoglutarate on stomach-by-pass induced arterial stiffness in rats. *International Journal of Nephrology and Renovascular Disease* 3, 73-84

**Harrison, A. P., Brüggemann, D., Bartels, E. M., Andrea, K. and Pierzynowski, S.** (2009) Healthy ageing: the beneficial effect of dietary supplementation with alpha-ketoglutarate on arterial elasticity in elderly mice. *Journal of Pre-Clinical and Clinical Research* 3, 024-030

**Harrison, A. P. and Pierzynowski, S. G.** (2008) Biological effects of 2-oxoglutarate with particular emphasis on the regulation of protein, mineral and lipid absorption/metabolism, muscle performance, kidney function, bone formation and cancerogenesis, all viewed from a healthy ageing perspective state of the art - review article. *Journal of Physiology and Pharmacology* 59, 91-106

**Harrison, A. P., Tygesen, M. P., Sawa-Wojtanowicz, B., Husted, S. and Tatara, M. R.** (2004) α-Ketoglutarate treatment early in postnatal life improves bone density in lambs at slaughter. *Bone* 35, 204-209

**Hato, T., Tabata, M. and Oike, Y.** (2008) The Role of Angiopoietin-Like Proteins in Angiogenesis and Metabolism. *Trends in Cardiovascular Maedicine* 18, 6-14

**Haywood, M. T.** (2011) Prolidase Deficiency: A child with persistent lower extremity ulcerations. *The Foot and Ankle Online Journal* 4, 4

**He, L., Li, H., Huang, N., Tian, J., Liu, Z., Zhou, X., Yao, K., Li, T. and Yin, Y.** (2016) Effects of Alpha-Ketoglutarate on Glutamine Metabolism in Piglet Enterocytes in Vivo and in Vitro. *J Agric Food Chem* 64, 2668-73

**Heino, J., Huhtala, M., Kapyla, J. and Johnson, M. S.** (2009) Evolution of collagen-based adhesion systems. *Int J Biochem Cell Biol* 41, 341-8

**Henry, S. P., Takanosu, M., Boyd, T. C., Mayne, P. M., Eberspaecher, H., Zhou, W., de Crombrugghe, B., Hook, M. and Mayne, R.** (2001) Expression pattern and gene characterization of asporin. a newly discovered member of the leucine-rich repeat protein family. *J Biol Chem* 276, 12212-21

**Hildebrand, M.** (1974). Early Development and Integument. In *Analysis of Vertebrate Structure*, (ed. W. International), pp. 85-112. United States of America: John Wiley & Sons.

**Hu, S. M., Li, F., Yu, H. M., Li, R. Y., Ma, Q. Y., Ye, T. J., Lu, Z. Y., Chen, J. L. and Song, H. D.** (2005) The mimecan gene expressed in human pituitary and regulated by pituitary transcription factor-1 as a marker for diagnosing pituitary tumors. *Journal of Clinical Endocrinology & Metabolism* 90, 6657-6664

**Huang da, W., Sherman, B. T. and Lempicki, R. A.** (2009a) Bioinformatics enrichment tools: paths toward the comprehensive functional analysis of large gene lists. *Nucleic Acids Res* 37, 1-13

**Huang da, W., Sherman, B. T. and Lempicki, R. A.** (2009b) Systematic and integrative analysis of large gene lists using DAVID bioinformatics resources. *Nat Protoc* 4, 44-57

**Hughes, A. L.** (2002) Adaptive evolution after gene duplication. *Trends Genet* 18, 433-4

**Hutton, J. J., Trappel, A. and Udenfriend, S.** (1966) Requirements for alpha-ketoglutarate, ferrous ion and ascorbate by collagen proline hydroxylase. *Biochemical and Biophysical Research Communications* 24, 179-84

**Huxley-Jones, J., Robertson, D. L. and Boot-Handford, R. P.** (2007) On the origins of the extracellular matrix in vertebrates. *Matrix Biology* 26, 2-11

**Hyman, L. H.** (1956). VI: The comparative anatomy of the skin and exoskeleton. In *Comparative Vertebrate Anatomy*, pp. 79-98. Chicago, Illinois, USA: The University of Chicago Press.

**Ibarz, A., Costa, R., Harrison, A. P. and Power, D. M.** (2010) Dietary keto-acid feed-back on pituitary activity in gilthead sea bream: Effects of oral doses of AKG. A proteomic approach. *General and Comparative Endocrinology* 169, 284-292

**Ibarz, A., Pinto, P. I. and Power, D. M.** (2013) Proteomic Approach to Skin Regeneration in a Marine Teleost: Modulation by Oestradiol-17beta. *Mar Biotechnol (NY)*

**Icardo, J. M.** (2012). The Teleost Heart: A Morpholical Approach. In *Ontogeny and Phylogeny of the Vertebrate Heart*, eds. D. Sedmera and T. Wang), pp. 35-53: Springer.

**Iger, Y. and Abraham, M.** (1990) The process of skin healing in experimentally wounded carp. *Journal of Fish Biology* 36, 421-437

**Infante, C., Manchado, M., Asensio, E. and Canavate, J. P.** (2007) Molecular characterization, gene expression and dependence on thyroid hormones of two type I keratin genes (sseKer1 and sseKer2) in the flatfish Senegalese sole (Solea senegalensis Kaup). *BMC Dev Biol* 7, 118

**Insenser, M., Montes-Nieto, R., Vilarrasa, N., Lecube, A., Simo, R., Vendrell, J. and Escobar-Morreale, H. F.** (2012) A nontargeted proteomic approach to the study of visceral and subcutaneous adipose tissue in human obesity. *Molecular and Cellular Endocrinology* 363, 10-19

**Iozzo, R. V.** (1997) The family of the small leucine-rich proteoglycans: Key regulators of matrix assembly and cellular growth. *Critical Reviews in Biochemistry and Molecular Biology* 32, 141-174

**Iozzo, R. V.** (1999) The biology of the small leucine-rich proteoglycans - Functional network of interactive proteins. *Journal of Biological Chemistry* 274, 18843-18846

**Iozzo, R. V. and Murdoch, A. D.** (1996) Proteoglycans of the extracellular environment: Clues from the gene and protein side offer novel perspectives in molecular diversity and function. *Faseb Journal* 10, 598-614

**Iozzo, R. V. and Schaefer, L.** (2010) Proteoglycans in health and disease: novel regulatory signaling mechanisms evoked by the small leucine-rich proteoglycans. *FEBS J* 277, 3864-75

**Iozzo, R. V. and Schaefer, L.** (2015) Proteoglycan form and function: A comprehensive nomenclature of proteoglycans. *Matrix Biology* 42, 11-55

**Ito, Y., Oike, Y., Yasunaga, K., Hamada, K., Miyata, K., Matsumoto, S., Sugano, S., Tanihara, H., Masuho, Y. and Suda, T.** (2003) Inhibition of angiogenesis and vascular leakiness by angiopoietin-related protein 4. *Cancer Res* 63, 6651-7

**Jackson, S., Gilchrist, H. and Nesbitt, L. T., Jr.** (2007) Update on the dermatologic use of systemic glucocorticosteroids. *Dermatol Ther* 20, 187-205

**Jaillon, O., Aury, J. M., Brunet, F., Petit, J. L., Stange-Thomann, N., Mauceli, E., Bouneau, L., Fischer, C., Ozouf-Costaz, C., Bernot, A. et al.** (2004) Genome duplication in the teleost fish Tetraodon nigroviridis reveals the early vertebrate proto-karyotype. *Nature* 431, 946-57

**Jeong, E. Y., Kim, S., Jung, S., Kim, G., Son, H., Lee, D. H., Roh, G. S., Kang, S. S., Cho, G. J., Choi, W. S. et al.** (2013) Enhancement of IGF-2-induced neurite outgrowth by IGF-binding protein-2 and osteoglycin in SH-SY5Y human neuroblastoma cells. *Neuroscience Letters* 548, 249-254

**Jiang, S., Zhao, L., Purandare, B. and Hantash, B. M.** (2010) Differential expression of stem cell markers in human follicular bulge and interfollicular epidermal compartments. *Histochem Cell Biol* 133, 455-65

**Jones, D., Taylor, W. and Thornton, J.** (1992) The rapid generation of mutation data matrices from protein sequences. *Comput Appl Biosci.* 8, 275-82

**Kadomatsu, T., Endo, M., Miyata, K. and Oike, Y.** (2014) Diverse roles of ANGPTL2 in physiology and pathophysiology. *Trends Endocrinol Metab* 25, 245-54

**Kampmann, A., Fernandez, B., Deindl, E., Kubin, T., Pipp, F., Eitenmuller, I., Hoefer, I. E., Schaper, W. and Zimmermann, R.** (2009) The proteoglycan osteoglycin/mimecan is correlated with arteriogenesis. *Molecular and Cellular Biochemistry* 322, 15-23

**Karna, E., Miltyka, W., Wołczynskib, S. and Pałka, J. A.** (2001) The potential mechanism for glutamine-induced collagen biosynthesis in cultured human skin fibroblasts. *Comparative Biochemistry and Physiology Part B* 130, 23-32

**Kishi, S., Slack, B. E., Uchiyamad, J. and Zhdanova, I. V.** (2009) Zebrafish as a Genetic Model in Biological and Behavioral Gerontology: Where Development Meets Aging in Vertebrates – A Mini-Review. *Gerontology* 55

**Kishi, S., Uchiyama, J., Baughman, A. M., Goto, T., Lin, M. C. and Tsai, S. B.** (2003) The zebrafish as a vertebrate model of functional aging and very gradual senescence. *Experimental Gerontology* 38, 777-786

**Kobayashi, T., Iwasaki, T., Amagai, M. and Ohyama, M.** (2010) Canine follicle stem cell candidates reside in the bulge and share characteristic features with human bulge cells. *J Invest Dermatol* 130, 1988-95

**Kobe, B. and Deisenhofer, J.** (1995) Proteins with leucine-rich repeats. *Curr Opin Struct Biol* 5, 409-16

**Kondo, S., Kuwahara, Y., Kondo, M., Naruse, K., Mitani, H., Wakamatsu, Y., Ozato, K., Asakawa, S., Shimizu, N. and Shima, A.** (2001) The medaka rs-3 locus required for scale development encodes ectodysplasin-A receptor. *Curr Biol* 11, 1202-6

**Kowalik, S., Filip, R. S., Śliwa, E., Tatara, M. R., Pierzynowski, S. and Studzinski, T.** (2005) Influence of alpha-ketoglutarate on bone mineral density of the femur in piglets. *Bull. Vet. Inst. Pulawy* 49, 343-348

**Krasnov, A., Skugor, S., Todorcevic, M., Glover, K. A. and Nilsen, F.** (2012) Gene expression in Atlantic salmon skin in response to infection with the parasitic copepod Lepeophtheirus salmonis, cortisol implant, and their combination. *BMC Genomics* 13, 130

**Kubota, Y., Oike, Y., Satoh, S., Tabata, Y., Niikura, Y., Morisada, T., Akao, M., Urano, T., Ito, Y., Miyamoto, T. et al.** (2005a) Cooperative interaction of Angiopoietin-like proteins 1 and 2 in zebrafish vascular development. *Proc Natl Acad Sci U S A* 102, 13502-7

**Kubota, Y., Oike, Y., Satoh, S., Tabata, Y., Niikura, Y., Morisada, T., Akao, M., Urano, T., Ito, Y., Miyamoto, T. et al.** (2005b) Isolation and expression patterns of genes for three angiopoietin-like proteins, Angptl1, 2 and 6 in zebrafish. *Gene Expr Patterns* 5, 679-85

**Lamalice, L., Le Boeuf, F. and Huot, J.** (2007) Endothelial cell migration during angiogenesis. *Circ Res* 100, 782-794

**Lambert, B. D., Filip, R., Stoll, B., Junghans, P., Derno, M., Hennig, U., Souffrant, W. B., Pierzynowski, S. and Burrin, D. G.** (2006) First-Pass Metabolism Limits the Intestinal Absorption of Enteral a-Ketoglutarate in Young Pigs. *The Journal of Nutrition - Nutrient Physiology, Metabolism, and Nutrient-Nutrient Interactions*, 2779-2784

**Larkin, M. A., Blackshields, G., Brown, N. P., Chenna, R., McGettigan, P. A., McWilliam, H., Valentin, F., Wallace, I. M., Wilm, A., Lopez, R. et al.** (2007) Clustal W and clustal X version 2.0. *Bioinformatics* 23, 2947-2948

**Larsson, A.** (2014) AliView: a fast and lightweight alignment viewer and editor for large datasets. *Bioinformatics* 30, 3276-8

**Lauter, G., Söll, I. and Hauptmann, G.** (2011) Two-color fluorescent in situ hybridization in the embryonic zebrafish brain using differential detection systems. *BMC Developmental Biology* 11, 43

**Lazado, C. C. and Caipang, C. M.** (2014) Mucosal immunity and probiotics in fish. *Fish Shellfish Immunol* 39, 78-89

**Lee, E. C., Desai, U., Gololobov, G., Hong, S., Feng, X., Yu, X. C., Gay, J., Wilganowski, N., Gao, C., Du, L. L. et al.** (2009) Identification of a new functional domain in angiopoietin-like 3 (ANGPTL3)

and angiopoietin-like 4 (ANGPTL4) involved in binding and inhibition of lipoprotein lipase (LPL). *J Biol Chem* 284, 13735-45

**Li, A., Xue, Y., Jin, C., Wang, M. and Yao, X.** (2006) Prediction of Nepsilon-acetylation on internal lysines implemented in Bayesian Discriminant Method. *Biochem Biophys Res Commun* 350, 818-24

**Li, X., Mohan, S., Gu, W. and Baylink, D. J.** (2001) Analysis of gene expression in the wound repair/regeneration process. *Mamm Genome* 12, 52-9

**Louis, A., Roest Crollius, H. and Robinson-Rechavi, M.** (2012) How much does the amphioxus genome represent the ancestor of chordates? *Brief Funct Genomics* 11, 89-95

**Ma, Q. Y., Zhang, X. N., Jiang, H., Wang, Z. Q., Zhang, H. J., Xue, L. Q., Chen, M. D. and Song, H. D.** (2011) Mimecan in pituitary corticotroph cells may regulate ACTH secretion and the HPAA. *Molecular and Cellular Endocrinology* 341, 71-77

**Ma, Q. Y., Zuo, C. L., Ma, J. H., Zhang, X. N., Ru, Y., Li, P., Pan, C. M., Liu, Z., Cao, H. M., Chen, M. D. et al.** (2010) Glucocorticoid up-regulates mimecan expression in corticotroph cells. *Molecular and Cellular Endocrinology* 321, 239-244

**Maisonpierre, P. C., Suri, C., Jones, P. F., Bartunkova, S., Wiegand, S., Radziejewski, C., Compton, D., McClain, J., Aldrich, T. H., Papadopoulos, N. et al.** (1997) Angiopoietin-2, a natural antagonist for Tie2 that disrupts in vivo angiogenesis. *Science* 277, 55-60

**Manuel, J. A. and Gawronska-Kozak, B.** (2006) Matrix metalloproteinase 9 (MMP-9) is upregulated during scarless wound healing in athymic nude mice. *Matrix Biol* 25, 505-14

**Matias Santos, D., Rita, A. M., Casanellas, I., Brito Ova, A., Araújo, I. M., Power, D. and Tiscornia, G.** (2016) Ear wound regeneration in the African spiny mouseAcomys cahirinus. *Regeneration* 3, 52-61

**Matsumoto, R. and Sugimoto, M.** (2007) Dermal matrix proteins initiate re-epithelialization but are not sufficient for coordinated epidermal outgrowth in a new fish skin culture model. *Cell & Tissue Research* 327, 349-265

**Matsushima, N., Ohyanagi, T., Tanaka, T. and Kretsinger, R. H.** (2000) Super-motifs and evolution of tandem leucine-rich repeats within the small proteoglycans--biglycan, decorin, lumican, fibromodulin, PRELP, keratocan, osteoadherin, epiphycan, and osteoglycin. *Proteins* 38, 210-25

**McEwan, P. A., Scott, P. G., Bishop, P. N. and Bella, J.** (2006) Structural correlations in the family of small leucine-rich repeat proteins and proteoglycans. *J Struct Biol* 155, 294-305

**Merline, R., Schaefer, R. M. and Schaefer, L.** (2009) The matricellular functions of small leucine-rich proteoglycans (SLRPs). *J Cell Commun Signal* 3, 323-35

**Metz, J. R., Vrieze, E. d., Lock, E.-J., Schulten, I. E. and Flik, G.** (2012) Elasmoid scales of fishes as model in biomedical bone research. *J. Appl. Ichthyol.* 28, 382-387

**Midwood, K. S., Williams, L. V. and Schwarzbauer, J. E.** (2004) Tissue repair and the dynamics of the extracellular matrix. *Int J Biochem Cell Biol* 36, 1031-7

**Mikesh, L. M., Aramadhaka, L. R., Moskaluk, C., Zigrino, P., Mauch, C. and Fox, J. W.** (2013) Proteomic anatomy of human skin. *Journal of Proteomics* 84, 190-200

**Miyabe, K., Tokunaga, H., Endo, H., Inoue, H., Suzuki, M., Tsutsui, N., Yokoo, N., Kogure, T. and Nagasawa, H.** (2012) GSP-37, a novel goldfish scale matrix protein: identification, localization and functional analysis. *The Royal Society of Chemistry* 159, 463-481

**Monnot, M. J., Babin, P. J., Poleo, G., Andre, M., Laforest, L., Ballagny, C. and Akimenko, M. A.** (1999) Epidermal expression of apolipoprotein E gene during fin and scale development and fin regeneration in zebrafish. *Dev Dyn* 214, 207-15

**Montserrat, N., Sanchez-Gurmaches, J., Garcia de la Serrana, D., Navarro, M. I. and Gutierrez, J.** (2007) IGF-I binding and receptor signal transduction in primary cell culture of muscle cells of gilthead sea bream: changes throughout in vitro development. *Cell Tissue Res* 330, 503-13

**Muiznieks, L. D. and Keeley, F. W.** (2013) Molecular assembly and mechanical properties of the extracellular matrix: A fibrous protein perspective. *Biochim Biophys Acta* 1832, 866-75

**Murawala, P., Tanaka, E. M. and Currie, J. D.** (2012) Regeneration: the ultimate example of wound healing. *Semin Cell Dev Biol* 23, 954-62

**Nehls, M., Pfeifer, D., Schorpp, M., Hedrich, H. and Boehm, T.** (1994) New member of the winged-helix protein family disrupted in mouse and rat nude mutations. *Nature* 372, 103-7

**Nelson, K. E., Paulsen, I. T. and Fraser, C. M.** (2001) Microbial genome sequencing: a window into evolution and physiology. *Asm News* 67, 310-317

**Nestle, F. O., Kaplan, D. H. and Barker, J.** (2009) Psoriasis. *N Engl J Med* 361, 496-509
**Nicholas KB, Nicholas HB and DWI, D.** (1997) GeneDoc: Analysis and visualization of genetic variation *EMBNEW.NEWS* 4, 14

**Ohira, Y., Shimizu, M., Ura, K. and Takagi, Y.** (2007) Scale regeneration and calcification in goldfish Carassius auratus: quantitative and morphological processes. *Fisheries Science* 73, 46-54

**Ohno, S.** (1970). Evolution by gene duplication: Springer-Verlag.

**Oike, Y., Akao, M., Kubota, Y. and Suda, T.** (2005) Angiopoietin-like proteins: potential new targets for metabolic syndrome therapy. *Trends Mol Med* 11, 473-9

**Oike, Y., Yasunaga, K., Ito, Y., Matsumoto, S., Maekawa, H., Morisada, T., Arai, F., Nakagata, N., Takeya, M., Masuho, Y. et al.** (2003) Angiopoietin-related growth factor (AGF) promotes epidermal proliferation, remodeling, and regeneration. *Proc Natl Acad Sci U S A* 100, 9494-9

**Okazaki, H., Hirakawa, S., Shudou, M., Nakaoka, Y., Shirakata, Y., Miyata, K., Oike, Y., Hashimoto, K. and Sayama, K.** (2012) Targeted overexpression of Angptl6⁄angiopoietin-related growth factor in the skin promotes angiogenesis and lymphatic vessel enlargement in response to ultraviolet B. *J Dermathology* 39, 366-374

**Olczyk, P., Mencner, L. and Komosinska-Vassev, K.** (2014) The role of the extracellular matrix components in cutaneous wound healing. *Biomed Res Int* 2014, 747584

**Olin, T., Bergstrom, E., Jungvid, H. and Decken, A. v. d.** (1992) Effect of dietary acids (AKG) on intermediary metabolism of nutrients in Atlantic salmon (*Salmo salar*) during 17-b-estradiol induced vitellogenin synthesis. *Acta Agric. Scand.* 42, 246-253

**Olson, R.** (1961) The Skin of Amphioxus. *Zeitschrift fur Zellforschung* 54, 90-104

**Ono, M., Shimizugawa, T., Shimamura, M., Yoshida, K., Noji-Sakikawa, C., Ando, Y., Koishi, R. and Furukawa, H.** (2003) Protein region important for regulation of lipid metabolism in angiopoietin-like 3 (ANGPTL3) - ANGPTL3 is cleaved and activated in vivo. *Journal of Biological Chemistry* 278, 41804-41809

**Pal, M., Tan, M. J., Huang, R. L., Goh, Y. Y., Wang, X. L., Tang, M. B. and Tan, N. S.** (2011) Angiopoietin-like 4 regulates epidermal differentiation. *PloS One* 6, e25377

**Palau, N., Julia, A., Ferrandiz, C., Puig, L., Fonseca, E., Fernandez, E., Lopez-Lasanta, M., Tortosa, R. and Marsal, S.** (2013) Genome-wide transcriptional analysis of T cell activation reveals differential gene expression associated with psoriasis. *BMC Genomics* 14, 825

**Palka, J. A.** (1996) The role of prolidase as an enzyme participating in the metabolism of collagen. *Rocz Akad Med Bialymst* 41, 149-60

**Park, H., Huxley-Jones, J., Boot-Handford, R. P., Bishop, P. N., Attwood, T. K. and Bella, J.** (2008) LRRCE: a leucine-rich repeat cysteine capping motif unique to the chordate lineage. *BMC Genomics* 9, 599

**Paus, R.** (2010) Exploring the "Thyroid–Skin Connection": Concepts, Questions, and Clinical Relevance. *J Invest Dermatol* 130, 7-10

**Pavlidis, M. and Mylonas, C.** (2011). Sparidae: Biology and aquaculture of gilthead sea bream and other species: Wiley-Blackwell.

**Peek, R., Kammerer, R. A., Frank, S., Otte-Holler, I. and Westphal, J. R.** (2002) The angiopoietin-like factor cornea-derived transcript 6 is a putative morphogen for human cornea. *J Biol Chem* 277, 686-93

**Pekny, M. and Lane, E. B.** (2007) Intermediate filaments and stress. *Exp Cell Res* 313, 2244-54

**Perez, M. I. and Kohn, S. R.** (1994) Cutaneous manifestations of diabetes mellitus. *J Am Acad Dermatol* 30, 519-31; quiz 532-4

**Persson, P., Björnsson, B. T. and Takagi, Y.** (1999) Characterization of morphology and physiological actions of scale osteoclasts in the rainbow trout. *Journal of Fish Biology* 54, 669-684

**Perumal, S., Antipova, O. and Orgel, J. P.** (2008) Collagen fibril architecture, domain organization, and triple-helical conformation govern its proteolysis. *Proc Natl Acad Sci U S A* 105, 2824-9

**Petersen, T. N., Brunak, S., von Heijne, G. and Nielsen, H.** (2011) SignalP 4.0: discriminating signal peptides from transmembrane regions. *Nat Methods* 8, 785-6

**Petrie, T. A., Strand, N. S., Yang, C. T., Rabinowitz, J. S. and Moon, R. T.** (2014) Macrophages modulate adult zebrafish tail fin regeneration. *Development* 141, 2581-91

**Philips, N., Auler, S., Hugo, R. and Gonzalez, S.** (2011) Beneficial Regulation of Matrix Metalloproteinases for Skin Health. *Enzyme Research* 2011

**Pond, S. L. K., Murrell, B., Fourment, M., Frost, S. D. W., Delport, W. and Scheffler, K.** (2011) A Random Effects Branch-Site Model for Detecting Episodic Diversifying Selection. *Molecular Biology and Evolution* 28, 3033-3043

**Poss, K. D., Keating, M. T. and Nechiporuk, A.** (2003) Tales of regeneration in zebrafish. *Dev Dyn* 226, 202-10

**Procopio, W. N., Pelavin, P. I., Lee, W. M. and Yeilding, N. M.** (1999) Angiopoietin-1 and -2 coiled coil domains mediate distinct homo-oligomerization patterns, but fibrinogen-like domains mediate ligand activity. *J Biol Chem* 274, 30196-201

**Putnam, N. H., Butts, T., Ferrier, D. E., Furlong, R. F., Hellsten, U., Kawashima, T., Robinson-Rechavi, M., Shoguchi, E., Terry, A., Yu, J. K. et al.** (2008) The amphioxus genome and the evolution of the chordate karyotype. *Nature* 453, 1064-71

**Quilhac, A. and Sire, J.-Y.** (1999) Spreading, Proliferation, and Differentiation of the Epidermis After Wounding a Cichlid Fish, *Hemichromis bimaculatus*. *The Anatomical Record* 254, 435-451

**Rai, A. K., Srivastava, N., Nigam, A. K., Kumari, U., Mittal, S. and Mittal, A. K.** (2012) Healing of cutaneous wounds in a freshwater teleost, Labeo rohita: scanning electron microscopical investigation. *Microsc Res Tech* 75, 890-7

**Rakers, S., Gebert, M., Uppalapati, S., Meyer, W., Maderson, P., Sell, A. F., Kruse, C. and Paus, R.** (2010) 'Fish matters': the relevance of fish skin biology to investigative dermatology. *Experimental Dermatology* 19, 313-324

**Rakers, S., Klinger, M., Kruse, C. and Gebert, M.** (2011) Pros and cons of fish skin cells in culture: long-term full skin and short-term scale cell culture from rainbow trout, Oncorhynchus mykiss. *Eur J Cell Biol* 90, 1041-51

**Rakers, S., Niklasson, L., Steinhagen, D., Kruse, C., Schauber, J., Sundell, K. and Paus, R.** (2013) Antimicrobial peptides (AMPs) from fish epidermis: perspectives for investigative dermatology. *J Invest Dermatol* 133, 1140-9

**Redd, M. J., Cooper, L., Wood, W., Stramer, B. and Martin, P.** (2004) Wound healing and inflammation: embryos reveal the way to perfect repair. *Philos Trans R Soc Lond B Biol Sci* 359, 777-84

**Richardson, R., Slanchev, K., Kraus, C., Knyphausen, P., Eming, S. and Hammerschmidt, M.** (2013) Adult zebrafish as a model system for cutaneous wound-healing research. *J Invest Dermatol* 133, 1655-65

**Roca, F. J., Sepulcre, M. A., Lopez-Castejon, G., Meseguer, J. and Mulero, V.** (2006) The colony-stimulating factor-1 receptor is a specific marker of macrophages from the bony fish gilthead seabream. *Mol Immunol* 43, 1418-23

**Rodriguez, A., Esteban, M. A. and Meseguer, J.** (2003) Phagocytosis and peroxidase release by seabream (Sparus aurata L.) leucocytes in response to yeast cells. *Anat Rec A Discov Mol Cell Evol Biol* 272, 415-23

**Ronquist, F., Teslenko, M., van der Mark, P., Ayres, D. L., Darling, A., Hohna, S., Larget, B., Liu, L., Suchard, M. A. and Huelsenbeck, J. P.** (2012) MrBayes 3.2: efficient Bayesian phylogenetic inference and model choice across a large model space. *Syst Biol* 61, 539-42

**Rosenbloom, J. and Cywinski, A.** (1976) Inhibition of proline hydroxylation does not inhibit secretion of tropoelastin by chick aorta cells. *FEBS Letters* 65

**Rotllant, J., Guerreiro, P. M., Anjos, L., Redruello, B., Canario, A. V. and Power, D. M.** (2005a) Stimulation of cortisol release by the N terminus of teleost parathyroid hormone-related protein in interrenal cells in vitro. *Endocrinology* 146, 71-6

**Rotllant, J., Redruello, B., Guerreiro, P. M., Fernandes, H., Canario, A. V. M. and Power, D. M.** (2005b) Calcium mobilization from fish scales is mediated by parathyroid hormone related protein via the parathyroid hormone type 1 receptor. *Regulatory Peptides* 132, 33-40

**Rutten, E. P., Engelen, M. P., Schols, A. M. and Deutz, N. E.** (2005) Skeletal muscle glutamate metabolism in health and disease: state of the art. *Current Opinion in Clinical Nutrition & Metabolic Care* 8, 41-51

**Salinas, I., Zhang, Y. A. and Sunyer, J. O.** (2011) Mucosal immunoglobulins and B cells of teleost fish. *Dev Comp Immunol* 35, 1346-65

**Sameshima, S., Nakao, M. and Somamoto, T.** (2012) Diversity of CD2 subfamily receptors in cyprinid fishes. *Results Immunol* 2, 25-34

**Santulli, G.** (2014) Angiopoietin-Like Proteins: A Comprehensive Look. *Front Endocrinol (Lausanne)* 5, 4

**Sasaki, T., Majamaa, K. and Uittog, J.** (1987) Reduction of Collagen Production in Keloid Fibroblast Cultures by Ethyl-3,4-dihydroxybenzoate. *The Journal of Biological Chemistry* 262, 9397-9403

**Schaefer, L. and Iozzo, R. V.** (2008) Biological functions of the small leucine-rich proteoglycans: From genetics to signal transduction. *Journal of Biological Chemistry* 283, 21305-21309

**Schaffeld, M. and Schultess, J.** (2006) Genes coding for intermediate filament proteins closely related to the hagfish "thread keratins (TK)" alpha and gamma also exist in lamprey, teleosts and amphibians. *Exp Cell Res* 312, 1447-62

**Schreder, A., Pierard, G. E., Paquet, P., Reginster, M. A., Pierard-Franchimont, C. and Quatresooz, P.** (2010) Facing towards epidermal stem cells (Review). *Int J Mol Med* 26, 171-4

**Schreml, S., Szeimies, R. M., Prantl, L., Landthaler, M. and Babilas, P.** (2010) Wound healing in the 21st century. *J Am Acad Dermatol* 63, 866-81

**Scott, P. G., Dodd, C. M., Bergmann, E. M., Sheehan, J. K. and Bishop, P. N.** (2006) Crystal structure of the biglycan dimer and evidence that dimerization is essential for folding and stability of class I small leucine-rich repeat proteoglycans. *J Biol Chem* 281, 13324-32

**Scott, P. G., McEwan, P. A., Dodd, C. M., Bergmann, E. M., Bishop, P. N. and Bella, J.** (2004) Crystal structure of the dimeric protein core of decorin, the archetypal small leucine-rich repeat proteoglycan. *Proc Natl Acad Sci U S A* 101, 15633-8

**Seeley, R., Stephens, T. and Tate, P.** (2001). Anatomy and Physiology: Lusodidacta.

**Seifert, A. W., Kiama, S. G., Seifert, M. G., Goheen, J. R., Palmer, T. M. and Maden, M.** (2012a) Skin shedding and tissue regeneration in African spiny mice (Acomys). *Nature* 489, 561-5

**Seifert, A. W. and Maden, M.** (2014). New Insights into Vertebrate Skin Regeneration, vol. 310, pp. 129-169. International Review of Cell and Molecular Biology: Elsevier Inc.

**Seifert, A. W., Monaghan, J. R., Voss, S. R. and Maden, M.** (2012b) Skin regeneration in adult axolotls: a blueprint for scar-free healing in vertebrates. *PloS One* 7, e32875

**Shan, L., Yu, X. C., Liu, Z., Hu, Y., Sturgis, L. T., Miranda, M. L. and Liu, Q.** (2009) The angiopoietin-like proteins ANGPTL3 and ANGPTL4 inhibit lipoprotein lipase activity through distinct mechanisms. *J Biol Chem* 284, 1419-24

**Shanahan, C. M., Cary, N. R. B., Osbourn, J. K. and Weissberg, P. L.** (1997) Identification of osteoglycin as a component of the vascular matrix - Differential expression by vascular smooth muscle cells during neointima formation and in atherosclerotic plaques. *Arteriosclerosis Thrombosis and Vascular Biology* 17, 2437-2447

**Siddiq, A., Aminova, L. R. and Ratan, R. R.** (2008) Prolyl 4-hydroxylase activity-responsive transcription factors: From hydroxylation to gene expression and neuroprotection. *Front Biosci.* 13, 2875–2887

**Sire, J.-Y. and Akimenko, M.-A.** (2004) Scale development in fish: a review, with description of sonic hedgehog (shh) expression in the zebrafish ( *Danio rerio*). *International Journal of Developmental Biology* 48, 233-247

**Sire, J.-Y., Huysseune, A. and Meunie, F. J.** (1990) Osteoclasts in teleost fish: Light- and electron-microscopical observations. *Cell & Tissue Research* 260, 85-94

**Skugor, S., Glover, K. A., Nilsen, F. and Krasnov, A.** (2008) Local and systemic gene expression responses of Atlantic salmon (Salmo salar L.) to infection with the salmon louse (Lepeophtheirus salmonis). *BMC Genomics* 9, 498

**Slominski, A., Wortsman, J., Paus, R., Elias, P. M., Tobin, D. J. and Feingold, K. R.** (2008) Skin as an endocrine organ: implications for its function. *Drug Discov Today Dis Mech* 5, 137-144

**Slominski, A., Wortsman, J., Tuckey, R. C. and Paus, R.** (2007) DIFFERENTIAL EXPRESSION OF HPA AXIS HOMOLOG IN THE SKIN. *Molecular and Cellular Endocrinology* 265-266, 143-149

**Slominski, A., Zbytek, B., Nikolakis, G., Manna, P. R., Skobowiat, C., Zmijewski, M., Li, W., Janjetovic, Z., Postlethwaite, A., Zouboulis, C. C. et al.** (2013) Steroidogenesis in the skin: implications for local immune functions. *J Steroid Biochem Mol Biol* 137, 107-23

**Son, E. D., Choi, G. H., Kim, H., Lee, B., Chang, I. S. and Hwang, J. S.** (2007) Alpha-Ketoglutarate Stimulates Procollagen Production in Cultured Human Dermal Fibroblasts, and Decreases UVB-Induced Wrinkle Formation Following Topical Application on the Dorsal Skin of Hairless Mice. *Biol. Pharm. Bull.* 30, 1395-1399

**Soo, C.** (2000) Differential expression of matrix metalloproteinases and their tissue-derived inhibitors in cutaneous wound repair--a correction. *Plast Reconstr Surg* 106, 236-7

**Steentoft, C., Vakhrushev, S. Y., Joshi, H. J., Kong, Y., Vester-Christensen, M. B., Schjoldager, K. T., Lavrsen, K., Dabelsteen, S., Pedersen, N. B., Marcos-Silva, L. et al.** (2013) Precision mapping of the human O-GalNAc glycoproteome through SimpleCell technology. *EMBO J* 32, 1478-88

**Steinert, P. M.** (2001) Keratins: dynamic, flexible structural proteins of epithelial cells. *Curr Probl Dermatol* 54, 193-198

**Stet, R. J., Hermsen, T., Westphal, A. H., Jukes, J., Engelsma, M., Lidy Verburg-van Kemenade, B. M., Dortmans, J., Aveiro, J. and Savelkoul, H. F.** (2005) Novel immunoglobulin-like transcripts in teleost fish encode polymorphic receptors with cytoplasmic ITAM or ITIM and a new structural Ig domain similar to the natural cytotoxicity receptor NKp44. *Immunogenetics* 57, 77-89

**Sundarraj, N., Fite, D., Belak, R., Sundarraj, S., Rada, J., Okamoto, S. and Hassell, J.** (1998) Proteoglycan distribution during healing of corneal stromal wounds in chick. *Exp Eye Res* 67, 433-42

**Suri, C., Jones, P. F., Patan, S., Bartunkova, S., Maisonpierre, P. C., Davis, S., Sato, T. N. and Yancopoulos, G. D.** (1996) Requisite role of angiopoietin-1, a ligand for the TIE2 receptor, during embryonic angiogenesis. *Cell* 87, 1171-80

**Tanaka, K., Matsumoto, E., Higashimaki, Y., Katagiri, T., Sugimoto, T., Seino, S. and Kaji, H.** (2012) Role of osteoglycin in the linkage between muscle and bone. *J Biol Chem* 287, 11616-28

**Tasheva, E. S. and Conrad, G. W.** (2003) The UV responsive elements in the human mimecan promoter: a functional characterization. *Mol Vis* 9, 1-9

**Tasheva, E. S., Funderburgh, M. L., McReynolds, J., Funderburgh, J. L. and Conrad, G. W.** (1999) The bovine mimecan gene. Molecular cloning and characterization of two major RNA transcripts generated by alternative use of two splice acceptor sites in the third exon. *J Biol Chem* 274, 18693-701

**Tasheva, E. S., Koester, A., Paulsen, A. Q., Garrett, A. S., Boyle, D. L., Davidson, H. J., Song, M., Fox, N. and Conrad, G. W.** (2002) Mimecan/osteoglycin-deficient mice have collagen fibril abnormalities. *Mol Vis* 8, 407-15

**Taşkiran, D., Taşkiran, E., Yercan, H. and Kutay, F. Z.** (1999) Quantification of Total Collagen in Rabbit Tendon by the Sirius Red Method. *Tr. J. of Medical Sciences* 29, 7-9

**Tatara, M. R., Brodzki, A., Krupski, W., Sliwa, E., Silmanowictz, P., Majcher, P., Pierzynowski, S. G. and Studzinski, T.** (2005) Effects of α-ketoglutarate on bone homeostasis and plasma amino acids in turkeys. *Poultry Science Association* 84, 1604-1609

**Tatara, M. R., Majcher, P., Krupski, W., Pierzynowski, S. G. and Studzinski, T.** (2004a) Influence of alpha-ketoglutarate on cortical bone density, geometrical properties and mechanical endurance of the humerus in turkeys. *Bull. Vet. Ins. Pulawy* 48, 461-465

**Tatara, R. M., Pierzynowski, S., Majcher, P., Krupski, W., Brodki, A. and Studzinski, T.** (2004b) Effect of alpha-ketoglutarate (AKG) on mineralisation, morphology and mechanical endurance of femur and tibia in turkey. *Bull. Vet. Ins. Pulawy* 48, 305-309

**Taylor, A. F.** (2002) Osteoblastic glutamate receptor function regulates bone formation and resorption. *J Musculoskelet Neuronal Interact* 2, 285-90

**Thamamongood, T. A., Furuya, R., Fukuba, S., Nakamura, M., Suzuki, N. and Hattori, A.** (2012) Expression of osteoblastic and osteoclastic genes during spontaneous regeneration and autotransplantation of goldfish scale: a new tool to study intramembranous bone regeneration. *Bone* 50, 1240-9

**Thomas, M. and Augustin, H. G.** (2009) The role of the Angiopoietins in vascular morphogenesis. *Angiogenesis* 12, 125-37

**Tocaj, A., Filip, R., Lindergard, B., Wernerman, J., Studzinski, T., Ohman, K. and Pierzynowski, S.** (2003) Alpha-ketoglutarate (AKG) inhibit osteoporosis development in postmenopausal women. *Journal of Bone and Mineral Research* 18, S267-S267

**Tournefier, A., Laurens, V., Chapusot, C., Ducoroy, P., Padros, M. R., Salvadori, F. and Sammut, B.** (1998) Structure of MHC class I and class II cDNAs and possible immunodeficiency linked to class II expression in the Mexican axolotl. *Immunol Rev* 166, 259-77

**Toyono, T., Usui, T., Yokoo, S., Taketani, Y., Nakagawa, S., Kuroda, M., Yamagami, S. and Amano, S.** (2015) Angiopoietin-like 7 is an anti-angiogenic protein required to prevent vascularization of the cornea. *PloS One* 10, e0116838

**Uhlen, M., Fagerberg, L., Hallstrom, B. M., Lindskog, C., Oksvold, P., Mardinoglu, A., Sivertsson, A., Kampf, C., Sjostedt, E., Asplund, A. et al.** (2015) Proteomics. Tissue-based map of the human proteome. *Science* 347, 1260419

**Umikawa, M., Umikawa, A., Asato, T., Takei, K., Matsuzaki, G., Kariya, K. and Zhang, C. C.** (2015) Angiopoietin-like protein 2 induces proinflammatory responses in peritoneal cells. *Biochemical and Biophysical Research Communications* 467, 235-241

**Vadon-Le Goff, S., Hulmes, D. J. S. and Moali, C.** (2015) BMP-1/tolloid-like proteinases synchronize matrix assembly with growth factor activation to promote rnorphogenesis and tissue remodeling. *Matrix Biology* 44-46, 14-23

**Venkatesh, B.** (2003) Evolution and diversity of fish genomes. *Current Opinion in Genetics & Development* 13, 588-592

**Vickaryous, M. and Sire, J. Y.** (2009) 'The integument story: origins, evolution and current knowledge'. *J Anat* 214, 407-8

**Vieira, F. A., Gregório, S. F., Ferraresso, S., Thorne, M. A., Costa, R., Milan, M., Bargelloni, L., Clark, M. S., Canario, A. V. and Power, D. M.** (2011) Skin healing and scale regeneration in fed and unfed sea bream, *Sparus auratus*. *BMC Genomics* 12, 490

**Vieira, F. A., Pinto, P. I., Guerreiro, P. M. and Power, D. M.** (2012) Divergent responsiveness of the dentary and vertebral bone to a selective estrogen-receptor modulator (SERM) in the teleost Sparus auratus. *Gen Comp Endocrinol* 179, 421-7

**Vieira, F. A., Thorne, M. A., Stueber, K., Darias, M., Reinhardt, R., Clark, M. S., Gisbert, E. and Power, D. M.** (2013) Comparative analysis of a teleost skeleton transcriptome provides insight into its regulation. *Gen Comp Endocrinol* 191, 45-58

**Waddington, R. J., Roberts, H. C., Sugars, R. V. and Schonherr, E.** (2003) Differential roles for small leucine-rich proteoglycans in bone formation. *Eur Cell Mater* 6, 12-21; discussion 21

**Wang, X. B., Ford, B. C., Praul, C. A. and Leach, R. M.** (2005) Characterization of the non-collagenous proteins in avian cortical and medullary bone. *Comparative Biochemistry and Physiology B-Biochemistry & Molecular Biology* 140, 665-672

**Wang, Y. H., Ma, Y., Lue, B. J., Xu, E., Huang, Q. and Lai, M.** (2007) Differential expression of mimecan and thioredoxin domain-containing protein 5 in colorectal adenoma and cancer: A proteomic study. *Experimental Biology and Medicine* 232, 1152-1159

**Ward, N. L. and Dumont, D. J.** (2002) The angiopoietins and Tie2/Tek: adding to the complexity of cardiovascular development. *Semin Cell Dev Biol* 13, 19-27

**Welborn, J. R., Shpun, S., Dantzler, W. H. and Wright, S. H.** (1998) Effect of a-ketoglutarate on organic anion transport in single rabbit renal proximal tubules. *American Journal of Physiology: Renal Physiology* 274, 165-174

**Wells, A., Nuschke, A. and Yates, C. C.** (2016) Skin tissue repair: Matrix microenvironmental influences. *Matrix Biol* 49, 25-36

**Werner, S. and Grose, R.** (2003) Regulation of wound healing by growth factors and cytokines. *Physiol Rev* 83, 835-70

**Wernerman, J., Hammarqvist, F. and Vinnars, E.** (1990) Alpha-ketoglutarate and postoperative muscle catabolism. *Lancet* 335, 701-3

**Wertheimer, E., Spravchikov, N., Trebicz, M., Gartsbein, M., Accili, D., Avinoah, I., Nofeh-Moses, S., Sizyakov, G. and Tennenbaum, T.** (2001) The Regulation of Skin Proliferation and Differentiation in the IR Null Mouse: Implications for Skin Complications of Diabetes. *Endocrinology* 142, 1234-1241

**Wirén, M., Permert, J. and Larsson, J.** (2002) a-Ketoglutarate–Supplemented Enteral Nutrition:Effects on Postoperative Nitrogen Balance andMuscle Catabolism. *Nutrition* 18, 725-728

**Witten, P. E.** (1997) Enzyme histochemical characteristics of osteoblasts and mononucleated osteoclasts in a teleost fish with acellular bone (*Oreochromis niloticus*, Cichlidae). *Cell & Tissue Research* 287, 591-599

**Witten, P. E., Hansen, A. and Hall, B. K.** (2001) Features of Mono- and Multinucleated Bone Resorbing Cells of the Zebrafish Danio rerio and Their Contribution to Skeletal Development, Remodeling, and Growth. *Journal of Morphology* 250, 197-207

**Wu, N., Yang, M., Gaur, U., Xu, H., Yao, Y. and Li, D.** (2016) Alpha-Ketoglutarate: Physiological Functions and Applications. *Biomol Ther (Seoul)* 24, 1-8

**Xiao, Y., Jiang, Z., Li, Y., Ye, W., Jia, B., Zhang, M., Xu, Y., Wu, D., Lai, L., Chen, Y. et al.** (2015a) ANGPTL7 regulates the expansion and repopulation of human hematopoietic stem and progenitor cells. *Haematologica*

**Xiao, Y., Wei, X., Jiang, Z., Wang, X., Ye, W., Liu, X., Zhang, M., Xu, Y., Wu, D., Lai, L. et al.** (2015b) Loss of Angiopoietin-like 7 diminishes the regeneration capacity of hematopoietic stem and progenitor cells. *J Hematol Oncol* 8, 7

**Xu, Z., Parra, D., Gomez, D., Salinas, I., Zhang, Y. A., von Gersdorff Jorgensen, L., Heinecke, R. D., Buchmann, K., LaPatra, S. and Sunyer, J. O.** (2013) Teleost skin, an ancient mucosal surface that elicits gut-like immune responses. *Proc Natl Acad Sci U S A* 110, 13097-102

**Yates, C. C., Hebda, P. and Wells, A.** (2012) Skin wound healing and scarring: fetal wounds and regenerative restitution. *Birth Defects Res C Embryo Today* 96, 325-33

**Yau, M. H., Wang, Y., Lam, K. S. L., Zhang, J. L., Wu, D. H. and Xu, A. M.** (2009) A Highly Conserved Motif within the NH2-terminal Coiled-coil Domain of Angiopoietin-like Protein 4 Confers Its Inhibitory Effects on Lipoprotein Lipase by Disrupting the Enzyme Dimerization. *Journal of Biological Chemistry* 284, 11942-11952

**Yeh, J. T., Yeh, L. K., Jung, S. M., Chang, T. J., Wu, H. H., Shiu, T. F., Liu, C. Y., Kao, W. W. and Chu, P. H.** (2010) Impaired skin wound healing in lumican-null mice. *Br J Dermatol* 163, 1174-80

**Young, M. F., Bi, Y., Ameye, L. and Chen, X.-D.** (2003) Biglycan knockout mice: New models for musculoskeletal diseases. *Glycoconjugate Journal* 19, 257-262

**Zhang, Y. A., Salinas, I., Li, J., Parra, D., Bjork, S., Xu, Z., LaPatra, S. E., Bartholomew, J. and Sunyer, J. O.** (2010) IgT, a primitive immunoglobulin class specialized in mucosal immunity. *Nat Immunol* 11, 827-35

**Zheng, J. K., Umikawa, M., Cui, C. H., Li, J. Y., Chen, X. L., Zhang, C. Z., Hyunh, H. D., Kang, X. L., Silvany, R., Wan, X. et al.** (2012) Inhibitory receptors bind ANGPTLs and support blood stem cells and leukaemia development. *Nature* 485, 656-+